(12)

RADC-TR-83-108
Final Technical Report
May 1983

RELIABILITY MODELING OF CRITICAL ELECTRONIC DEVICES

IIT Research Institute

David W. Colt and Joseph J. Steinkirchner

APPROVED FOR PUBLIC RELEASE; DISTRIBUTION UNLIMITED

ROME AIR DEVELOPMENT CENTER
Air Force Systems Command
Griffiss Air Force Base, NY 13441

This report has been reviewed by the RADC Public Affairs Office (PA) and is releasable to the National Technical Information Service (NTIS). At NTIS it will be releasable to the general public, including foreign nations.

RADC-TR-83-108 has been reviewed and is approved for publication.

APPROVED: Lester J. Gubbins

LESTER J. GUBBINS
Project Engineer

APPROVED: W. S. Tuthill

W. S. TUTHILL, COLONEL, USAF
Chief, Reliability & Compatibility Division

FOR THE COMMANDER: John P. Huss

JOHN P. HUSS
Acting Chief, Plans Office

If your address has changed or if you wish to be removed from the RADC mailing list, or if the addressee is no longer employed by your organization, please notify RADC (RBET) Griffiss AFB NY 13441. This will assist us in maintaining a current mailing list.

Do not return copies of this report unless contractual obligations or notices on a specific document requires that it be returned.

UNCLASSIFIED

SECURITY CLASSIFICATION OF THIS PAGE (When Data Entered)

REPORT DOCUMENTATION PAGE		READ INSTRUCTIONS BEFORE COMPLETING FORM
1. REPORT NUMBER RADC-TR-83-108	2. GOVT ACCESSION NO. A133705	3. RECIPIENT'S CATALOG NUMBER
4. TITLE (and Subtitle) RELIABILITY MODELING OF CRITICAL ELECTRONIC DEVICES		5. TYPE OF REPORT & PERIOD COVERED Final Technical Report Oct 81 - Jan 83
		6. PERFORMING ORG. REPORT NUMBER N/A
7. AUTHOR(s) David W. Coit Joseph J. Steinkirchner		8. CONTRACT OR GRANT NUMBER(s) F30602-81-C-0236
9. PERFORMING ORGANIZATION NAME AND ADDRESS IIT Research Institute 10 West 35th Street Chicago IL 60616		10. PROGRAM ELEMENT, PROJECT, TASK AREA & WORK UNIT NUMBERS 62702F 23380253
11. CONTROLLING OFFICE NAME AND ADDRESS Rome Air Development Center (RBET) Griffiss ADB NY 13441		12. REPORT DATE May 1983
		13. NUMBER OF PAGES 380.
14. MONITORING AGENCY NAME & ADDRESS(if different from Controlling Office) Same		15. SECURITY CLASS. (of this report) UNCLASSIFIED
		15a. DECLASSIFICATION/DOWNGRADING SCHEDULE N/A

16. DISTRIBUTION STATEMENT (of this Report)

Approved for public release; distribution unlimited.

17. DISTRIBUTION STATEMENT (of the abstract entered in Block 20, if different from Report)

Same

18. SUPPLEMENTARY NOTES

RADC Project Engineer: Lester J. Gubbins (RBET)

19. KEY WORDS (Continue on reverse side if necessary and identify by block number)

Reliability	Semiconductor Lasers	Electronic Filters
Failure Rate	Helium Cadmium Lasers	Solid State Relays
Magnetrons	Helium Neon Lasers	Time Delay Relays (Electronic)
Vidicons	Crystals	Circuit Breakers
Cathode Ray Tubes	Nd:YAG Lasers	I. C. Sockets (See Reverse)

20. ABSTRACT (Continue on reverse side if necessary and identify by block number)

This report presents failure rate prediction procedures for magnetrons, vidicons, cathode ray tubes, semiconductor lasers, helium-cadmium lasers, helium-neon lasers, Nd:YAG lasers, electronic filters, solid state relays, time dealy relays (electronic hybrid), circuit breakers, I.C. Sockets, thumbwheel switches, electromagnetic meters, fuses, crystals, incandescent lamps, neon glow lamps and surface acoustic wave devices. Collected field failure rate data were utilized to develop and

DD FORM 1 JAN 73 1473 EDITION OF 1 NOV 65 IS OBSOLETE

UNCLASSIFIED

SECURITY CLASSIFICATION OF THIS PAGE (When Data Entered)

evaluate the procedures. The reliability prediction procedures are presented in a form compatible with MIL-HDBK-217.

Item #19 (continued)

Thumb Wheel Switches
Electromagnetic Meters
Fuses
Incandescent Lamps
Neon Lamps
Surface Acoustic Wave Devices

PREFACE

This final report was prepared by IIT Research Institute, Chicago, Illinois, for the Rome Air Development Center, Griffiss AFB, New York, under Contract F30602-81-C-0236. The RADC technical monitor for this program was Mr. Lester J. Gubbins (RBET). This report covers the work performed from October 1981 to January 1983.

The principal investigators for this project were Mr. D.W. Coit and Mr. J.J. Steinkirchner with valuable assistance provided by Dr. N.P. Murarka, Mr. D.W. Fulton, Mr. D. Dylis, Mr. S. Flint, Mr. K. Dey, Mr. W. Cesare and Mr. M. Rossi. Data collection efforts for this program were coordinated by Mr. J. Carey.

Approved by,

H.A. Lauffenburger
Manager of Reliability Technology
IIT Research Institute

Submitted by,

J.J. Steinkirchner
Manager of Reliability Programs
IIT Research Institute

Management Summary

The objective of this 6400 engineering manhour effort was to develop failure rate prediction models for the following thermionic, coherent light emitting, passive and electromechanical devices:

- o Magnetrons (including low power C.W.)
- o Vidicons
- o Cathode Ray Tubes
- o Lasers
- o Electronic Filters
- o Solid State Relays
- o Electronic Time Delay Relays
- o Circuit Breakers
- o I.C. Sockets
- o Thumbwheel Switches
- o Electromagnetic Meters
- o Fuses
- o Crystals
- o Incandescent Lamps
- o Glow Lamps
- o Surface Acoustic Wave Devices

The derived prediction models are intended to provide the ability to predict the total device reliability as a function of the characteristics of the device, the technology employed in producing the device and those external factors, e.g., environmental stresses, circuit application, etc. which have a significant affect on device reliability. The prediction models are to be incorporated into MIL-HDBK-217.

The general approach used for the development of the prediction models was as follows:

- o Identify critical factors which were thought to ultimately impact the reliability of a device. These factors were identified from

published literature and from the shared experiences of the personnel asigned to the project (IITRI corporate memory).

- Hypothesize a model form based on the critical factors and IITRI's corporate memory.
- Use failure experience data to evaluate the accuracy of the hypothesized model form and to generate numerical estimates for the parameters included in the model.

Most of the devices considered in this study effort are not used extensively in military equipments. Therefore, the general model development approach usually had to be modified. Approach modifications included the use of life test data or physics of failure information in lieu of field experience data, the assumption that present MIL-HDBK-217 relationships for similar components could be applied to the device, and the use of survey data obtained from a previous RADC study to develop environmental factors. The depth and extent to which modifications to the general model development approach were made for a particular device is discussed in the applicable section of this report.

The data on which this study are based are comprised of field experience and life test data. Collectively these data represent more than 29.4 billion device operating hours and some 5,428 failures.

Failure rate prediction models were developed for the following devices:

- Vidicons
- Semiconductor Lasers
- Helium-Cadmium Lasers
- Electronic Filters
- Solid State Relays
- I.C. Sockets
- Thumbwheel Switches
- Surface Acoustic Wave Devices

In addition, the prediction procedures for the following devices were revised:

- o Magnetrons
- o Electronic Time Delay Relays
- o Circuit Breakers
- o Meters
- o Fuses
- o Crystals
- o Incandescent Lamps
- o Cathode Ray Tubes

Due to the lack of sufficient field experience data, the failure rate prediction models for the following devices could not be revised:

- o Helium-Neon Lasers
- o Ruby Rod Lasers
- o Nd:YAG Rod Lasers
- o CO_2 Lasers
- o Argon Ion Lasers
- o Neon Glow Lamps

With the exception of Nd:YAG rod lasers and neon glow lamps, these devices are rarely used in military systems.

Both the new and the revised failure rate prediction procedures greatly improve upon existing failure rate prediction capabilities. Therefore, it is recommended that the proposed failure rate prediction models presented in this technical report, be incorporated into MIL-HDBK-217.

TABLE OF CONTENTS

TABLE OF CONTENTS (CONT'D)

TABLE OF CONTENTS (CONT'D)

TABLE OF CONTENTS (CONT'D)

TABLE OF CONTENTS (CONT'D)

LIST OF FIGURES

LIST OF TABLES

LIST OF TABLES (CONT'D)

LIST OF TABLES (CONT'D)

LIST OF TABLES (CONT'D)

LIST OF TABLES (CONT'D)

1.0 INTRODUCTION

1.1 Objective

The objective of this study effort was to develop failure rate prediction models for the following thermionic, coherent light emitting, passive and electromechanical devices:

- o Magnetrons (including low power C.W.)
- o Vidicons
- o Cathode Ray Tubes
- o Lasers
- o Electronic Filters
- o Solid State Relays
- o Electronic Time Delay Relays
- o Circuit Breakers
- o I.C. Sockets
- o Thumbwheel Switches
- o Electromagnetic Meters
- o Fuses
- o Crystals
- o Incandescent Lamps
- o Glow Lamps
- o Surface Acoustic Wave Devices

The derived prediction methodologies are intended to provide the ability to predict the total device reliability as a function of the characteristics of the device, the technology employed in producing the device, and those external factors, e.g., environmental stresses, circuit application, etc. which have a significant affect on device reliability. The prediction methodology was formatted in a form compatible with MIL-HDBK-217.

1.2 Background

Failure rate and mean-time-between-failure prediction capabilities are essential tools in the development and maintenance of reliable electronic equipments. Predictions performed during the design phase yield early estimates of the anticipated equipment reliability and provide a quantitative basis for performing proposal evaluations, design trade-off analyses, reliability growth monitoring and life-cycle cost studies. While the majority of the device models in MIL-HDBK-217 afford reasonably accurate predictions, the same cannot be said for the devices enumerated in Section 1.1. Vidicons, electronic filters, solid state relays, I.C. sockets and surface acoustic wave devices are not represented by a model, while the models for the remaining devices are inadequate or may have become obsolete as a consequence of advancing technology.

1.3 Modeling Approach

The general approach used for the development of viable prediction methodologies for these critical electronic devices is described in this section.

Critical factors which were thought to ultimately impact the reliability of a device were identified for each critical device. These factors which were considered in detail included:

- Function
- Technology
  - Fabrication Techniques
  - Fabrication Process Maturity
  - Failure Mode/Mechanism Experience
- Complexity
- Effectiveness of Process Controls
- Effectiveness of Screening and Test Techniques
- Operating Temperature and Environment
- Application Considerations

The information required to identify these factors was obtained from the shared experiences of the personnel working on the study (IITRI corporate memory) and from the literature search discussed in Section 2.1.

A model form was hypothesized based on information obtained from IITRI's corporate memory and from the literature search discussed in Section 2.1. Data obtained from the data collection effort discussed in Section 2.2 were analyzed to evaluate the accuracy of the hypothesized model form and to generate numerical estimates for the parameters included in the model.

Field failure experience data were utilized where ever possible. In some instances insufficient field experience data were available, and either life test data and/or physics of failure information and/or the present relationships between factors in the current MIL-HDBK-217 models were used to derive numerical estimates for the parameters included in the proposed model.

A detailed discussion of the modeling approach used to develop each model is presented in the model development section for each model.

1.4 Report Organization

This technical report is organized as follows:

Section 1.0 - A general introduction concerning the objective of the study, the rationale for the study and the basic modeling approach used.

Section 2.0 - A general discussion of the data collection and literature search(s) employed.

Section 3.0 - A general discussion of the statistical procedures used in the data analyses and model development

Section 4.0 thru Section 18.0 - Detailed discussions of the applicable part descriptions, part failure modes/mechanisms, proposed model, model development approach, references and bibliography.

Section 19.0 - Conclusion and recommendations.

Appendix A - Revision pages for MIL-HDBK-217.

2.0 DATA/INFORMATION COLLECTION TECHNIQUES

2.1 Literature Review

A comprehensive literature review was performed for each device type considered in the study. The purpose of the review was to identify all published information which was thought to be relevant to the reliability of the critical devices. Literature sources searched included the Reliability Analysis Center automated library information retrieval system, the National Technical Information Service (NTIS), the Defense Technical Information System (DTIS), the Government Industry Data Exchange Program (GIDEP), the RADC Technical Library and the John Crerar library. Additionally, manufacturers and users of the devices were queried to supply useful information.

The primary objective of the literature review was to locate references whose content could be used to define relevant device characteristics and to hypothesize a model form, to supplement the data analysis process and to provide the reliability models with a sound theoretical foundation.

The information sources that were identified and utilized in the study are presented in the appropriate section.

2.2 Data Collection and Preliminary Analysis

The modification of current failure rate prediction models or the development of new prediction methodologies should be derived from field failure rate data obtained from monitored systems. This section presents the basic data collection procedure followed and the preliminary analyses used to develop useful databases for the devices.

The Reliability Analysis Center operated by the IIT Research Institute at Griffiss Air Force Base was solicited to aid in the data collection process. The Reliability Analysis Center regularly pursues the collection of parts reliability data including those devices to be analyzed in this study.

Data resources which had been collected and summarized prior to the initiation of this study were available for analysis. However, the requirements for extensive data resources necessitated additional data collection activities to supplement the existing information.

A survey of commercial, industrial and government organizations was conducted shortly after the beginning of the study. Organizations contacted either manufactured, used or were similarly connected with one or more of the devices considered in this study. Information requested included field experience data, pre-production and production equipment tests, failure analysis reports and physical construction details. A sum total of over 787 organizations were contacted. Approximately 15% of all organizations contacted during the data collection effort submitted information pertaining to one or more of the critical electronic devices. A primary concern of the majority of contributors was the proprietary nature of the information and the desire to remain anonymous. For this reason, none of the data contributors in this study will be identified.

A prerequisite to the summarization of data was the identification of all parameters and factors influencing the reliability of the devices. A task was defined at the beginning of the program whose goal was a reliability evaluation based solely on theoretical considerations. These theoretical studies served to identify the important parameters which were then further investigated using data analysis. Identification of construction details and process controls which were theoretically believed to have an effect on reliability were pursued for each source of data.

All data items received during the data collection efforts were reviewed for completeness of detail and examined for any inherent biases. Any data submittal which displayed obvious biases were not considered in this study. Those reports lacking sufficient detail were not considered until the necessary additional information was acquired.

A summary of the collected and reduced data is given in Table 2.2-1. Table 2.2-1 presents part operating hours and recorded failures for each

device type. A detailed list of the data collected on each device type is presented in the appropriate section.

TABLE 2.2-1: DATA SUMMARY BY DEVICE

Device	Device Operate Hours ($X 10^6$)	Number of Failures
Magnetrons	6.941	1950
Vidicons	8.542	479
Cathode Ray Tubes	5.079	91
Semiconductor Lasers	4.051	354
Helium-Cadmium Lasers	0.358	90
Helium-Neon Lasers	4.708	25
Nd:YAG Lasers	0.176	25
Electronic Filters	580.955	73
Solid State Relays	23853.760	702
Time Delay Relays	4.012	6
Circuit Breakers	334.198	379
I.C. Sockets	3478.129	2
Thumbwheel Switches	5.485	19
Meters	60.799	108
Fuses	800.401	185(1)
Crystals	44.469	16
Incandescent Lamps	213.433	893
Neon Lamps	60.877	27
Surface Acoustic Wave Devices	1.577	2
Totals	29467.950	5425

Notes: (1) includes both failures and replacements

3.0 DATA ANALYSIS

3.1 Statistical Analysis Techniques

In order to evaluate the relationships between device failure rate and potential failure rate model parameters, various statistical analysis techniques were employed. A brief discussion of each technique which was applicable to this study is given in this section.

Stepwise Multiple Linear Regression Analysis. Regression analysis is an important statistical tool and was used to develop the failure rate prediction models for the majority of the critical electronic devices. A more thorough discussion of stepwise multiple linear regression analysis is given in reference 1. A brief description follows.

The stepwise multiple linear regression analysis technique assumes a preliminary model of the form

$$Y = b_0 + b_1X_1 + b_2X_2 + \ldots + b_iX_i$$

where Y is the resultant dependent variable, X_1, $X_2,\ldots,X_i$ are the independent variables which are thought to influence the value of Y, and b_1, $b_2,\ldots,b_i$ are the coefficients which are to be found by the regression.

To perform a regression, a number of data points, each consisting of a known Y and its corresponding X variables, are required. A proper regression also requires that the X variables be independent and that there are many more data points than X variables.

The analysis orders the X (independent) variables according to their relative significance with respect to the Y (dependent) variable. The first step considers only the independent variable with the highest signficance. b_0 and b_1 are computed such that the sum of the squares of (Y' - Y) is a minimum. Y' is the calculated dependent variable and Y is the observed

dependent variable. The second X variable is then considered and b_0, b_1 and b_2 are computed such that the sum of the sqares of (Y' - Y) is again a minimum. If the improvement in the estimate afforded by the inclusion of this second variable is significant with respect to a given confidence level, the variable is accepted as part of the model. If considering the second variable does not result in a significant improvement the model remains,

$$Y = b_0 + b_1X_1$$

In the case where the second variable is accepted, the regression analysis continues until all of the significant X variables have been identified and the corresponding b_i coefficients have been calculated. However, whenever a new variable is included in the fitted model, all previously included variables are retested for significance and eliminated if insignificant.

Failure rate prediction models are rarely in the additive form the stepwise linear regression analysis assumes. However, by using transformations, many possible model forms can assume the additive form. An example can best illustrate this point. The Arrhenius relationship is applicable to many electrical devices and takes the following form,

$$\lambda = A \exp(-B/T)$$

where T is the independent variable, λ is the dependent variable and A and B are constants. By taking the logarithm of each side the equation becomes,

$$\ln\lambda = \ln A - \frac{B}{T}$$

which can be solved by regression analysis with 1/T the independent variable and $\ln\lambda$ the dependent variable. Other transformations are available such that stepwise multiple linear regression can be used to quantify a variety of failure rate model forms.

The previous paragraphs have discussed how regression analysis can be useful in developing failure rate prediction models in which failure rate is a function of quantitative variables such as temperature, frequency or peak power level. However, there are often significant variables which can not be measured on a continuous quantitative scale. Application environment and manufacturing quality level are examples of variables which are qualitative. Numerically it is difficult to relate "ground benign" environmental stress to "airborne inhabited fighter" environmental stress although one is known to be worse than the other. In order to determine numerical quantities for qualitative factors in a regression analysis, a matrix of "dummy variables" (0 or 1) is used as the independent variables. The regression solution by least squares gives numerical values of the coefficients (b_i) which can be used to calculate numerical quantities corresponding to the appropriate qualitative category. An example can best illustrate this method. Take for example a part type wnich is represented by a multiplicative model and has four clearly defined quality levels based on the amount of screening. The four quality levels are signified as q_1, q_2, q_3 and q_4. The following matrix of "dummy variables" given in Table 3.1-1 show quality level as a function of X_1, X_2 and X_3.

TABLE 3.1-1: EXAMPLE OF QUALITATIVE REGRESSION ANALYSIS

	"Dummy Variables"		
Quality Level	X_1	X_2	X_3
q_1	0	0	0
q_2	1	0	0
q_3	0	1	0
q_4	0	0	1

Failure rate data for q_1 quality level parts is entered into the regression by setting (X_1, X_2, X_3) equal to (0, 0, 0) and data for q_2 quality level parts is entered by setting (X_1, X_2, X_3) equal to (1, 0, 0) and so on. Determination of coefficients for variables X_1, X_2, and X_3 allow for computation of quality factor values by the following equations:

$$\pi_Q = \exp (b_1X_1 + b_2X_2 + b_3X_3)$$

$$\pi_{Q1} = \exp (0 + 0 + 0) = 1.0$$

$$\pi_{Q2} = \exp (b_1 + 0 + 0) = e^{b1}$$

$$\pi_{Q3} = \exp (0 + b_2 + 0) = e^{b2}$$

$$\pi_{Q4} = \exp (0 + 0 + b3) = e^{b3}$$

This example was set up such that a q_1 quality factor is equal to one. Any of the other quality factors could have been set equal to one without changing the overall results. The relative differences caused by changing which quality factor was set equal to one would be compensated for by a change in the base failure rate. Generally the qualitative category which is anticipated to have the lowest failure rate is chosen to be set equal to one.

To apply stepwise multiple linear regression analysis, the assumed model form should be either a linear equation or capable of being transformed into a linear equation. All the example equations given thus far in this section have been linear equations. An example of a nonlinear equation is,

$$\lambda p = (b_o + b_1X_1) \exp (b_2X_2 + b_3X_3 + b_4X_4)$$

This equation can not be transformed into a linear equation and still meet all requirements necessary for regression analysis. However models of this form often represent the failure rate of electronic and electromechanical part types. Included in this study are magnetrons and rotary switches which are best represented by nonlinear failure rate prediction models. Nonlinear equations are very difficult to solve by regression analysis and therefore several alternatives were considered.

One approach to nonlinear regression is to approximate the nonlinear equation by a linear equation. An approximation of this type can be very

accurate as long as there are clearly defined minimum and maximum values for the independent variables which are part of the approximation. This approach was used for magnetrons. The assumed form for magnetron failure rate with and without the approximation are given below.

$$\lambda_p = \lambda_b (Ar + B) f^c P^d \pi_E \quad \text{, empirical model form}$$

$$\lambda_p = \lambda_b (ar^b) f^c P^d \pi_E \quad \text{, model form with approximation}$$

where r, f and P are independent variables and λ_b, A, B, a, b, c and d are constants. All factors are clearly defined in Section 4.3. r is a ratio which can vary from 0 to 1. The approximation proved to be very accurate for r values from 0.2 to 1.

Another approach to nonlinear regression is to transform the assumed equation form such that the right hand side of the equation (independent variables and coefficients) is linear. The resulting left hand side of the equation is treated as the dependent variable. This approach does not strictly adhere to the theoretical requirements necessary for application of stepwise multiple linear regression analysis. However, this is often done in reliability modeling efforts and errors caused by this transformation are minimal if applied carefully. An example would be normalizing the failure rate for environment before applying regression. Another example is the rotary switch failure rate prediction model which is given by the following equation:

$$\lambda_p = (\lambda_1 + \lambda_2 N) \pi_E \pi_{cyc} \pi_L$$

where N is an independent variable, λ_p is the dependent variable, λ_1 and λ_2 are constants and π_E, π_{cyc} and π_L are modifying factors which were assumed correct for all types of rotary switches. In order to apply regression analysis so that λ_1 and λ_2 can be determined, the equation is transformed (or normalized) to the following form,

$$\lambda_p/(\pi_E\ \pi_{cyc}\ \pi_L) = \lambda_1 + \lambda_2 N$$

If the entire left hand side of this equation is treated as the dependent variable, then the equation becomes linear and regression can be applied.

F Ratio and Critical F. The F Ratio and Critical F are statistical parameters which are used in conjunction with regression analysis to determine significance of independent variables. The Critical F value is the value from the F table (given in Reference 1) corresponding to the degrees of freedom of the model (equal to the number of data points minus the number of b_i coefficients minus one). This number may be used to test the significance of each variable as it is considered for addition to or deletion from the model. The F ratio value for a regression is the quotient of the mean square due to regression and the mean square due to residual variation. If the F Ratio value for any independent variable is greater than the critical F value, then it is considered a significant factor influencing failure rate and is included in the regression analysis model.

Standard Error of Estimate. The standard error of estimate gives an indication of the confidence of an individual b_i coefficient determined from a regression analysis. The standard error is equal to the square root of the residual mean square (the estimate of the variance about the regression). Upper and lower confidence limits of the regression coefficients can be determined from the standard error and are given for a predetermined confidence (α) by,

$$b_i \pm t_{n-2}\ (S.E.)$$

where

b_i = regression coefficient

t_{n-2} = 1 - ½ α percentage point of a t - distribution with n-2 degrees of freedom

n = number of observations

S.E. = standard error of estimate

When the assumed failure rate model form is a multiplicative model, the upper and lower confidence limit values are not exact but are approximate due to the transformation. Values for the t - distribution are given in Reference 1.

Multiple Coefficient of Determination. The multiple coefficient of determination is equal to the ratio of the sum of squares of the variance explained by the regression to the sum of the squares of the variance of the observed data. The correlation coefficient is often used as a means to select the optimal form of a failure rate prediction model (i.e. linear, exponential). The coefficient ranges from 0 to 1.0. A coefficient value of 1.0 indicates a perfect fit between the model and observed data.

The Correlation Coefficient. The correlation coefficient is a measure of the relation between any two variables. It varies between -1 and 1 (from perfect negative to perfect positive correlation).

Chi-Squared Goodness of Fit Test. The chi-squared goodness of fit test compares observed data to expected values to determine whether the data is representative of the hypothesized distribution. The chi-squared statistic is given by the following equation.

$$\chi^2 = \Sigma \frac{(o-e)^2}{e}$$

where

χ^2 = chi-squared value
o = observed value
e = predicted value

The chi-squared statistic indicates whether the observed events differ from predicted values at a set level of significance for a given degrees of

freedom. Relatively lower chi-squared values indicate a better fit between observed data and predicted values. Chi-squared tables are given in Reference 2.

Chi-squared Confidence Intervals. The chi-squared statistic is used to identify a confidence interval around the failure rate point estimate for an exponentially distributed failure rate. Different samples yield different intervals; some of these intervals will contain the true failure rate point estimate and some will not. It is possible to define a 90% interval such that 90% of all possible intervals (of which ours is just one) will contain the true failure rate point estimate. Assumptions concerning data censoring are made in order to calculate the confidence interval values. These values are calculated as follows:

$$\text{Lower Confidence Limit} = \frac{\chi^2\,(1-\alpha,\ 2r)}{2T}$$

$$\text{Point estimate} = \frac{r}{T}$$

$$\text{Upper Confidence Limit} = \frac{\chi^2\,(1-\alpha,\ 2r+2)}{2T}$$

where

r = numer of failures
T = total part hours
$\chi^2(\alpha)$ = Chi-squared value corresponding to a particular confidence level and degrees of freedom (obtained from Chi-square tables, given in Reference 2)

Kolmogorov-Smirnov Goodness of Fit Test. This test performs essentially the same function as the chi-squared test. It is also a non-parametric test which indicates the goodness of fit by analyzing the maximum difference between observed and predicted values for a theoretical cumulative distribution. If the maximum difference is larger than a preselected critical value for a given level of significance, then the observed events

would not appear to follow the assumed theoretical distribution. The Kolmogorov-Smirnov test is generally used when testing the goodness of fit of a Weibull distribution. A more thorough description and K-S critical value tables are given in reference 2.

Homogeneity Test for Merging Data. A computerized program developed by IITRI was utilized to determine whether failure rate data from diverse sources can be merged. This method is presented in detail in Reference 3. A brief description of this test is presented in this section.

Given data of the form,

r_1 failures in time t_1
r_2 failures in time t_2
etc.

mean time between failure (MTBF) can be computed for each data record and an observed histogram of frequency of occurence vs. MTBF can be determined. The computerized program then uses Monte Carlo simulation to hypothesize a theoretical distribution of MTBF. If all data records are from the same underlying distribution, then the observed and simulated distributions should be in agreement. If the simulated deviates significantly from the observed distribution, then some nonhomogeneity is indicated. The Kolmogorov-Smirnov goodness of fit test is used as the relative measure of whether the observed and simulated distributions are in agreement and the data can be merged. Several reasons for failure rate data not merging are the existence of outliers which can be natural or due to poor data collection practices, or that the data records are not similar in regard to all significant variables effecting failure rate.

The statistical techniques described in this section represent useful tools applicable to reliability modeling efforts. It must be emphasized, however, that all reliability prediction models derived in this study are

based on a sound theoretical basis. The statistical techniques are most useful as a complement to engineering analyses and not as a substitute.

3.2 Data Deficiencies and Data Quality Control

Reliability modeling of electronic or electromechanical components ideally requires a large database of failure rate data available for analysis. The part types considered in this study effort can be classified as low population or low usage parts. Therefore, development of failure rate databases which are both plentiful and accurate, is difficult, if not impossible. This section presents a brief overview of inherent problems with available data and data quality control measures implemented to insure accurate failure rate prediction models.

Available sources of failure rate data are generally either life test data supplied from part manufacturers or equipment level field experience data. Each type of data has several inherent difficulties.

Life test data generally are of a high statistical quality because there is very little uncertainty with regard to recorded failures, number of parts on test, test time, operating conditions and environmental conditions. However, caution must be applied when using this type of data for reliability modeling efforts. Often the life test conditions are at an elevated temperature or voltage to accelerate the frequency of observed failures. Extrapolation of failure rates obtained at the accelerated conditions to more normal operating conditions may introduce error, if extrapolation is possible at all. Another problem associated with life test data obtained from part manufacturers is one of validity. The majority of part manufacturers are unquestionably honest. However, the question arises as to whether the data which is supplied is representative of all life testing performed.

Several measures were implemented to minimize the detrimental effects of using life test data. First, for part types where field experience data was

available, life test data was only used to complement field experience data. Second, only life test data with operating and temperature conditions which are typical of a ground, benign environment were used in regression analyses in conjunction with field experience data. The proposed failure rate prediction model for semiconductor lasers was the only model presented in this report which was based primarily on life test data.

Field experience data are the more desirable type of data since they represent what actually occurred in the field and this is what the proposed model attempts to predict. The inherent difficulties with field experience data are related to the accuracy with which a failure can be defined, the precision with which the number of part hours can be measured, and the ability to determine the stresses applied to a part.

A problem associated with all sources of field experience data is that individual times to failure can not be determined. Data is available in the form of R failures observed in T part hours. The part hours represent a cumulative count of part hours from individual components. The result of this data deficiency is that the exponential hazard rate function must be applied to all part types. For most electronic parts it has been documented that this assumption does not introduce significant error. For electromechanical parts and other part types where degradation failure mechanisms are significant, the constant failure rate calculated by dividing the observed failures by the recorded part hours represents the random failure rate plus an average degradation failure rate contribution.

The best sources of field experience data are from military systems where the number of observed failures and equipment operating hours are precisely recorded because of contractual agreements. Examples of government contracts which require monitoring of failures and part hours are Reliability Improvement Warrenty (RIW) and Life-Cycle Cost (LCC) contracts. Specific military equipments of this type which were utilized in this study effort are the AN/ARN-118 TACAN radio set, the AN/UYK-7 Navy computer and

the AN/ARC-164 radio set. Unfortunately there are relatively few military equipments of this type.

A more plentiful source of failure rate data for fielded military equipments are maintenance data systems maintained by the different branches of the armed forces. The largest of these are the AFM66-1 system maintained by the U.S. Air Force, the 3M system maintained by the U.S. Navy and the Sample Data Collection system maintained by the U.S. Army, TSARCOM. These systems are designed to provide equipment-level statistics such as availability and equipment mean time between failures. Some also provide information on failed components in order to assist in spares provisioning and logistics support. None of these systems is intended to track reliability to the piece-part level. It has been found, however, that this can be done with some degree of accuracy by using the failure records from one of the maintenance data systems.

There are several major problems associated with using one of the maintenance data systems as a source of part level failure rate data. The major problem is that the data provides the analyst with the number of part replacements and not the number of part failures. It is very difficult to separate true failures from part replacements which were secondary failures or which were due to operator error, maintenance error or other factors. Several measures can be taken to minimize the difference between "replacements" and "failures". First, data should only be collected on part types where the ratio of replacement rate to failure rate is known to be low. Maintenence technicians often replace many board mounted components such as resistors before finding the actual failed component. Second, caution should be applied when collecting data on part types which are easily replaced and the replacement possibly not recorded. Parts of this type are incandescent lamps and fuses. Third, other codes included in the maintenance data summaries such as "action taken" code, "when discovered" code, "type maintenance" code and "how malfunctioned" code must be analyzed. Failures which occur during periods of nonoperation, or part replacements which are due to operator or maintenance error can often be identified by analyzing

these codes. The U.S. Army Sample Data Collection system maintained by TSARCOM, St. Louis, MO includes a chargeability code to denote whether part replacements are true failures for the ground transportable generator sets which they collect data on. This is an encouraging development and if implemented on a broad scale, it would increase the accuracy of data collected from maintenance data collection systems.

Field failure experience data samples for most electronic and electromechanical parts are necessarily restricted because the average mean time to failure (approximately 10^5 to 10^7 part hours) is, in many cases, much longer than the technology has been available. However good the failure rate data, it can only cover the first few percentiles of the probability density function. One result of these relatively high mean time to failures for most part types is the presence of data records with zero observed failures.

For "zero failure" data records, the standard method of dividing the number of observed failures by the part hours results in a constant failure rate value of zero. This value is intuitively unsatisfactory. Zero observed failures can be a result of a very low intrinsic part failure rate, but it can also be a result of insufficient collected part hours. Any potential data record will exhibit zero failures if the data collection time period is short enough. To compute a more realistic estimate of failure rate for "zero failure" data records, an upper 60% confidence limit is used. It can be said with a 60% probability that the actual part failure rate is within the range of zero and the upper 60% confidence limit. This method of failure rate estimation is unprecise and regression analysis should be avoided when a large percentage of the data points are "zero failure" point estimates. Numerically, estimating a failure rate by assuming it is equal to the 60% upper confidence limit is equivalent to assuming 0.9 failures.

When it is necessary to include failure rate estimates without observed failures in a regression analysis, caution should be applied. For similar part types operated in similar environmental conditions, the upper limit failure rate values should only be used when the failure rate estimate is

relatively low compared to failures rates computed from data entries with observed failures. In the case where an upper 60% confidence limit is higher than failure rate estimates from data entries with observed failures, then the "zero failure" data entry should not be considered in the analysis. In these cases it can be assumed that insufficient part hours were recorded to expect an observed failure, and not that the intrinsic part failure rate for the "zero failure" data entry was higher than the failure rates for the data entries with failures.

To determine which "zero failure" data entries include sufficient part hours to include in the regression analysis, a preliminary regression analysis should be preformed using only failure rates computed with observed failures. All upper 60% confidence limit failure rate estimates which are both higher than the preliminary regression solution estimate and higher than failure rate estimates for similar part types in similar environment conditions, should not be included in the analysis.

Reliability modeling efforts require the analysis of empirical data and therefore it is essential not only that data be collected, but that the collected data be of a high quality. Every attempt was made in this study effort to insure that all collected data was both accurate and representative of the part type being studied.

3.3 Environmental Factor Evaluation and Derivation

The quantity of application environment categories included in MIL-HDBK-217 increased from nine categories in MIL-HDBK-217B (September 1974) to eleven categories in MIL-HDBK-217C (April 1979). The next revision of MIL-HDBK-217 will include 26 environment category options because of the conclusions presented in References 4 and 5. This relatively high number of environmental factor options increases reliability prediction accuracy but presents a major problem to the reliability modeling analyst. Most of the part types included in this study effort are low population or low usage parts. It is difficult to obtain large amounts of data for these part types.

Field failure rate data can generally be obtained for these low population parts in approximately five or less environmental categories because of the data limitations. Therefore, derivation of a complete series of environmental factors is impossible by the desired data analysis technique which includes analysis of data in each of the 26 environment category options. This section presents the alternate measures which were utilized to develop environmental factors for the part types considered in this study.

The initial approach utilized for part types which are currently included in MIL-HDBK-217 was to use the available data to determine whether the existing environmental factors accurately represent the combined effects of environmental stresses. This, of course, can only be attempted for device failure rate prediction models which include an environmental factor. Point estimate environmental factor values and confidence intervals around the point estimate value were calculated for each environment category where data is available. If each of the existing MIL-HDBK-217D environmental factors, for environments with failure rate data, falls within the confidence interval calculated from the data, then it can be assumed that the entire series of 26 environmental factors can be applied to the particular part type in question. This was the approach taken for cathode ray tubes and magnetrons.

One approach which was taken for part types either not included in MIL-HDBK-217D or included in MIL-HDBK-217D but without environmental factors, was to make assumptions based on theoretical physics of failure information. If a part type which is included in MIL-HDBK-217D has construction similarities and similar anticipated failure modes and mechanisms, then the environmental factors for the analogous part type were analyzed with the available data to determine if they were applicable. If the available failure rate data did not identify discrepancies between the data and the environmental factors under consideration, then the series of environmental factors were applied to the part type in question. This approach was taken for vidicons, helium-cadmium lasers, semiconductor lasers, circuit breakers, I.C. sockets and surface acoustic wave devices.

Several of the part types included in this study effort are hybrid parts composed of discrete components soldered in place on a printed wiring board and packaged in a single housing. Assembly level environmental factors can be computed for these part types if the internal piece part composition is known on a representative sample. A complete series of environmental factors can be computed by using the following equation if each series of environmental factors for the internal parts is normalized to a ground, benign factor equal to one:

$$\pi_{E,j} = \sum_{i=1}^{n} (\lambda_i \ \pi_{E,ij}) / \sum_{i=1}^{n} (\lambda_i)$$

where

$\pi_{E,j}$ = assembly level environmental factor for the j^{th} environment

λ_i = predicted failure rate in the ground benign environment for the i^{th} component

$\pi_{E,ij}$ = environmental factor for the i^{th} component in the j^{th} environment

This equation can be applied if one or more series of environmental factors is not normalized to a ground, benign factor equal to one by dividing each factor ($\pi_{E,ij}$) by the ground, benign factor and then multiplying the base failure rate by the same value. Parts composed of discrete components are available in various compositions for an identical part function. Therefore, proper application of this environmental factor computation method should include calculation of environmental factors for a variety of parts, and an average environmental factor value proposed for each environment. Available failure rate data can then be used to either verify or disprove the calculated values. This approach was utilized for solid state relays and time delay relays.

For part types where none of the previously described approaches were applicable or where application of one of the previously described approaches was unsuccessful, an alternate environmental factor derivation

process was developed. The alternate approach was based on the assumption that an environmental factor relation can be determined where environmental factor is a function of the "environmental stress ratios" obtained from Reference 5 and presented in Table 3.3-1. The environmental stress ratio is a relative index of combined environmental stress severity. The numerical environmental stress ratio values were determined by Martin Marietta Corporation, Orlando FL based on a survey of reliability experts. The survey results provide a possible ranking of environmental factors to be applied in cases where only limited data resources are available. The survey results also provide a quantitative measure of the relative differences between expected failure rate for different environments. To determine absolute (as compared to relative) numerical environmental factor values, field failure rate data are required from a minimum of four different environment categories. The methodology to be described in the following paragraph can be applied when data are available from two or three environments. However, without data from a minimum of four environments, biased data in an individual environment category can result in an environmental factor relation which is essentially nonsense.

The numerical failure rate data from the different environment categories should be similar in regard to all significant failure rate model parameters except for environment. If there are apparent differences other than environment, then the data should be normalized to compensate for the apparent differences. Thus, the numerical differences between the data points are primarily a function of the effect of environmental stress and statistical noise. A regression analysis is then preformed where the environmental stress ratio is the independent variable and the normalized failure rate is the dependent variable. By applying different transformations on the dependent and independent variable, the environmental factor relation can be changed to several general forms. Three examples of environmental factor relation form are given below:

1) $\lambda_n = K\,\pi_E = AS + B$
2) $\lambda_n = K\,\pi_E = A(S)^B$
3) $\lambda_n = K\,\pi_E = A\,\exp(BS)$

where

λ_n = predicted normalized failure rate

K = normalization constant

π_E = environmental factor

S = environmental stress ratio

A,B = regression contants

TABLE 3.3-1: ENVIRONMENTAL STRESS RATIOS

Environment	Abbreviation	Rank	Environmental Stress Ratio
ground, benign	GB	1	1.0
ground, fixed	GF	3	2.7
ground, mobile	GM	7	11.5
manpack	MP	8	12.5
naval, sheltered	NS	5	7.3
naval, unsheltered	NU	10	16.8
naval, undersea, unsheltered	NUU	14	20.6
naval, benign, submarine	NSB	4	6.0
naval, hydrofoil	NH	12	19.2
airborne, inhabited, transport (1)	AIT	6	10.2
airborne, inhabited, fighter (2)	AIF	13	19.5
airborne, uninhabited, transport (1)	AUT	15	23.1
airborne, uninhabited, fighter (2)	AUF	17	33.5
airborne, rotary wing	ARW	16	27.6
missile, launch	ML	19	42.7
cannon, launch	CL	20	720.6
undersea, launch	USL	18	37.1
missile, free flight	MFF	9	12.6
airbreathing missile, flight	MFA	11	17.6
space, flight	SF	2	2.1

Notes: (1) includes bomber and cargo aircrafts
(2) includes attack, trainer and fighter aircrafts

The correlation coefficient is used as a measure of relative fit between the regression solutions and the normalized failure rates.

The results of this environmental factor derivation process can be used in two basic ways. In the instance where data are available from relatively few environment categories, but the data are of high quality, the environmental factor derivation process can be used to determine

environmental factors for only those environment categories without data. In the instances where data are available from more environment categories, but are of questionable quality, then the environmental factor derivation process can be used to derive the entire set of environmental factors. In those instances, it can be assumed that the observed environmental factors which are too high or too low cancel each other out, and therefore, the regression solution represents the best estimates for environmental factor.

The environmental factor derivation process was used to derive the environmental factors for filters, meters, fuses, crystals and incandescent lamps. This process has two major deficiencies. First, the numerical rank of environment factors derived by this method are the same for all part types. In practice, the rankings of environmental factors are similar for most part types, but not identical. The second deficiency is that the environmental stress ratios were determined before the release of Reference 4. Reference 4 recommended that the four original avionic environmental factors be replaced by ten factors. Environmental stress ratios given in Reference 5 are only available for four avionic environments (airborne inhabited fighter, airborne inhabited transport, airborne uninhabited fighter, airborne uninhabited transport). Therefore, each series of environmental factors derived by this method proposes fixed inhabited and uninhabited values for the original fighter (attack, trainer and fighter) and transport (cargo and bomber) environment categories.

In conclusion, environmental factors were determined for each part type considered in this study except neon lamps. Table 3.3-2 presents a summary showing method of environmental factor development versus part type. Each section of this report pertaining to model development includes a discussion of the method used to determine the applicable environmental factors.

3.4 References

1. Draper, N.R. and H. Smith, Applied Regression Analysis, Wiley, 1966.

TABLE 3.3-2: ENVIRONMENTAL FACTOR DEVELOPMENT

Part Type	Verify Existing Factors	Assume Factors of Similar Part	Piece Part Prediction Method	Environmental Factor Derivation Process
Magnetrons	X			
Vidicons		X		
CRTs	X			
He-Cd lasers		X		
Semiconductor lasers		X		
Filters				X
Solid State Relays			X	
Time Delay Relays			X	
Circuit Breakers		X		
I.C. Sockets		X		
Thumbwheel Switches		X		
Meters				X
Fuses				X
Crystals				X
Incandescent Lamps				X
SAWs		X		

2. Siegel, S., Non-Parametric Statistics for the Behavioral Sciences, McGraw-Hill, 1955.

3. Dey, K.A., Statistical Analysis of Noisy and Incomplete Failure Data, 1982 Proceedings, Annual Reliability and Maintainability Symposium.

4. Edwards, E., S. Flint and J. Steinkirchner, Avionic Environmental Factors for MIL-HDBK-217, Final Technical Report, RADC-TR-81-374, January, 1982.

5. Kremp, B.F. and E.W. Kimball, Revision of Environmental Factors for MIL-HDBK-217B, Final Technical Report, RADC-TR-80-299, September, 1980.

4.0 MAGNETRONS

4.1 Device Description

A magnetron is in effect a diode with the input electrodes being a cathode and an anode. The high frequency is usually taken from a magnetron by means of either a coaxial line or a waveguide. There have also been magnetrons that employed special radiators to deflect the high frequency energy. The magnetron has the advantage over other microwave tubes in that it is relatively simple to operate and has relatively low internal resistance. Its primary disadvantage is the extent to which it can be electronically tuned. Magnetrons are available which can be operated under either CW or pulsed conditions. Some tubes are small enough to be held in the hand while others are so heavy they must be picked up by mechanical means. The operating voltage for the tubes range from a few hundred volts to many tens of thousands of volts. Magnetrons may have the magnetic source attached to the tube to form a complete unit or the magnet may be separate.

Pulsed magnetrons have been developed covering frequency ranges from a few hundred MHz to 100 GHz. Peak power from a few KW to several megawatts have been obtained with typical efficiencies of 30 - 40%. Continuous wave magnetrons have also been developed with power levels of a few hundred watts in tunable tubes at an efficiency of 30%. Pulsed magnetrons are used primarily in radar applications as sources of peak power. Pulsed modulation is obtained by applying a negative rectangular voltage pulse to the cathode with the anode at ground potential.

Magnetrons may be either fixed frequency, mechanically tunable or electrically tunable. Mechanical tuning of conventional magnetrons can be accomplished by moving capacitive tuners near the anode straps or capacitive regions of the quarter wave resonators. Tuner motion is produced by a mechanical connection through flexible bellows in the vacuum wall. Voltage tunable magnetrons use a circular-format, re-entrant stream injected beam which interacts with a standing wave on a low Q resonant structure.

Pulsed magnetrons are available in both conventional and coaxial designs. Coaxial magnetrons differ from conventional magnetrons in that they have an internal stabilizing cavity. The stabilizing cavity greatly improves frequency stability. The coaxial design also includes higher efficiency, improved r-f output spectrum and longer life as its attributes.

4.2 Failure Modes and Mechanisms

A magnetron tends to react to total incident energy, and to some degree is affected by variations in heat, radiation and each power supply as if they were signals. Similarly, variations in external electric and magnetic fields may affect performance. Therefore, application environment has a significant effect on magnetron performance. Proper magnetron selection for a particular application environment minimizes the effects of environmental stress.

The reason for the envelope and seals is to provide electrical and magnetic insulation and protect the electron ballistics by keeping the vacuum within the tube constant. Loss of vacuum may occur due to deterioration of a seal or a puncture or crack in the envelope. The deterioration of a seal and the subsequent loss of vacuum is a function of the seal type, length of the seal, thermal cycling, ambient temperature and number of pins in the connector. The tube envelope, the seal, the filament and in some cases, the cathode may be damaged by shock and/or vibration.

A partial loss of seal will result in a contaminated environment which may poison the cathode or cause the filament to burn-up and which may result in either tube degradation or catastrophic failure. The cathode must be capable of carrying high current densities, especially in pulsed operation, and be able to withstand considerable bombardment by electrons. An emissive coating is required which will quickly recover in the event of poisoning and which is also highly conductive, electrically and thermally; otherwise the potential difference across the emissive coating may result in breakdown through the coating. Good thermal conductivity is necessary to prevent the

surface of the cathode from becoming overheated which leads to either melting or deterioration. The factors that influence cathode life are cathode bombardment which may be accelerated by mismatches in output coupling and cathode temperature.

The filament provides thermal energy sufficient to excite the electrons in the cathode to a state where some of the electrons obtain enough energy to escape. The primary failure mode of the filament is an open and its occurence is a function of temperature cycling, oxidation, shock, vibration, applied power and method of applying power.

The magnetic circuit may be an integral part of the tube or it may be a separate device. In either case, the failure or degradation of the magnetic circuit may result in catastrophic failure or degradation in tube operation. For example, if the magnetic field strength is too low the magnetron will oscillate in another mode than the π mode, or the efficiency will be low. If the field strength is too high, the appropriate anode voltage will also be too high and there will be a risk of anode flashover.

4.3 Magnetron Failure Rate Prediction Model

This section presents the proposed failure rate prediction model for magnetrons. The proposed model is:

$$\lambda_p = \lambda_b \, \pi_u \, \pi_E \, \pi_C$$

where

λ_p = magnetron failure rate (failures/10^6 filament hours)

π_u = utilization factor (see Table 4.3-1)

π_E = environmental factor (see Table 4.3-2)

π_C = construction factor
= 1, CW magnetrons (rated power < 5 kw)
= 1, coaxial pulsed magnetrons
= 5.4, conventional pulsed magnetrons

λ_b = base failure rate (failures/10^6 filament hours)
= 18, CW magnetrons (rated power < 5 kw)
= 19 $(f)^{0.73}$ $(P)^{0.20}$, pulsed magnetrons

where

f = frequency (GHz)
P = rated peak power (Mw)

TABLE 4.3-1: UTILIZATION FACTOR

Utilization (radiate hrs./filament hrs.)	π_u
0.0	0.44
0.1	0.50
0.2	0.55
0.3	0.61
0.4	0.66
0.5	0.72
0.6	0.78
0.7	0.83
0.8	0.89
0.9	0.94
1.0	1.0

$\pi_u = 0.44 + 0.56\ (R)$, R = radiate hrs./filament hrs.

TABLE 4.3-2: ENVIRONMENTAL FACTOR

Environment	π_E	Environment	π_E
G_B	1.0	A_{IA}	4.0
G_F	2.0	A_{IF}	20
G_M	4.0	A_{UC}	13
M_P	36	A_{UT}	16
N_{SB}	13	A_{UB}	19
N_S	13	A_{UA}	5.0
N_U	20	A_{UF}	30
N_H	56	S_F	1.0
N_{UU}	60	M_{FF}	36
A_{RW}	80	M_{FA}	50
A_{IC}	11	U_{SL}	106
A_{IT}	13	M_L	160
A_{IB}	15	C_L	2000

4.4 Failure Rate Model Development

The approach utilized for model development of magnetrons was to identify significant variables by analysis of magnetron failure rate data. The model parameters were quantified with the same data. At the conclusion of each step, the results were given a thorough theoretical analysis. The magnetron failure rate data collected in support of this study is presented in Table 4.4-1. Life test data supplied by magnetron manufacturers and field experience data received from Sacramento ALC and summarized by IITRI comprised the majority of all collected data.

Application and construction variables were identified for magnetrons and are presented in Table 4.4-2. These variables represent possible failure rate model parameters whose values were determined whenever possible for all collected data.

TABLE 4.4-1 MAGNETRON FAILURE RATE DATA

ENTRY NO.	TYPE (1)	FREQUENCY (GHz)	PEAK POWER LEVEL (Kw)	TUNING (2)	COOLING (3)	R (4)	ENVIRONMENT	PART NO	FAILURES	PART HOURS (5)
1	C.W	4.31	< 1	Elec.	None	1.0	GB	6177A	2	84,000
2 (6)	Conv.	8.83	40	None	F.A.	1.0	GB	2J50	0	3,500
3 (6)	"	9.05	40	Mech.	"	1.0	GB	2J51A	0	3,500
4	"	9.35	40	None	"	1.0	GB	2J55	1	5,200
5 (6)	"	3.05	20	"	"	1.0	GB	2J70A	0	4,000
6	"	3.05	50	"	"	1.0	GB	2J70B	3	17,900
7 (6)	"	6.43	180	"	"	1.0	GB	4J58	0	1,000
8 (6)	"	1.29	400	Mech.	"	1.0	GB	5J26	0	1,500
9 (6)	"	2.80	800	"	"	1.0	GB	5586	0	1,200
10	"	3.30	1000	"	"	1.0	GB	5795	2	9,400
11 (6)	"	9.32	250	None	"	1.0	GB	6002	0	1,000
12	"	8.80	1	Mech.	"	1.0	GB	6248	4	29,600
13	"	5.64	175	Mech.	"	1.0	GB	6344	2	23,000
14	"	2.81	4500	None	Liquid	1.0	GB	6410A	3	6,200
15 (6)	"	1.30	1000	Mech.	F.A.	1.0	GB	6517	0	1,500
16	"	9.08	40	"	"	1.0	GB	7256	4	46,200
17	"	2.78	3500	"	Liquid	1.0	GB	7529	2	3,600
18	C.W.	(7)	< 1	(7)	None	1.0	GF	(7)	5	157,000
19	Conv.	2.80	800	Mech.	F.A.	0.85	GF	5586	19	70,000
20	"	2.80	800	"	"	0.95	GF	5586	131	250,800
21	"	2.81	4500	None	Liquid	0.09	GF	6410A	2	6,000
22	"	2.81	4500	"	"	0.14	GF	6410A	3	11,470
23	"	2.81	4500	"	"	0.25	GF	6410A	3	20,900
24	"	2.81	4500	"	"	0.37	GF	6410A	4	8,120
25	"	2.81	4500	"	"	0.46	GF	6410A	6	16,330
26	"	2.81	4500	"	"	0.53	GF	6410A	4	8,650
27	"	2.81	4500	"	"	0.65	GF	6410A	20	76,000
28	"	2.81	4500	"	"	0.75	GF	6410A	25	86,000
29	"	2.81	4500	"	"	0.85	GF	6410A	72	210,000
30	"	2.81	4500	"	"	0.95	GF	6410A	273	810,000
31	"	2.80	800	None	F.A.	0.85	GF	8798	10	30,440
32	"	2.80	800	"	"	0.95	GF	8798	91	180,000
33	"	2.78	3500	Mech.	Liquid	0.08	GF	QK-327A	2	19,000
34	"	2.78	3500	"	"	0.19	GF	QK-327A	1	2,630
35	"	2.78	3500	"	"	0.27	GF	QK-327A	4	14,450
36	"	2.78	3500	"	"	0.37	GF	QK-327A	8	16,900
37	"	2.78	3500	"	"	0.47	GF	QK-327A	6	13,680
38	"	2.78	3500	"	"	0.54	GF	QK-327A	6	15,430
39	"	2.78	3500	"	"	0.65	GF	QK-327A	14	22,000
40	"	2.78	3500	"	"	0.75	GF	QK-327A	15	31,000
41	"	2.78	3500	"	"	0.85	GF	QK-327A	90	280,000
42	"	2.78	3500	"	"	0.95	GF	QK-327A	446	1,150,000
43	"	2.81	4500	None	"	0.07	GF	QK-338A	1	3,430
44	"	2.81	4500	"	"	0.17	GF	QK-338A	6	16,700
45	"	2.81	4500	"	"	0.29	GF	QK-338A	10	31,800
46	"	2.81	4500	"	"	0.32	GF	QK-338A	3	9,150
47	"	2.81	4500	"	"	0.45	GF	QK-338A	3	13,810
48	"	2.81	4500	"	"	0.55	GF	QK-338A	13	26,000
49	"	2.81	4500	"	"	0.67	GF	QK-338A	6	12,570
50	"	2.81	4500	"	"	0.78	GF	QK-338A	9	28,580
51	"	2.81	4500	"	"	0.85	GF	QK-338A	37	74,000
52	"	2.81	4500	"	"	0.95	GF	QK-338A	95	250,000
53	Coax.	2.80	3000	Mech.	"	0.06	GF	VMS-1143A	1	46,900
54	"	2.80	3000	"	"	0.16	GF	VMS-1143A	2	217,000
55	"	2.80	3000	"	"	0.34	GF	VMS-1143A	1	56,600
56	"	2.80	3000	"	"	0.48	GF	VMS-1143A	1	43,380
57	"	2.80	3000	"	"	0.69	GF	VMS-1143A	3	17,130
58	"	2.80	3000	"	"	0.76	GF	VMS-1143A	1	31,900
59	"	2.80	3000	"	"	0.89	GF	VMS-1143A	5	86,700
60	"	2.80	3000	"	"	0.95	GF	VMS-1143A	21	40,000
61	"	2.80	3000	"	"	0.33	GF	VMS-1143B	1	10,000
62	"	2.80	3000	"	"	0.50	GF	VMS-1143B	1	5,630
63 (6)	"	2.80	3000	"	"	0.67	GF	VMS-1143B	1	1,500
64	"	2.80	3000	"	"	0.89	GF	VMS-1143B	1	64,100
65	"	2.80	3000	"	"	0.97	GF	VMS-1143B	8	73,560
66	Conv.	1.30	1000	"	F.A.	0.22	GM	400615	2	7,010
67	"	1.30	1000	"	"	0.39	GM	400615	7	34,950
68	"	1.30	1000	"	"	0.42	GM	400615	3	10,860
69	"	1.30	1000	"	"	0.55	GM	400615	11	16,920
70	"	1.30	1000	"	"	0.65	GM	400615	25	77,750
71	"	1.30	1000	"	"	0.74	GM	400615	15	52,400
72	"	1.30	1000	"	"	0.86	GM	400615	3	3,470
73	"	1.30	1000	"	"	0.95	GM	400615	6	19,850
74	"	2.80	800	"	"	0.06	GM	5586	2	9,440
75	"	2.80	800	"	"	0.16	GM	5586	5	10,500
76	"	2.80	800	"	"	0.26	GM	5586	10	49,120
77	"	2.80	800	"	"	0.36	GM	5586	33	126,820
78	"	2.80	800	"	"	0.45	GM	5586	75	280,000
79	"	2.80	800	"	"	0.55	GM	5586	50	170,000
80	"	2.80	800	"	"	0.65	GM	5586	28	94,000
81	"	2.80	800	"	"	0.75	GM	5586	25	50,000
82	"	3.30	1000	"	"	0.04	GM	5795	4	37,250
83	"	2.80	800	"	"	0.19	GM	8798	2	11,300
84	"	2.80	800	"	"	0.24	GM	8798	1	3,460
85	"	2.80	800	"	"	0.37	GM	8798	10	49,750
86	"	2.80	800	"	"	0.45	GM	8798	26	110,000
87	"	2.80	800	"	"	0.55	GM	8798	17	61,000
88	"	2.80	800	"	"	0.65	GM	8798	16	55,000
89	"	2.80	800	"	"	0.78	GM	8798	8	26,250

TABLE 4.4-1: MAGNETRON FAILURE RATE DATA (CONT'D)

ENTRY NO.	TYPE (1)	FREQUENCY (GHz)	PEAK POWER LEVEL (Kw)	TUNING (2)	COOLING (3)	R (4)	ENVIRONMENT	PART NO.	FAILURES	PART HOURS (5)
90	Coax.	5.64	1000	Mech.	F.A.	0.04	GM	SFD-313	3	43,300
91	"	5.64	1000	"	"	0.25	GM	SFD-313	1	8,000
92	"	9.05	200	Elec.	"	0.15	GM	SFD-354	1	3,400
93	"	9.05	200	"	"	0.24	GM	SFD-354	3	23,000
94	"	9.05	200	"	"	0.36	GM	SFD-354	1	2,200
95 (6)	"	9.05	200	"	"	0.50	GM	SFD-354	1	1,170
96	"	9.05	200	"	"	0.58	GM	SFD-354	1	6,120
97	"	9.05	200	"	"	0.65	GM	SFD-354	1	3,410
98	"	9.05	200	"	"	0.74	GM	SFD-354	1	4,560
99	"	(8)	1500	None	"	0.06	GM	SFD-369	2	12,730
100	"	(8)	1500	"	"	0.18	GM	SFD-369	2	70,240
101	"	(8)	1500	"	"	0.25	GM	SFD-369	4	66,850
102	"	(8)	1500	"	"	0.36	GM	SFD-369	2	51,620
103	"	(8)	1500	"	"	0.49	GM	SFD-369	5	42,610
104	"	(8)	1500	"	"	0.54	GM	SFD-369	4	25,250
105	"	(8)	1000	"	"	0.19	GM	SFD-385	4	63,680
106	"	(8)	1000	"	"	0.25	GM	SFD-385	6	157,300
107	"	(8)	1000	"	"	0.36	GM	SFD-385	5	28,810
108	"	(8)	1000	"	"	0.46	GM	SFD-385	3	33,020
109	"	(8)	1000	"	"	0.55	GM	SFD-385	3	9,220
TOTALS									1950	6,940,930

NOTES.

(1) C.W. = continuous wave, Conv. = conventional, Coax. = coaxial
(2) Elec.= electrical, Mech. = mechanical
(3) F.A. = forced air
(4) R = radiate hours/filament hours, filament hours = radiate hours + standby hours
(5) filament hours, radiate hours = (R) x (filament hours)
(6) insufficient part hours to introduce into the regression analysis
(7) unknown
(8) operating frequency is classified for SFD-369 and SFD-385 magnetrons

TABLE 4.4-2: MAGNETRON CONSTRUCTION AND APPLICATION VARIABLES

I. Operation Mode
   A. Continous Wave (CW)
   B. Pulsed

II. Type
   A. Conventional
   B. Coaxial

III. Tuning Availability
   A. No Tuning
   B. Mechanical Tuning
   C. Electrical Tuning

IV. Peak Power Level
   A. Rated
   B. Actual

V. Type of Output Port

VI. Magnetic Source Location
   A. Internal
   B. External

VII. Tube Envelope Material

VIII. Tube Dimensions

IX. Heater Voltage Type and Level
   A. Rated Voltage
   B. Actual Voltage

X. Operating Temperature
   A. Rated
   B. Actual

XI. Application Environment

XII. Ratio of Radiate hours to Filament hours

It was the intent of this study effort to analyze the effects of standby operation on failure rate. The raw data for a particular tube type operating in a similar application was merged according to the ratio of radiate operating hours to filament operating hours. Standby operation for a magnetron is the period of time when voltage is applied to the filament but the magnetron is not radiating. Failure rates were calculated for each data entry by dividing the observed failures by the filament hours. It was assumed that a particular magnetron type operating under identical conditions would exhibit a unique radiate and standby failure rate. It was also assumed that the failure rate of magnetrons operating in the radiate mode would be greater than the failure rate in the standby mode and that for applications with intermediate amounts of standby operation the failure rate would be a linear relation between the two extreme cases which are no standby and total standby. Therefore a general magnetron failure rate prediction model is given by,

$$\lambda_p = (AR + B)\ \lambda_b\ \pi_1\ \pi_2\ \ldots$$

where

λ_p = magnetron failure rate (failures/10^6 filament hours)
R = radiate hours/filament hours
A,B = constants
λ_b = base failure rate
π_i = modifying factor(s)

An equation of this form is nonlinear and linear regression analysis can not be directly applied. A brief discussion of nonlinear models is included in Section 3.1. As suggested in Section 3.1, a linear equation form was used to approximate the nonlinear part of the preliminary magnetron failure rate prediction model. The approximation is as follows:

$$a(R)^b \simeq AR + B$$

where a, b, A and B are constants and R is the ratio of radiate to filament hours. This approximation proved to be accurate for R values ranging from 0.2 to 1.0.

Stepwise multiple linear regression analysis was then applied to the pulsed magnetron failure rate data. All data records, except where noted in Table 4.4-1, were entered into the regression analysis. The variables which were introduced into the regression are given in Table 4.4-3.

Three regression analyses were necessary. The initial regression analysis identified frequency, rated peak power, magnetron type, ratio of radiate to filament hours, environment and tuning as significant variables at the 70% confidence level. The results from the initial regression were rejected, however, as being inconsistent with theory. Strict interpertation of the initial results were that fixed frequency and mechanically tunable magnetrons have a similar failure rate and that electrically tunable magnetrons have a failure rate 4.2 times as high. Also the results indicated that magnetrons operating in a ground, benign and ground, fixed environments have a similar failure rate and that magnetrons operating in a ground, mobile environment have a failure rate 1.7 times as high. Both of these results seemed to be inconsistent with theory. Mechanically and electrically tunable magnetrons would both be expected to exhibit a higher observed failure rate than fixed frequency magnetrons. However a factor of 4.2 is unreasonable. Tunable magnetrons are similar to fixed frequency magnetrons except with the addition of electrical or mechanical components. The anticipated failure rates of the additional components are small in comparison to the tube failure rate. Inspection of the raw data given in Table 4.4-1 reveals that the only data entries with electrical tuning (data entries 92-98) also operated in the ground, mobile environment. The relatively higher failure rates computed for data entries 92 to 98 were considered to be due to the application environment and not because of the electrical tuning components. The reason for this apparent shortcoming in the regression analysis is that a complete database for magnetrons was not

TABLE 4.4-3: MAGNETRON VARIABLE IDENTIFICATION

Parameter	Variable(s)	Factor
frequency	$X_1 = \ln(f)$	$(f)^{b1}$
rated peak power	$X_2 = \ln(P)$	$(P)^{b2}$
type	X_3	
coaxial		$\exp(b_3 X_3)$
conventional		1.0
		$\exp(b_3)$
tuning	X_4, X_5	
fixed frequency		$\exp(b_4 X_4 + b_5 X_5)$
mechanical		1.0
electrical		$\exp(b_4)$
		$\exp(b_5)$
environment	X_6, X_7	
GB		$\exp(b_6 X_6 + b_7 X_7)$
GF		1.0
GM		$\exp(b_6)$
		$\exp(b_7)$
output port	X_8	
coaxial		$\exp(b_8 X_8)$
waveguide		1.0
		$\exp(b_8)$
cooling	X_9	
liquid		$\exp(b_9 X_9)$
forced air		1.0
		$\exp(b_9)$
radiate hrs/filament hrs	$X_{10} = \ln(R)$	$(R)^{b10}$

obtained. To be able to evaluate both environment and tuning, data would have to have been available for each tuning option in several different environment categories.

A second regression analysis was preformed without tuning availability as an input variable. The results from this analysis are given in Table 4.4-4 and correspond to the following preliminary failure rate prediction model. Each variable was significant at a 90% confidence level.

$$\lambda_p = 15.5\ (f)^{0.732}\ (P)^{0.204}\ (\exp(1.69X_3))\ (R)^{0.360}\pi_E$$

where

λ_p = magnetron failure rate (failures/10^6 hours)
f = frequency (GHz)
P = rated peak power (Mw)
X_3 = 0, coaxial magnetrons
= 1, conventional magnetrons
R = radiate hours/filament hours
π_E = environmental factor
= 1.0, GB
= 1.9, GF
= 3.2, GM

This preliminary model was then modified to resemble existing MIL-HDBK-217D models.

TABLE 4.4-4: RESULTS OF THE REGRESSION ANALYSIS

Variable (Xi)	Coefficient (bi)	Standard Error	F-Ratio
X_1	0.7318	0.2123	11.88
X_2	0.2039	0.938	4.73
X_3	1.6887	0.1701	98.50
X_6	0.6302	0.3273	3.71
X_7	1.1543	0.2876	16.11
X_{10}	0.3602	0.0866	17.66
Constant	2.7406	--	--

The observed relationship between failure rate and ratio of radiate hours to filament hours was designated as the utilization factor. It was considered desirable to transform the approximate utilization factor form ($\pi_u = K(R)^{0.360}$) to the form originally assumed ($\pi_u = AR + B$). The approximate model form was sufficiently accurate for the majority of ratio values ($R > 0.20$). However, low ratio values resulted in approximate utilization factor values approaching zero. Therefore, a utilization factor of the assumed form was deemed necessary. A third regression analysis was performed to obtain numerical estimates for the utilization factor constants. All data entries were normalized for frequency, rated peak power, magnetron type and environment. The normalization function is,

$$\pi_u' = \lambda_o/(15.5(f)^{0.732}(P)^{0.204}\ (\exp(b_3X_3))\pi_E) = AR + B$$

where

λ_o = observed magnetron failure rate

and the results of the regression analysis were,

$$\pi_u' = 0.678\ (R) + 0.533$$

It was desired that the utilization factor be normalized to a value of one for applications where radiate hours equals filament hours. Therefore, the following modification was made to the preliminary magnetron failure rate prediction model.

$$\pi_u' = 0.678\ (R) + 0.533$$

$$\pi_u = 0.825\ \pi_u' = 0.560\ (R) + 0.440$$

$$\lambda_p = (15.5/0.825)\ (f)^{0.732}\ (P)^{0.204}\ (\exp(1.69X_3))\ \pi_u\ \pi_E$$

$$= 18.8\ (f)^{0.732}\ (P)^{0.204}\ (\exp(1.69X_3))\ \pi_u\ \pi_E$$

It was decided to include frequency and rated peak power into an equation for base failure rate. The magnetron base failure rate then becomes,

$$\lambda_b = 18.8\ (f)^{0.732}\ (P)^{0.204}$$

where

λ_b = base failure rate (failures/10^6 hours)

A construction factor (π_C) was defined to account for magnetron type. The equation ($\pi_C = \exp(1.69\ X_3)$) when solved for X_3 = 1 and 0 gives the following construction factors:

conventional magnetron, 5.42
coaxial magnetron, 1.0

Data were collected from three environment categories. The observed environmental factors along with upper and lower confidence limits are given in Table 4.4-5.

TABLE 4.4-5: OBSERVED MAGNETRON ENVIRONMENTAL FACTORS

Environment	L 20%CL	observed π_E	U 80%CL
GB	--	1.0	--
GF	1.42	1.88	2.48
GM	2.49	3.17	4.05

The observed ground, fixed environmental factor and the observed ground, benign environmental factor are consistent with the existing MIL-HDBK-217D electron tube environmental factors. However, the magnitude of the observed environmental factor for the ground mobile environment is significantly lower than the existing MIL-HDBK-217D value. A probable explanation is that proper magnetron selection can minimize the effects of environmental stress.

For other tube types, such as cathode ray tubes, an identical part type can be used in a wide variety of environments. For magnetrons, different part types with similar specifications can be obtained depending on the intended application environment. Therefore proper selection of available magnetrons is essential for minimizing the effects of the environment.

The existing MIL-HDBK-217D electron tube environmental factors cannot be applied to magnetrons without introducing error. However, it is essential that a complete set of environmental factors be developed so that a proposed failure rate prediction model can apply to a maximum number of potential applications. In order to determine a complete set of environmental factors, a review was initiated of previous revisions of MIL-HDBK-217. MIL-HDBK-217B, Notice 2 dated 17 March 1978 expanded the number of magnetron base failure rate options from two to nine. Additionally, this revision of MIL-HDBK-217 included the environmental factors presented in Table 4.4-6. Table 4.4-6 also includes the observed magnetron environmental factors, upper and lower confidence intervals and the MIL-HDBK-217B, Notice 2 factors normalized to a ground, benign value equal to one. Analysis of Table 4.4-6 resulted in the conclusion that these factors can be accurately applied to magnetrons. For application environment options which were not included in MIL-HDBK-217B, Notice 2, the existing MIL-HDBK-217D electron tube factors are proposed except for the naval, submarine environment. The naval, sheltered factor was also applied to the naval, submarine environment so the environmental factor rankings are consistent with MIL-HDBK-217D. Use of these factors should result in slightly pessismistic failure rate calculations.

TABLE 4.4-6: ENVIRONMENTAL FACTOR COMPARISONS

Environment	MIL-HDBK-217B Notice 2 Factors	MIL-HDBK-217B Notice 2 Factors Normalized	Observed Factors L 20%CL	PT EST	U 80%CL
GB	0.5	1.0	--	1.0	--
SF	0.5	1.0	--	--	--
GF	1.0	2.0	1.42	1.88	2.48
AI	6.5	13	--	--	--
NS	6.5	12	--	--	--
GM	2.0	4.0	2.49	3.17	4.05
AU	8.0	16	--	--	--
NU	10	20	--	--	--
ML	80	160	--	--	--

Two data records (data entries 1 and 18) were available for low power continuous wave (CW) magnetrons. It was assumed that one series of environmental factors were applicable to all magnetron types whether pulsed or CW. Therefore, the part hours were normalized for environment and a base failure rate was determined by dividing the sum total of failures by the sum total of normalized part hours. In equation form,

$$\lambda_{b,cw} = \Sigma f/(\Sigma T\ \pi_E)$$
$$= (2 + 5)/((0.084)(1.0) + (0.157)(2.0))$$
$$= 17.6 \text{ failures}/10^6 \text{ hours}$$

where

$\lambda_{b,cw}$ = continuous wave magnetron base failure rate
f = observed failures
T = observed part hours
π_E = environmental factor

This base failure rate only applies to CW magnetrons with a rated peak power less than 5Kw. It was also assumed that the utilization factor derived for pulsed magnetrons would also apply to CW magnetrons. The construction factor (π_C) was set at a value of 1.0.

Computation of the base failure rate for CW magnetrons completes the magnetron failure rate prediction model development. The proposed model represents magnetron failure rate as a function of magnetron type, frequency, rated peak power, environment and amount of standby. The proposed model increases prediction accuracy and extends prediction capabilities, particularly in regard to coaxial and CW magnetrons, and it is recommended that the proposed model be added to MIL-HDBK-217D.

4.5 References

1. Farney, George K., Crossed-Field Tubes, Electronics Engineers' Handbook, Second Edition, Fink, Donald G. and Christiansen, Donald, McGraw-Hill, 1982.

5.0 VIDICONS

5.1 Device Description

The term vidicon is frequently used as a generic term for a photoconductive camera tube. Vidicon is used to describe return beam vidicons, lead oxide vidicons and silicon diode vidicons. In the usual vidicon a homogeneous type of photoconductive layer is employed which will freely accept the mobile photo generated carriers needed to replenish those extracted from the layers. The vidicon has many advantages compared to other types of television tubes. It is relatively small in size, has a simple and rugged structure, is low in cost and does not require critical adjustment in operation. At the same time such tubes can produce high resolution images and a high signal to noise ratio under proper illumination. In addition to their use in black and white and color cameras for television pick ups, vidicons are used with special photoconductors for pick up of images in the infrared, ultraviolet and x-ray parts of the spectrum.

The basic elements of a typical vidicon tube are shown in the cross-sectional diagram in Figure 5.1-1. The photoconductive layer is supported on the glass face plate of the tube envelope. Between the photoconductor and the faceplate a transparent electrode is provided, which acts as the target back plate. In operation, the input image projected on to the photoconductor produces conductivity variations in this layer causing previously established surface charges to leak to the back plate. Upon recharging the photoconductor surface to its equilibrium potential by the reading beam, output voltage variations are produced across the load resistor connected to the back plate. The scanning beam is usually focused and deflected by magnetic coils. Tubes are also designed for operation with electrostatic focusing and deflection, or electrostatic focusing and magnetic deflection. The glass envelope of a typical vidicon is approximately one inch in diameter and six inches in length, although there are vidicons with envelope diameters ranging from approximately one-half to four and one-half inches.

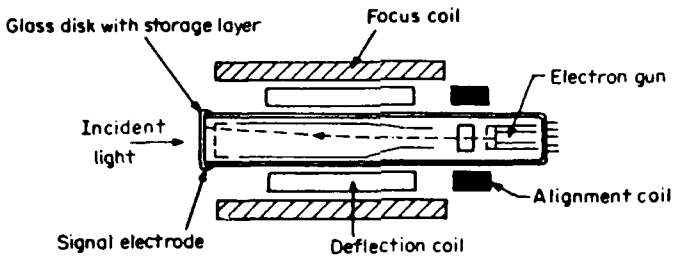

FIGURE 5.1-1: CROSS-SECTIONAL DIAGRAM OF A TYPICAL VIDICON

Prior to writing, the surface of the photoconductive layer is assumed to be at zero potential, having been charged to this equilibrium potential during previous scanning by the reading beam. With a dc voltage of +20V on the back plate, a uniform electric field is established across the photoconductor. During writing, an image of light or other radiation to which the photoconductor is sensitive, is projected on to the photoconductive layer. This generates free carriers. The resulting increased conductivity allows a fraction of the local surface charge to leak to the back plate, causing the surface to shift toward back plate potential. A pattern of potential variations is thus established on the photoconductor surface.

During reading, which is usually simultaneous with writing, the photoconductor is scanned by the primary beam. Since the surface potential of all photoconductors is low with respect to the reading gun cathode potential, the secondary emission ratio is less than unity. Each of the elements is thus shifted back to its equilibrium potential (i.e., the potential of the reading gun cathode). As each element is shifted to ground potential in scanning, a capacitive current is produced through the target

whose magnitude varies in accordance with the charge deposited by the beam. These time varying currents in turn produce a half tone output signal voltage across the load resistor. In normal operation, the scanning of the photoconductor during reading acts to shift the elements down to a potential which is close to the equilibrium (ground) potential. This automatically erases stored information. Ideally this should be accomplished in a single scan. In practice, several scans may be required to fully discharge or erase the target because of the capacitance of the target and velocity spread of the primary beam.

Relatively few target materials have been found which satisfy the requirements imposed in the photoconductive layer by vidicons. To enable charge storage, the dielectric relaxation time or R-C constant in the dark must be considerably longer than frame time. For operation at conventional TV frame rates, a target resistivity of approximately 10^{12} Ω-cm is required. In addition, the response time of the photoconductor to changes in illumination should be approximately a frame time or less to prevent lag or image smear in the case of moving scenes. The choice of photoconductive target material is the construction variable which best characterizes vidicons. The following paragraphs present a brief description of the three photoconductive materials most often used.

The photoconductor target material used in most commercial applications is antimony trisulfide (Sb_2S_3). The material is relatively stable and has spectral sensitivity peaked in the red between 700 - 800 nanometers (nm). However, by evaporating the material in a residual gas atmosphere to form a porous layer, its response can be shifted to 550 nm in the green. This will more closely match the response of the eye. One of the limitations of Sb_2S_3 is its photoconductive decay time. After cutoff of the input light, several TV frame times are required for the photoconductivity to fall to 10%. Because of the long tail of the decay curve, objectionable image smear occurs particularly at low input light levels.

The photoconductive material generally used in military applications is a silicon diode array. Silicon target vidicons offer extremely high sensitivity, low dark current, exceptional resistance to image burn and high resolution capabilities. The spectral response for silicon target vidicons ranges from 380 to 1100 nm. This broad spectral response range extends into the near infrared.

For direct pick up of x-ray images a number of experimental vidicons have been developed. One of the target materials is lead monoxide, (PbO). A major problem associated with PbO targets is a fatigue effect whereby irradiation of the layer with x-rays during application of voltage causes a gradual increase in image persistence. This is also accompanied by a loss in sensitivity and the development of nonuniformities. Such effects are believed to be partially associated with the loss of oxygen from the PbO. For pickup of color images, the input image is separated optically into three color components. In operation, a single reading beam is used and the tube is scanned in the same manner as a conventional vidicon. Output signals are generated simultaneously across the three load resistors corresponding to the three color components of the input image. One of the problems of such tubes is signal lag caused by the relatively high layer capacitance of the target junction. Vidicons with a PbO photoconductive material are often used in applications when a clear, color picture is required.

5.2 Failure Modes and Mechanisms

Vidicons tend to react to total incident energy, and to some degree are affected by variations in heat, light and radiation, and each power supply as if the power supplies were signals. Similarly, variations in external electrical and magnetic fields may affect performance. Therefore, application environment has a significant effect on vidicon performance.

The function of the envelope and seals are to provide electrical insulation and to protect the electron ballistics within the tube by keeping the vacuum within the tube constant. Loss of vacuum may occur due to

deterioration of a seal or microcrack in the tube envelope. The deterioration of a seal and the subsequent loss of vacuum is a function of the seal type, vidicon bulb diameter, exposure to thermal cycling and ambient temperature. A crack in the envelope may occur, especially in the neck area, due to shock and/or vibration stresses. A partial loss of seal will result in a contaminated internal tube environment which may poison the cathode or the photoconductive target and may result in tube degradation or catastrophic failure. Failure of the vidicon cathode accelerated by a contaminated internal tube environment is the dominant failure mode for vidicons.

Another important factor regarding vidicon reliability is that the cathode must be capable of carrying high current densities and be able to withstand considerable bombardment by electrons as well as by ions. An emissive coating is required which will quickly recover in the event of poisoning and is also highly conductive, electrically and thermally. Otherwise, the potential difference across the emissive coating may result in breakdown through the coating. Good thermal conductivity is necessary to prevent the surface of the cathode from overheating, and then either melting or deteriorating.

Exposure to shock or vibration may result in the repositioning of the grids, electrodes and deflection plates. The repositioning of the grids, electrodes and deflection plates may result in either performance degradation or catastrophic failure depending on the magnitude of the repositioning.

The filament provides thermal energy sufficient to excite the electrons in the cathode to a state where some of the electrons obtain enough energy to escape. The primary failure mode of the filament is an open. The frequency of this failure mode is a function of temperature cycling, oxidation, shock, vibration, applied power and method of applied power.

An important problem in vidicons is image lag caused by incomplete discharge or shift of the photoconductive to equilibrium potential in a single scan of the reading beam. This effect tends to be more noticeable at low input levels when the magnitude of the potential pattern established in writing is low. If the image lag phenomenon becomes severe, then the vidicon must be replaced. Image lag is a degradation failure mechanism. To insure adequate discharge of the photoconductive surface in a single scan, the total capacitance of the target should be sufficiently low. Separate consideration also requires that the photoconductive layer have a total capacitance which never exceeds a certain value. This is based upon the fact that sufficient charge must be deposited on the surface by the reading beam to produce an output current substantially greater than the noise currents of the load resister and video amplifier.

In the usual vidicon, the output signal increases linearly with increasing input light. At high signal levels optical overloading occurs. Optical overloading is defined as that illumination for which all of the target plate shows effects that persist long enough for the human eye to detect the persistence. As the intensity of a point in the field of view increases, a level is reached where the output saturates. The output signal no longer increases with input light. With further increase in source intensity, the saturated point on the target material begins to spread into surrounding areas because of lateral current flow in the photoconductive target, internal reflections in the faceplate and flow in the output optics. This phenomenon is known as blooming and is most predominately noticed in vidicons with Sb_2S_3 photoconductive material.

In operation, the target backplate potential is frequently varied to produce optimum sensitivity and image quality. As the backplate voltage is increased, the photocurrent is increased because of a higher electrical field across the photoconductor. However, above a certain voltage the dark current increases rapidly causing objectionable non-uniformities in the picture background and reducing the signal to noise ratio. At low inputs the

operation of vidicons is limited by thermal noise generated by the load resistor and the succeeding amplifier.

The most frequently observed failure modes for vidicons are degradation modes. Therefore it would be anticipated that the instantaneous failure rate function would be increasing in time. Unfortunately, data to support this hypothesis is nonexistent. Therefore, the vidicon failure rate prediction models to be presented in Section 5.3 represent an average failure rate with respect to the anticipated equipment life. Time to failure data for cathode ray tubes (which have certain construction similarities to vidicons) indicate that the constant failure rate assumption does not introduce significant errors.

5.3 Vidicon Failure Rate Prediction Model

This section presents the proposed failure rate prediction model for vidicons. The proposed model only applies to vidicons with antimony trisulfide (Sb_2S_3) or silicon diode array photoconductive materials. The proposed model is:

$$\lambda_p = \lambda_b \times \pi_E$$

where

λ_p = predicted vidicon failure rate in failures/10^6 hours
λ_b = base failure rate
= 51 failures/10^6 hours, Sb_2S_3 vidicons
= 48 failures/10^6 hours, silicon target vidicons
π_E = environmental factor (see Table 5.3-1)

TABLE 5.3-1: ENVIRONMENTAL FACTOR

Environment	π_E	Environment	π_E
G_B	0.5	A_{IA}	2.0
G_F	1.0	A_{IF}	10.0
G_M	9.0	A_{UC}	6.5
M_P	18.0	A_{UT}	8.0
N_{SB}	7.6	A_{UB}	9.5
N_S	7.6	A_{UA}	2.5
N_U	13.0	A_{UF}	15.0
N_H	28.0	S_F	0.5
N_{UU}	30.0	M_{FF}	18.0
A_{RW}	40.0	M_{FA}	25.0
A_{IC}	5.5	U_{SL}	53.0
A_{IT}	6.5	M_L	61.0
A_{IB}	7.5	C_L	1000.0

5.4 Failure Rate Model Development

The approach utilized for model development of vidicons was to assume a model form based on physics of failure information. The model parameters were quantified by analysis of life test data, field experience data and comparisons with devices having similar construction characteristics. The vidicon failure rate data collected in support of this study is presented in Table 5.4-1.

Application and construction variables were identified for vidicons and are presented in Table 5.4-2. The application and construction variables represent possible failure rate model parameters which were determined whenever possible for all collected data. Significant model parameters could not be identified exclusively by data analysis due to the relative scarcity of accurate field experience and life test data. Therefore, based on theoretical analysis of vidicon reliability characteristics it was determined that the application environment and choice of photoconductive

TABLE 5.4-1: VIDICON FAILURE RATE DATA

Entry No.	Photoconductive Material	Tube Diameter	Environment	Quality	Equipment(4)	Failures	Part Hours
1	Silicon Diode	1"	GF	Commercial	AN/GXS-2	291	7,480,000
2	Silicon Diode	(1)	AUA	(1)	AN/AXQ-13	1	13,000
3	Silicon Diode (2)	(1)	AUB	(1)	AN/AAQ-6	164	201,000
4	Sb_2S_3	1"	GB	Commercial	life test	14	400,000
5	Sb_2S_3	2/3"	GB	Commercial	life test	4	300,000
6	Silicon Diode	1/2"	(3)	Commercial	life test	5	148,000
7	(1)	(1)	Dormant	(1)	dormant storage	3	20,590,000
TOTALS						482	29,132,000

NOTES:

(1) Unknown.

(2) Assumed.

(3) Life testing at elevated temperature (ambient temp. = 47^{o} C).

(4) Test data is noted.

TABLE 5.4-2: VIDICON CONSTRUCTION AND APPLICATION VARIABLES

I. Photoconductive Material
   A. Chemical Compound
      1. Sb_2S_3
      2. PbO
      3. Other
   B. Silicon Semiconductor

II. Image Range
   A. Visible
   B. Infrared
   C. Ultraviolet
   D. X-Ray

III. Tube Dimensions
   A. Diameter
   B. Length

IV. Focus Method
   A. Magnetic
   B. Electrostatic

V. Deflection Method
   A. Magnetic
   B. Electrostatic

VI. Color vs. Black and White

VII. Heater Voltage and Current
   A. Rated
   B. Actual

VIII. Grid Voltages
   A. Rated
   B. Actual

IX. Temperature
   A. Rated
   B. Actual

X. Application Environment

XI. Manufacturing Quality Level

material were the two dominate factors effecting vidicon failure rate. Many other factors effect vidicon reliability, but the number of model parameters is limited by the available data.

Failure rate data was collected from four different environment categories. However, it was determined that there was insufficient empirical data to develop a unique series of environmental factors for vidicons. Therefore, the existing MIL-HDBK-217D environmental factors for other tube types were analyzed to investigate whether they could be applied to vidicons. A single series of environmental factors is currently applied to all tube types included in MIL-HDBK-217D except for traveling wave tubes (TWTs). It was assumed that these existing tube environmental factors could also be applied to vidicons without introducing error because of construction similarities with other tube types such as cathode ray tubes. The additional avionic environmental factors presented in RADC-TR-81-374 (Ref. 1) were also included in the proposed vidicon failure rate prediction model. Although the vidicon failure rate data presented in Table 5.4-1 is not sufficient to confirm these factors, the data does appear to be in agreement with the existing tube environmental factors.

The failure rate data (data entries 1, 2, 3, 4 and 5) were normalized for environment and merged to determine base failure rate values for vidicons with Sb_2S_3 and silicon diode photoconductive materials. No failure rate data was available for vidicons with other photoconductive materials such as lead oxide (PbO). Therefore, the proposed failure rate prediction model is limited to vidicons with Sb_2S_3 and silicon diode photoconductive materials. The normalized failure rate point estimates, lower 10% and upper 90% confidence limit values are presented in Table 5.4-3.

TABLE 5.4-3: NORMALIZED FAILURE RATES

Photoconductive Material	Normalized Failures	Normalized Part Hrs. ($X10^6$)	Base Failure Rates ($F/10^6$ hrs.) L 10%CL	PT EST	U 90%CL
Sb_2S_3	456	9.423	45.51	48.39	51.42
Silicon Diode	18	0.350	36.48	51.43	70.58

The results presented in Table 5.4-3 are in complete agreement with the anticipated failure modes and mechanisms of vidicons. As stated in Section 5.2, the dominant failure mode for vidicons is failure of the cathode, which is physically similar for each vidicon type. Therefore, the results showing that the normalized failure rates were numerically close was expected. Degradation failure mechanisms associated with the photoconductive material such as blooming and image lag are noticed more frequently with Sb_2S_3 photoconductive material. Therefore, the normalized failure rate for Sb_2S_3 vidicons being higher was also expected.

The homogeneity test for merging data described in Section 3.1 was applied to the data (normalized for environment) to determine whether the two base failure rate point estimates given in Table 5.4-3 differ significantly. The results of the test indicate that the Kolmogorov-Smirnov statistic is equal to 0.310 which is less than the critical value at 5% significance equal to 0.565. This means that all normalized failure rate data could have been merged. However, the point estimate base failure rates are in agreement with theoretical analyses and show proper discrimination against device construction. Therefore the optimal base failure rates to be applied to vidicons are those given in Table 5.4-3 and the proposed vidicon failure rate prediction model is,

$$\lambda_p = \lambda_b \times \pi_E$$

where

λ_p = predicted vidicon failure rate

λ_b = base failure rate

= 48, Sb_2S_3 (antimony trisulfide) photoconductive material

= 51, silicon diode photoconductive material

π_E = environmental factors

= existing MIL-HDBK-217D electron tube factors.

All of the data collected were for mature vidicon devices. Since there were no data available to prove or disprove the learning curve (π_L) factor currently in MIL-HDBK-217D, this factor was retained for the current model. The proposed operating failure rate model then becomes:

$$\lambda_p = \lambda_b \times \pi_E \times \pi_L$$

where

λ_p, λ_b, π_E and π_L were defined in Section 5.3

The proposed failure rate prediction model for vidicons improves the overall utility of MIL-HDBK-217D. The existing absence of a vidicon model has impaired reliability prediction capabilities for surveillance equipments like the AN/GXS-2 Ground Intrusion Detection system.

5.5 Bibliography

Dervishian, Ed, Some Simple, Practical Pointers for Routine Maintenance of Closed-Circuit TV, Plant Engineering, February, 1976, pp. 51-52.

McMann, Renville H., Jr., Television Cameras, Chapter 20, Electronics Engineers' Handbook, Second Edition, McGraw-Hill, 1982.

Welmer, Paul K., From Camera Tubes to Solid-State Sensors, RCA Review, Vol. 36, September, 1975.

Westinghouse Electric Corporation, Imaging Devices Product Catelog.

6.0 CATHODE RAY TUBES

6.1 Part Description

The cathode ray tube (CRT) is the most common display device used due to its flexibility of performance, resolution, dynamic range and simplicity of hardware. The CRT consists of an electron emitting element or cathode with an electron beam forming and control structure. The electron beam is positioned and focused on a phosphor. Focusing and positioning or deflection can be obtained by either electrostatic or magnetic fields. The energy of the electron beam excites the particles of a phosphor screen which emits the energy as light. Color of light, storage or decay rate of emission and light conversion efficiency depend on the properties of phosphor.

Typical electrostatic and magnetic deflection systems are shown in Figures 6.1-1 and 6.1-2. Electrostatic deflection tubes utilize an electric field to deflect the electron beam. Deflecting electrode plates are mounted in pairs on each side of the beam. A potential difference between the plates deflects the beam in proportion to the established field intensity. Two pairs of orthogonal plates are generally mounted sequentially on the beam path to allow deflection in both x and y planes. Minimum distortion of the beam and maximum deflection linearity are achieved by applying equal and opposite voltages to the deflection plates. Apertures to limit the beam size are also employed to minimize beam interaction with the deflection fields and deflection defocusing. The complexity of the electrode design and the required sensitivity of the design limit the application of this deflection approach.

The deflection is an inverse function of the beam potential. To increase brightness with electrostatic deflection and minimize deflection voltage requirements and overall tube length, it is common to use a post acceleration type tube. In this type tube, the beam is deflected at an intermediate potential and then is accelerated to a final potential. The deflection system is generally operated at around ground or chassis potential and the

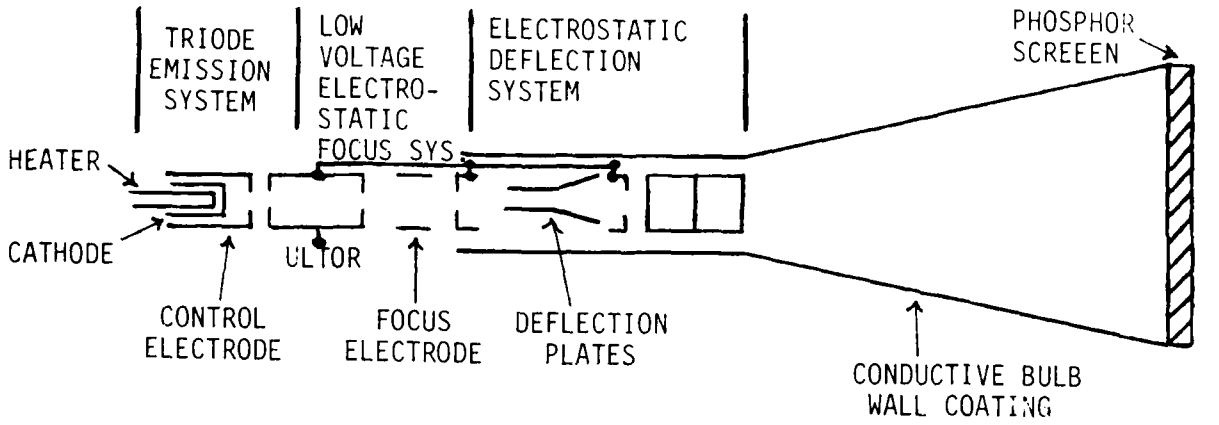

FIGURE 6.1-1: ELECTROSTATIC DEFLECTION SYSTEM

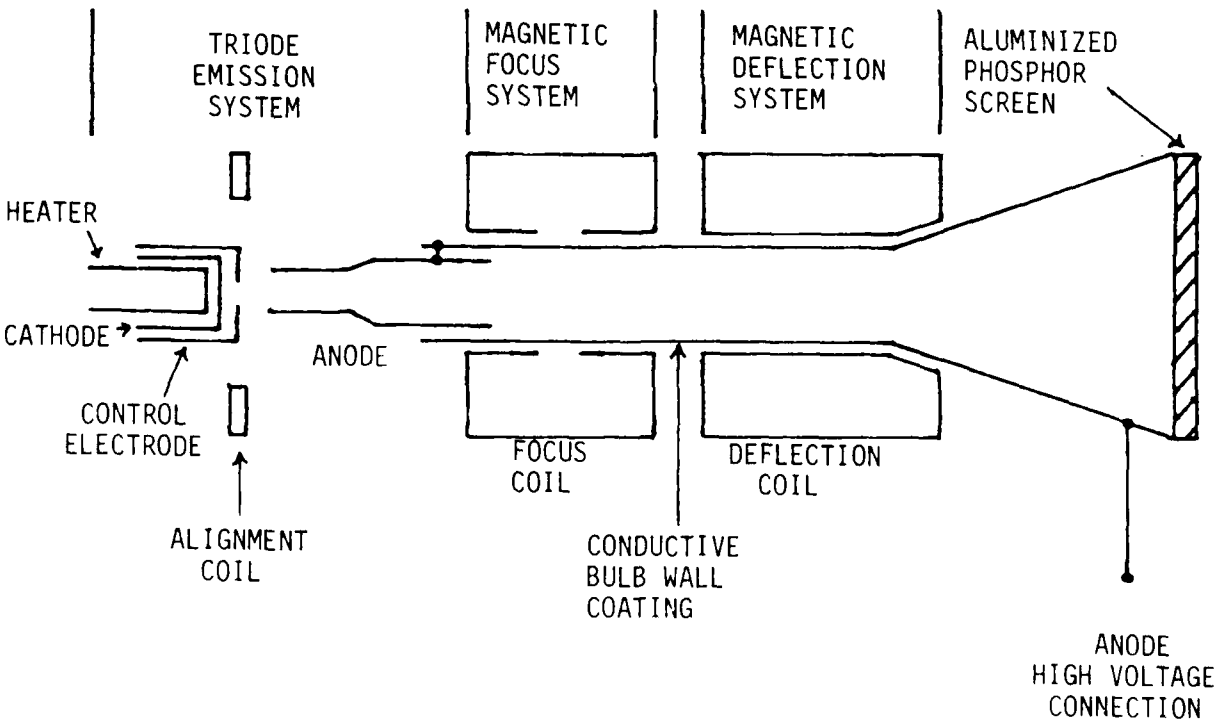

FIGURE 6.1-2: MAGNETIC DEFLECTION SYSTEM

electron gun is operated at a negative potential equivalent to the intermediate accelerating voltage. To improve the linearity and beam focus, a high resistance spiral is often used on the inside of the bulb between the intermediate voltage anode and the final anode to obtain a linear post acceleration field.

Electromagnetic deflection tubes have an electromagnet or deflection yoke positioned around the neck of the tube to provide a magnetic field for beam deflection. The deflection sensitivity of the magnetic tube is a linear function of the magnetic flux density and length of the magnetic field and is inversely proportional to the square root of the beam potential. Since the deflection varies inversely as the square root of beam potential, the advantage of post-acceleration with magnetic deflection is diminished as compared with electrostatic deflection tube.

Dual electrostatic-magnetic deflection is sometimes used for special purpose applications. Magnetic deflection is used for the major beam positioning with electrostatic deflection utilized for low-angle or minor deflection.

Focusing of the CRT electron beam is required to converge the beam into a usable spot on the face since the initial beam from the electron gun is diverging. Performance of the focusing system is a function of the ratio of the distance between the focusing lens and the screen to the distance between the focusing lens and the electron gun aperture.

The effective focus of the electron beam is limited by factors which are not optical in nature. Maximum resolution of the beam is a function of the current density and effective anode voltage. The space charge effect of the electron beam limits the minimum size of the beam. The size of the object at the CRT cathode also increases as the cathode current is increased. Increasing the screen grid potential increases the resolution of the spot by minimizing the effective aperture size of the electron beam at the expense of increasing the modulation requirements for the control grid. Another factor

limiting the focused resolution is the variation of the electron velocity and the fact that the paths of all electrons in the beam are not symmetrical around the center. Increasing the final anode voltage reduces the effect of variations in the initial velocities and directions of the electrons in the beam. CRT focusing is not analogous to optical focusing in that fields are not sharply confined.

CRT focusing may be either electrostatic or magnetic. Electrostatic focusing type tubes have either bipotential or unipotential guns. The bipotential type has a tetrode type gun and offers high resolution and moderate deflection defocusing. The unipotential CRT has a triode type gun and offers medium resolution and low deflection defocusing. Magnetic focusing tubes utilize an axial magnetic field concentric with the beam axis of the CRT to converge the electron beam. In magnetic focusing, electrons at an angle to the magnetic lines of force are deflected toward the line of the magnetic field. Thus if the center line of the magnetic field is not parallel and concentric with the center line of the beam, the beam shape and resultant spot will be distorted and aberrations of the beam will occur. Magnetic focusing generally provides better resolution, largely because the magnetic focus coil is necessarily located further from the gun and the magnification factor based on the ratio of object distance to image distance has the lower number. However, the magnetic focus tube has the largest spot growth or defocusing at the edge of the tube, owing to the larger beam bundle in the magnetic focus lens and to the sharper crossover at the screen caused by the lower ratio between the image distance and the object distance.

The major parameters for evaluation of deflection yokes are deflection sensitivity, inductance and speed. Other parameters are the accuracy of the orthogonality of the coils for xy deflection yokes, magnetic sensitivity, coupling between othorgonal coils and deflection defocusing of the yoke. Deflection defocusing of the CRT is a function of the uniformity of the magnetic field and fringing fields. Fringe fields at the ends of the yoke can be modified by shielding. However, such shields add time constants to the magnetic field and produce non-linearities in fast sweeps or require

increased settling time for random positioning. Cathode ray tubes are sensitive devices requiring careful shielding. Magnetic fields from transformers, fans or servomotors may require shielding at both the source and the tube. Fields from high current AC conductors near the tube may also modulate the display. Generally the shield must cover both the area between the yoke and gun and the bell of the tube near the face plate.

In the cathode ray tube the electron beam energy is converted to light by a phosphor. The phosphor is a luminescent material in which the energy of the electron beam is transferred to an electron in the phosphor crystal raising the energy level of the electron. The electron then releases a quantum of light energy when it returns to the initial or original state subsequent to the excitation. The period of light emission from the phosphor after excitation is termed the persistence of the phosphor. The nature of persistence, or decay characteristic as a function of time, may vary from logarithmic to exponential. The decay characteristic of phosphor is affected by variables such as anode voltage, repetition rate, duration of the excitation and current density of the electron beam. Selection of a phosphor requires the balancing of several factors. Among these are color, persistance, relative efficiency, resolution capability and its life time. Phosphor life time or its durability is normally related to the sensitivity of phosphor to overheating or burning. Since the efficiency of beam energy conversion to light is fairly low, most electron beam energy is dissipated as heat.

The contrast of a CRT is limited by reflected light from ambient illumination and scattering of light emitted by phosphor in the face plate. Light emitted from the written image results in halation or a series of concentric rings around the beam spot. With large area beam writing, the halation causes a general illumination of the phosphor reducing the CRT contrast. Halation is the effect of specular reflection of light that exceeds the critical angle of a glass-air interface. Another effect limiting display visibility is light reflection from various glass-air interfaces.

Anti-reflection coatings such as magnesium fluoride reduce these reflections.

The glass envelopes for CRT tubes are designed with a desired flat face for the viewer and minimum glass thickness to reduce the weight of the envelope. A flat face plate also leads to increased non-linearity and pattern distortion. Glass envelopes are designed and tested to withstand three to five times atmospheric pressure at a reasonable margin of safety. A metal cone may be utilized for the bell of the CRT. A rim on the metal cone supports the face plate, which is sealed to the rim under compression. This seal increases the face plate resistance to implosion. The metal cone is also self shielding to magnetic and electrostatic fields. The end of the metal cone is protected and insulated for safety.

6.2 Failure Modes and Mechanisms

Cathode ray tube reliability depends on the performance of the electron-optics and phosphor screen life time. Mechanical stresses may cause implosion of the tube, or broken connections and filaments. Degradation of the seals may cause cathode poisoning and eventually tube failure. Phosphor brightness and durability reduce with time resulting in low brightness or image distortion. High current densities cause burn-out and aging of the phosphor resulting in the fall-off of brightness. External fields may cause focusing degradation. Erosion and change in the characteristics of the cathode may deteriorate the electron beam resulting in low brightness or image distortion. An open filament (heater) causes a catastrophic failure.

The failure mechanisms most likely to be directly or indirectly responsible for these failure modes are excessive heat and ambient conditions. Both heat from the environment around the tube and heat generated within the tube create this adverse effect. Internal heat rise is due to one of two sources: the current flow from one element of the tube to another element, and power used to raise the electron-emitting cathode to operating temperature. The ambient conditions other than temperature that

are most likely to be directly or indirectly responsible for tube failure are shock, vibration and electromagnetic fields.

6.3 Cathode Ray Tube Prediction Model

This section presents the proposed failure rate prediction model for cathode ray tubes (CRTs). The proposed model is:

$$\lambda_p = \lambda_b \times \pi_E$$

where

λ_p = predicted CRT failure rate (F/10^6 hours)
λ_b = base failure rate (F/10^6 hours)
= 9.6 F/10^6 hours
π_E = environmental factor (Table 6.3-1)
π_L = learning factor (Table 6.3-2)

6.4 Failure Rate Model Development

The approach utilized for model development was to identify significant parameters by analysis of the CRT field experience failure rate data. The model parameters were then quantified using the same data. At the conclusion of each step, the results were given a thorough analysis to determine whether they were consistent with the theoretical physics of failure information. The CRT failure rate data collected in support of this study are presented in Table 6.4-1.

Application and construction variables were identified for CRTs. These variables which are listed in Table 6.4-2 represent factors which were determined whenever possible for all collected data.

TABLE 6.3-1: ENVIRONMENTAL MODE FACTORS

Environment	π_E	Environment	π_E
G_B	0.5	A_{IA}	2
G_F	1.0	A_{IF}	10
G_M	9	A_{UC}	6.5
M_P	18	A_{UT}	8
N_{SB}	7.6	A_{UB}	9.5
N_S	7.6	A_{UA}	2.5
N_U	13	A_{UF}	15
N_H	28	S_F	0.5
N_{UU}	30	M_{FF}	18
A_{RW}	40	M_{FA}	25
A_{IC}	5.5	U_{SL}	53
A_{IT}	6.5	M_L	61
A_{IB}	7.5	C_L	1000

TABLE 6.3-2: LEARNING FACTOR

t*(yrs)	1	2	3
π_L**	10	2.3	1

* t = number of years since introduction to military use

** $\pi_L = 10t^{-2.1}$ for $1 \leq t \leq 3$

$= 10$ for $t > 1$

$= 1$ for $t < 3$

TABLE 6.4-1: CRT FIELD EXPERIENCE DATA

Source	Type 1 (1)	Type 2 (2)	Env Mat (3)	Viewing Area (Sq in)	Env	Heater Volts (V)	Anode Volts (KW)	Grid Volts (4)	Qual (5)	DEF Method (6)	Focus Method (6)	No. Fail	OP Hours
1	S/1	B/P4	G	227	GF(9)	6.3	18	300	C	M	E	10	2135412
2	S/1	B/P4	G	346	GF(9)	6.3	18	300	C	M	E	4	237268
3	S/1	B/P4	G	491	GF(9)	6.3	18	---	C	M	E	0	711804
4	S/1	B/P31	-	154	GB(10)	6.3	16	300	M	M	E	0	16680
5	S/1	B/P31	-	24	AIC(11)	6.3	18	500	C	M	E	64	1160000
6	S/1	B/P31	-	332	GF(12)	6.3	18	(A)	C	M	E	2	78800
7	R/1	B/P31	-	429	GF(12)	6.3	18	(B)	C	M	M	0	105100
8	S/1	B/P4	-	143	GF(12)	6.3	16	(C)	C	M	E	0	35000
9	S/1	B/P4	-	74	GF(12)	12.6	16	---	C	M	E	0	52560
10	R/1	B/P31	-	122	GF(12)	6.3	8	---	C	E	E	1	35040
11	S/1	B/P31	-	70	AIC(13)	6.3	18	(D)	C	M	E	0	50668
12	S/1	B/(8)	G	154	AIC(13)	6.3	20	(D)	C	M	E	8	228006
13	R/4	C	M	415	GF(12)	6.3	15	---	C	M	E	1	203050
14	R	B	-	---	A(7)	--	--	---	C	-	-	1	10000
15	R	C	-	---	A(7)	--	--	---	C	-	-	0	20000
										Totals		91	5079388

Notes:
(1) R = round, S = rectangular; No. Present indicates No. of guns
(2) B = Black & White, C = Color; Alphanumeric indicates Phosphor type
(3) G = Glass, M = Metal
(4) A = -150V & 500V, B = -100V & 400V, C = 60V, 200V & 450V, D = 60V, 800V & 3.2KV
(5) C = Commercial, M = Military
(6) E = Electrostatic, M = Electromagnetic
(7) A = An accelerated lifetest that simulated the airborne environment
(8) Phosphor could be P1 or P39
(9) AN/GYQ-18
(10) Life test data
(11) Commercial airline, equipment type unknown
(12) Radar
(13) E-3A

TABLE 6.4-2: CRT CONSTRUCTION AND APPLICATION VARIABLES

I. Tube Dimensions
   A. Length
   B. Screen Width (or radius)
   C. Screen Height

II. Focus and Deflection Method
   A. Magnetic
   B. Electrostatic

III. Color vs. Black and White

IV. Number of Guns

V. Anode Voltage
   A. Rated
   B. Actual

VI. Heater Voltage and Level
   A. dc
   B. ac
      1. Frequency
   C. Rated Voltage
   D. Actual Voltage

VII. Operating Temperature
   A. Rated
   B. Actual

VIII. Application Environment

IX. Manufacturing Quality Level

X. Grid Voltage(s)
   A. Rated
   B. Actual

XI. Operation Mode
   A. Operating
   B. Stand by

XII. Tube Envelope Material and Phosphor Type

XIII. Cathode Voltage
   A. Rated
   B. Actual

Stepwise multiple linear regression analysis as described in Section 3.1 was applied to the CRT data. Theoretically, temperature, envelope material, and grid voltages should be significant variables effecting failure rate; however, the amount of data available did not allow for the inclusion of these variables in the analysis. The regression analysis resulted in the following failure rate prediction model:

$$\lambda_p = \lambda_b \times \pi_E$$

wnere

λ_p = CRT failure rate in failures/10^6 hours
λ_b = base failure rate
= 9.626 F/10^6 hours
π_E = environmental factor

The environmental factor was significant at the 0.90 confidence level. One other factor, magnetic vs. electrostatic deflection method, was significant at the 0.70 confidence level. The regression showed a 0.29:1 difference between magnetic and electrostatic deflection respectively. The difference is consistent with theory since the elements necessary for electrostatic deflection are an integral part of the tube whereas the elements necessary for electromagnetic deflection are not part of the tube. However, due to the unbalanced nature of the data (only one data entry with electrostatic deflection) and the fact that the approximately 3:1 ratio did not seem warranted, this factor was not included in the model. The details of the regression analysis are given in Table 6.4-3:

TABLE 6.4-3: RESULTS OF CRT REGRESSION ANALYSIS

Variable	Coefficient (bi)	Standard Error	F-Ratio
λ_b	2.264416 (1)	--	--
π_E, A_{IC}	1.223334 (1)	0.6180	3.92
π_E, G_F	1.0	--	--

Notes: (1) factor = exp(bi)

Environment was identified as a significant variable in the regression analysis; however, only two data points were included in the analysis (G_F and A_{IC}). The standard error statistic (Table 6.4-3) allows for the calculation of confidence intervals for a factor. Table 6.4-4 presents the point estimate, lower 20% confidence limit and upper 80% confidence limit for the A_{IC} environment along with the current A_{IC} environmental factor (reference 1).

TABLE 6.4-4: A_{IC} ENVIRONMENTAL FACTOR CONFIDENCE INTERVALS

Parameter	L 20%CL	PT EST	U 80%CL	Current Factor
A_{IC}	2.0	3.4	5.9	5.5

Since the current factor lies within the 60% confidence interval of the observed factor, there is no reason to assume that the current factor is incorrect. It was then assumed that the current set of environmental factors given in reference 1 are still valid.

All of the data collected were for mature CRT devices. Since there were no data available to prove or disprove the learning curve (π_L) factor currently in MIL-HDBK-217D, this factor was retained for the current model. The proposed operating failure rate model is then:

$$\lambda_p = \lambda_b \times \pi_E \times \pi_L$$

where

λ_p, λ_b π_E and π_L were defined in Section 6.3

All of the data used for this study were from the field environment. No information were available to identify if a failure occurred during an operating, nonoperating or standby state. Therefore, it had to be assumed that the predicted failure rate included the contribution of the operating,

nonoperating and standby failures. The inclusion of any nonoperating or standby failures should not bias the operating failure rate model too heavily because 8 of the 11 data points used in the analysis were from systems that normally operate 24 hrs/day 7 days/week, and one of the A_{IC} data points (by far the largest) was from the commercial airlines where equipment usage is quite high (50%).

6.5 References and Bibliography

References

1. Edwards, E., et.al., Avionic Environmental Factors For MIL-HDBK-217, Final Technical Report, RADC-TR-81-374, January, 1982.

Bibliography

Annon., Determination of the Reliability Parameters for the 813H-1 CRT Assembly (CPN 618-1631-001).

Arno, Robert G., Nonelectronic Parts Reliability Data, Reliability Analysis Center Publication NPRD-2, Summer, 1981.
Brain, Jake, Determining the Phospor Life of A Cathode Ray Tube, Thomas Electronics, Inc. Internal Report.

Corson, Bayard R., Some Reliability Characteristics of CRT Cathode Assemblies, IEEE Transactions on Reliability, Vol. R-23, No. 4, October, 1974, pp. 226-230.

Edwards, E., et.al., Avionic Environmental Factors For MIL-HDBK-217, Final Technical Report, RADC-TR-81-374, January, 1982.

Fink, Donald G., and Christianson, Donald, Editors, Electronics Engineers' Handbook, Second Edition, McGraw-Hill, 1982, Chapters 6, 7, 8, 9, 11, 20, 25.

Galves, J.P. and Brun, J., Reliability of High-Brightness CRT's For Airborne Displays, AGARD-CP-261 Conference Proceedings, No. 261, April 1979, pp. 26-1 to 26-14.

IIT Research Institute, Electronic Reliability Design Handbook, Volume II, Contract Data Item, Contract F30602-78-C-0081, 1981.

Sinharoy, S., et. al., Surface Stability Studies on Some CRT Phosphors, Journal of Electrochemical Society: Solid-State Science and Technology, January, 1981, pp. 205-208.

7.0 LASERS

The current version of MIL-HDBK-217 contains failure rate models for the following laser types:

Helium/Neon
Argon Ion
CO_2 Sealed
CO_2 Flowing
Solid State, Nd:YAG Rod
Solid State, Ruby Rod

In addition the laser section of the handbook contains failure rate models for Xenon and Krypton flash lamps.

A data collection effort was initiated to acquire physics of failure information, life test data and field experience data on the lasers and flash tubes listed above, plus two additional laser types which were identified as potential laser sources for military applications. These additional laser types are Helium-Cadium and Semiconductor Diode. The data collection effort fell short of expectations in that sufficient data for reliability modeling could be obtained only for Helium/Neon, Nd:YAG Solid State, Helium/Cadmium and Semiconductor Diode lasers. It was found that the remaining laser types are rarely used in military applications and therefore sufficient field experience data for modeling was unavailable.

The approach proposed for model development was to identify significant variables from the literature (Table 7.0-1) and to use these variables to quantify the field experience and life test data. It was intended that physics of failure information would be used to hypothesize a model form and that regression techniques would be applied to the failure rate data to identify significant variables and to derive parameters for the significant model variables. With the exception of semiconductor diode lasers, there was insufficient data collected to apply this approach. The approach that was used to develop each model is described in the following subsections.

TABLE 7.0-1: LASER CONSTRUCTION AND APPLICATION VARIABLES

I. Type and Lasing Material
   - A. Solid
     1. Lasing Material
   - B. Liquid
     1. Lasing Material
   - C. Gas
     1. Lasing Material
   - D. Semiconductor
     1. Lasing Material

II. Power Level
   - A. Continuous
     1. Rated
     2. Actual
   - B. Pulse
     1. Rated
     2. Actual

III. Rated Life
   - A. Hours
   - B. Pulses

IV. Pumping Mechanism
   - A. Type
     1. Optical
     2. Chemical
     3. Electrical
        - a. Discharge
          - i. Transverse
        - b. Current
   - B. Components
     1. List Quantity and Type
     2. List Temperature and Stress Level for Each Component[1]
   - C. Number of Firings (flashes)
     1. Rated
     2. Actual
   - D. Output Energy Level
     1. Rated
     2. Actual

V. Material
   - A. Tube
     1. Quartz
     2. Glass
     3. Etc.

TABLE 7.0-1: LASER CONSTRUCTION AND APPLICATION VARIABLES (CONT'D)

- B. Seal
  - 1. Epoxy
  - 2. Glass
- C. Lens
  - 1. Quantity
    - a. Quartz
    - b. Glass

VI. Q-Switch
- A. Type
  - 1. Electrooptical
  - 2. Rotating Prism (mirror)
  - 3. Acoustooptical
  - 4. Saturable Absorber
- B. Components
  - 1. List Quantity and Type
  - 2. List Temperature and Stress Levels for Each Component

VII. Firing Circuit (Pulse forming)
- A. Components
  - 1. List Quantity and Type
  - 2. List Temperature and Stress Levels for Each Component

VIII. Power Supply
- A. Components
  - 1. List Quantity and Type
  - 2. List Temperature and Stress Levels for Each Component

IX. Mirrors
- A. Quantity
  - 1. Totally Reflective
  - 2. Partially Reflective
- B. Seal Type
  - 1. Hermetic
  - 2. Dust
  - 3. None
- C. Alignment
  - 1. Adjustable
  - 2. Nonadjustable
- D. Material
  - 1. List All Materials
    - a. Reflective
    - b. Substrate

X. Cooling Circuit
- A. Type
  - 1. Forced Air

TABLE 7.0-1: LASER CONSTRUCTION AND APPLICATION VARIABLES (CONT'D)

2. Liquid
3. Gas
4. None

B. Components
1. List Quantity and Type
2. List Temperature and Stress Levels for Each Component

XI. Auxiliary Circuits
A. Type
1. Input/output Valves
a. Liquid
b. Gas
2. Mixing Chamber
3. Frequency Doubling Crystal

B. Components
1. List Quantity and Type
2. List Temperature and Stress Levels for Each Component

XII. Temperature (Ambient or Tube)
A. Rated
B. Actual

XIII. Operating Environment

XIV. Manufacturing Quality Level

Additional Information

I. Part Designation
A. Military
B. Commercial

NOTE: 1) Temperature and Stress Level are those required to calculate a MIL-HDBK-217 Part Stress Level Failure Rate.

It is proposed that the current Argon Ion, CO_2 Sealed, CO_2 Flowing and Solid State, Ruby Rod models be retained until sufficient field experience data are available to reanalyze them.

7.1 Semiconductor Lasers

7.1.1 Device Description

Various semiconductor materials have been shown to exhibit laser properties when an electric field is applied. These are sometimes referred to as injection lasers. Semiconductor lasers are finding applications in areas such as range-finding, pollution detection and communication. The wide range of wavelengths obtainable, inherent simplicity of large scale manufacture, compatibility with electronic circuitry and small size can be expected to result in large scale applications.

The most common form of semiconductor laser consists of a p-type and n-type material forming a p-n junction. Electrodes are attached to the opposite faces of the material and are connected to a power supply (pulsed and/or DC). When the p-n junction is forward biased optical radiation is generated, electrons in conduction band recombine with a hole in the valence band to give a quantum of radiation with energy equal to the energy difference between the two states. This radiation is called recombination radiation. If a sufficient population inversion in the junction area is achieved, (i.e. greater number of electrons in conduction band than holes in the valence band), then recombination may be stimulated and laser action is possible. The wavelength of the laser transition is determined by the size of the band gap. One of the simplifications of diode lasers as compared to other lasers is that no external mirrors are needed to provide feedback. The high reflectivity due to the refractive index difference at the air-diode interface is sufficient. The diodes are cleaved along material crystal planes and the parallelism of the reflecting surfaces is assured.

The most extensively studied semiconductor laser is the Ga-As diode laser. Typical construction of a double heterostructure stripe Ga-As diode laser is shown in Figure 7.1-1. The laser may operate in the pulsed or CW mode. Excitation is carried out by an electrical current and results in relatively large temperature increases. CW operation usually requires an efficient cooling system.

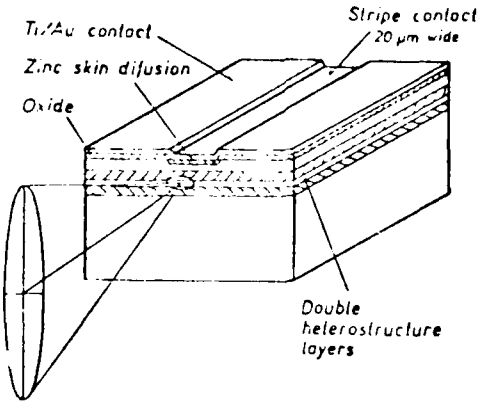

FIGURE 7.1-1: DOUBLE-HETEROSTRUCTURE STRIPE LASER

Semiconductor lasers that are fabricated from a single semiconductor (eg GaAs) are called homojunction lasers. Heterojunction lasers are fabricated from more than one type of material. In both types of lasers, both injected electrons and emitted light must be confined to the junction region for an efficient stimulated emission process. In the homojunction laser the confinement of light to the junction region is a consequence of the free electrons and holes. They serve to increase the refractive index so that light is reflected internally rather than out of the junction region. Although this confinement mechanism works sufficiently well to allow the homojunction lasers to operate, the current density is high and efficiency is low. Some light spreads out of the region reducing the amount available to provide stimulated emission. The electrons are injected into various distances in the p-type region before they recombine.

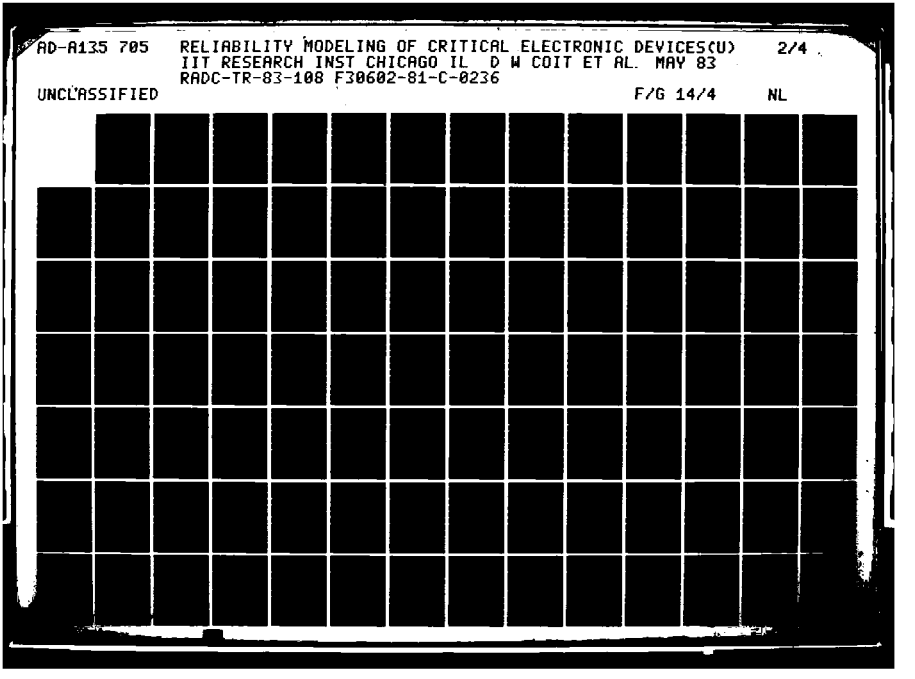

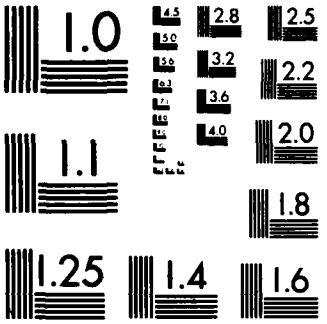

MICROCOPY RESOLUTION TEST CHART
NATIONAL BUREAU OF STANDARDS-1963-A

A much higher lasing efficiency and a much lower threshold current density is obtained when two materials are used to form a junction. Materials such as Gallium Arsenide and Aluminum Arsenide and its admixture Gallium Aluminum Arsenide have different refractive indexes and band gaps. The discontinuity in refractive indexes causes radiation generated within the junction to be reflected back into the region giving higher lasing efficiency. The band gap difference confines the carriers to the junction region and thereby reduces the threshold current density. Heterojunction lasers are of two types. The single heterojunction laser is formed by depositing p+type $Ga_xAl_{1-x}As$ layer on n-type Ga-As. The double heterostructure consists of a triple structure of p-type Ga-As sandwiched between p^+ type and n-type $Ga_xAl_{1-x}As$. The triple structure is frequently mounted on n-type Ga-As substrate with p-type Ga-As on top to provide contact. The double heterostructure approach reduces the threshold current density to about 2000 amp/cm^2 as compared to 8000 amp/cm^2 for single heterostructure and 100000 amp/cm^2 for homostructure lasers. Coupled with the decrease in threshold current density is a corresponding increase in power efficiency due to stricter confinement of the radiation to active region.

Semiconductor lasers are very susceptible to failure due to reverse bias; therefore, extreme care should be taken to ensure that the laser circuitry is resistant to voltage transients.

7.1.2 Laser Failure Modes

Semiconductor laser failure modes can be separated into three categories -catastrophic, gradual degradation and functional degradation. The first depends on optical flux density, bulk defects and metalization and bonding anomolies that have been documented for other semiconductor devices. The second is related to the electron-hole recombination process and is strongly affected by the laser technology and operating conditions. The third category is related to the ability of the laser to function in specific design applications. One study (Ref. 14) reported a 2:1 ratio between

catastrophic and gradual degradation failure during a life test of approximately 100 double heterojunction GaAlAs stripe geometry lasers. Other studies have shown that self-sustained-oscillations and frequency shifts occur in a large portion of the devices (≈50%) and that these failure mechanisms may impact the ability of the laser to perform in different applications. Therefore, although most of the reliability literature stresses the gradual degradation phenomena, catastrophic failures and functional failures may account for a large portion of the laser failure rate.

7.1.2.1 Catastrophic Failure Mechanisms

Catastrophic degradation mechanisms that have been documented fall into two categories - P-side metalization breakdown and catastrophic facet damage.

P-Side Metalization Breakdown

P-Side metalization breakdown is attributed to metal penetration into the semiconductor material (Ref. 16). No data were presented in the literature to describe the rate at which this mechanism occurs or the activating media, although, since it is a metal diffusion process, temperature is probably the major activating influence.

Catastrophic Facet Damage

Catastrophic degradation due to facet damage occurs at optical power densities greater than several milliwatts per micrometer of emitting facet width after short operating times (Ref. 10). The physical process leading to this failure mechanism has been documented in the literature (Ref. 10, 16), and has been found to be a function of optical power density and pulse length. Two equations that describe the critical flux density are (Ref. 16):

Critical Optical Flux Density (qc)

$qc \propto t^{-\frac{1}{4}}$ (100ns < t < 10-50us) (7.1-1)

$qc \simeq$ Constant (t > 10-50us)

and

$qc \propto t^{-\frac{1}{2}}$ (300ns < t < 1us) (7.1-2)

$qc =$ Constant (t > 1us)

Equation 7.1-1 was derived from test data on 15um wide stripe geometry double heterojunction lasers. For 300ns pulses, qc was found to be approximately $3MW/CM^2$. Equation 7.1-2 was derived from test data on broad-contact homojunction devices. For 300ns pulses, qc was found to be approximately $4MW/CM^2$.

Facet damage is believed to reduce the facet reflectivity and thus increase the threshold current and reduce the differential quantum efficiency (Ref. 10). The effects of catastrophic facet damage can be mitigated by the use of a half-wavelength ($\lambda/2$) dielectric facet coating such as Al_2O_3 (Ref. 16). The degree to which facet coatings affect the reliability of a semiconductor laser has been shown to be a function of the thickness of the coating, the dielectric material (Al_2O_3, SiO_2) and the construction of the laser (Ref. 10, 15, 16). The reliability impact of facet damage on some of the more advanced laser devices such as stripe geometry buried heterostructure, narrow stripe or V-groove lasers may differ from what was given above for the broad-contact homojunction and stripe geometry double heterojunction lasers.

7.1.2.2 Gradual Degradation Failure Mechanisms

The gradual degradation of semiconductor lasers has been attributed to the following failure mechanisms: dark line defects (DLDs), dark spot defects (DSDs), thermal resistance degradation, homogeneous degradation, and non-catastrophic facet deterioration. The nature of these mechanisms and

their affect on the reliability of a semiconductor laser will be discussed in the following paragraphs.

Dark Line Defects (DLDs) and Dark Spot Defects (DSDs)

Both DLDs and DSDs propagate during operation. They are both regions of high non-radiative recombination so that the carriers injected into that region do not contribute to the luminescent output. Additionally, light travelling in the junction plane can be absorbed in these regions, since they are regions of loss, which results in further reduction in laser output. One study (Ref. 5) suggests that DSDs can develop into DLDs. Both DLDs and DSDs initiate at native defects in the semiconductor material. Sources of DLDs, that have been identified include crystal edges, stacking faults, DSDs and various kinds of surface damages induced by scratches, indentations, and non-uniform bonding. Sources of DSDs are substrate dislocation, segregrated impurities, and macroscopic foreign particles such as carbon powder. Both DLDs and DSDs are activated by the presence of strain or temperature gradients and result in the rapid degradation of the laser. One study (Ref. 10) reported a thermal activation energy of 0.1ev for this mechanism. These degradation mechanisms were more prevalent in earlier versions of semiconductor lasers. The newer lasers and more sophisticated manufacturing and quality assurance techniques have reduced the impact of this degradation mechanism on the life of the laser. One suggested method of screening is a short (50-100 hour) high temperature (70°C) burn-in (Ref. 10). However, if the 0.1ev thermal activation energy is correct, accelerating the temperature from room ambient (≈20°C) to 70°C would only have a 2:1 difference in expected life; therefore, a room ambient test of 100 to 200 hours would have the same effect. In addition, strain was reported as another activating mechanism. High temperature operation may, in fact, reduce the strain and, therefore, defeat the purpose of the screen. A better screen may be temperature cycling or temperature-vibration for 50-100 hours.

Thermal Resistance Degradation

The increase in thermal resistance in Au-In metalization systems is attributed to contact deterioration. Investigation of the effect has shown that it is due to intermetallic and void formation in the indium used to solder the Au-evaporated chip to the gold plated header (Ref. 15). The growth of the intermetallic compounds is a function of the temperature, the length of time of exposure to that temperature and the initial ratio of the gold to the indium (Ref. 21). A temperature-intermetallic growth figure is shown in reference 21. The rate of intermetallic growth as given by the figure appears to follow an exponential curve of the form:

$$\text{Intermetallic growth} = A\,T^{n},\ 20 \leq T(^{o}C) \leq 60 \qquad (7.1\text{-}3)$$

where

$A \simeq 10^{-8}$
$n \simeq 5.0$ to 6.0
T = temperature (^{o}C)

The knee of the curve is at approximately 40°C. Reference 21 recommends an ambient temperature limit of 40°C for wire bonds. Reference 10 reports a thermal activiation energy of 0.6ev for contact deterioration in indium solder based systems. The data shown by the figure given in reference 21 was fitted to the standard Arrhenius equation using two points at 50°C and 60°C. The result was a thermal activation energy of 2.14ev. It should be pointed out that the use of the Arrhenius relationship with an apparent activation energy of 2.14eV for prediction purposes would give a lower intermetallic growth rate than that observed in reference 21 between 20 and 60°C. Equation 7.1-3 is more nearly accurate for temperatures between these temperatures.

Thermal resistance degradation then appears to be an exponential function of time and temperature. There was not enough data to determine the exact form of the function from the literature.

Homogeneous Degradation

Homogeneous degradation is a gradual degradation that occurs in lasers. Reference 10 reports that this degradation process is both current density (J) and temperature dependent and is reported to be caused by defects formed by small non-radiative centers. The number of non-radiative centers increases in proportion to the number of radiative centers resulting in reduced laser output power. Homogeneous degradation then may be some increasing function of current and temperature. There was not sufficient data to determine the form of the equation or its parameters from the literature; however, from reference 10 the current density and temperature dependence are bounded by:

$$1/\tau \propto J^n, \quad 1.5 \leq n \leq 2.0 \tag{7.1-4}$$

$$1/\tau \propto A \exp\left(\frac{Ea}{KT}\right), \quad 0.3 \leq Ea \leq 0.95 \tag{7.1-5}$$

where

$1/\tau$ = degradation rate
J = current density
A = constant
E_a = apparent activation energy
K = boltzman's constant
T = temperature (^oK)

Non-catastrophic Facet Deterioration (Erosion)

Reference 16 reports that non-catastrophic facet deterioration (erosion) is a gradual degradation of the laser facets which is caused by some photochemical reaction at the facet. This deterioration is enhanced by the ambient conditions and optical flux densities. It was also reported that the gradual oxidation introduces extra non-radiative recombination centers near the facet causing the threshold to rise and introducing losses resulting

in a decrease in external quantum efficiency. Reference 10 reports that the presence of oxygen or moisture in the ambient gases in contact with the facet accelerates facet erosion, and that the facet erosion decreases the mirror reflectivity and increases the non-radiative recombination rate at the facets. Reference 10 also reports that facet erosion can be prevented by coating the facet with a Al_2O_3 half-wave length thick film. A half-wave film is used in order to leave the facet reflectively, and hence, the threshold current unchanged. The application of a quarter-wavelength thick film would decrease the reflectivity, and hence, increase the threshold current which would accelerate other failure mechanisms. The coating is believed to provide a moisture barrier. Reference 13 also reports that facet erosion is a function of optical flux and ambient gases.

Non-catastrophic facet deterioration is some function of optical flux, ambient and facet coating. Data were not available to determine the form of the function or its parameters from the literature; however, references 13 and 15 report that a significant decrease in degradation occurs (>2X) when facet coatings are utilized.

7.1.2.3 Functional Degradation Failure Mechanisms

Functional degradation failure mechanisms that have been documented fall into three categories, Intensity Pulsations, Optical Frequency Shifts and Emission Symmetry Changes.

Intensity Pulsations

Intensity pulsations are self sustained oscillations (SSOs) that have been reported to occur at frequencies between 200MHZ and 3GHZ and at a modulation depth approaching 100% (Ref. 9, 10, 16, 28). The onset of SSOs could be detrimental if the laser was being used in a digital application. The failure mechanisms that cause these SSOs have yet to be confirmed, but there have been suggestions that either second order mode locking or switching between two lateral filaments, or effects associated with

electron-photon interactions in the presence of non-uniform gain or loss, or the effect of saturable absorbers in the active region are the cause (Ref. 16). The absorber may result from a localized region of lower population inversion, caused by a region of non-radiative recombination, surface recombination at the facets or the unpumped regions at the edges of the stripe. The absorption in these areas will decrease with increasing pumping, giving rise to a Q-switching effect (Ref. 16). One study (Ref. 9) reported that SSOs were present in new devices and that the SSOs become enhanced by forward-biased operation and/or elevated temperature. Data were not available to derive an equation describing laser degradation or failure due to SSOs. A second study (Ref. 28) reported that SSOs were present after testing at elevated temperatures.

Several studies (Ref. 9, 10, 16, 28) have addressed this failure mode. The distribution of devices that exhibited SSOs after lifetesting on a group of AlGaAs double-heterostructure lasers (Ref. 28) is shown in Table 7.1-1:

TABLE 7.1-1: SSO DISTRIBUTION

	STRONG SSO	WEAK SSO	NO SSO	TOTAL NO. OF DEVICES
Lasers that degraded* during lifetest	10	8	12	30
Lasers that did not degrade* after aging				
4000 hour	4	3	5	12
521 hour	0	0	5	5
0 hour	0	0	18	18
TOTAL	14	11	40	65

*Optical Power output degradation

Another study (Ref. 9) reported that 64 out of 103 samples (62%) exhibited SSOs and that greater than 50% were converted from a stable laser to a pulser during a 50-60 hour test. The data indicates that, at least for these two batches of lasers, SSOs could be a major failure mode depending on the

circuit and application. The data also indicates that the onset of SSOs may be time dependent and associated with other degradation mechanisms.

Optical Frequency Shifts and Light Intensity Changes

Optical frequency shifts are basically small alterations in the beam direction and mode shape. These changes could be caused be minor internal degradation which perturbs the cavity parameters in the junction plane without significantly changing the efficiency (Ref. 10). Data were not available to determine if operational parameters such as current and temperature are activating influences, or to quantify the percentage of devices that exhibit a frequency shift.

Emission symmetry changes are light intensity differences at the two ends of the laser. The light intensity at one end is not the same as the other and the difference varies with aging and drive current. One study (Ref. 9) reported that 47 out of 95 (49%) of the samples exhibited an emission symmetry change in the light polarized perpendicular to the junction plane after accelerated testing. Light polarized in this manner was defined as transverse magnetic (TM). Reference 9 also reported emission symmetry changes in the light polarized parallel to the junction plane but the percentage of devices that exhibited a change was not reported. Light polarized in this manner was defined as transverse electric (TE). Data were not available to determine if operational parameters such as current and temperature are activating influences.

TM and TE emission symmetry changes and optical frequency shifts may affect the performance of the laser in systems such as single-mode fiber optical communications links and optical disks. The design engineer should be aware of these devices characteristics, and design circuitry that are tolerant of them.

7.1.3 Semiconductor Laser Reliability Prediction Procedure

The semiconductor laser failure rate is calculated using the following equation:

$$\lambda_p = \lambda_D \pi_E \qquad (7.1\text{-}6)$$

where

λ_p = total device failure rate (F/10^6hours)
λ_D = average degradation failure rate (F/10^6hours)
π_E = environmental factor (Table 7.1-2)

The failure rate prediction procedure is as follows:

STEP 1: Calculate the average failure rate
STEP 1A: Calculate the average optical power output degradation rate using the following equation:

$$\tau_p = \tau_b \times \pi_T \times \pi_I \times \pi_C \times \pi_A \times \pi_F \qquad (7.1\text{-}7)$$

where

τ_p = semiconductor laser optical power output degradation rate (%/1000 hours)

τ_b = base degradation rate (%/1000 hours) (Table 7.1-3)

π_T = temperature factor

$$= \exp\left[\frac{-E}{(T + 273)}\right], \quad T = \text{Case Temperature } (^oC)$$

where E = apparent activation energy/Boltzman's Constant (Table 7.1-3)

π_T is valid for $+25^{\circ}C \leq T \leq +100^{\circ}C$

π_C = construction factor (Table 7.1-4)

π_A = application factor (Table 7.1-5)

π_F = pulsed duty cycle factor

$= \sqrt{\text{pulsed duty cycle}}$ (Table 7.1-6)

π_I = (forward peak current (ma))$^{0.68}$

π_I is valid for $0 \leq I \leq 25$ amps

STEP 1B: Calculate the Mean life of the device by the following procedure:

1) P_S = rated optical power output (mw)
2) define required optical power output (P_R)
3) calculate the allowable degradation (D) as follows:

$$D\ (\%) = \frac{P_S - P_R}{P_S} \times 100 \qquad (7.1\text{-}8)$$

4) mean life (u) = $D(\%)/\tau p$

Note: Each laser must be replaced when it reaches Pr to make the calculated mean life (u) valid.

STEP 1C: Calculate the average failure rate using:

$$\lambda_D = 1/u\ (F/10^6 \text{ hours}) \qquad (7.1\text{-}9)$$

STEP 2: Calculate the average semiconductor laser failure rate using the equation:

$$\lambda_P = \lambda_D \times \pi_E\ (F/10^6 \text{ hours}) \qquad (7.1\text{-}10)$$

TABLE 7.1-2: ENVIRONMENTAL MODE FACTORS

Environment	π_E
G_B	1
G_F	2.4
G_M	7.8
M_P	7.7
N_{SB}	3.7
N_S	5.7
N_U	11
N_H	12
N_{UU}	13
A_{RW}	17
A_{IC}	2.5
A_{IT}	3.5
A_{IB}	3.5
A_{IA}	5.5
A_{IF}	8
A_{UC}	3
A_{UT}	5.5
A_{UB}	5.5
A_{UA}	8
A_{UF}	10
S_F	1
M_{FF}	7.8
M_{FA}	11
U_{SL}	23
M_L	26
C_L	450

TABLE 7.1-3: DEGRADATION EQUATION PARAMETERS

Device Type	E	(τ_b X10^5)
AlGaAs	4635	2.21
GaAs	4635	2.81
InGaAs/InGaAsP	5784	188

TABLE 7.1-4: CONSTRUCTION FACTORS

Construction	π_C
Facet Coat or Hermetic Package	1.0
No Facet Coat	3.3

TABLE 7.1-5: APPLICATION FACTOR

Application	π_A
Variable Current Source with optical feedback	1.0
Fixed Current Source	1.5

TABLE 7.1-6: PULSED DUTY CYCLE FACTOR

Duty Cycle	π_F*
1.0	1.00
0.9	0.95
0.8	0.90
0.7	0.85
0.6	0.75
0.5	0.70
0.4	0.65
0.3	0.55
0.2	0.45
0.1	0.30

*$\pi_F = \sqrt{\text{duty cycle}}$

7.1.4 Model Limitations

The procedure described in paragraph 7.1.3 applies to the following device constructions:

AlGaAs DH Stripe
GaAs SH Stripe
InGaAs/InGaAsP DH Stripe

The models only apply if the optical flux density is less than $3MW/CM^2$.

The procedure does not address the functional failure modes - self-sustained-oscillations (SSOs), TM & TE symmetry change and frequency shift. An estimate of the expected percentage of devices that may exhibit these failure modes is:

Self-Sustained-Oscillations (SSOs)	53%
TM Symmetry Change	49%
TE Symmetry Change	unknown
Frequency Shift	unknown

As can be seen from the data, these failure modes may occur in a large percentage of the devices. It is impossible at this time to quantify their impact on system reliability since they are not parameters that are specified in the device data sheets, no definition of failure exists, and no field data are available. It should also be noted that more than one of these failure modes may occur in the same device, and that the probability of this occurring is unknown.

The temperature and drive current extremes that were available to derive the factors π_T and π_I are given in Table 7.1-7.

TABLE 7.1-7: TEMPERATURE AND CURRENT LIMITS

Variable	Upper Value	Lower Value
Temperature	+ 100°C	+ 22°C
Drive Current	25 amps	50 ma

There were two data points at -35°C; however, these were not utilized to derive the π_T factor. The models are then limited to temperatures and currents between the ranges given above.

The procedure assumes that the catastrophic failure rate and degradation rate are constant.

7.1.5 Model Development

All of the data collected during this study effort were obtained from either life tests or special research studies. With the exception of two sources of data (Ref. 3, 21) all of the data were obtained from published articles or manufacturer's product catalogs. Over 50 letters were written to semiconductor laser manufacturers and researchers, and one trip was made to a major semiconductor laser manufacturer to obtain reliability information and data. No reliability data were obtained from any of these inquiries.

The data and information extracted from the literature are listed in Table 7.1-8.

The approach to model development for semiconductor lasers was to hypothesize a preliminary model form and general values for the model parameters based on data and information extracted from the literature. The life test data extracted from the literature was then used to develop empirical estimates for the model parameters based on all of the available data. The average degradation rate model was deemed necessary since parameter degradation occurs early in the life of the device and the constant hazard rate assumption over the life of the equipment may not be accurate. The development of this model is presented in the following paragraphs.

TABLE 7.1-8: TEST DATA

REF	DEVICE TYPE (7)	TEST CURRENT (Ma) (2)	TEST TEMP (°C)	TEST FREQ (3)	TEST MEAS. (6)	NO. TESTED	NO. FAILED	TOTAL DEVICE (HOURS)	TEST LENGTH (HOURS)	DEGRADATION RATE (/ 1000 HOURS) CURRENT	DEGRADATION RATE (/ 1000 HOURS) POWER	MEDIAN LIFE (HOURS)
2	III	260	27	1	L	6	-	150,000	25,000	-	1.0	50,000
8	II	160	90	1	S	11	-	33,500	4,500	19.1	-	1,047
8	II	160	55	1	S	1	-	3,500	3,500	6.1	-	3,279
8	II	160	25	1	S	4	-	24,000	6,000	1.2	-	16,667
8	II	V	25	1	L	4	-	12,000	3,000	3.2	-	6,250
8	II	V	25	1	S	20	0	10,000	500	-	-	(1)10,929
10	I	180	70	1	L	40	38	119,300	10,000	-	26.3	1,900
10	I	V	70	1	L	40	37	187,450	10,000	-	18.2	2,747
10	I	V	70	1	L	7	6	58,100	18,000	-	14.0	3,571
10	I	V	22	1	L	24	7	750,000	>40,000	-	0.6	80,000
13	I	C	22	1	L	8	1	84,000	11,000	-	0.9	55,556
13	II	C	22	1	L	1	0	18,000	>18,000	-	6.3	7,353
14	III	V	55	1	L	72	20	-	10,000	-	12.5	4,000
17	II	170	70	1	L	100	74	450,506	14,500	-	11.1	4,500
17	II	C	70	1	L	1	-	10,000	10,000	-	2.5	20,000
19	IA	V	18	1	-	16	-	-	25,000	0.7	-	28,571
19	IA	V	18	1	-	13	-	-	25,000	0.6	-	33,333
22	IA	V	90	1	L	-	-	-	-	8.0	-	2,500
22	IA	V	90	1	L	-	-	-	10,500	15.0	-	1,333
22	IA	V	24	1	L	-	-	-	-	2.0	-	10,000
23	I	200	100	1	S	15	-	-	-	39.2	-	510
23	I	200	90	1	S	15	-	-	-	32.2	-	621
23	I	200	80	1	S	15	-	-	-	10.2	-	1,961
23	I	200	70	1	S	15	-	-	-	3.7	-	5,405
23	I	200	60	1	S	15	-	-	-	1.5	-	13,333
23	I	200	22	1	L	8	2	154,000	22,000	-	-	77,000
23	I	450	22	1	L	1	1	21,334	21,334	-	4.0	12,500
23	II	200	22	1	L	2	2	9,000	5,500	-	-	4,000
1	VI	25,000	27	2	L	-	-	-	-	-	11.5	4,348
6	X	C	70	1	-	-	-	-	-	-	-	11,000
3	VI	11,000	22	3	L	63	0	636,552	10,104	-	-	(1)695,700
3	VI	11,000	65	3	L	9	0	90,936	10,104	-	-	(1) 99,384
3	VI	11,000	-35	3	L	9	0	90,936	10,104	-	-	(1) 99,384
3	VI	11,000	65 & -35	3	L	9	0	90,936	10,104	-	-	(1) 99,384
9	II	V	70	1	L	103	64	6,180	60	-	-	(4) 97
9	II	V	70	1	L	95	47	5,700	60	-	-	(5) 121
15	IA	V	18	1	S	-	-	-	>30,000	1.0	-	20,000
15	IA	V	55	1	S	4	-	16,000	4,000	0.7	-	28,571
15	IA	V	70	1	S	5	-	20,000	4,000	1.9	-	10,526
15	IA	V	90	1	S	4	-	16,000	4,000	9.0	-	2,222
18	X	V	25	1	L	6	-	12,000	2,000	6.0	-	3,333
18	X	0	25	1	S	-	-	500	500	0	-	-
18	X	50	25	1	S	-	-	500	500	15.0	-	1,333
18	X	75	25	1	S	-	-	25	500	27.0	-	741
18	X	100	25	1	S	-	-	10	500	36.0	-	556
24	VIIA	150	20	1	L	1	-	4,500	4,500	-	0.7	71,428
24	VIIA	C	70	1	S	-	-	-	-	-	-	1,050
24	VIIA	C	80	1	S	-	-	-	-	-	-	400
24	VIIA	C	90	1	S	-	-	-	-	-	-	650
24	VIIA	C	100	1	S	-	-	-	-	-	-	550
25	VIIA	150	22	1	L	1	-	-	12,300	1.2	3.2	15,625
25	VIIA	100	70	1	S	4	-	-	12,000		[illegible]	45,454
15	II	C	25	1	L	5	-	1,500	300		[illegible]	6,494
15	II	C	25	1	L	26	-	7,800	300		13.5	3,704
31	IX	V	70	1	L	30	18	237,190	11,500	-	-	9,300
29	I	V	70	1	L	12	0	120,000	10,000	1.7	-	11,765
29	I	V	70	5	L	15	0	150,000	10,000	0.7		28,377
29	I	V	70	4	L	7	0	70,000	10,000	0.5	-	40,000
29	I	V	70	6	L	8	0	80,000	10,000	0.4	-	80,000
30	X	120	60	1	L	3	-	17,100	5,700	3.7	-	5,405
30	X	195	60	1	L	4	-	4,000	1,000	29.1	-	687
28	I	V	70	1	L	40	35	190,000	10,000	-	-	4[illegible]6,000
28	I	V	70	1	L	12	7	48,000	4,000	-	-	4 6,357
29	I	V	70	1	L	5	0	2,605	521	-	-	4[illegible]12,332
28	I	V	-	-	-	19	0	-	-	-	-	-
25	VIIA	100	70	1	S	4	-	48,000	12,000	-	1.4	35,714
Totals							354	4,051,000				

NOTES:

(1) 60% Lower Confidence Level
(2) V - Current varied to maintain a set output
C - Current constant but magnitude is unknown
(3) 1 - CW (100% duty cycle)
2 - 5KHZ, 200 ns pulse (0.1% duty cycle)
3 - 500 HZ, 80 ns pulse (0.005% duty cycle)
4 - 10 MHZ, 20% duty cycle with 90% threshold current bias
5 - 10 MHZ, 60% duty cycle with 90% threshold current bias
6 - 10 MHZ, 50% duty cycle with 50% threshold current bias
(4) MTTF for self sustained oscillations
(5) MTTF for frequency shift
(6) L - Lasing mode
S - Spontaneous mode (LED)
(7) 'A' after ROMAN Numerial indicates that presence or absence of facet coating is unknown

7.1.5.1 Preliminary Model Development

The following preliminary failure rate model was developed entirely from the data and information extracted from the sources listed in the references:

Degradation Rate:

$$\tau_p = \tau_b \times \pi_C \times \pi_E \times \pi_F \times \pi_A \qquad (7.1\text{-}11)$$

where

τ_p = semiconductor laser optical power output degradation rate (%/1000 hours)
π_A = application factor
π_C = construction factor
π_E = environmental factor
π_F = duty cycle factor

$$\tau_b = AI^n \quad \exp\left[\frac{-E_a}{KT}\right] \qquad (7.1\text{-}12)$$

where

A = Constant
I = drive current
$1.5 \leq n \leq 2.0$
K = Boltzman's constant
T = Case temperature (^oK)
E_a = apparent activation energy

$0.3 \leq E_a \leq 1.1$

The rationale for the adoption of the degradation rate model form and the parameters included in the model is presented below.

A review of the literature disclosed that at least three of the failure mechanisms associated with semiconductor lasers, dark line defects (DLDs), dark spot defects (DSDs) and catastrophic facet damage, result in the rapid degradation of the device; and that a high temperature burn-in in the order of fifty to one hundred hours would eliminate most of the devices that would fail because of these mechanisms. The review also disclosed that the occurrence of DLDs and DSDs is a function of stresses that are induced by the process materials and/or by the manufacturing process. Another failure mechanism, ohmic contact degradation, has been found (reference 21) to be a function of the bond materials. A fifth failure mechanism, facet erosion, has been found to be a function of optical power density and the moisture or oxygen content of the atmosphere in contact with the facet where both increasing optical power density and the presence of oxygen or moisture increases the degradation rate of the laser. A good oxygen and moisture barrier, then, whether it is a facet coating or a hermetic package is important for device reliability. Therefore, because of the reasons listed above, a quality factor should be included in the failure rate model. There are, however, at this time no defined quality levels for semiconductor lasers. According to one semiconductor laser manufacturer, semiconductor lasers are still custom devices and any testing or screening that is performed varies considerably and is defined by the procurement specification. Because there are no defined quality levels and because most of the data collected are for non-packaged devices that were subjected to routine testing, no quality level factors could be developed that are a function of test or screen level.

Data were collected from several sources (reference 13, 15, 23) that showed a correlation between laser performance and the presence or absence of facet coatings. These data are as follows: Reference 13 shows a 7.6:1 improvement factor, reference 23 shows a 1.7:1 improvement factor and reference 15 shows a 1.8:1 improvement factor. The geometric average of the degradation rate given in these three references for Al_2O_3 facet coated lasers and non-facet coated lasers is 2.3%/1000 hours and 6.6%/1000 hours respectively which gives a ratio of 2.9 or approximately 3.0. The tests were

performed on non-packaged devices. Since the facet coat protects the laser facet from the environment, the use of a hermetic package should provide similar protection. Based on these data the construction factors (π_C) shown in Table 7.1-9 were assumed.

TABLE 7.1-9: CONSTRUCTION FACTORS

Construction	π_C
Lower*	1.0
Plastic,** with Al_2O_3 Facet Coating	1.0
Plastic,** no Facet Coating	3.0

*Applies to all hermetic packaged devices
**Applies to all non-hermetic packaged devices

A review of the literature also disclosed that, except for the degradation that occurs because of facet erosion, facet damage, and to some extent DLDs and DSDs, the failure mechanisms and their activating influences that impact semiconductor lasers are the same as those that impact LEDs. These similarities; plus the fact that no field failure experience data were available to develop separate environmental factors for semiconductor lasers, led to the assumption that the environmental factors for Opto-electronic Devices given in MIL-HDBK-217D would adequately account for the reliability impact of environment on semiconductor lasers.

The duty cycle factor (π_F) is based on work performed by Yoshida et.al (reference 29) where they showed that the laser diode degradation rate was proportional to duty cycle, operating current and temperature. The duty cycle function was given as:

$$\text{Degradation rate} \propto (\text{duty cycle})^{0.5} \qquad (7.1\text{-}13)$$

This relationship was based on three data points; 20, 50 and 100% duty cycle, where the relative degradation rate, which is defined as the pulsed operating

degradation rate divided by the CW operating degradation rate, versus duty cycle measured is given in Table 7.1-10.

TABLE 7.1-10: DUTY CYCLE DEGRADATION RATES

Relative Degradation Rate				
Lower Bound	Measured Point Estimate	Upper Bound	Calculated	Duty Cycle (%)
--	1.0	--	1.0	100
0.16	0.38	0.96	0.71	50
0.17	0.27	0.45	0.45	20

The measured values shown above are approximations because they were extracted from a figure. The confidence limit used to generate the upper and lower bounds was not given. Based on these data the duty cycle factors SHOWN IN Table 7.1-11 were assumed.

TABLE 7.1-11: ASSUMED DUTY CYCLE FACTORS

Duty Cycle (%)	π_F
100	1.0
90	0.95
80	0.90
70	0.85
60	0.75
50	0.70
40	0.65
30	0.55
20	0.45
10	0.30

The application factor (π_A) is based on work performed by Ettenberg, et.al. (Ref. 10) where one of their studies was a comparison of laser

lifetime considering two definitions of failure; the first when the laser drops to half its initial output at constant current and the second where the laser can no longer emit 1.25mw at the 70°C heat sink temperature. The tests were conducted on 40 low-threshold (≈50ma) oxide-defined stripe lasers. The operating conditions were initial power output ≈4mw CW at 70°C heat sink temperature. The median times-to-failure were:

Time to 50% Power Degradation - 1900 hours
Time to <1.25 mw output - 3800 hours

If a linear degradation rate is assumed, the degradation rates for the two failure definitions are:

Time to 50% Power Degradation = ((4-2)/4)/1000 hours or 26.3%/1000 hours
Time to <1.25 mw output = ((4-1.25)/4)/3800 hours or 18.1%/1000 hours

These two failure definitions correspond to two possible laser circuit designs -constant current and variable current with an optical feedback circuit. Based on the data given above the two application factors shown in Table 7.1-12 were assumed.

TABLE 7.1-12: APPLICATION FACTORS

Application	π_A
Variable Current W Optical Feedback	1.0
Constant Current	1.5

Of course, if optical feedback is employed, additional external components would be required for the design. The application factor can then be used by the circuit designer to perform reliability trade-off studies.

The base degradation rate factor, τ_b, has been found to be a function of temperature, drive current, optical power density, laser construction and definition of failure. The greatest difficulties encountered during the

model development were grouping and cataloguing the various lasers used in the lifetests, and determining a common definition of failure that would be applicable for all device types. The following table defines the lasers that were used for the derivation of the base degradation rate (τ_b). These lasers were grouped into one of the categories given in Table 7.1-13.

TABLE 7.1-13: LASER CATEGORIES

Device Type	Laser Construction
I	AlGaAs DH Stripe with facet coat
II	AlGaAs DH Spripe w/o facet coat
III	AlGaAs DH Stripe hermetic package
IV	GaAs SH Stripe with facet coat
V	GaAs SH Stripe w/o facet coat
VI	GaAs SH Strip hermetic package
VII	InGaAs/InGaAsP DH Stripe with facet coat
VIII	InGaAs/InGaAsP DH Stripe w/o facet coat
IX	AlGaAs DH V-Groove Stripe with facet coat
X	AlGaAs DH with Stripe w/o facet coat
X	AlGaAs DH with buffered Stripe w/o facet coat
X	AlGaAs DH V-Groove Stripe w/o facet coat

The definition of failure used throughout most of the life tests was that optical power output had degraded a set amount, usually 50%. Two methods of tests were used. One was that current was held constant; the second was that current was increased and device case temperature held constant until the device failed to generate a set output usually 30-50% of initial at a maximum current level. References 10 and 23 equated a 20% threshold increase to a 50% reduction in power output. This rationale was used to equate the two failure definitions.

Table 7.1-8 lists the data extracted from the references. It should be noted that the measured numerics are, in most cases, approximations since they were extracted from figures shown in the reference.

The degradation rate model developed herein can be used to predict the degradation rate of the laser due to facet degradation, contact deterioration, dark line defects, dark spot defects and homogeneous degradation. It will not predict the expected number of failures due to self-sustained oscillations and/or frequency shifts or waveshape changes. The following paragraphs discuss the magnitude of these last two failure modes.

Paoli (reference 9) conducted experiments that showed that 62% of a group of laser diodes, which were initially stable, exhibted pulsations and that 49% of the same group of laser diodes exhibited a change in the emission symmetry of the light polarized perpendicular to the junction plane (TM) following a 50-60 hour, 70°C burn-in. The actual test data showed that 64 out of 103 devices exhibited pulsations after the burn-in. The literature also stated that there were many other devices that exhibited pulsations prior to the burn-in. The exact number was not given, but the percentages were 16, 30, 24 and 5% from wafers A, B, C and D respectively. If the number of samples from wafers A, B, C and D subjected to the burn-in were increased by the percentages given, then the actual number of failures would be 88 failures out of 127 devices. Relating this to a failure rate based on the 50-60 hour burn-in gives 69.3%/55 hour or 12,600F/10^6 hours. The χ^2 80% confidence limits about this estimate are 11,024F/10^6 hours and 14,316F/10^6 hours.

The actual test data showed that 47 out of 95 devices exhibited a TM Emission Symmetry change during the 50-60 hour burn-in. This corresponds to a 49.5%/55 hour or 9,000F/10^6 hour failure rate. The 80% confidence limits about this estimate are 7,560F/10^6 hour and 10,718F/10^6 hours.

The results of this study showed that a large percentage of devices exhibited these failure modes during the first 50 hours of a high temperature burn-in, and, therefore, that a 70°C, 60-hour burn-in and screen would eliminate a large portion of the devices that could possibly fail due to these failure modes.

Another study (reference 28) also showed that SSOs are a major failure mode; however, this study indicated that a longer burn-in (>500 hours) may be required to screen out the susceptible devices. The data shown in Table 7.1-14 were generated during the study.

TABLE 7.1-14: SSO DISTRIBUTION

Following these test Conditions	STRONG SSO	WEAK SSO	NO SSO	TOTAL
Degraded (1)	10	8	12	30
Aged 4000 hours (2)	4	3	5	12
Aged 521 hours (2)	0	0	5	5
No Aging	0	0	18	18
Total	14	11	40	65

Notes: 1) Lasers that had failed to generate a minimum stimulated emission at 70°C during a 70°C life test but which continued to operate CW at room temperature.

2) Aging was at 70°C with no appreciable degradation.

As can be seen the percentage of lasers that exhibited SSOs is approximately the same for the degraded and the aged 4000 hour devices (60% and 58%).

Based on the data given above, it is obvious that SSOs and TM emission symmetry changes are major failure modes; however, insufficient data were available to allow for their incorporation into the failure rate prediction model. It is proposed that the model be defined as excluding these failure modes. It is recommended that, if these failure modes could result in a circuit failure, that the devices be screened to eliminate any devices exhibiting SSOs and that the screen include a 70°C burn-in of at least 60 hours duration. As was mentioned previously, data were not available to derive a factor for the predicton model that would account for these failure modes. This was because, except for the two references listed above, the

life tests did not address these failure modes, and the data given in these two references were somewhat contradictory.

The data shown in Table 7.1-15 is given to aid the designer in assigning a failure numeric for these failure modes.

TABLE 7.1-15: FUNCTIONAL DEGRADATION MODE DISTRIBUTION

Failure Mode	Ref	Percentage of devices that failed during: 60 hour 70°C Screen	521 hour 70°C Screen	4000 hour 70°C Screen
TM Emission Symmetry change	9	49.3	---	---
SSOs	9	69.3	---	---
SSOs	28	---	0.0	58.3

This failure numeric would be an additive factor in that it would be considered along with the failure rate generated by the failure rate prediction model. If the limited 4000 hour data were used, an average failure rate of 58.3%/4000 hours or 146F/10^6hours would be added to the failure rate generated by the failure rate prediction model to account for the SSO failure mode. By comparison, the failure rate generated by the prediction model for a AlGaAs facet coated DH stripe laser used in a ground, fixed environment at 55°C with a fixed dc current source at 100ma and the allowable degradation is 50% or 266 F/10^6 hours. It should be noted again that the potential contribution of this failure mode to the device failure rate is significant, but that it may be controllable by the circuit design.

7.1.5.2 Model Refinement

Model refinement consisted in fitting the data shown in Table 7.1-8 to the preliminary model forms. The regression technique described in Section 3.1 was used to fit the data.

Due to the limited amount of data, it was necessary to fix the parameter E_a at 0.4ev for GaAs and AlGaAs devices. The value of 0.4ev for E_a was chosen for GaAs and AlGaAs devices since it agrees with the results obtained by Ritchie et. al. (Ref. 8) when both the Arrhenius relationship and current are considered in the degradation model with the current factor normalized out.

The data in Table 7.1-8 for device types, I, II, III, IV, V, VI, IX, and X were regressed (regression No. 1) to develop the application factor π_A, the duty cycle factor (π_F), the construction factor (π_C) and current factor (I^n). The data for device types I, II, III, IV, V and VI were then regressed with degradation rate as the dependent variable (regression No. 2) to develop the base degradation rate factor (τ_b) for the AlGaAs and GaAs devices. The data for device types VII and VIII were regressed (regression No. 3) to develop the temperature relationship (E_a) and base degradation rate (τ_b) for the InGaAs/InGaAsP devices. In the second and third regressions the factors π_A, π_F, π_C and I^n were fixed at the values derived in the first regression. The purpose of the second and third regressions was to obtain the temperature relationship since the literature (Ref. 10, 16, 20) indicated that InGaAs/InGaAsP devices were more temperature sensitive than the GaAs and AlGaAs devices.

The results of the regression were:

$$\tau_p = \tau_b \times \pi_T \times I^n \times \pi_C \times \pi_A \times \pi_F \qquad (7.1\text{-}14)$$

where

τ_p = semiconductor laser degradation rate (%/1000 hours)
τ_b = base degradation rate (%/1000 hours)
π_T = temperature factor

$$= \exp\left[\frac{-E}{(T + 273)}\right], \quad T = \text{Case Temp } (^oC), \; E = Ea/K$$

I = current (ma)

and where

n = constant of regression
π_C = construction factor
π_A = application factor
π_F = duty cycle factor
= F^m

and where

F = duty cycle
m = constant of regression

and with the constants as shown in Table 7.1-16 where the standard error statistic was used to calculate confidence intervals about the derived factors where possible.

TABLE 7.1-16: MODEL CONSTANTS

(A) π_C, Construction Factor

Construction	π_C		
	L 20% Limit	PT EST	U 80% Limit
Facet Coat or Hermetic	--	1.0	--
W/O Facet Coat	2.1	3.3	5.1

(B) π_A, Application Factor

Application	π_A		
	L 20% Limit	PT EST	U 80% Limit
Variable Current Source with optical feedback	--	1.0	--
Fixed Current Source	0.90	1.5	2.44

(C) π_I, Current Factor

Device Type	n		
	L 20% Limit	PT EST	U 80% Limit
AlGaAs	0.12	0.68	1.23
GaAs	0.12	0.68	1.23
InGaAs/InGaAsP	0.12	0.68	1.23

(D) τ_b, Base Degradation Rate

Device Type	τ_b (X 10^5)		
	L 20% Limit	PT EST	U 80% Limit
AlGaAs	--	1.534	--
GaAs	1.095	1.952	3.481
InGaAs/InGaAsP	--	130.9	--

(E) π_T, Temperature Factor

Device Type	E*		
	L 20% Limit	PT EST	U 80% Limit
AlGaAs	--	-4635	--
GaAs	--	-4635	--
InGaAs/InGaAsP	-11390	-5784	-3687

* E = Apparent Activation Energy (EA)/Boltzman's constant (8.63 X 10^{-5})

(F) π_F, Duty Cycle Factor

	m	
L 20% Limit	PT EST	U 80% Limit
0.15	0.50	0.84

In order to derive a prediction model for a non-constant failure rate device, an expression for the hazard function (in time) is required. For practical purposes, it is required to express this as a cumulative average over time; i.e., $\frac{1}{t}\int_0^t h(u)\,du$, where h(u) is the hazard function and u a dummy variable for integration.

We require an expression for

$$H(t) = \frac{1}{t} \int_0^t h(u)\, du \qquad (7.1\text{-}16)$$

where $h(u) = \dfrac{f(u)}{1 - F(u)}$

and where f(u) is the failure (probability) density function and F(u) is the associated cumulative density function.

So, for example, if f(u) is exponential,

$$h(u) = \frac{\lambda e^{-\lambda u}}{1 - (1 - e^{-\lambda u})} \qquad (7.1\text{-}17)$$

$$\frac{\lambda e^{-\lambda u}}{e^{-\lambda u}} = \lambda, \text{ as expected}$$

so, $H(t) = \dfrac{\lambda t}{t} = \lambda$, again as expected.

However if the p.d.f. is lognormal,

$$f(u) = \frac{1}{2\pi\, \sigma\, u}\, e^{-\frac{1}{2}\left(\frac{\ln u - \mu}{\sigma}\right)^2} \qquad (7.1\text{-}18)$$

where μ and σ are respectively the mean and standard deviation of the associated normal distribution of ln u;

then

$$H(t) = \frac{1}{t} \int_0^t \frac{f(u)}{1 - \int_0^u f(v)\, dv}\, du \qquad (7.1\text{-}19)$$

where v is a second dummy variable of integration

Clearly, solution of 7.1-19 will be analytically tedious, and probably impossible (given the difficulty of solving even the regular normal integral).

Weibull approximation

The similar shapes of the lognormal and Weibull over certain ranges of σ and β, suggest that the readily soluble Weibull hazard may be appropriate. This approach was investigated. The approach is discussed in the following paragraphs. The data given in Table 7.1-17 were available with times-to-failure, median life(u) and standard deviation (σ). Table 7.1-17 also lists the Weibull and lognormal parameters for the data sets.

TABLE 7.1-17: WEIBULL AND LOGNORMAL PARAMETERS COMPARISONS

Ref	Log Normal Parameters		Weibull Parameters	
	μ	σ	θ	β
10	80000	15500	90000	1.15
10(1)	1900	550	3000	1.05
10(1)	3800	1250	5800	1.10
14	40000	2000	33500	0.65
17	4500	800	5000	0.95
19	74000	22000	105000	1.40
31	8800	1650	13000	0.80
31	11000	4450	13500	1.50

Notes: (1) Same devices with different failure criteria.

The data were graphed on Weibull probability paper giving the Weibull estimates for characteristic life (θ) and slope (B) shown above. The Kolmogorov-Smirnov (K-S) test described in Section 3.1 was used on the data given above to determine if the Weibull slope was significantly different from 1.0. The results of the test are given in Table 7.1-18.

TABLE 7.1-18: K-S TEST RESULTS

Ref	No. of Failures	Maximum Deviation	K-S Statistic (0.2 Significance Level)	Conclusion
10	7	.04	.40	No Difference
10	37	.14	.18	No Difference
10	38	.06	.17	No Difference
14	22	.21	.23	No Difference
17	74	.05	.12	No Difference
19	15	.27	.28	No Difference
31	9	.10	.36	No Difference
31	9	.10	.36	No Difference

Based on the results of the K-S test, it was assumed that the failure distribution of semiconductor laser could be described by a Weibull slope of 1.0.

The degradation rate equation, 7.1-14 described previously, was derived from the time to 50% failure (median life) of the devices. The Weibull Characteristic life (θ) is the time to 63% failure. The median life estimate was converted to a characteristic life estimate by revising the base degradation rate (τ_b) constant. The technique used and the revision factor is given below:

Given: τ = time to 50% failures

$$F(t) = 1 - \exp\left[-(t/\theta)^B\right] \qquad (7.1\text{-}20)$$

θ = time to 63% failures

B = 1.0

t = τ = time to 50% failures

Then: $.5 = 1 - e^{-\tau/\theta}$

$= e^{-t/\theta}$

or: $\theta = 1.44\ \tau$ (7.1-21)

The following (average Weibull hazard rate) equation was then used to derive an estimate of the failure rate:

$$\lambda_{avg} = \frac{T^{b-1}}{\theta^b} \qquad (7.1\text{-}22)$$

where

T = operating time

b = Weibull slope

θ = Characteristic life

λ_{avg} = Average hazard rate

For the semiconductor laser

b = 1, and
$\theta = \tau_p$

Giving

$$\lambda_{avg} = 1/\tau_p \qquad (7.1\text{-}23)$$

The relationship $1/\tau_p$ was set equal to λ_D. Since the data used to derive this factor were all life test data, since the physics of failure information extracted from the literature suggests that environment may have a significant impact on the failure rate of these devices, and since the same information suggests that the failure modes of LEDs are similar to these for semiconductor lasers, the LED environmental factor was incorporated into the prediction model. The proposed model for semiconductor lasers is then

$$\lambda_p = \lambda_D \pi_E \qquad (7.1\text{-}24)$$

7.1.6 References

1. RCA, Solid State IR Emitters and Injection Lasers, OPT-113C, October 1979.

2. RCA, Optical Communications Products - Solid State IR Emitters, Lasers, Photodiodes and Systems, OPT-115, June 1979.

3. Feldhake, Leo, Naval Electronics Center, Indianapolis Ind., Telephone Conversation, 19 May 1982.

4. Svacek, Joseph F., Transmitter feedback techniques stablize laser-diode output, EDN, March 5, 1980, p 107.

5. Ito, Ryolchi, Nakashima, Hisao, Etal., Degradation Sources in GaAs - AlGaAs Double - Heterostructure Lasers, IEEE Journal of Quantum Electronics, Vol QE-11, July 1975, pp. 551-556.

6. Wolk, Claus, Gottsmann, Hartmut, etal., Criteria for Designing V-Groove Lasers, IEEE Journal of Quantum Electronics, Vol. QE-17, No. 5, May 1981, pp. 756-758.

7. Hwang, C.J. and Svacek, Joseph S., Long lived diode lasers, Laser Focus, June 1979.

8. Ritchie, S., Godfrey, R.F., etal., The temperature dependence of degradation mechanisms in long-lived (GaAl) As DH lasers, Journal of Applied Physics, June 1978, pp. 3127-3132.

9. Paoli, Thomas L., Changes in the Optical Properties of CW (AlGa)As Junction Lasers During Accelerated Aging, IEEE Journal of Quantum Electronics, Vol QE-113, May 1977, pp. 351-359.

10. Ettenberg, Michael and Kressel, Henry, The Reliability of (AlGa)As CW Laser Diodes, IEEE Journal of Quantum Electronics, Vol. QE-16, No. 2., February 1980, pp. 186-196.

11. DeLoach Jr., B.C., Hakki, B.W., etal., Degradation of CW GaAs Double-Heterojunction Lasers at 300K, Proceedings of IEEE, Vol. 61, July 1973, pp. 1042-1044.

12. Barnes, C.E., Neutron Damage in Epitaxial GaAs Laser Diodes, Journal of Applied Physics, Vol. 42, No. 1, April 1971, pp. 1941-1949.

13. Ladany, I., Ettenberg, M., etal., Al_2O_3 half-wave films for long-life CW lasers, Applied Physics Letters, Vol. 30, January 1977, pp. 87-88.

14. Thompson, Alan, The Reliability of a Practical $Ga_{1-x}Al_xAs$ Laser Device, IEEE Journal of Quantum Electronics, Vol. QE-15, No. 1, January 1979, pp. 11-13.

15. Newman, D.H. and Ritchie, S., Degradation Pnenomena in Gallium Aluminium Arsenide Stripe Geometry Lasers, Cqechoslovak Journal of Physics, Vol. B30, 1980, pp. 336-344.

16. Newman, D.H. and Ritchie, S. Reliability and Degradation, Chapter 6, Reliability and degradation of lasers and LEDs, John Wiley and Sons, 1981, pp. 301-361.

17. Hartman, R.L., Schumaker, N.E. and Dixon, R.W., Continuously Operated (Al, Ga) As double-heterostructure lasers with 70°C lifetimes as long as two years, Applied Physics Letters, Vol. 31, December 1977, pp. 756-759.

18. Kobayashi, Takeshi and Furukawa, Yoshitaka, Recombination Enhanced Annealing Effect in AlGaAs/GaAs Remote Junction Heterostructure Lasers, IEEE Journal of Quantum Electronics, Vol. QE-15, No. 8, August 1979, pp. 674-684.

19. Kirkby, P.A. and Cox, A.A., GaAs Lasers - A Family of Laser Structures Emerging for New Applications, Microelectronics Reliability Vol. 19, 1980, pp. 633-644.

20. Yamakoshi, S., Abe, Masayaki, etal., Reliability of High Radiance InGaAsP/InP LEDs Operating in the 1.2-1.3um Wavelength, IEEE Journal of Quantum Electronics, Vol. QE-17, No. 2, February 1981, pp. 167-173.

21. Goddard Space Flight Center, Product Assurance Briefs, PAB No. 82-01, March 31, 1982.

22. Robertson, M.J., Wakefield, B. and Hutchinson, P., Strain-related degradation phenomena in long-lived GaAlAs stripe lasers, Journal of Applied Physics, Vol. 52, No. 7, July 1981, pp. 4462-4466.

23. Kressel, H., Ettenberg, M. and Ladany, I., Accelerated step-temperature aging of Al_xGa_{1-x} As heterojunction laser diodes, Applied Physics Letters, Vol. 32, March 1978, pp. 305-308.

24. Olsen, G.H., Nuese, C.J. and Ettenberg, M., Reliability of Vapor-Grown InGaAs and InGaAsP Heterojunction Laser Structures, IEEE Journal of Quantum Electronics, Vol. QE-15, No. 8, August 1979, pp. 688-693.

25. Olsen, G.H., InGaAsP laser Diodes, SPIE, Vol. 224, Fiber Optics for Communications and Control, 1980, pp. 113-121.

26. Botez, D. and Herskowitz, G.J., Components for Optical Communications Systems: A Review, Proceedings of the IEEE, Vol. 68, No. 6, June 1980, pp. 689-731.

27. Ettenberg, M., A Statistical study of the reliability of oxide-defined stripe CW lasers of (AlGa) As, Journal of Applied Physics, Vol. 50, No. 3, March 1979, pp. 1195-1202.

28. Channin, D.J., Ettenberg, M. and Kressel, H., Self-sustained oscillations in (AlGa)As oxide-defined stripe lasers, Journal of Applied Physics, Vol. 50, No. 11, November 1979, pp. 6700-6706.

29. Yoshida, Jun-Ichi, etal., Degradation Behavior of AlGaAs Double-Heterostructure Laser Diodes Aged Under Pulsed Operating Conditions, IEEE Journal of Quantum Electronics, Vol. QE-18, No. 5, May 1982, pp. 879-884.

30. Shimizu, Hirokazu, etal., Improvement in Operation Lives of GaAlAs Visable Lasers by Introducing GaAlAs Buffer Layers, IEEE Journal of Quantum Electronics, Vol. QE-17, No. 5, May 1981, pp. 763-767.

31. Arnold, Gunther, etal., Long-Term Behavior of V-Groove Lasers at Elevated Temperature, IEEE Journal of Quantum Electronics, Vol. QE-17, No. 5, May 1981, pp. 759-762.

7.2 Helium-Cadmium Lasers

7.2.1 Device Construction

The helium-cadium (He-Cd) laser is a low current, high voltage, continuous wave, gas discharge laser. The laser exits a single blue line at 442 nm. Typical tube currents are in the 50-100ma region, and typical tube voltages are in the 1.5KV range. Current density in the bore is $\simeq 4A/CM^2$, dissipation $\simeq 3W/CM$ of length and gas pressure are $\simeq 6$ Torr. Power outputs range from 5 to 50 mw. Total tube dissipation is quite low and units are cooled by natural convection (Ref 1). The construction of a He-Cd laser tube is shown in Figure 7.2-1. The primary uses of He-Cd lasers are commercial recorders, reprographics, spectroscopy and Q/A scanning.

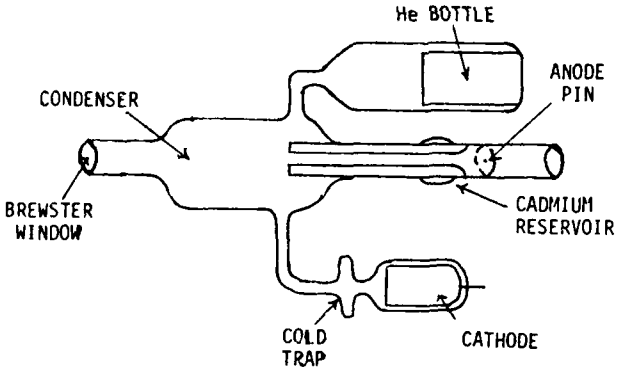

FIGURE 7.2-1: HELIUM-CADMIUM LASER TUBE

Principle design considerations relating to the lifetime of the device include (Ref 1):

- o Minimizing He gas cleanup via depositing Cd metal and cathode sputtering,

- o Maintaining a uniform mix of He gas and Cd vapor in the discharge,
- o Protection of Brewster windows from condensing Cd, and
- o Blockage of the optical path by deposits of Cd.

7.2.2 Failure Modes/Mechanisms

The primary failure modes and associated mechanisms of a He-Cd laser are:

- o Power output degradation
  - Helium gas loss due to
    - o cathode sputtering
    - o burial of He under condensing Cd
    - o wall diffusion
  - Cadmium depletion from the reservior
    - o normal vaporization
    - o cataphoretic transport down the bore to the condenser
  - Discharge contamination by impure gases resulting from materials out gassing or incomplete processing
  - Growth of Cd deposits into the optical beam in the vicinity of the condenser
- o Filament Failure
- o Rapid gas loss
  - Glass Crack
  - Seal Leak
- o Resonator/Beam Misalignment

Failure mechanism distributions reported by two data sources are presented in Table 7.2-1 along with a distribution based on the combined results.

TABLE 7.2-1: HELIUM-CADMIUM FAILURE MECHANISM DISTRIBUTION

Failure Mechanism	Source 2		Source 1		Combined (1)	
	Number Failures	Percent Cont.	Number Failures	Percent Cont.	Number Failures	Percent Cont.
Cadmium Depletion	28	35.5	1	9.1	29	24.6
Condenser Blockage	35	44.3	--	--	35	25.9
Helium Depletion	1	1.3	2	18.2	3	8.3
Resonator/Beam Misalign	3	3.8	--	--	--	--
Filament Failure	2	2.5	--	--	--	1.1
Plasma Tube Leak	2	2.5	--	--	--	--
Over Pressure Tube	3	3.8	--	--	3	2.2
Miscellaneous	5	6.3	--	--	--	4.0
Glass Crack	--	--	6	54.5	8	24.5
Cathode Contaminated	--	--	1	9.1	1	3.8
Tube Alignment/ glass stress	--	--	1	9.1	4	5.6
TOTALS	**79**	**100.0**	**11**	**100.0**	**90**	**100.0**

Notes: (1) Combined calculated using following assumption:

- o Plasma tube leak = Glass crack
- o Resonator/Beam Misalign = Tube Alignment/glass stress
- o Percent contribution weighted by operating hours because of wearout mechanisms

$$\% \text{ Cont.} = \frac{FR(\text{Source one}) + FR(\text{Source two})}{\text{Total Failure Rate (Source one + Source two)}}$$

7.2.3 Helium-Cadmium Failure Rate Model

$$\lambda_{He\text{-}Cd} = \pi_E \lambda_{MEDIA} + \pi_E \lambda_{COUPLING}$$

where

$\lambda_{He\text{-}Cd}$ = helium-cadmium laser failure rate in f/10^6 operating hours.
π_E = environmental application factor, determined from Table 7.2-2.
λ_{MEDIA} = failure rate contribution of the lasing media.
= 228 failures/10^6 operating hours.
$\lambda_{COUPLING}$ = failure rate contribution of the laser coupling hardware.
= 0.1 failures/10^6 operating hours.

It should be noted that the helium-cadmium laser failure rate prediction model can be simplified and rewritten as:

$$\lambda_{He\text{-}Cd} = 228.1 \pi_E$$

7.2.4 Model Development

The approach utilized was to hypothesize a model form based on the theory of operation and physics of failure of the laser. Data were collected; however, there was insufficient data to support this preliminary model form. It was then considered appropriate to adopt the model form of the current Helium-Neon laser. This is a realistic assumption because of the similarity in construction and application between the two laser types. A unique media parameter was then derived for the helium-cadium laser.

The following preliminary model was hypothesized:

$$\lambda_{He\text{-}Cd} = \lambda_c + \lambda_d$$

TABLE 7.2-2: ENVIRONMENTAL MODE FACTORS

Environment	π_E	Environment	π_E
G_B	0.2	A_{IA}	5
G_F	1	A_{IF}	7
G_M	5	A_{UC}	6
M_P	2.3	A_{UT}	5
N_{SB}	1.1	A_{UB}	10
N_S	5	A_{UA}	8
N_U	5	A_{UF}	10
N_H	3.6	S_F	0.2
N_{UU}	3.9	M_{FF}	2.4
A_{RW}	5.2	M_{FA}	3.3
A_{IC}	3	U_{SL}	7.0
A_{IT}	3	M_L	8
A_{IB}	6.5	C_L	N/A

where

$\lambda_{He\text{-}Cd}$ = helium-cadmium laser failure rate in failures/10^6 operating hours.

λ_c = random failure rate contribution (F/10^6 hours)

λ_d = average degradation failure rate contribution (F/10^6 hours)

$$\lambda_d = \frac{1}{(T_2 - T_1)} \int_{T_1}^{T_2} h(t)\, dt$$

where

$T_2 - T_1$ = operate time or replacement interval

$h(t)$ = the hazard rate function

Empirical data were received from two proprietary sources. The source 1 data shown in Table 7.2-3 are life test times-to-failure on 18 devices.

TABLE 7.2-3: LIFE TEST TIME-TO-FAILURE

Device	Time-To-Failure (hours)
1	500
2	1000
3	2400
4	2840
5	2908
6	3200
7	4190
8	4196
9	4300
10	4500
11	5100
12-18	Did not fail
Total Hours	58198

The definition of failure used was when the power output of the tube dropped to less than 50% of specified power. The tubes tested were all nominally 10MW specified power. These laser tubes are terminated in Brewster windows. Two cavity mirrors are used; a flat high reflector and a 60cm (curvature) output coupler. No failures were recorded on the optics. Six of the failures (Pin s l failures (glass crack)) were identified as attributed to manufacturing errors (infant mortality) that have been eliminated, one (1) was tube alignment thai is probably a random failure, and four (4) were wearout failures.

The source 2 data shown in Tab'e 7.2-4 are field experience data on 100 devices used in a commercial environment. The de. inition of failure used was when the power output of the tube dropped to 60% :f the original output power. Thirteen (13) of the 79 failures were infant mortality failures (≈0 operate hours), two (2) were random failures and 64 were wearout failures.

Table 7.2-4 also shows the failure experience data from source 1 and failure rate estimates for both data sources.

TABLE 7.2-4: EMPIRICAL FAILURE DATA

Source	Sample Size	No. Failed	Device Operate Hours	Failure Rate ($F/10^6$ hours) L10% CL	PT EST	U90% CL	Environment
2	100	79	300,000	226	263	306	GF
1	18	11	58,198	121	189	285	GB

The time-to-failure data from source 1 were plotted on Weibull probability paper (Figure 7.2-2). A linear regression of the data gave a best fit estimate of the median life and slope of 6800 hours and 1.3 respectively. A slope of 1.3 indicates a slightly increasing hazard rate relatively close to a slope of 1.0 which indicates a constant hazard rate. The Weibull hazard rate function is:

$$H(t) = \frac{b}{\Theta b} (t)^{b-1} \qquad (7.2\text{-}1)$$

where from the data

$\Theta = 6800$

$b = 1.3$

t = operate time

An average failure rate for the life of the device could be calculated from the TTF data as follows:

$$\lambda_{avg} = \frac{1}{T} \int_0^T h(t)\, dt \qquad (7.2\text{-}2)$$

or

$$\lambda_{avg} = \frac{T^{b-1}}{\Theta b}$$

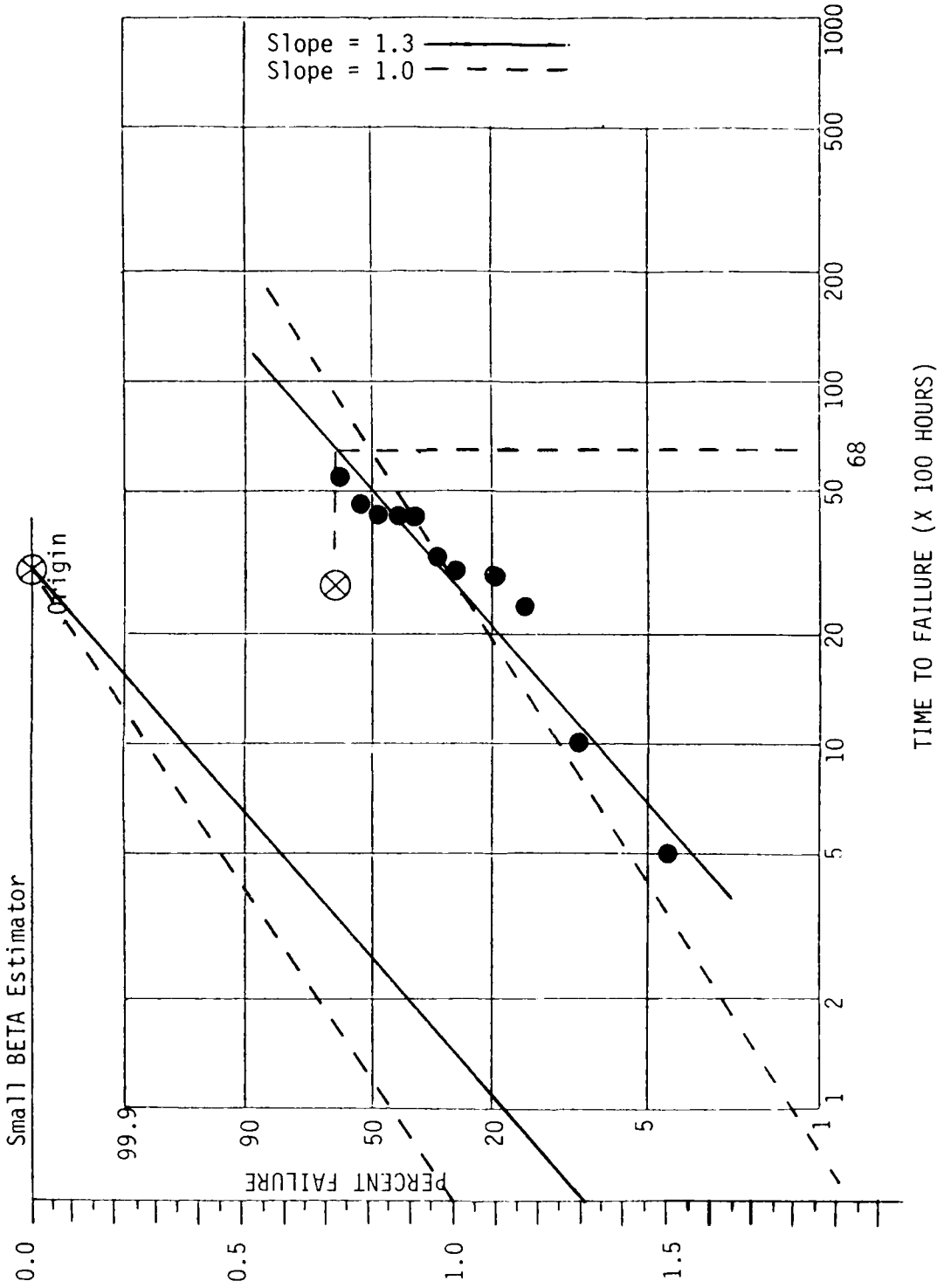

FIGURE 7.2-2: WEIBULL PLOT SOURCE 1 LIFE TEST DATA

Since only one data point was available with time to failure data, a time dependent model of this form was not deemed appropriate. A line was drawn through the data with a slope of 1.0 (Figure 7.2-2). The Kolmogorov-Smirnov (K-S) test described in Section 3.1 was used to determine if the data were significantly different from a distribution with a slope of 1.0. The conclusion of the test was that there was no significant difference at the 0.2 significance level. Therefore the assumption of an exponential failure rate model does not introduce significant errors.

It was then assumed that the following model which was derived from the He-Ne model was correct except for the media failure rate contribution. This is an accurate assumption because of the similarity in construction and application between the two laser types.

$$\lambda_{He\text{-}Cd} = \pi_E(\lambda_{Media} + \lambda_{Coupling})$$

where

$\lambda_{He\text{-}Cd}$ = helium-cadmium laser failure rate in f/10^6 operating hours
π_E = environmental factor (Table 7.2-2)
λ_{Media} = failure rate contribution of the lasing media
$\lambda_{Coupling}$ = failure rate contribution of the laser coupling hardware
= 0.1 failures/10^6 operating hours

The data in Table 7.2-4 were then categorized by infant mortality, wearout and random failures. The life test data (π_E = 0.2) were normalized to the ground fixed environment (π_E = 1.0) by multiplying the operating hours by 0.2. The normalized hours were used to calculate an average wearout failure rate, a catastrophic (random failure) failure rate and a combined wearout and catastrophic failure rate (Table 7.2-5).

TABLE 7.2-5: NORMALIZED FAILURE RATES

Failure Type	No. Failed	Operate Hours	Failure Rate ($F/10^6$ hours) L10%CL	PT EST	U90%CL
Infant mortality	19	-	-	-	-
Random	3	311,640	3.5	9.6	21.4
Wearout	68	311,640	185.0	218.2	256.2
Random & Wearout	71	311,640	194	228	266

The random failure rate is 9.6 $F/10^6$ hours, and the average wearout failure rate is 218.2 $F/10^6$ hours. The MTTF for wearout failures is 4583 hours which is in agreement with published estimates (5000 hours) for the life of the tube (ref 3 and 4). λ_{media} was then determined to be 228 Failures/10^6 operating hours. The predicted and observed data are listed in Table 7.2-6. The observed data does not include the contribution of the infant mortality failures.

TABLE 7.2-6: PREDICTED/OBSERVED FAILURE RATES

		Failure Rate (Failures/10^6 hours)			
		Predicted		Observed	
Observation	Env		L10%CL	PT EST	U90%CL
1	G_B	45.6	42	86	159
2	G_F	228.1	186	220	259

7.2.5 References

1. Martin Marietta Aerospace, Laser Reliability Prediction, Final Technical Report, RADC-TR-75-210, August 1975.

2. Dowley, M.W., Reliability and Commercial Lasers, Applied Optics, Vol. 21, No. 10, May 1982.

3. Dowley, M.W., Helium Cadmium Lasers in Commercial Systems, Unpublished draft article.

4. Annon., Lasers and Applications, Laser Application Matrix, September 1982.

7.3 Helium-Neon Lasers

7.3.1 Device Construction

The helium-neon (He-Ne) laser is a low current, high voltage, continuous wave, gas discharge laser. The laser exhibits a single red line at 633nm. Typical tube currents are in the 5 ma region, and typical tube voltages are in the 10KV range. The He-Ne gas mixture is typically 6:1 at a pressure of 2-3 Torr. Power outputs range from 0.5 to 50 mw. The construction of a He-Ne laser tube is shown in Figure 7.3-1. The primary uses of He-Ne lasers are video discs, laser printers, communications, bar graph scanners, positional alignment, gyros and reprographics.

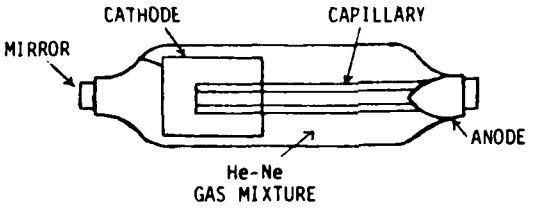

FIGURE 7.3-1: HELIUM-NEON LASER TUBE

7.3.2 Failure Modes/Mechanisms

The principal long-term failure mechanism is a progressive reduction in gas pressure and a change in the gas mix ratio. These changes result in a loss of power (Ref. 1). The loss of gas pressure is principally due to burial of gas under material sputtered from the cathode. A secondary loss is due to gas diffusion through the glass envelope. Cathode sputtering is due to energetic ions striking the cathode and knocking off atoms of cathode

material. It is intensified by the presence of impurities, particularly water vapor and hydrocarbons, in the gas discharge which can be present as a result of imperfect processing or result from partially leaking or outgassing seals (Ref. 1). A second time dependent failure mechanism is the degradation of the dielectric coatings exposed to the discharge. This mechanism is a function of the optical power output and is more prevalent with laser radiation density outputs approximately equal to $100w/CM^2$ (Ref. 1). $100w/CM^2$ corresponds to a laser with an output in the 7 to 10mw range.

7.3.3 Helium-Neon Failure Rate Model

$$\lambda_{He\text{-}Ne} = \pi_E \lambda_{MEDIA} + \pi_E \lambda_{COUPLING}$$

where

$\lambda_{He\text{-}Ne}$ = helium-neon laser failure rate in failures/10^6 operating hours.
π_E = environmental application factor, determined from Table 7.3-1.
λ_{MEDIA} = failure rate contribution of the lasing media.
= 84 failures/10^6 operating hours.
$\lambda_{COUPLING}$ = failure rate contribution of the laser coupling hardware.
= 0.1 failures/10^6 operating hours.

It should be noted that the helium-neon laser failure rate prediction model can be simplified and rewritten as:

$$\lambda_{He\text{-}Ne} = 84.1 \pi_E$$

7.3.4 Model Development

The approach utilized was to hypothesize a model form based on the theory of operation and physics of failure of the laser. Data were collected; however, there were insufficient data to support this preliminary model form. It was then necessary to adopt the current model form for the Helium-Neon laser. One exception is that the extended set of laser environmental

factors (π_E) given in RADC-TR-81-374 (Ref. 2) were adopted in lieu of the factors given in MIL-HDBK-217D.

TABLE 7.3-1: ENVIRONMENTAL MODE FACTORS

Environment	π_E	Environment	π_E
G_B	0.2	A_{IA}	5
G_F	1	A_{IF}	7
G_M	5	A_{UC}	6
M_P	2.3	A_{UT}	5
N_{SB}	1.1	A_{UB}	10
N_S	5	A_{UA}	8
N_U	5	A_{UF}	10
N_H	3.6	S_F	0.2
N_{UU}	3.9	M_{FF}	2.4
A_{RW}	5.2	M_{FA}	3.3
A_{IC}	3	U_{SL}	7.0
A_{IT}	3	M_L	8
A_{IB}	6.5	C_L	N/A

The following preliminary model was hypothesized:

$$\lambda_{He\text{-}Ne} = \lambda_c + \lambda_d$$

where

$\lambda_{He\text{-}Ne}$ = helium-neon laser failure rate ($F/10^6$ hrs)
λ_c = random failure rate contribution ($F/10^6$ hrs)
λ_d = average degradation failure rate contribution ($F/10^6$ hrs)

$$\lambda_c = \lambda_{media} + \lambda_{coupling}$$

where

λ_{media} = Laser tube catastrophic failure rate

$\lambda_{media} = \lambda_b \times \pi_Q \times \pi_E$

$\lambda_{coupling}$ = Laser optics catastrophic failure rate

$\lambda_{coupling} = \Sigma\lambda_{os}(i) \times \hat{\pi}_E \times \hat{\pi}_Q$ (os = optical surface)

and where

λ_b = base failure rate (function of tube construction and power rating)

π_Q = quality factor for laser tube

π_E = environmental factor for laser tube

$\lambda_{os}(i)$ = base failure rate for the optical surface (i). It is a function of the type of optics (lens, prism, etc.), its construction, and optical power density.

$\hat{\pi}_Q$ = quality factor for the optics

$\hat{\pi}_E$ = environmental factor for the optics

λ_d = laser tube and optics degradation failure rate

$$\lambda_d = \frac{1}{(T_2 - T_1)} \int_{T_1}^{T_2} h(t)\, dt$$

where

$T_2 - T_1$ = operate time or replacement interval

$h(t)$ = hazard rate and is a function of operate time, tube construction, tube power output, optical power density, tube and optics quality, cleanliness, and environment.

Empirical data were received from four sources, one of which is proprietary. The data summaries are shown in Table 7.3-2. The life test data ($\pi_E = 0.2$) were normalized to the ground fixed environment ($\pi_E = 1.0$) by multiplying the operating hours by 0.2. The normalized data were merged by

TABLE 7.3-2: HELIUM-NEON LASER DATA

Source	PWR (mw)	Env	Sample Size	No. Fail 100%	No. Fail 80%	Total Operate Hrs	Failure Rate (F/10^6 Hrs)(3) L 10%	PT EST	U 90%	Comments
1	2.0	G_F	2985	9	9(1)	4092000	1.3	2.2	3.5	Hand Held Bar Code Reader Avg 5 hrs/Day Operation. Top (MAX) for any device is 11,700 hrs. TAvg/device = 2,800 Hrs.
2	0.3	G_3	4	0	0	19948	--	46.2(4)	115.6	Life test data. Two definitions of failure, when power output drops below 100% and 80%.
	1.0	G_B	20	4	2	173682	3.1	11.5	30.6	
	2.0	G_B	4	1	0	63864	--	14.4(4)	36.1	
	2.0	G_B	28	5	3	233400	4.7	12.8	28.6	
3	0.5	G_B	5	4(2)	1(1,2)	110000	1.0	9.1	35.4	Life test data. Each device run for 22,000 hours.
4	2.0	G_F	1	0	0	200	--	4610(4)	11525	Field data on instrumentation equipment.
	3.0	G_F	1	0	0	300	--	3073(4)	7683	
	5.0	G_F	4	1	1(1)	8150	12.9	122.7	477.3	
	10.0	G_F	1	0	0	1200	--	768.3(4)	1921	
	50.0	G_F	1	1	1(1)	5500	19.2	181.8	707.3	
TOTAL	--	--	3054	25	17	4708244	2.5	3.6	5.0	

NOTES: (1) Field data with failure criteria unknown. Assumed equipment would operate until power dropped to 80%.
(2) Data extrapolated from a figure.
(3) Failure rates calculated on 80% power output failures.
(4) 60% upper confidence level.

source (Table 7.3-3). A homogeneity test for merging data from diverse sources (described in Section 3.1) was applied to the environmental normalized data. This test was applied because of uncertainty in the operating hour estimates for the source 1 data. The results indicate that the four data entries do not merge. Additionally the test indicated that the source 1 data was divergent from the other data entries. The homogeneity test was run a second time with the source 2,3 and 4 data. The second test indicated that these three data entries can be successfully merged. Results of the two homogeneity tests are presented in Table 7.3-4. As described in Section 3.1, the data entries can be successfully merged if the Kolmogrov-Smirnov (K-S) statistic is less than the K-S critical value. The 5% significance level was chosen for this test.

TABLE 7.3-3: NORMALIZED-MERGED DATA

Source	No.* Failed	Operate Hours	Failure Rate ($F/10^6$ hours) L10%CL	PT EST	U90%CL
1	9	4092000	1.3	2.2	3.5
2	5/10	98179	24.8/63.3	50.9/101.8	94.5/156.9
3	1/4	22000	4.8/79.3	45.4/181.8	176.7/363.4
4	2	15350	34.6	130.3	346.6
TOTAL	17/25	4227529	2.8/4.4	4.0/5.9	5.6/7.7

* Devices that failed to meet 80% of output power/devices that failed to meet 100% of output power

TABLE 7.3-4: HOMOGENEITY TEST

Test No.	No. of Data Entries	K-S Statistic	K-S Critical Value	Results
1	4	0.690	0.680	can not be merged
2	3	0.110	0.785	can be merged

The data from sources 2,3 and 4 were merged by the rated power of the tube (Table 7.3-5). The data were graphed (Figure 7.3-2). The graph suggested that the failure rate of the tube may be of the form:

$$\lambda_b = A\ P^B$$

A regression analysis (described in Section 3.1) was run on the source 2, 3 and 4 failure experience data. The $\leq$ 80% of rated power failure criteria was chosen since the literature (Ref. 1) indicated that most laser equipment designs have a built-in safety margin which will allow them to operate successfully as long as the output of the tube is greater than 80% of rated. The results of the regression are:

$$\lambda_b = 54.8\ P^{0.32}$$
$$R = 0.936 = \text{correlation coefficient}$$

where

λ_b = Ground fixed failure rate ($F/10^6$ hours)
P = rated tube power in milliwatts (mw)

The results of the regression are graphed in Figure 7.3-2. Although the regression indicated that the tube failure rate is a function of the tube rated power, it was felt that the data used to derive the equation were too sparse to include in the proposed failure rate equation.

TABLE 7.3-5: DATA MERGED BY TUBE RATED POWER

Rated Power (mw)	Sample Size	No. Failed	Operate Hours	Failure Rate ($F/10^6$ hours) L10%CL	PT EST	U90%CL
0.5	5	1	22000	4.8	45.4	176.8
1.0	20	2	34736	15.3	57.6	153.2
2.0	33	3	59653	18.4	50.3	112.0
5.0	4	1	8150	12.9	122.7	477.3
50.0	1	1	5500	19.2	181.8	707.3

The normalized data from Table 7.3-6 sources 2, 3 and 4 were merged to derive a revised estimate for the λ_{media} estimate currently in MIL-HDBK-217. Since the current MIL-HDBK-217 λ_{media} estimate of $84F/10^6$ hours lies within the 80% confidence interval of the data collected from sources 2, 3 and 4, there is no reason to reject the current estimate. Therefore it is proposed

that the current MIL-HDBK-217 estimate for λ_{media} be retained. The data listed in Table 7.3-2 were graphed vs the predicted failure rate (Figure 7.3-3). The 80% confidence interval or the upper 60% confidence limit are also shown on the graph. As can be seen by the graph the predicted value lies within the confidence bounds of 9 of the 11 data entries, and it lies above the other two data entries (prediction is pessimistic).

TABLE 7.3-6: REVISED λ_{media} ESTIMATE

Sample Size	No. Failed	Operate Hours	Failure Rate ($F/10^6$ hours) L10%CL	PT EST	U90%CL
69	8	135529	34.3	59.0	95.9

No optics failures were reported from the four data sources; hence no data were available to derive a revised estimate for the current MIL-HDBK-217 estimate for $\lambda_{coupling}$. Therefore it is proposed that the current MIL-HDBK-217 prediction model and estimate of $\lambda_{coupling}$ be retained.

7.3.5 References and Bibliography

References

1. Dowley, Mark W., Reliability and Commercial Lasers, Applied Optics, Vol. 21, No. 10, May, 1982.

2. IIT Research Institute, Avionic Environmental Factors for MIL-HDBK-217, Final Technical Report, RADC-TR-81-374, January, 1982.

Bibliography

Annon., Coherent Announces Automated Manufacture of Helium Neon Lasers, Product Brochure, 1982.

Dowley, Mark W., Reliability and Commercial Lasers, Applied Optics, Vol. 21, No. 10, May, 1982.

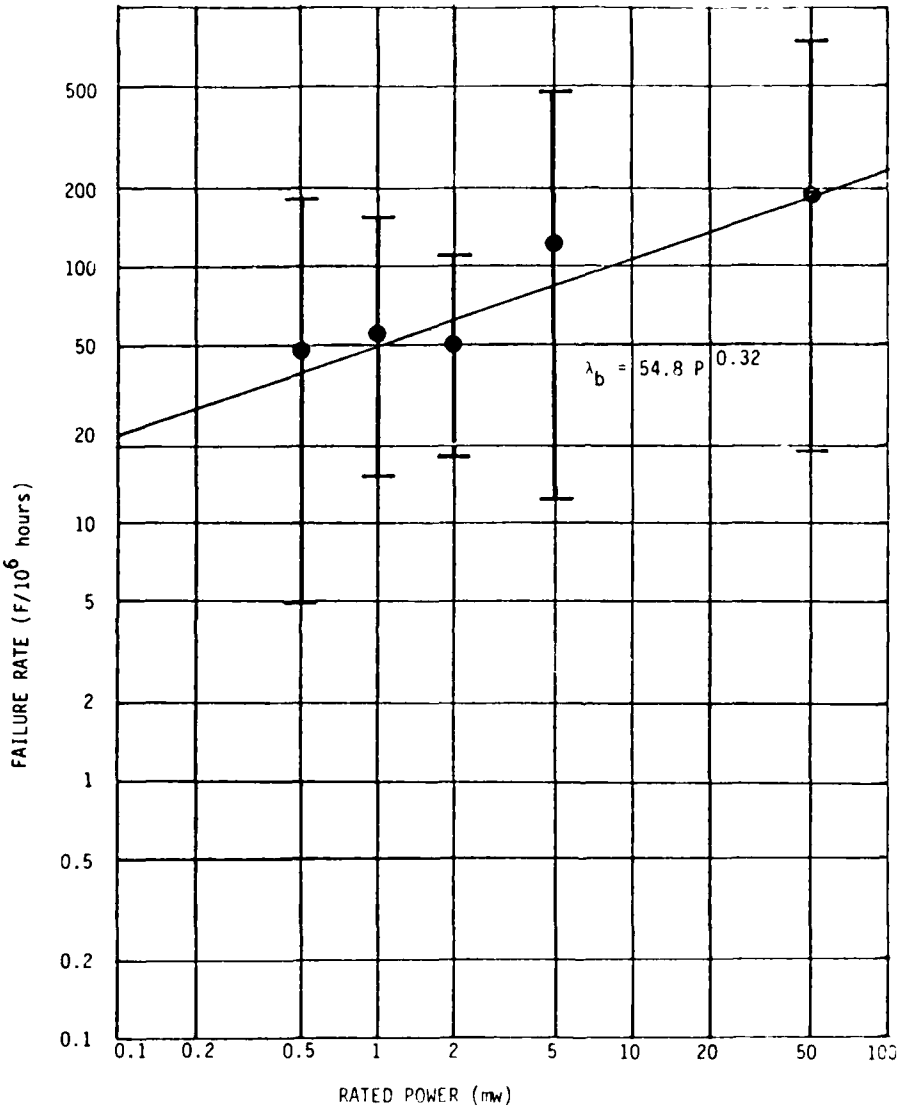

FIGURE 7.3-2: FAILURE RATE VS RATED POWER

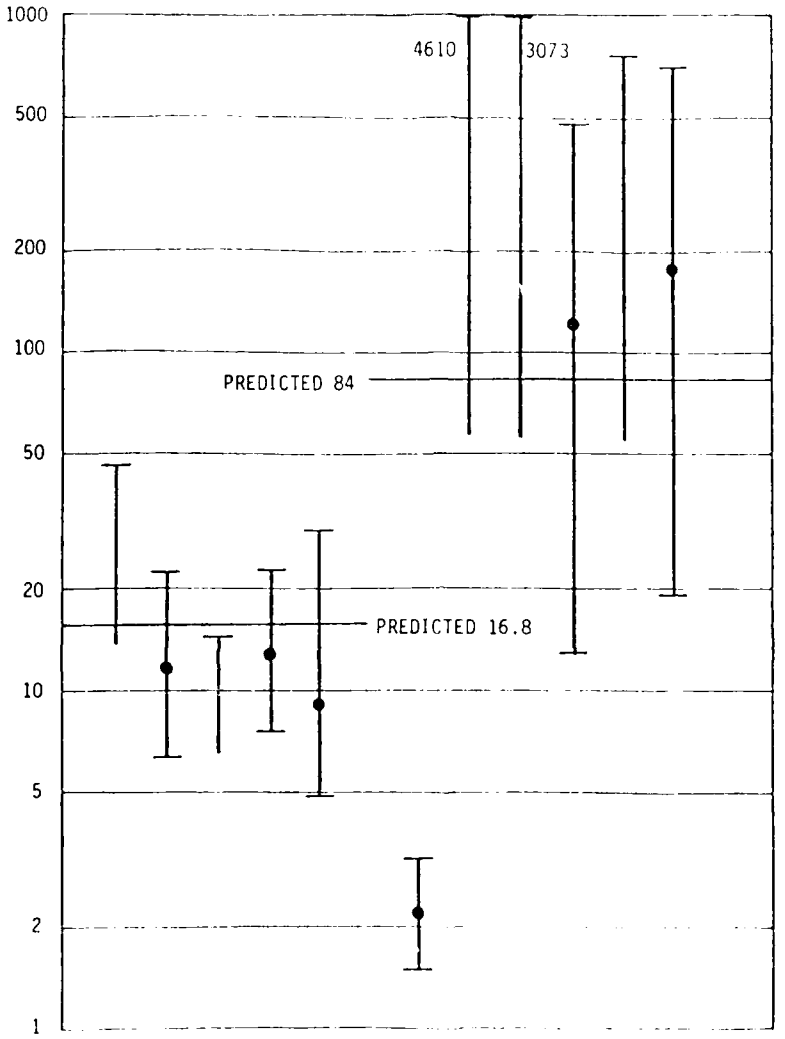

FIGURE 7.3-3: PREDICTED VS OBSERVED FAILURE RATES

Horowitz, Daniel J., Lasers (Coherent Sources), Electronic Engineers' Handbook, Second Edition, McGraw-Hill, 1982.

Martin Marietta Aerospace, Laser Reliability Prediction, Final Technical Report, RADC-TR-75-210, August, 1975.

Prather, T.W. and Ramsay, I.A., Mean Time Between Failures Data on Hughes Helium-Neon Lasers, Report No. 1, September, 1981.

7.4 Solid State, Nd:YAG Rod Laser

7.4.1 Device Construction

The Solid State Nd:YAG rod laser is a flashlamp-pumped laser that utilizes a neodymium doped yttrium-aluminum-garnet (Nd:YAG) rod as the lasing medium. The laser may be designed to operate in either the CW or pulsed mode. The Nd:YAG laser is an assembly comprised of the following subassemblies or elements:

- Nd:YAG Rod
- Flashlamp
- Optical train
- Q-Switch
- Flashlamp power supply
- Cooling system

The design of each Nd:YAG laser may be different because the type of flashlamp, optical train, Q-switch, power supply and cooling system may vary from design to design. The only element that is unique is the Nd:YAG rod and its dimensions may vary. The military users of Nd:YAG lasers include target designators and target range finders. A detailed description of Nd:YAG lasers and their components is given in reference 1.

7.4.2 Failure Modes/Mechanisms

The failure modes/mechanisms discussed below were extracted chiefly from reference 1. The major life-limiting characteristic of Nd:YAG laser systems is the requirement for periodic replacement of the flashlamp. The most predominant failure mode of flashlamps is degradation sputter resulting from a deposition mechanism which is a function of derating. Degradation of the flashlamp can also be caused by light absorption in color centers formed by impurities (chiefly aluminum and lithium) in the quartz tube. The type of cooling circuit, pulse forming network and prepulsing or simmering circuit is known to impact the life of the tube.

Greater than 90 percent of the "random" type failure mechanisms are associated with dust on optical surfaces, misalignment or the cooling system. Failure of the charging capacitor is known to be the predominant problem experienced in the laser power supply.

7.4.3 Solid State, Nd:YAG Rod Laser Failure Rate Model

This section presents the failure rate prediction model for Nd:YAG lasers. The model is:

$$\lambda_{Nd:YAG} = \pi_E \lambda_{MEDIA} + \lambda_{PUMP} + \pi_E \pi_C \pi_{OS} \lambda_{COUPLING}$$

where

$\lambda_{Nd:YAG}$ = the solid state neodymium doped yttrium-aluminum-garnet rod laser failure rate in failures/10^6 operating hours.

π_E = the environmental application factor, and its value is determined from Table 7.4-1.

λ_{MEDIA} = the failure rate contribution of the lasing media, and its value is 0.1 failures/10^6 operating hours for Nd:YAG lasers.

λ_{PUMP} = the failure rate contribution of the pumping mechanism which, for solid state lasers, is highly affected by the flashlamp or flash tube contribution and can be expressed as:

$$\lambda_{PUMP} = \pi_E \times \lambda_{PUMP\ HOURS}$$

where

π_E = the environmental application factor, and its value is determined from Table 7.4-1.

$\lambda_{PUMP\ HOURS}$ = the failure rate contribution of the flashlamp or flash tube in failures/10^6 operating hours, and its value is determined by converting pump pulses from failures per 10^6 pulses to failures/10^6 operating hours. The value for $\lambda_{PUMP\ HOURS}$ is determined as indicated in Figures 7.4-1 or 7.4-2 as applicable.

π_C = the coupling cleanliness factor, and its value is to be determined from Table 7.4-2.

π_{OS} = the number of active optical surfaces and is determined from Figure 7.4-3.

$\lambda_{COUPLING}$ = the failure rate contribution of the laser coupling hardware; that is, lenses, mirrors, prisms, exit window, etc. Its value is 16.3 failures/10^6 operating hours for solid state Nd:YAG lasers.

It should be noted that the solid state Nd:YAG laser failure rate prediction model can be rewritten as:

$$\lambda_{Nd:YAG} = \pi_E\ (0.1 + \lambda_{PUMP\ HOURS} + 16.3\ \pi_C\ \pi_{OS})$$

TABLE 7.4-1: Nd:YAG ENVIRONMENTAL FACTORS

Environment	π_E	Environment	π_E
G_B	0.2	A_{IA}	5
G_F	1	A_{IF}	7
G_M	5	A_{UC}	6
M_P	2.3	A_{UT}	5
N_{SB}	1.1	A_{UB}	10
N_S	5	A_{UA}	8
N_U	5	A_{UF}	10
N_H	3.6	S_F	0.2
N_{UU}	3.9	M_{FF}	2.4
A_{RW}	5.2	M_{FA}	3.3
A_{IC}	4	U_{SL}	7
A_{IT}	3	M_L	8
A_{IB}	6.5	C_L	N/A

TABLE 7.4-2: COUPLING CLEANLINESS FACTORS

CLEANLINESS LEVEL (1)	π_C
Rigorous cleanliness procedures, equipment, and trained maintenance personnel. Plus bellows provided over optical train.	1
Minimal precautions during opening, maintenance, repair, and testing. Plus bellows provided over optical train.	30
Minimal precautions during opening, maintenance, repair, and testing. No bellows provided over optical train.	60

Notes: (1) Although sealed systems tend to be reliable once compatible materials have been selected and proven, extreme care must still be taken to prevent the entrance of particulates during manufacturing, field flashlamp replacement, or routine maintenance/repair. Contamination is the major cause of solid state laser malfunction, and special provisions and vigilance must continually be provided to maintain the cleanliness level required. π_C values can vary from 1 up to 60.

The empirical formula used to determine $\lambda_{PUMP\ HOURS}$ for xenon lamps is:

$$\lambda_{PUMP\ HOURS\ XENON} = \left[\pi_{REP}\right] \left[2000 \left[\frac{E_j}{dL\sqrt{T}}\right]^{8.58}\right] \left[\pi_{COOL}\right] \text{ failures/}10^6 \text{ hours}$$

where

$\lambda_{PUMP\ HOURS\ XENON}$ is the failure rate contribution of the xenon flashlamp or flashtube* in failures/10^6 operating hours. The flashlamps evaluated herein are linear types used for military solid state laser systems.

π_{REP} is the pulse or repetition rate factor used to convert from failures per 10^6 pulses to failures/10^6 operating hours, and its value is determined by multiplying the number of pulses/second by 3600.

E_j is the flashlamp or flashtube input energy per pulse in joules, and its value is determined from the actual or design input energy parameter except that for input energy levels equal to or less than 30 joules, $E_j = 30$.

d is the flashlamp or flashtube inside diameter in millimeters, and its value is determined from the actual design parameter of the flashlamp utilized.

L is the flashlamp or flashtube arc length in inches, and its value is determined from the actual design parameter of the flashlamp utilized.

T is the truncated pulse width in microseconds, and its value is determined from the actual design parameter of the pulse forming network (PFN) used to pulse the flashlamp or flashtube. Pulse tails do not affect reliability, and the maximum value of T is 100 microseconds for any truncated pulse width exceeding 100 microseconds. For shorter duration pulses, pulse width is to be measured at 10 percent of the maximum current amplitude.

π_{COOL} is the cooling factor due to various cooling media immediately surrounding the flashlamp or flashtube, and its value is 1.0 for gas cooling and 0.1 for liquid cooling.

*Note: Typical values for Xenon flashlamps in military Nd:YAG rangefinders and designators are E_j = 40 joules, d = 4 millimeters, L = 2 inches, and T = 100 microseconds. The repetition or pulse rate ranges from 1 to 20 pps, and the lamps are normally liquid cooled.

FIGURE 7.4-1: DETERMINATION OF $\lambda_{PUMP\ HOURS}$ FOR XENON FLASHLAMPS

The empirical formula used to determine $\lambda_{PUMP\ HOURS}$ for Krypton lamp is:

$$\lambda_{PUMP\ HOURS\ KRY\ TON} = 625 \left[10^{(0.9\ \frac{P}{L})} \right] \pi_{COOL} \quad \text{failures}/10^6 \text{ hours}$$

where

$\lambda_{PUMP\ HOURS\ KRYPTON}$ is the failure rate contribution of the krypton flashlamp or flashtube in failures/10^6 operating hours. The flashlamps evaluated herin are the continuous wave (CW) type and are most widely used for commercial solid state applications. They are approximately 7mm in diameter and 5 to 6 inches long. Average power is typically 4 KW.

P is the average input power in kilowatts, and its value is determined from the actual design parameter for the flashlamp utilized.

L is the flashlamp or flashtube arc length in inches, and its value is determined from the actual design parameter of the flashlamp utilized.

π_{COOL} is the cooling factor due to various cooling media immediately surrounding the flashlamp or flashtube, and its value is 1.0 for gas cooling and 0.1 for liquid cooling.

FIGURE 7.4-2: DETERMINATION OF $\lambda_{PUMP\ HOURS}$ FOR KRYPTON FLASHLAMPS

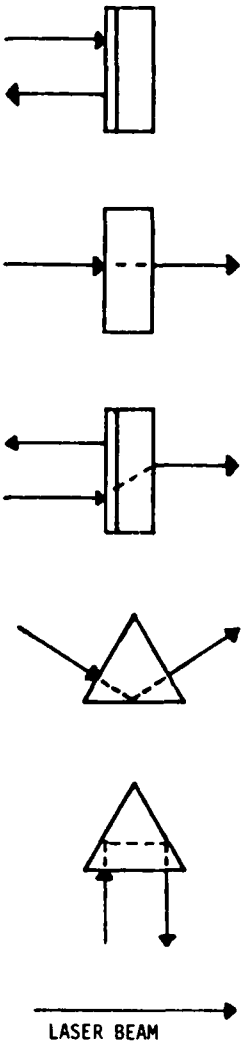

(A) Totally reflective (TR) mirror
one active optical surface
Count = 1

(B) LENS/WINDOW
Two active optical surfaces
Count = 2

(C) Partially reflective (PR) mirror
Two active optical surfaces
Count = 2

(D) PRISM
Two active optical surfaces
Count = 2

LASER BEAM

Only active optical surfaces are counted. An active optical surface is an external surface with which the laser energy or beam interacts. Internally reflecting surfaces are not counted.

FIGURE 7.4-3: TYPES OF OPTICAL SURFACES AND COUNT

7.4.4 Model Development

The model development approach used was to assume that the current model form in MIL-HDBK-217D was correct, and to use the limited amount of field experience data that was available to verify or disprove the model parameters. If the data indicated that the current parameters were incorrect, then it was planned to revise them to reflect the results of the analysis of the data. The failure experience data collected in support of this study are presented in Table 7.4-3. It should be noted that the source 1 through 4 data were obtained from the U.S. Air Force Maintenance Data System and that the data are part replacements. The observed replacements then should present an upper bound on the true number of failures incurred. Technical information collected to allow for the calculation of a predicted failure rate is presented in Table 7.4-4. A prediction was made on the source 1 through 4 data. The prediction results were compared with the observed failure rate (Table 7.4-5). A comparison of the predicted vs. observed failure rate for those entries with observed failures showed the following:

- The laser prediction was pessimistic for three of the four sources and for the group as a whole, and accurate for one of the sources,
- The rod prediction was optimistic for all four sources and for the group as a whole,
- The lamp prediction was optimistic for three sources, pessimistic for the other source and accurate for the group as a whole,
- The optics prediction was pessimistic for all four sources and for the group as a whole.

The published literature (Ref. 1, 2, 3, 4) indicated that the inclusion of a "simmer" circuit should improve the life of the flashlamp. The data were examined to determine if it substantiated these claims. A multiplicative variable (A) was added to the xenon flash tube model. The revised xenon failure rate model was set equal to the observed point estimate failure rate equation (observed failures/operating time) to derive a

TABLE 7.4-3: Nd:YAG FAILURE EXPERIENCE DATA

Source	Env	OP HRS	No. of Shots ($X 10^6$)	No. of Failures			Failure Rate $F/10^6$ hours			Failure Rate $F/10^6$ Pulses		
				Rod	Lamp	Optics	Rod	Lamp	Optics	Rod	Lamp	Optics
1	A_{UF}	3517	126.6	2	5	3	569	1422	853	0.016	0.039	0.024
2	A_{UF}	1713	116.8	1	0	2	584	538(2)	1168	0.008	0.008(2)	0.017
3	A(1)	1883	12.6	0	0	0	490(2)	490(2)	490(2)	0.073(2)	0.073(2)	0.073(2)
4	A_{UF}	4600	165.6	0	3	0	200(2)	652	200(2)	0.006(2)	0.018	0.006(2)
5	G_B(3)	--	--	-	-	-	--	--	--	--	0.1667	--
6	G_B(3)	--	--	-	-	-	--	--	--	--	0.0556	--
7	(4)	164000	--	0	-	-	5.6	--	--	--	--	--
8	(4)	--	524.1	9	-	-	--	--	--	0.017	--	--
Total		175713	945.7	12	8	5						

Notes: (1) Rel Demo Test with conditions representative of an airborne environment

(2) Upper 60% Confidence limit used to estimate the failure rate where no failues were observed

(3) life test data

(4) environment and equipment type unknown

Table 7.4-4: Nd:YAG PREDICTIONS

Source	Description	π_E	λ_{media}	π_C	π_{os}	π_{coup}	π_{rep} (X1000)	E_j (j)	d (mm)	L (in)	T (μS)	π_{cool}	λ_p F/10^6 hrs
1	ASQ-153, Freon-optic coolant, Pockels Cell Modulator, Xenon Flashlamp, E_j = 13.5J, no simmer CKT	10	0.1	1	17	16.3	36	30	5	3	100	0.1	2779
2	AVQ-25, Water-Glycol coolant, E_j, T, L and d unknown assumed Avg of sources 1&2. Simmer circuit, Pockels cell modulator	10	0.1	1	25	16.3	68.4	30	4.5	3.1	100	0.1	3518
3	Same as source 2 (Note 1)	10	0.1	1	25	16.3	7.2	30	4.5	3.1	100	0.1	3288
4	AVQ-27, T = 120us, Gas, Nitrogen Coolant, Xenon Flashtube, E_j = 16J, no simmer CKT, Pockels cell modulator	10	0.1	1	19	16.3	36	30	4	3.3	100	1	3315

Notes: (1) Rel Demo Test

TABLE 7.4-5: PREDICTED AND OBSERVED FAILURE RATES

Source	Failure Rate ($F/10^6$ hours)															
	Rod				Lamp				Optics				Lasers			
	Pred	Observed			Pred	Observed			Pred	Observed			Pred	Observed		
		L 10%CL	PT EST	U 90%CL		L 10%CL	PT EST	U 90%CL		L 10%CL	PT EST	U 90%CL		L 10%CL	PT EST	U 90%CL
1	1.0	151	569	1513	72.5	692	1422	2637	2771	313	853	1899	2844	1768	2843	4379
2	1.0	61.5	584	2271	257	---	538(1)	1346	4075	310	1168	3106	4333	642	1751	3900
3	1.0	--	490(1)	1224	27	---	490(1)	1224	4075	---	490(1)	1224	4103	--	490(1)	1224
4	1.0	--	200(1)	501	2170	239	652	1485	3097	---	200(1)	501	5268	652	1485	3097
Total	1.0(2)	93.4	256	570	632(2)	397	683	1109	2526(2)	208	427	792	3159(2)	951	1195	1916

Notes: (1) Upper 60% Confidence limit

(2) Arithmetic Average

normalized estimate for variable A. The source 2 and 3 data were combined since they are the same system and both entries had zero failures. The results are given in Table 7.4-6.

TABLE 7.4-6: SIMMER CIRCUIT ANALYSIS

Source	Circuit Type	Normalized Variable	Results
1	No Simmer	19.6	10 X worse than source 2 & 3
2&3	Simmer	1.88	--
4	No Simmer	0.300	6 X better than source 2 & 3

As the data shows, the results are inconclusive; therefore, even though the literature claims that a simmer circuit improves the life of the tube, the data neither confirms nor denies it. The source 5 data is life test data on tubes without a simmer circuit and the source 6 data is life test data on tubes using a simmer circuit. These data show a 3:1 failure rate improvement for tubes used with a simmer circuit. One of the reasons why the results are inclusive may be due to the method of determining the total number of shots accumulated by each data source. The number of equipment operating hours was obtained through field inquiries while the number of shots per hour was determined from technical information. It is not known whether the lasing mechanism was inhibited during a portion of equipment operation. If it were inhibited for a portion of the time then the observed failure rate calculated for the laser would be optimistic. For instance, it is known that the lasing mechanism of the AVQ-25 was inhibited for a portion of the operating time during the Rel Demo test. The equipment which normally operates at 10 or 20 shots/second was run during the Rel Demo test on the average 1.85 shots/second of operate time. Since the data were inconclusive as to the accuracy of the xenon lamp model as a whole, it is proposed that the current prediction model be retained until more field experience data become available.

From discussions held with optics experts, it has been determined that optical power density is a factor that should be included in the optics portion of the model; however, no data were obtained that could be used to develop this hypothesis. The comparison between the predicted and observed failure rates indicated that the optics model may be overly pessimistic, and that the rod model may be overly optimistic. The data from sources 1 & 2 would indicate that the rod model may be optimistic (predicts a lower failure rate) by over two orders of magnitude, and that the optics model may be pessimistic (predicts a higher failure rate) by a factor of three. Since all of the available data are from the same environment (A_{UC}), it could not be determined if the base failure rates (λ_{media} and $\lambda_{coupling}$) are in error, and/or if it is the environmental factor (π_E) that is an error.

Since there was not sufficient data to revise the current model, it is proposed that it be retained until data becomes available.

7.5 References and Bibliography

References

1. Martin Marietta Corporation, Laser Reliability Prediction, Final Technical Report, RADC-TR-75-210, August, 1975.

2. ILC Technology, Liquid Cooled Flashlamp Catalog.

3. IBID., Air Cooled Linear Flashlamp Catalog.

4. IBID., Internal Report, 1982.

Bibliography

EG&G Electro-optics Product Catalog.

ILC Technology, Liquid Cooled Flashlamp Catalog.

IBID., Air Cooled Linear Flashlamp Catalog.

Martin Marietta Corporation, Laser Reliability Prediction, Final Technical Report, RADC-TR-75-210, August, 1975.

Paget, Fred W., Xenon Flash tube Power Supplies, Journal of the Society of Illuminating Engineers, Vol. 4, October, 1974, pp. 223-228.

Pettifer, R.E., et.al., A Reliable 60KV Flashlamp Triggering System, Journal of Physics E, Scientific Instruments, Vol. 8, 1975.

Rehmet, M., Xenon Lamps, IEE Proceedings, Vol. 127, PT.A, No. 3, April, 1980, pp. 190-195.

8.0 ELECTRONIC FILTERS

8.1 Device Construction

The devices considered in this section are RFI/EMI filters per MIL-F-15733; band pass, high pass, low pass and band suppression filters per MIL-F-18327 and similar nonstandard filters of each type.

MIL-F-15733 filters may be a packaged assembly constructed of discrete components soldered in place on a printed circuit card, or a hybrid type of device consisting of capacitive-inductive elements mounted in a metal can. RFI/EMI filters allow relatively low frequencies (50 to 400Hz) to pass unaffected while reducing the power level of higher frequencies. Sources of RFI/EMI vary from natural phenomenom such as lightning and cosmic noise to man induced interference from radio transmitters and florescent lights. These devices are not only useful in protecting electronic equipments from unwanted RFI/EMI signals, but they can be used to protect the environment from RFI/EMI signals generated within an equipment.

Several different internal circuit configurations are available for RFI/EMI filters. Figure 8.1-1 presents the most popular inductor-capacitor (LC) circuit configurations. Figure 8.1-2 presents the construction of a ceramic-ferrite RFI/EMI filter. Reference 1 discusses the relative merits of each circuit configuration. Filters used on AC power lines generally use toroidal wound inductors and wound paper or paper-plastic capacitors. Ceramic filters are widely used for low voltage applications because of their small size. These devices also use toroidal inductors but the use of monolithic ceramic, discoidal capacitors results in a significant reduction in overall volume as compared to filters using paper or plastic dielectrics. Another type of ceramic filter used for RFI/EMI suppression uses a ferrite bead (Figure 8.1-2) as the inductive element. Here the ferrite bead functions not as a true inductor, but as an absorber of RF energy.

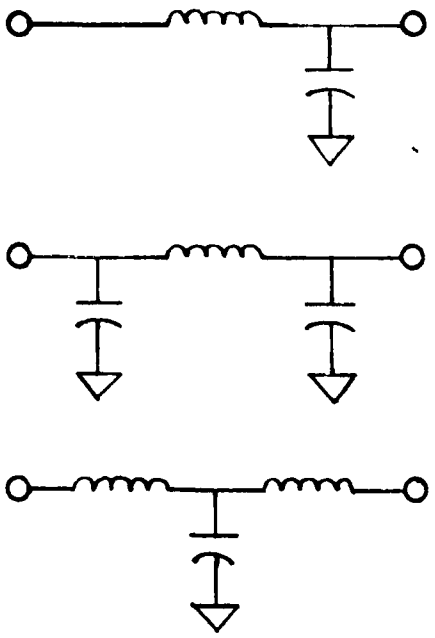

(a) L - filter

(b) π - filter

(c) T - filter

FIGURE 8.1-1: TYPICAL LC LOW PASS FILTER CIRCUITS

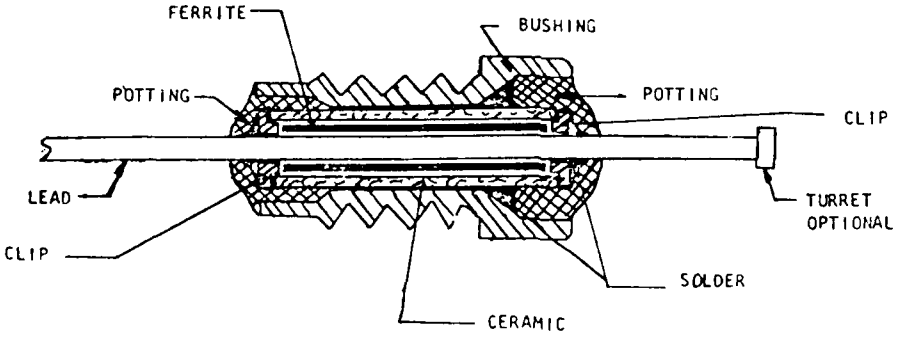

FIGURE 8.1-2: TYPICAL CERAMIC-FERRITE RFI FILTER

The family of filters per MIL-F-18327 include high pass, low pass, band pass, band suppression and dual function types. These filters are in fact packaged assemblies constructed of discrete components soldered in place on a printed circuit card. The components are arranged in electrical circuits which provide the frequency discrimination and insertion - loss characteristics required. The assembly is either enclosed in a metal can or encapsulated in plastic.

The function of these filters is to provide for transmission through the filter, at acceptable power levels, of energy at desired frequencies while providing for attenuation of energy at undesired frequencies. Figure 8.1-3 presents power output versus frequency graphs for band pass, high pass, low pass and band suppression filters.

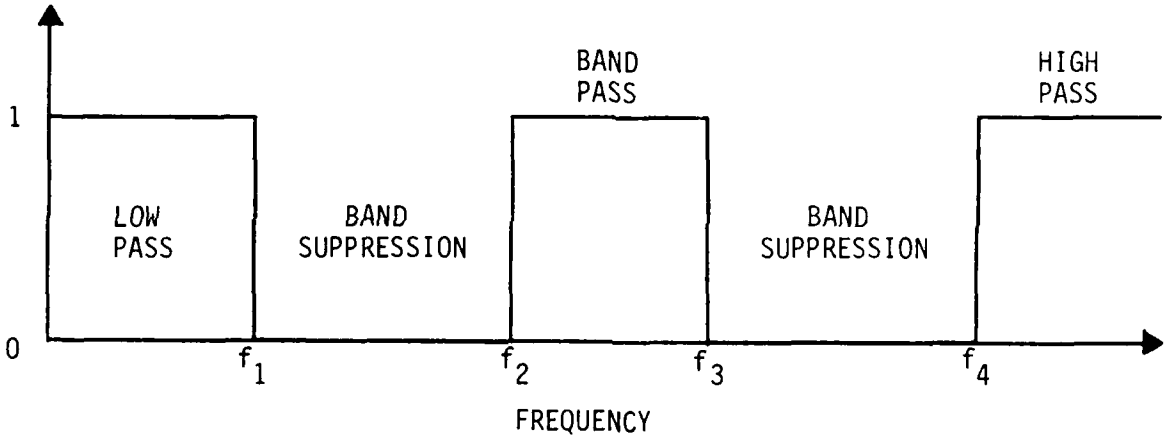

FIGURE 8.1-3: POWER OUTPUT VERSUS FREQUENCY

The low pass filter passes frequencies lower than f_1 and attenuates frequencies greater than f_1. The band suppression filter passes frequencies below f_1, between f_2 and f_3 and greater than f_4, and attenuates frequencies between f_1 and f_2, and between f_3 and f_4. The band pass filter passes frequencies between f_2 and f_3, and attenuates all other frequencies. The high pass filter passes frequencies greater than f_4 and attenuates frequencies lower than f_4.

The most distinquishable construction characteristic of these type filters is the principal resonator. The principal resonator is generally an LC circuit or a crystal. Two examples of typical filter constructions are given in Table 8.1-1.

TABLE 8.1-1: EXAMPLES OF FILTER CONSTRUCTION

Device Type	Low Pass LC Filter	Band Pass Crystal Filter
RF Transformer	0	3
RF Coil	4	0
Paper/Plastic Capacitor	2	0
Plastic Capacitor	5	0
Mica Capacitor	1	0
Ceramic Capacitor	0	3
Variable Ceramic Capacitor	0	3
Crystal	0	6
Printed Wiring Board	1	1
Solder Connections	24	30

The examples of filter construction given in Table 8.1-1 each represent just one possible construction option for a particular filter type. There are many ways of designing and constructing the desired filter given an identical filter performance specification.

8.2 Filter Failure Modes and Mechanisms

The failure mechanisms and the distribution of failure modes of filters since they are packaged assemblies are a function of the design and manufacturing techniques used. Several of the failure modes that are characteristic of filters are given in Table 8.2-1.

TABLE 8.2-1: FILTER FAILURE MODES

Input Shorted to Ground
No Output
High Insertion Loss
Output Shorted to Ground
Input Open
Cutput Open
Low Attenuation at Frequency

8.3 Electronic Filter Failure Rate Prediction Procedure

This Section presents the proposed failure rate prediction procedure for non-tunable electronic filters. The prediction procedure is:

Step 1: If a Parts List and/or Schematic Diagram are available.

Step 1A: Calculate a failure rate for each particular component in the filter assembly using the correct model from the following sections in MIL-HDBK-217:

Integrated Circuits	Section 5.1.2
Discrete Semiconductors	Section 5.1.3
Resistors	Section 5.1.6
Capacitors	Section 5.1.7
Inductive Devices	Section 5.1.8
Printed Wiring Assemblies	Section 5.1.13
Crystals	Section 5.1.16

Step 1B: Sum the failure rate contribution for each component. The filter failure rate (λ_p) then is:

$$\lambda_p = \sum_{i=1}^{n} \lambda_i$$

where

λ_p = filter failure rate ($F/10^6$ hours)

λ_i = failure rate of each individual component ($F/10^6$ hours)

Step 2: If a parts list, but no schematic diagram is available, or if the component complement can be determined by other means, e.g., disection.

Step 2A: Calculate a failure rate for each component type and for the filter as an assembly using the procedure discussed in MIL-HDBK-217, Section 5.2.

Step 3: If no parts list or schematic diagram are available, calculate the filter failure rate using the proposed model:

$$\lambda_p = \lambda_b \times \pi_Q \times \pi_E$$

where

λ_p = filter failure rate ($F/10^6$ hours)

λ_b = base failure rate

= 0.0219 $F/10^6$ hours for MIL-F-15733, ceramic/ferrite construction (Styles FL10-16, 22, 24, 30-35, 38, 41-43, 45, 47-50, 61-65, 70, 81-93, 95, 96)

= 0.120 $F/10^6$ hours for MIL-F-15733, discrete LC components (Styles FL37, 53, 74)

= 0.120 $F/10^6$ hours for MIl-F-18327, discrete LC components (Composition 1)

= 0.265 $F/10^6$ hours for MIL-F-18327, discrete LC and crystal components (Composition 2)

π_Q = quality factor

= 1.0, MIL-SPEC quality

= 2.9, lower quality

π_E = environmental factor (Table 8.3-1).

TABLE 8.3-1: ENVIRONMENTAL FACTORS

Environment	π_E	Environment	π_E
G_B	1	A_{IA}	8.8
G_F	2.1	A_{IF}	8.8
G_M	6	A_{UC}	10
M_P	6.4	A_{UT}	13
N_{SB}	3.7	A_{UB}	10
N_S	4.3	A_{UA}	13
N_U	7.9	A_{UF}	13
N_H	8.7	S_F	1.7
N_{UU}	9.2	M_{FF}	6.4
A_{RW}	11	M_{FA}	8.2
A_{IC}	5.5	U_{SL}	14
A_{IT}	8.8	M_L	16
A_{IB}	5.5	C_L	120

8.4 Failure Rate Model Development

The approach utilized for model development was to treat the filter as a packaged assembly. The rationale for this approach is based on the following facts:

- the filter is a packaged assembly comprised of discrete components.
- every filter is functionally a frequency suppression circuit; however, the circuit design and consequently the quantity, quality and type of components used in the design varies between manufacturers.
- The filter MIL-SPEC is a functional specification and does not specify or limit internal construction.

However, it was recognized that it may not be possible for the reliability analyst to obtain the parts list and/or schematic diagram for a filter; therefore a default prediction procedure was necessary.

The approach used for development of a default filter failure rate prediction model was to identify and quantify model parameters by analysis of field experience data. The filter failure rate data collected in support of this study effort are presented in Table 8.4-1.

Application and construction variables which were considered as possible filter failure rate model modifying parameters are presented in Table 8.4-2. The application and construction variables were determined whenever possible for all collected data. The selection of variables to be included in the proposed filter failure rate prediction model was based solely on the analysis of field experience data.

Stepwise multiple linear regression analysis as described in Section 3.1 was applied to the filter failure rate data. Data records which were included in the regression analysis are indicated in Table 8.4-1. Other data records included insufficient part hours to estimate a failure rate without observed failures, or insufficient detail was obtained, or the entry was identified as an outlier or the part was outside the scope of the study. Construction was assumed to be discrete LC unless otherwise indicated. The regression analysis resulted in the following filter failure rate prediction model:

$$\lambda_p = \lambda_b \times \pi_Q \times \pi_E$$

where

λ_p = predicted filter failure rate in failures/10^6 hours

λ_b = base failure rate

= 0.0407 F/10^6 hours for ceramic-ferrite construction

= 0.105 F/10^6 hours for discrete LC component construction

= 0.0698 F/10^6 hours for discrete LC and crystal component construction

TABLE 8.4-1: FILTER FIELD EXPERIENCE DATA

SOURCE	EQUIP	FUN (1)	ENC (2)	COM (3)	FREQ (Hz)	QUAL (4)	ENV	NO. FAIL	OPHRS (x10^6)
1 (6)	BRD-7	C	C	-	-	C	NSB	0	0.092
2	SQS-26	D	-	-	-	C	NS	0	0.532
3	SQS-26	C	-	-	-	C	NS	2	25.135
4	ARC-164	B	A	A	-	C	AIB	0	0.161
4	ARC-164	B	A	A	-	C	AIC	1	0.113
5	COMM	C	-	-	-	C	AIC	4	0.917
6 (8)	COMM	C	C	-	-	C	AIC	2	0.229
7	ALQ-117	A	A	-	-	C	AUB	1	0.161
8	ARN-118	C	-	-	-	C	AUB	1	0.237
8	ARN-118	C	-	-	-	C	AUC	5	2.244
9	ARN-118	C	C	-	63M	C	AUB	0	0.237
9	ARN-118	C	C	-	63M	C	AUC	0	2.244
10	ARN-118	C	-	-	-	C	AUB	3	0.237
10	ARN-118	C	-	-	-	C	AUC	2	2.244
11	ALQ-117	C	-	-	-	C	AUB	0	4.824
12	ARN-118	C	-	-	-	C	AUA	2	9.529
12	ARN-118	C	-	-	-	C	AUT	6	1.157
12	ARN-118	C	-	-	-	C	AUF	2	0.492
13	ARN-118	C	-	-	-	C	AUA	5	0.529
13	ARN-118	C	-	-	-	C	AUT	1	1.157
13	ARN-118	C	-	-	-	C	AUF	1	0.492
14	ARN-118	C	C	-	63M	C	AUA	0	0.529
14	ARN-118	C	C	-	63M	C	AUT	0	1.157
14	ARN-118	C	C	-	63M	C	AUF	0	0.492
15 (6)	ARN-118	C	-	-	-	C	ARW	1	0.063
16	GRR-23	C	-	B	-	C	GM	0	0.253
16	GRR-24	C	-	B	-	C	GM	0	1.701
17 (6)	BRD-7	C	C	B	-	C	NSB	1	0.184
18 (6)	BRD-7	C	C	B	-	C	NSB	0	0.184
19 (6)	BRD-7	C	C	B	-	C	NSB	0	0.275
20 (6)	BRD-7	C	C	B	-	C	NSB	0	0.275
21	ARC-164	C	A	B	-	C	AIB	0	0.322
21	ARC-164	C	A	B	-	C	AIC	0	0.226
22	ARC-164	C	A	B	-	C	AIB	1	0.161
22	ARC-164	C	A	B	-	C	AIC	0	0.113
23	ARC-164	C	A	B	-	C	AIB	0	0.161
23	ARC-164	C	A	B	-	C	AIC	0	0.113
24	GRR-23	F	B	A	-	C	GM	0	1.521
24	GRR-24	F	B	A	-	C	GM	0	10.207
25	UYK-7	F	-	D	400	C	GF	0	21.414
26	UYK-7	F	-	D	-	C	GF	2	16.061
27	RADAR	F	-	-	-	C	GF	10	314.758
28 (6)	GYQ-18	F	A	C	60	C	GF	0	2.491
29 (6)	GYQ-18	F	C	A	400	C	GF	0	1.424
30 (6)	GYQ-18	F	C	A	60	C	GF	0	0.712
31 (6)	UYK-7	F	-	D	400	C	NSB	0	0.222
32 (6)	UYK-7	F	-	D	-	C	NSB	0	0.167
33 (6)	BRD-7	F	C	D	400	M	NSB	1	0.184
34	BRD-7	F	C	D	-	C	NSB	0	2.203
35 (6)	BRD-7	F	C	D	400	C	NSB	0	0.734
36	BRD-7	F	C	D	-	C	NSB	2	31.123
37 (6)	BRD-7	F	C	D	-	C	NSB	0	0.734
38	BRD-7	F	C	D	-	C	NSB	0	2.203
39 (6)	BRD-7	F	C	D	-	C	NSB	0	0.918
40 (6)	BRD-7	F	C	-	-	C	NSB	0	0.184
41 (6)	BRD-7	F	C	-	-	C	NSB	0	0.275
42 (6)	BRD-7	F	C	-	-	C	NSB	0	0.275
43	TSQ-73	F	-	-	-	C	GM	0	14.760
44	TSQ-73	F	-	-	-	C	GM	0	0.369
45	ARC-164	F	C	A	-	M	AIB	0	0.643
45	ARC-164	F	C	A	-	M	AIC	0	0.551
46	ALQ-117	F	C	A	-	M	AUB	0	1.286
47	ARN-118	F	-	A	400	M	AUB	0	0.474
47	ARN-118	F	-	A	400	M	AUC	0	4.488
48	ARN-118	F	-	-	400	C	AUB	0	0.711
48	ARN-118	F	-	-	400	C	AUC	0	6.732
49	ALQ-117	F	-	A	-	C	AUB	1	0.161
50	ALQ-117	F	-	A	-	C	AUB	0	1.126
51	ALQ-117	F	-	A	-	C	AUB	0	0.643
52	ALQ-117	F	-	A	-	C	AUB	1	10.432
53	ALQ-117	F	-	A	-	C	AUB	0	1.026
54	ALQ-117	F	-	A	-	C	AUB	0	0.322
55	ALQ-117	F	-	A	-	C	AUB	0	0.322
56	ALQ-117	F	-	A	-	C	AUB	0	4.824
57	ARN-118	F	-	-	400	C	AUA	0	1.587
57	ARN-118	F	-	-	400	C	AUT	0	3.471
57	ARN-118	F	-	-	400	C	AUF	0	1.476
58	ARN-118	F	-	A	400	M	AUA	0	1.058
58	ARN-118	F	-	A	400	M	AUT	0	2.314
58	ARN-118	F	-	A	400	M	AUF	0	0.984

TABLE 8.4-1: FILTER FIELD EXPERIENCE DATA (CONT'D)

SOURCE	EQUIP	FUN (1)	ENC (2)	COM (3)	FREQ (Hz)	QUAL (4)	ENV	NO. FAIL	DPHRS ($\times 10^6$)
59 (6)	ARN-118	F	-	-	400	C	ARW	0	0.126
60 (6)	ARN-118	F	-	A	400	M	ARW	0	0.189
61 (6)	GYQ-18	F	A	C	60	C	GF	0	0.356
62 (6)	BRD-7	-	-	-	-	M	NSB	0	0.092
63 (6)	BRD-7	F	A	-	60	C	NSB	0	0.092
64 (6)	BRD-7	F	A	-	-	C	NSB	0	0.092
65 (6)	BRD-7	C	C	B	-	C	NSB	0	0.092
66 (6)	BRD-7	C	C	B	-	C	NSB	0	0.092
67 (6)	BRD-7	C	C	B	-	C	NSB	0	0.092
68 (6)	BRD-7	C	C	B	-	C	NSB	0	0.092
69 (6)	BRD-7	C	C	B	-	C	NSB	0	0.092
70 (6)	BRD-7	C	C	B	-	C	NSB	0	0.092
71 (6)	BRD-7	C	C	B	-	C	NSB	0	0.092
72 (6)	BRD-7	C	C	B	-	C	NSB	0	0.092
73 (6)	BRD-7	C	C	B	-	C	NSB	0	0.092
74 (6)	BRD-7	C	C	B	-	C	NSB	0	0.092
75 (6)	BRD-7	C	C	B	-	C	NSB	0	0.092
76 (6)	ALQ-117	F	-	A	-	C	AUB	0	0.161
77 (6)	TSQ-73	A	C	-	-	C	GM	0	0.123
78 (6)	RADAR	B	-	-	-	-	GF	0	0.223
79 (6)	ARN-118	C	C	-	63M	C	ARW	0	0.063
80 (6)	ARN-118	C	-	-	-	C	ARW	0	0.063
81 (6)	ARC-164	B	-	-	-	C	AI	0	0.320
82 (6)	ARC-164	B	-	-	-	C	AI	0	0.080
83 (7)	RADAR	-	-	-	-	C	GF	0	28.174
84 (6)	RADAR	C	-	-	-	C	GF	0	0.889
85 (6)	SQS-26	C	-	-	-	C	NS	0	0.532
86 (7)	SQS-26	-	-	-	-	C	NS	0	2.015
87	SQS-26	F	-	-	-	C	NS	0	6.839
88 (6)	ARC-164	F	-	-	-	C	AI	0	0.080
89 (6)	ARC-164	C	-	-	-	C	AI	0	0.080
90 (6)	ARC '64	C	-	-	-	C	AI	0	0.080
91 (6)	ARC 4	C	-	-	-	C	AI	0	0.240
92 (6)	ARC-164	C	-	-	-	C	AI	0	0.160
93 (6)	ARC-164	F	-	-	-	C	AI	0	0.080
94 (6)	ARC-164	F	-	-	-	C	AI	0	0.080
95 (6)	ARC-164	C	-	-	-	C	AI	0	0.080
96 (9)	GRR-24	G	-	-	-	C	GM	4	1.701
97 (9)	GRR-23	G	-	-	-	C	GM	1	0.253
98 (7)	SENSOR	-	-	A	-	C	GF	0	8.360
99 (8)	BRD-7	F	C	-	400	C	NSB	4	0.184
100	-	F (5)	-	-	-	C	GF	1	0.736
101 (9)	PWR EQUIP	F	-	-	60	C	GF	4	3.326
102 (9)	PWR EQUIP	F	-	-	60	C	GF	2	3.211
103 (9)	PWR EQUIP	F	-	-	60	C	GF	0	0.642
TOTAL								73	580.955

NOTES: (1) A = High Pass, B = Low Pass, C = Band Pass, D = Band Suppression
F = RFI, G = Tunable
(2) A = Metal Encased (non-hermetic), B = Encapsulated (non-hermetic)
C = Hermetically Sealed
(3) A = LC, B = Crystal, C = Other Electromechanical, D = Ferrite
(4) C = Commercial quality, M = MIL-SPEC quality
(5) EMI Filter
(6) Insufficient part hours
(7) Insufficient detail
(8) Identified as an outlier
(9) Part outside scope of study

TABLE 8.4-2: FILTER CONSTRUCTION AND APPLICATION VARIABLES

I. Function
   A. High Pass
   B. Low Pass
   C. Band Pass
   D. Band Suppression
   E. Dual Functioning
   F. Radio Frequency Interference
   G. Tunable

II. Enclosure Type
   A. Metal Encased (non-hermetic)
   B. Encapsulated (non-hermetic)
   C. Hermetically Sealed

III. Composition
   A. LC
   B. Crystal
   C. Other Electromechanical
   D. Ferrite
   E. Other

IV. Quantity of Terminals

V. Current Level
   A. Rated
   B. Actual

VI. Voltage Level
   A. Rated
   B. Actual

VII. Frequency

VIII. Temperature (^{o}C)
   A. Rated
   B. Actual

IX. Quality Level

X. Environment

π_Q = quality factor
= 1.0, MIL-SPEC quality
= 2.9, lower quality
π_E = environmental factor
= 1.0, GF
= 1.17, NS
= 1.83, NSB
= 2.02, GM
= 14.04, AIT
= 7.3, AUT
= 4.2, AUF

and where

AIT = Airborne Inhabited Transport
AUT = Airborne Uninhabited Transport
AUF = Airborne Uninhabited Fighter

It should be noted that the base failure rate constants given above differ from the value given in Section 8.3. This apparent discrepancy is due to normalization of the environmental factors, and because the values given in Section 8.3 are the upper 90% confidence bound for two of the categories. The regression analysis assumed a ground, fixed environmental factor equal to one because no data were available from a ground, benign environment. The base failure rate estimates for the filters constructed using discrete components was set at the upper 90% confidence limit to insure that an optimistic (lower than what would actually be observed in the field 90% of the time) failure rate was not predicted by the default technique. A secondary reason for using this upper bound was to force the analyst to utilize one of the first two techniques whenever possible since these techniques should generate a more nearly accurate estimate of the true failure rate. The proposed filter failure rate prediction model environmental factors were normalized to a ground, benign factor equal to one to be consistent with existing MIL-HDBK-217D models. The details of the

regression analysis are given in Table 8.4-3. Base failure rate, quality factor and environment factor were defined by the following equations:

$\lambda_b = \exp(b_o + b_1X_1 + b_2X_2)$
$X_1, X_2 = (0,0)$, RFI Filters, ferrite-ceramic
$X_1, X_2 = (1,1)$, Discrete LC with crystal
$X_1, X_2 = (0,1)$, Discrete LC
$\pi_Q = \exp(b_3X_3)$
$X_3 = 0$, MIL-SPEC
$X_3 = 1$, lower quality
$\pi_E = \exp(b_4X_4 + b_5X_5 + b_6X_6 + b_7X_7 + b_8X_8 + b_9X_9)$
$X_4, X_5, X_6, X_7, X_8, X_9 = (0,0,0,0,0,0)$, GF
$X_4, X_5, X_6, X_7, X_8, X_9 = (1,0,0,0,0,0)$, NS
$X_4, X_5, X_6, X_7, X_8, X_9 = (0,1,0,0,0,0)$, NSB
$X_4, X_5, X_6, X_7, X_8, X_9 = (0,0,1,0,0,0)$, GM
$X_4, X_5, X_6, X_7, X_8, X_9 = (0,0,0,1,0,0)$, AIT
$X_4, X_5, X_6, X_7, X_8, X_9 = (0,0,0,0,1,0)$, AUT
$X_4, X_5, X_6, X_7, X_8, X_9 = (0,0,0,0,0,1)$, AUF

The X_i variables are "dummy variables" used to quantify qualitative factors.

TABLE 8.4-3: RESULTS OF FILTER REGRESSION ANALYSIS

Variable (X_i)	Coefficient (b_i)	Standard Error	F-Ratio
X_1	0.951720	0.5764	2.74
X_2	-0.411436	0.9241	0.20
X_3	1.067148	0.9048	1.39
X_4	0.157188	1.0703	0.02
X_5	0.605001	0.9994	0.37
X_6	0.702430	0.9554	0.54
X_7	2.642144	1.0633	6.17
X_8	1.988904	0.7691	6.69
X_9	1.435398	0.9850	2.12
Constant	-3.201837		

The variables X_1, X_7 and X_8 were significant at the 90% confidence level. The variable X_9 was significant at the 80% confidence level, and X_3 was significant at the 70% confidence level. The remaining variables were forced into the equation by assuming a 0.0 critical f-ratio. The standard error statistic allows for the calculation of confidence intervals for quality factor, environmental factors and base failure rate. Table 8.4-4 presents the point estimate, lower 20% confidence limit and upper 80% confidence limit for these factors.

TABLE 8.4-4: RESULTS OF FILTER REGRESSION ANALYSIS

Parameter	Point Estimate	Lower 20% CL	Upper 80% CL
λ_b, ferrite	0.0407	--	--
λ_b, Discrete LC	0.105	0.0645	0.172
λ_b Discrete LC with crystal	0.0698	0.0195	0.250
π_Q, MIL-SPEC	1.0	--	--
π_Q, Lower quality	2.9	1.35	6.28
π_E, GF	1.0	--	--
π_E, NS	1.17	0.47	2.91
π_E, NSB	1.83	0.78	4.29
π_E, GM	2.02	0.90	4.55
π_E, AIT	14.04	5.68	34.71
π_E, AUT	7.31	1.33	14.07
π_E, AUF	4.20	1.82	9.71

Analysis of the data only allowed for determination of seven environmental factors. To improve the utility of the proposed model, a complete series of environmental factors was determined. There is no part type currently included in MIL-HDBK-217D whose environmental factors adequately represent the effects of environmental stress on filters. Therefore, the methodology described in Section 3.3 was applied to the seven observed environmental factors to derive an applicable series of factors. This method assumes that an environmental factor relation can be determined

where environmental factor is a function of the "environmental stress ratios" given in Reference 2. The results of the environmental factor derivation are given by the following equations:

$$\pi_{E1} = 0.539\ (S)^{0.732}$$

$$\pi_{E2} = (S)^{0.732}$$

$$R^2 = 0.63$$

where

π_{E1} = environmental factors normalized to a ground, fixed $\pi_E = 1$
π_{E2} = environmental factors normalized to a ground, benign $\pi_E = 1$
S = environmental stress ratio
R^2 = correlation coefficient

It was considered desirable for the environmental factors included in the proposed filter failure rate prediction model to be normalized to a ground, benign factor equal to one. The preliminary failure rate prediction model obtained by the regression analysis was normalized to a ground, fixed environmental factor equal to one. Therefore, the base failure rate constants given in Table 8.4-4 were multiplied by a factor of 0.539 and the appropriate set of environmental factors (π_{E2}) was included in the proposed model. Thus, the proposed base failure rates are:

λ_b = .0219, ferrite construction
λ_b = .120, discrete LC construction
λ_b = .265, discrete LC and crystal construction

The complete set of environmental factors normalized to a ground, benign factor equal to one is presented in Table 8.3-1.

Normalization of the base failure rate and the environmental factors concluded the failure rate prediction model development for filters. The proposed model presents failure rate as a function of construction, quality level and application environment. The use of this proposed model will improve the reliability prediction capabilities for equipments designed with filters.

8.5 References and Bibliography

References

1. Jones, Edwin C. Jr., and Hale, Harry W., Filters and Attenuators, Section 12, Electronics Engineers' Handbook, Second Edition, McGraw-Hill, 1982.

2. Kremp, B.F. and E.W. Kimball, Revision of Environmental Factors for MIL-HDBK-217B, Final Technical Report, RADC-TR-80-299, September, 1980.

Bibliography

Curtis Industries, Inc., RFI Power Line Filters, Catalog No. 481.

Electronic Products, EMI/RFI Filters, One Answer To Electrical Pollution, October, 1978, pp 35-40.

Eric Technological Products, LTD., Filter Connectors, Catalog FC-1255R.

Jones, Edwin C., Jr., and Hale, Harry W., Filters and Attenuators, Section 12, Electronics Engineers' Handbook, Second Edition, McGraw-Hill,, 1982.

Kremp, B.F. and E.W. Kimball, Revision of Environmental Factors for MIL-HDBK-217B, Final Technical Report, RADC-TR-80-299, September, 1980.

Mann, John E., Failure Analysis of Passive Devices, 16th Annual Reliability Physics Proceedings, 1978, pp 89-92.

9.0 SOLID STATE RELAYS

9.1 Part Description

A solid state relay (SSR) is a switching assembly (either hybrid or discrete components) which controls load currents through the use of solid state switches such as triacs, SCRs, or power transistors. These switching elements are controlled by input signals coupled to the switching devices through various isolation mechanisms such as reed relays, transformers, or optoisolators. Snubber circuits or zero-crossing detectors which reduce spikes and transients produced by interupting load currents are also used in some solid state relays.

Solid state relays in general incorporate the use of a heat sink to minimize operating temperature. These devices generate heat because of the voltage drop which is present in semiconductor devices. For example, a 40 amp SSR will typically drop 1.2 volts during conduction and in turn dissipate 50 watts of heat. However, no special system design is required because cooling and heat sinking methods are adequate.

9.2 Failure Modes and Mechanisms

Solid state relays are not susceptible to wear out from on/off cycling like electromechanical relays. Failures normally occur due to faulty SCR or triac switching. The most common failure mode is when a solid state relay falsely turns-on. Several failure mechanisms causing this phenomenom are:

1) operating temperatures which exceed the thyristor rating.

2) transients from the switched load or from an AC line could momentarily exceed the thyristor breakover voltage.

3) steeply rising load voltages could couple into the thyristor input through strong capacitances in the thyristor. (called dv/dt turn-on)

To help eliminate dv/dt turn-on, the use of back to back SCRs with reverse bias can be used in place of triacs in the solid state relay.

The main failure mechanism for solid state relays is mechanical fatigue of the power semiconductor structure due to thermal cycling. The effects of cycling can be controlled, however, through the matching of load cycling characteristics to relay characteristics.

9.3 Solid State Relay (SSR) Failure Rate Prediction Procedure

This Section presents the proposed failure rate prediction procedure for solid state relays. The prediction procedure is:

Step 1: If a Parts List and/or Schematic Diagram are available.

Step 1A: Calculate a failure rate for each particular component in the SSR assembly using the correct model from the following sections in MIL-HDBK-217:

Integrated Circuits	Section 5.1.2
Discrete Semiconductors	Section 5.1.3
Resistors	Section 5.1.6
Capacitors	Section 5.1.7
Inductive Devices	Section 5.1.8
Relays	Section 5.1.10
Printed Wiring Assemblies	Section 5.1.13

Step 1B: Sum the failure rate contribution for each component. The SSR failure rate (λ_p) then is:

$$\lambda_p = \sum_{i=1}^{n} \lambda_i$$

where

λ_p = SSR failure rate (F/10^6 hours)
λ_i = failure rate of each individual component (F/10^6 hours)

Step 2: If a parts list but no schematic diagram is available, or if the part complement can be determined by other means (e.g. disection).

Step 2A: Calculate a failure rate for each component type and for the SSR as an assembly using the procedure discussed in MIL-HDBK-217, Section 5.2.

Step 3: If no parts list or schematic diagram are available, calculate the SSR failure rate using the following model:

$$\lambda_p = \lambda_b \times \pi_E \times \pi_Q$$

where

λ_p = SSR failure rate (F/10^6 hours)
λ_b = base failure rate = 0.4 F/10^6 hours
π_E = environmental factor (see Table 9.3-1)
π_Q = quality Factor
= 1, MIL-SPEC quality
= 3, lower quality

TABLE 9.3-1: SSR ENVIRONMENTAL FACTORS

Environment	π_E	Environment	π_E
G_B	1	A_{IA}	13
G_F	3.3	A_{IF}	22
G_M	13	A_{UC}	11
M_P	10	A_{UT}	16
N_{SB}	5.2	A_{UB}	40
N_S	7	A_{UA}	24
N_U	17	A_{UF}	38
N_H	16	S_F	0.85
N_{UU}	17	M_{FF}	10
A_{RW}	23	M_{FA}	14
A_{IC}	6.5	U_{SL}	31
A_{IT}	9.5	M_L	35
A_{IB}	24	C_L	590

9.4 Failure Rate Model Development

The approach utilized for model development was to treat the SSR as a packaged assembly. The rationale for this approach is based on the following facts:

- the SSR is either a packaged assembly comprised of discrete components, or a hybrid assembly.
- every SSR is functionally a single pole-single throw (SPST) relay; however, the circuit design and consequently the quantity, quality and type of components used in the design varies between manufacturers.
- The SSR MIL-SPEC is a functional specification and does not specify or limit internal construction.

However, it was recognized that it may not be possible for the reliability analyst to obtain the parts list and/or schematic diagram for a SSR;

therefore a default prediction procedure was necessary. The following model was hypothesized which could be used when limited data were available:

$$\lambda_p = \lambda_b \times \pi_T \times \pi_Q \times \pi_E$$

where

λ_p = SSR failure rate ($F/10^6$ rs)
λ_b = base failure rate ($F/10^6$ hrs)
π_T = temperature factor
π_Q = quality factor
π_E = environmental factor

The SSR failure rate data collected in support of this study are presented in Table 9.4-1. Theoretically, environmental stress should have an effect on SSR reliability; however, since data were only available from two environments, the environmental factors could not be developed using regression techniques. Therefore, an alternate approach was developed. A weighted average π_E was calculated from a parts count prediction of a typical SSR and the environmental mode factors given in reference 1 and reference 2 (Table 9.4-2). The equation used to calculate the weighted average π_E is:

$$\pi_{Ej} = \Sigma \ (Qty_i \times FR_i \times \pi_{Eij}) \ / \ \Sigma \ (Qty_i \times FR_i)$$

where

π_{Ej} = weighted average environmental mode factor for environment j
Qty_i = number of part type i used in the assembly
FR_i = Failure rate of part type i
π_{Ei} = current environmental mode factor for part type i and environment j (reference 1)

TABLE 9.4-1: SSR FAILURE EXPERIENCE DATA

Source	Equipment Type	Env	Qual (1)	Load Type (2)	Temp (°C)	Output volts	No. Fail.	Operate Hours (X 10^6)	Failure Rate (F/10^6 hours) L 10%CL	PT EST	U 90%CL	U 60%CL
1	Solar System	GF	C	L	--	120	2	1.496	0.356	1.337	3.556	--
2	AN/UYK-7	GF	C	-	45	--	7	13.384	0.291	0.523	0.879	--
3	AN/UYK-7	GF	M	-	45	40	0	10.707	--	--	--	0.086
4	Traffic Control	GF	C	L	45	120	693	23827.2	0.028	0.029	0.030	--
5	Radar	GF	-	-	--	--	0	0.724	--	--	--	1.273
6	AN/UYK-7	NSB	M	-	45	40	0	0.111	--	--	--	8.306
7	AN/UYK-7	NSB	C	-	45	--	0	0.138	--	--	--	6.681
Total	--	--	-	-	--	--	702	23853.76	0.028	0.029	0.031	--

Notes: (1) C = Commercial, M = MIL-SPEC

(2) L = Lamp

TABLE 9.4-2: SSR ENVIRONMENT FACTOR INFORMATION

MIL-HDBK-217D ENVIRONMENTAL MODE FACTORS

Part Type	Qty	Qty^{X} F.R.	GB	GF	GM	MP	NSB	NS	NU	NH	NUU	ARW	AIC	AIT	AIB	AIA	AIF	AUC	AUT	AUB	AUA	AUF	SF	MFF	MFA	USL	ML	CL
Resistor, Film	9	0.194	1	2.4	7.8	8.8	4.2	4.7	14	14	15	19	2.5	3	9	6	6.5	7	6.5	20	15	15	0.4	8.9	12	26	30	510
Capacitor, Film	1	0.060	1	2.4	7.8	9.2	4.4	5.7	13	14	15	20	2.5	3	5.5	2.5	8	9.5	10	20	3	30	1	9.3	13	27	31	530
Diode, Signal	4	0.027	1	3.9	18	12	4.9	4.7	21	19	20	27	20	15	30	25	35	30	25	50	40	50	1	12	17	36	41	690
Transistor, NPN	1	0.025	1	5.8	18	12	11	8.6	21	19	20	27	9.5	15	40	20	35	15	25	65	35	60	0.4	12	17	36	41	690
Transistor, PNP	1	0.036	1	5.8	18	12	11	8.6	21	19	20	27	9.5	15	40	20	35	15	25	65	35	60	0.4	12	17	36	41	690
SCR	2	0.440	1	3.9	18	12	5.8	8.7	21	19	20	27	9.5	15	40	20	35	15	25	65	35	60	1	12	17	36	41	690
Optoisolator	1	0.210	1	2.4	7.8	7.7	3.7	5.7	11	12	13	17	2.5	3.5	3.5	5.5	8	3	5.5	5.5	8	10	1	7.8	11	23	26	450
PWB Assembly	1	0.003	1	2.3	7.7	6.9	4.1	5.3	12	13	14	19	2	5.5	8.5	5.5	7	6	15	25	15	20	1	8.7	12	26	29	500
Totals	19	0.995																										
Avg π_E	--	--	1	3.3	13.2	10.3	5.2	7.0	17.0	16.2	17.2	22.9	6.5	9.5	23.8	13.2	22.0	11.0	16.3	40.4	23.5	38.5	0.85	10.3	14.5	30.7	35	594

The factors were then rounded to two significant digits because of the uncertainity of the data.

The failure experience data shown in Table 9.4-1 for sources 1, 2, 3, 4 and 5 were normalized to the ground benign environment (G_B) by the π_E's derived above. The normalized data for sources 1, 2, 3 and 4 were then subjected to a regression analysis as described in Section 3.1 in order to ascertain if there was a significant difference between quality levels, and, if so, to derive a quantitative estimate of the difference. The source 5 data were deleted from the analysis because the quality level was unknown. The sources 6 and 7 data were deleted because of the low number of operating hours that were accumulated on the devices. The results of the regression are shown in Table 9.4-3.

TABLE 9.4-3: SSR REGRESSION ANALYSIS RESULTS

Variable	Coefficient (1)	STD-Error	F-Ratio
MIL-STD Quality	-1.173333 (0.3)	2.2983	0.26
Commercial Quality	(1.0)	--	--
Constant	-0.068846 (0.933)	--	--

Notes: (1) Numbers in paranthesis are the transformed parameters

Quality was found to be significant at the 30% level. The low level of significance was attributed to the sparsity of the data (4 data entries). Even though the level of significance was not high (30%), it is proposed that it be included in the prediction model since quality should be a significant factor affecting reliability. The proposed quality factors (π_Q) are:

MIL-STD Quality	1
Commercial Quality	3

The factors were rounded to one significant digit because of the uncertainty of the data.

The base failure rate factor (λ_b) was derived by taking the average value of the upper 90% confidence bounds on the source 1 through 5 and source 7 data. The upper 90% confidence bounds were calculated for data normalized to a MIL-SPEC part in a ground, benign environment. The source 5 data were assumed to be MIL-SPEC quality. This should be a realistic assumption since the equipment is a missile site radar. The average of the upper 90% confidence bounds was chosen to insure that an optimistic (lower than what would actually be observed in the field 90% of the time) failure rate was not predicted by the default technique. A secondary reason for using this upper bound was to force the analyst to utilize one of the first two techniques whenever possible since these techniques should generate a more nearly accurate estimate of the true failure rate. The data from source 6 was deleted from the analysis because no failures were observed and less than 1,000,000 normalized part hours were accumulated on the devices. The average of the 90% confidence bounds is $0.392F/10^6$ hours. Due to the uncertainty in the method of derivation, the base failure rate (λ_b) was rounded to $0.4\ F/10^6$ hours.

9.5 References and Bibliography

References

1. Edwards, E., et.al., Avionic Environmental Factors For MIL-HDBK-217, IIT Research Institute, Final Technical Report, RADC-TR-81-374, January, 1982.

2. Coit, David, W., Printed Wiring Assembly and Interconnection Reliability, Final Technical Report, RADC-TR-81-318, November 1981.

Bibliography

Coit, David, W., Printed Wiring Assembly and Interconnection Reliability, Final Technical Report, RADC-TR-81-318, November 1981.

Edwards, E., et.al., Avionic Environmental Factors For MIL-HDBK-217, IIT Research Institute, Final Technical Report, RADC-TR-81-374, January, 1982.

Fink, Donald G., and Christiansen, Donald, Editors, Electronics Engineers' Handbook, Second Edition, McGraw-Hill, 1982.

Howell, Dave, Electronic Products Forum on Solid State Relays, Electronic Products, February, 1977.

IIT Research Institute, Electronic Reliability Design Handbook, Volume II, Contract Data Item, Contract F30602-78-C-0281, 1981.

Weghorn, Frank, Solid State Relays, Electronics Products, Vol. 24, No. 6, October, 1981.

Yudewitz, Norman, Back to Relay Basics, Magnecraft Electric Company Pamphlet, 1980.

10.0 ELECTRONIC TIME DELAY RELAYS

10.1 Part Description

The relays described in this section are of the time delay type with either all solid state or hybrid (electromechanical relay and solid state delay) construction. Both of these types are classified as electronic time delay relays. The all solid state time delay relay utilizes a solid state circuit to perform the timing function and a solid state relay (described in Section 9.0) to perform the output switching function. The hybrid time delay relay utilizes a solid state circuit to perform the timing function and an electromechanical relay to perform the output switching function. Relays of these types are specified by MIL-R-83726. The time delay relays (TDRs) considered in this study then can be divided by output function and delay function. The output function is either accomplished by solid state circuitry or by an electromechanical relay. Since a description of the solid state output function and its associated failure modes and mechanisms has been discussed previously in this report (Section 9.0), and since descriptions of electromechanical relays and their associated failure modes and mechanisms are well documented (References 1, 2, 3), the discussion of the TDR part description and its associated failure modes and mechanisms will be limited to the time delay function.

The following discussion was extracted from reference 4. There are three basic methods of accomplishing the time delay function (RC Threshold, Frequency Counter or Digital Counter). The resistor-capacitor (RC) threshold designs generate the time delay by charging a capacitor through a resistor. Timing is accomplished by monitoring the voltage rise or fall across the capacitor. When a predetermined voltage is reached, relay driving circuitry turns on or off, depending on the relay function, and energizes or de-energizes the relay. A variable time delay circuit utilizes a variable resistor in the RC network, or a potentiometer to provide a variable reference for a voltage comparator. Frequency counting or dividing TDRs utilize a free-running oscillator. The oscillator output is applied to a

divider chain programmed to output a pulse at a specific count. This pulse is used to trigger the relay driving circuitry. Variable resistors are used in the variable time delay circuits to vary the oscillator frequency. Some frequency counting circuits have built-in programming switches to set the count needed to trigger the relay driver. A digital counter works on the same principle as the simple frequency counter, but has more sophisticated circuitry. The counter is programmed by external switches. The circuitry is driven by a crystal-controlled oscillator. By varying the counter programming instead of the frequency, greater accuracy is obtainable than for the RC threshold or frequency counter types. On-board memory and microprocessing will allow the digital counter type to provide several timing functions. The relay driver circuitry for all three types is necessarily heftier for the hydrid TDR since more current is required to actuate an electromechanical relay then to drive the input of a solid state relay. Figure 10.1-1 shows a function diagram for the three delay methods.

There are three basic timing modes associated with TDRs: delay-on-pull-in (DOPI), delay-on-drop-out (DODO) and interval-timing (IT).

DOPI relays provide a ' -on delay that begins the moment power is applied. The contacts close after the preset time has elapsed. If power is removed before the timing cycle is completed, the timer resets to zero.

DODO relays provide a turn-off delay that begins when a control voltage is removed. The word 'control' is important here because most DODOs require continuous power to maintain contact closure and timing function during the turn-off cycle. These devices monitor the presence of a control voltage or switch closure rather than the presence of main power. DODOs may use a latching relay to maintain contact closure after power is removed. An on-board storage capacitor holds sufficient charge to power the CMOS timing circuit and to energize the latching coil long enough to release the relay contacts.

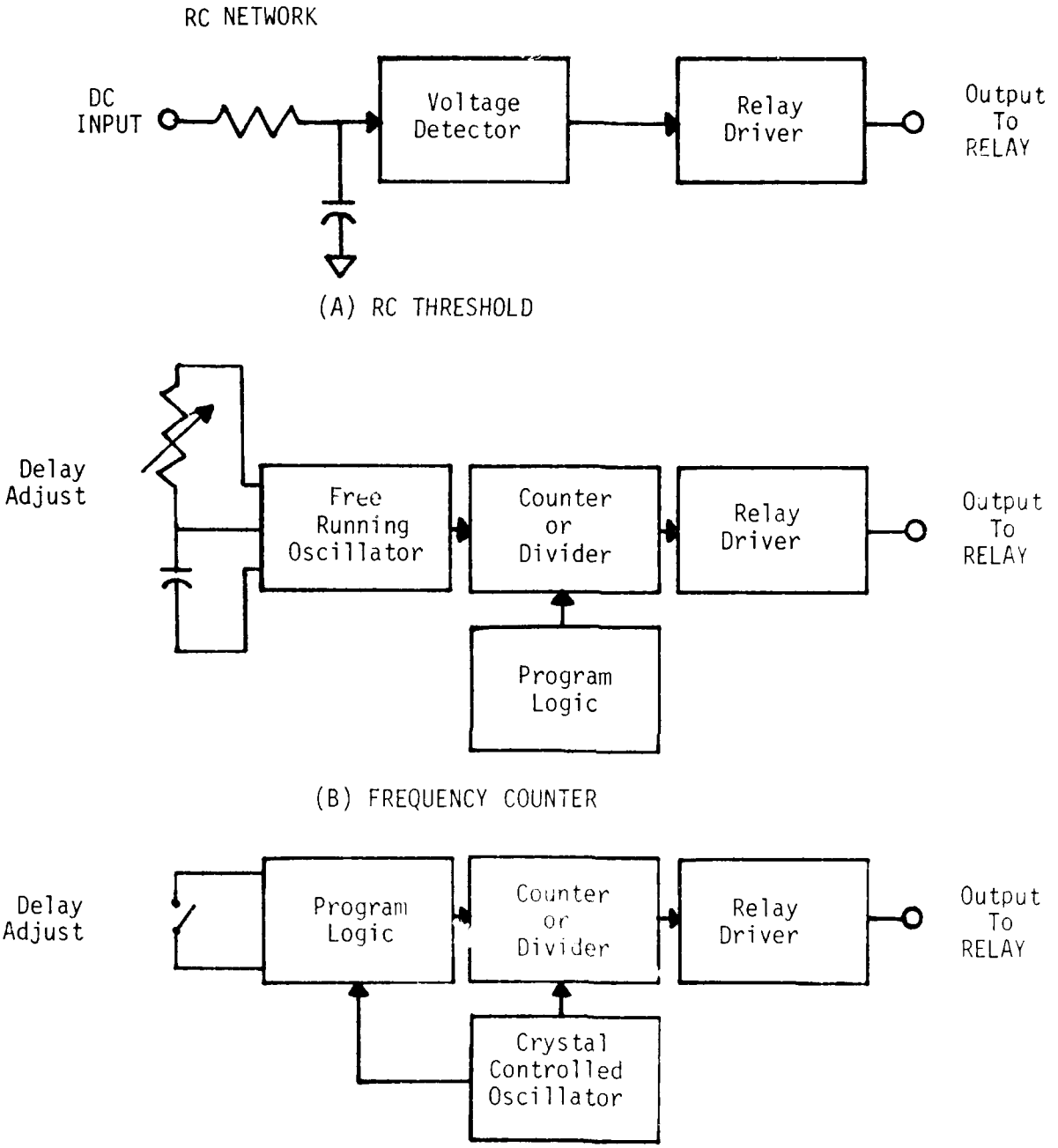

FIGURE 10.1-1: TDR DELAY METHODS

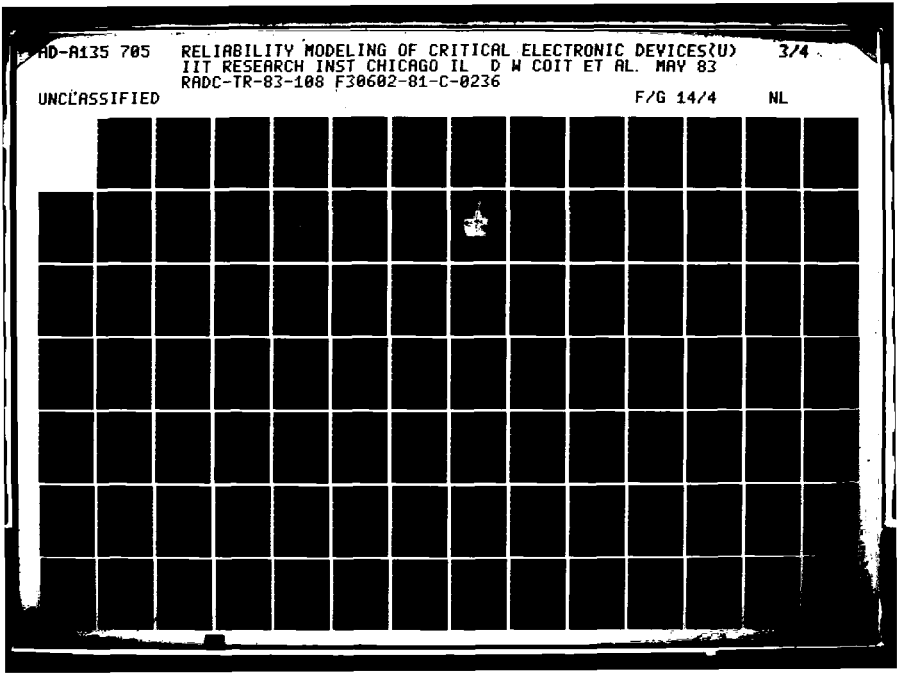

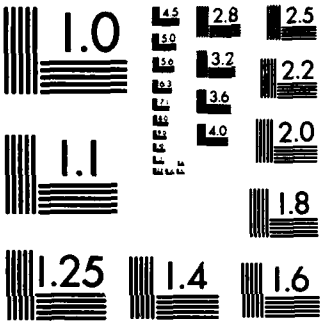

MICROCOPY RESOLUTION TEST CHART
NATIONAL BUREAU OF STANDARDS-1963-A

IT relays are a cross between DOPI and DODO devices. When power is applied, the timing cycle begins as it does in a DOPI relay. However, the contacts immediately close as in a DODO, and, as in a DODO, they open after the preset delay period has elapsed. Another similarity between the IT relay and the DODO relay is the need for continuous power. If power is removed before the timing cycle is completed, the contacts will open prematurely. There is a second type of IT relay that senses a control voltage or switch closure in the same manner as most DODOs. Although continuous operating power is required, the triggering signal can be a pulse of only a few milliseconds duration. These "one-shot" interval timers then start their timing cycle, closing the contacts and maintaining closure for the preset time interval.

The vast majority of TDRs offer a single timing function; however, there are versions that combine several timing functions in a common package. The most common is the DOPI/DODO. All hybrid relays with combined functions require continuous power for proper operation.

Parts lists were available on four hybrid DODO TDRs. As can be seen in Table 10.1-1, the quantity and type of components used to perform the delay function varies significantly among the relays. Although parts lists were not available for the DOPI or IT delay types, it is reasonable to assume that the complement of parts needed to perform those functions would differ from those given in Table 10.1-1. It is also obvious because of the differences in technology that the complement of parts needed for the frequency counting or digital counting TDRs would vary significantly from those given in Table 10.1-1. Therefore, since MIL-R-83726 is a functional specification, the technology and consequently the complement of parts used to obtain the desired function is up to the TDR manufacturer and can vary significantly for the same military part type.

TABLE 10.1-1: TDR PART COUNT

Relay Type MIL-R-83726/XXX

Part Type	023	043	043	Unknown
Transistor, NPN	6	3	2	3
Transistor, PNP	2	1	2	2
Transistor, UJT	0	1	0	0
Transistor, FET	1	0	1	1
Diode, Signal	6	5	7	8
Diode, Zener	3	2	2	2
Diode, SCR	0	0	1	0
Capacitor	5	3	4	6
Resistor	18	12	14	14
Potentiometer	0	0	1	0
Relay	1	1	1	1
Total	42	28	35	37

10.2 Failure Modes and Mechanisms

Since electronic TDRs are packaged assemblies, the failure modes and mechanisms associated with them are a function of the design and manufacturing techniques used. Several failure modes and operating characteristics and their associated effects that were given in references 4 and 5 are listed in Table 10.2-1.

Transients are a problem and most TDRs have built-in transient suppression networks to protect against false triggering and electrostatic discharge (ESD) damage to the internal components. The design engineer should insure that sufficient protection is provided (both internal and external) to assure reliable operation in the specified environment.

10.3 Electronic Time Delay Relay (TDR) Failure Rate Prediction Procedure

This Section presents the proposed failure rate prediction procedure for electronic time delay relays. The prediction procedure is:

Step 1: If a Parts List and/or Schematic Diagram are available.

TABLE 10.2-1: TDR FAILURE MODES/OPERATING CHARACTERISTICS AND EFFECTS

Type Delay	Failure Mode/Operating Characteristics	Effect on TDR
DOPI	Power Interrupted for short period	Timer may not reset, but instead pickup the count from the point at which power was removed
	False triggering caused by loss of power or a voltage transient on power line	relay contacts close briefly
DODO	Various component failures	relay drops out immediately after control voltage is removed
		relay drops out (after control voltage is removed) after a time delay exceeding the limit specified.
		relay does not drop out (after control voltage is removed) as long as operating voltage is applied
		relay does not pull in
		operating current > specified
		relay pulls in and then drops out after a time delay
		control current > specified

Step 1A: Calculate a failure rate for each particular component in the TDR assembly using the correct model from the following sections in MIL-HDBK-217:

Integrated Circuits	Section 5.1.2
Discrete Semiconductors	Section 5.1.3
Resistors	Section 5.1.6
Capacitors	Section 5.1.7
Inductive Devices	Section 5.1.8
Relays	Section 5.1.10
Printed Wiring Assemblies	Section 5.1.13

Step 1B: Sum the failure rate contribution for each component. The TDR failure rate (λ_p) then is:

$$\lambda_p = \sum_{i=1}^{n} \lambda_i$$

where

λ_p = TDR failure rate (F/10^6 hours)

λ_i = failure rate of each individual component (F/10^6 hours)

Step 2: If a parts list, but no schematic diagram is available, or if the part complement can be determined by other means (e.g., disection).

Step 2A: Calculate a failure rate for each component type and for the TDR as an assembly using the procedure discussed in MIL-HDBK-217, Section 5.2.

Step 3: If no parts list or schematic diagram are available and the TDR is a hybrid electronic TDR, calculate the TDR failure rate using the current MIL-HDBK-217 model for electronic time delay relays (MIL-HDBK-217D Section 5.1.10).

Step 4: If no parts list or schematic diagram are available and the TDR is an all solid state TDR, calculate the TDR failure rate using the proposed model:

$$\lambda_p = \lambda_D + \lambda_R$$

where

λ_p = TDR failure rate (F/10^6 hours)
λ_D = delay circuit failure rate (F/10^6 hours)
λ_R = relay circuit failure rate (F/10^6 hours)

Step 4A: Calculate the delay circuit failure rate (λ_D).

$$\lambda_D = \lambda_b \times \pi_E \times \pi_Q$$

where

λ_b = base failure rate = 0.5 F/10^6 hours
π_E = environmental factor (Table 10.3-1)
π_Q = quality factor
= 1, MIL-SPEC quality
= 4, lower quality

Step 4B: Calculate the relay circuit failure rate (λ_R) using the procedure given in MIL-HDBK-217, Section 5.1.10.2 (Proposed).

Step 4C: Calculate the total TDR failure rate (λ_p).

$$\lambda_p = \lambda_D + \lambda_R$$

TABLE 10.3-1: ENVIRONMENTAL FACTORS

Environment	π_E	Environment	π_E
G_B	1	A_{IA}	18
G_F	4.5	A_{IF}	30
G_M	16	A_{UC}	15
M_P	12	A_{UT}	21
N_{SB}	8.4	A_{UB}	58
N_S	8.8	A_{UA}	33
N_U	20	A_{UF}	52
N_H	18	S_F	0.58
N_{UU}	20	M_{FF}	12
A_{RW}	26	M_{FA}	17
A_{IC}	8.8	U_{SL}	35
A_{IT}	12	M_L	40
A_{IB}	35	C_L	680

10.4 Failure Rate Model Development

The approach utilized for model development was to treat the TDR as a packaged assembly. The rationale for this approach is based on the following facts:

- the TDR is a packaged assembly comprised of discrete components.
- every TDR is functionally a delay circuit and a switching circuit (relay); however, the circuit design and consequently the quantity, quality and type of components used in the design varies between manufacturers.
- The TDR MIL-SPEC is a functional specification and does not specify or limit internal construction.

However, it was recognized that it may not be possible for the reliability analyst to obtain the parts list and/or schematic diagram for a TDR;

therefore a default prediction procedure was necessary. The following model was hypothesized which could be used when limited data were available:

$$\lambda_p = \lambda_D + \lambda_R$$

where

λ_p = TDR failure rate (F/10^6 hours)
λ_D = delay circuit failure rate (F/10^6 hours)
$\lambda_D = \lambda_b \times \pi_E \times \pi_Q$
λ_b = base failure rate (F/10^6 hrs) (function of delay type (DOPI, DODO, IT, etc.))
π_E = environmental factor
π_Q = quality factor
λ_R = relay failure rate (F/10^6 hours)
λ_R = MIL-HDBK-217D Section 5.1.10 for electromechanical relays
λ_R = MIL-HDBK-217D Section 5.1.10.2 (Proposed) for solid state relays

The TDR failure rate data collected in support of this study are presented in Table 10.4-1. All of the data collected are for the hybrid DOPI type TDR; therefore, although the type of delay is seen as having an affect on reliability because each type requires a different complement of parts to perform its function, separate λ_b factors could not be derived. A second problem that arose from the data was that the failures could not be isolated to a specific part; consequently, it could not be determined whether it was a delay failure or a relay failure. The current MIL-HDBK-217 TDR failure rate model was investigated to determine its applicability and accuracy. An effort was undertaken to obtain the reliability predictions on the relays for which data were obtained so that the accuracy of the prediction could be checked. The predictions were not available. A second effort was initiated to obtain the necessary technical information (temperature, no. of cycles, stress ratio, etc.) from the applicable equipment technical orders. These technical orders were not available either. It was then necessary to make

TABLE 10.4-1: TDR FIELD EXPERIENCE DATA

Source	Conf	Qual (1)	Type (2)	Temp (°C)	Cycling Rate	Stress Ratio	Type Load (3)	Env	No. Fail	OP Hrs (X 10^6)	Failure Rate (F/10^6 hours) Observed L 10%CL	PT EST	U 90%CL	U 60%CL
1A	--	C	-	--	-	-	-	$G_F(4)$	2	0.226	2.35	8.85	23.5	--
1B	--	C	-	--	-	-	-	$G_F(4)$	0	0.110	--	--	--	8.38
1C	--	C	-	--	-	-	-	$G_F(4)$	2	1.321	0.403	1.51	4.03	--
1D	--	C	-	--	-	-	-	$G_F(4)$	0	0.163	--	--	--	5.66
1E	--	C	-	--	-	-	-	$G_F(4)$	1	0.569	0.185	1.76	6.84	--
2	--	-	1	--	-	-	-	$N_S(5)$	0	0.092	--	--	--	10.0
3	--	-	1	--	-	-	-	$G_F(6)$	0	0.480	--	--	--	1.92
4	SPDT	M	1	75	-	-	R	$A_{UB}(7)$	1	0.322	0.327	3.10	12.1	--
5	DPDT	M	1	75	-	-	R	$A_{UB}(7)$	0	0.161	--	--	--	5.73
6	DPDT	M	1	75	-	-	R	$A_{UB}(7)$	0	0.161	--	--	--	5.73
7	DPDT	M	1	75	-	-	R	$A_{UB}(7)$	0	0.161	--	--	--	5.73
8	DPDT	M	1	30	-	-	-	$G_M(8)$	0	0.246	--	--	--	3.75
9	DPDT	M	1	--	-	-	-	$A_{RW}(9)$	1	0.023	4.65	44.2	171	--
Total									6	4.012	7.85	1.50	2.62	--

Notes:
(1) C = lower quality, M = MIL-SPEC
(2) 1 = DOPI
(3) R = resistive
(4) Nuclear power plant equipment
(5) AN/SQS-26
(6) Radar
(7) AN/ALQ-117
(8) AN/TSQ-73
(9) OH-58C helicopter

assumptions regarding the usage of the parts so that the accuracy of the current model could be checked. The assumptions that were made are:

Source

1 thru 3 - Type = DPDT, temperature = 40°C, load = resistive, stress ratio = 0.75, cycling rate < 10/hour.

2 and 3 - Qual = MIL-SPEC

4 thru 7 - stress ratio = 0.75, cycling rate < 1/hour.

8 - load = resistive, stress ratio = 0.75, cycling rate < 10/hour.

These assumptions are for the most part reasonably accurate. The function of most TDRs is to turn circuitry on or off after a preset delay. One would not expect this to occur greater than once per hour on the average. The average temperature for G_F and N_S applications is approximately 23°C. The 40°C assumption allows for a 17°C internal rise within the equipment and relay enclosure. Source 2 and 3 are military equipments; therefore, it was assumed that the parts used would be MIL-SPEC or equivalent. The stress ratio is the recommended derated value for relays (reference 3). The assumption of a resistive load was made since the four points for which data were available (source 4-7) were used with resistive loads. The assumption of a DPDT configuration was made since five of the six points for which data were available employed a DPDT configuration. The 75°C temperature assumption for the A_{RW} environment was made to be consistent with the other airborne environments. It is probably a pessimistic assumption.

The data points for which all of the failure rate model parameters were the same and which had zero failures recorded were merged. The predicted and observed failure rates are given in Table 10.4-2. As can be seen, the data does not disprove the accuracy of the current model. Therefore it is proposed that the current model be retained as the default prediction method for hybrid electronic TDRs.

TABLE 10.4-2: PREDICTED AND OBSERVED FAILURE RATES

Source	No Fail	OP Hrs (X 10^6)	Predicted	Failure Rate (F/10^6 hours) Observed L 10%LC	PT EST	U 90%CL	U 60%CL
1A	2	0.227	2.62	2.35	8.85	23.5	
1C	2	1.321	2.62	0.403	1.51	4.03	
1E	1	0.569	2.62	0.185	1.76	6.84	
1B&1D	0	0.273	2.62			16.9	3.38
2	0	0.092	0.252			25.0	10.0
3	0	0.480	0.190			4.80	1.92
4	1	0.322	0.482	0.327	3.10	12.1	
5-7	0	0.483	0.826			4.77	1.91
8	0	0.246	0.323			9.37	3.75
9	1	0.023	2.534	4.65	44.2	171	
Total	7	4.036		0.965	1.73	2.92	

The current MIL-HDBK-217 relay prediction procedure does not address the all solid state electronic TDR (MIL-R-83726, Class C). A default prediction procedure was needed to address this class of relay. The default procedure adopted for solid state relays (Section 9.0) was also adopted for the delay portion of the all solid state TDR. The techniques used to develop the parameters for the λ_b, π_E and π_Q factors is discussed in the following paragraphs. The assumption had to be made prior to developing the parameters that the six observed failures occurred in the delay portion of the relay. This assumption may result in a pessimistic estimate for λ_b and an error in the π_Q parameters.

A weighted average π_E was calculated from the parts count predictions of typical TDRs given in Table 10.1-1, and the environmental mode factors given in reference 6 (Table 10.4-3). The equation used to calculate the weighted average π_E is:

$$\pi_{Ej} = \Sigma \ (Qty_i \times FR_i \times \pi_{Eij}) \ / \ \Sigma \ (Qty_i \times FR_i)$$

where

π_{Ej} = weighted average environmental mode factor for environment j
Qty_i = number of part type i used in the assembly
FR_i = Failure rate of part type i
π_{Ei} = current environmental mode factor for part type i and environment j (reference 1)

The factors were then rounded to two significant digits because of the uncertainity of the data.

The failure experience data shown in Table 10.4-2 were normalized to the ground benign environment (G_B) by the π_E's derived above. The normalized data were then subjected to a regression analysis as described in Section 3.1 in order to ascertain if there was a significant difference between quality levels, and, if so, to derive a quantitative estimate of the difference. The

TABLE 10.4-3: TDR ENVIRONMENT FACTOR INFORMATION

Part Type	Qty	Qty x F.R. (GB)	MIL-HDBK-217D ENVIRONMENTAL MODE FACTORS																											
			GB	GF	GM	MP	NSB	NS	NU	NH	NUU	AEW	AIC	AIT	AIB	AIA	AIF	AUC	AUT	AUB	AUA	AUF	SDF	MDF	MDA	USL	ML	CL
Resistor, Carbon	35	0.536	1	2.9	8.3	8.5	4	5.2	12	13	14	19	3	5	6.5	3.5	3.5	3	10	15	7	7	1	8.6	13	25	2	490
Resistor, Film	17	0.367	1	2.4	7.8	8.8	4.2	4.7	14	14	15	19	2.5	3	9	6	6.5	7	6.5	20	15	15	0.4	8.9	12	26	30	510
Resistor, Accurate WW	4	0.516	1	2.4	9.8	12	5.2	5.2	16	18	20	27	15	9	20	15	20	25	20	45	25	40	1.5	12	17	36	41	610
Resistor, Variable	1	0.300	1	2.9	11	18	5.7	5.7	15	27	29	39	6	3	10	4.5	7	15	7.5	25	10	15	1	18	25	53	61	1006
Resistor, PWR WW	2	0.432	1	1.5	8.3	11	4.9	4.9	14	16	17	23	1.5	3.5	10	7	7.5	5.6	7	20	15	15	0.6	11	15	31	36	610
Capacitor, Solid TANT	14	0.235	1	2.4	7.8	9.2	4.4	4.9	13	14	15	20	2.5	3	7	7.5	2.5	4.5	10	25	30	6	0.8	9.3	13	27	31	530
Capacitor, Ceramic	2	0.066	1	1.6	7.8	11	5	5.5	12.4	16	18	24	3	3	5	3	6	8	7.5	10	8	15	0.8	11	15	32	36	610
Capacitor, Non Solid TANT	2	1.200	1	1.4	10	11	5	6.7	15	16	17	23	6.5	2.5	10	4	6	20	8.5	40	15	20	1	11	15	31	36	610
Transistor, PNP/ NPN	21	12.64	1	5.8	18	12	9.8	9.8	21	19	20	27	9.5	15	40	20	35	15	25	65	35	60	0.4	12	17	36	41	690
Transistor, FET	3	1.410	1	4	18	12	6	8.6	21	19	20	27	9	7.5	40	30	35	15	10	65	50	55	0.6	12	17	36	41	690
Transistor, UJT	1	1.60	1	1	18	12	9.3	9.3	21	19	20	27	9.5	15	40	20	35	15	25	65	35	60	1	12	17	36	41	690
Diode, Signal	26	0.177	1	3.9	18	12	4.8	4.8	21	19	20	27	20	15	30	25	35	30	25	50	40	50	1	12	17	36	41	690
Diode, Zener	9	0.243	1	3.9	18	12	5.8	8.7	21	19	20	27	4.5	6.5	45	25	45	7.5	10	70	40	70	1	12	17	36	41	690
Diode, SCR	1	0.220	1	3.9	18	12	5.8	8.7	21	19	20	27	9.5	15	40	20	35	15	25	65	35	60	1	12	17	36	41	690
Totals	138	19.942	1																											
Avg π_E			1	4.5	16.4	11.8	8.4	8.8	19.6	18.5	19.6	26.4	8.8	12.4	34.6	18.3	30.1	14.8	21	58.5	32.6	52.1	0.58	11.8	16.7	35.2	40.2	675

source 2 and 3 data were deleted from the analysis because the quality level of the parts could not be ascertained. The results of the regression are shown in Table 10.4-4.

TABLE 10.4-4: TDR REGRESSION ANALYSIS RESULTS

Variable	Coefficient (1)	STD-Error	F-Ratio
MIL-STD Quality	(1.0)	--	--
Commercial Quality	1.4575 (4.3)	0.9875	2.18
Constant	-1.865537 (0.155)	--	--

Notes: (1) Numbers in paranthesis are the transformed parameters

Quality was found to be significant at the 80% level. The proposed quality factors (π_Q) are:

MIL-STD Quality	1
Commercial Quality	4

The factors were rounded to one significant digit because of the uncertainity of the data.

The base failure rate factor (λ_b) was derived by taking the average value of the upper 90% confidence bounds on the Table 10.4-2 source 1 and 4 through 8 data. The upper 90% confidence bounds were calculated for data normalized to a MIL-SPEC part in a ground, benign environment. The average of the upper 90% confidence bounds was chosen to insure that an optimistic (lower than what would actually be observed in the field 90% of the time) failure rate was not predicted by the default technique. A secondary reason for using this upper bound was to force the analyst to utilize one of the first two techniques whenever possible since these techniques should generate a more nearly accurate estimate of the true failure rate. The data from sources 2 and 3 were deleted from the analysis because the quality level of the part could not be determined. The source 9 data were deleted because of the low

number of operating hours that were accumulated on the devices. The average of the 90% confidence bounds is $0.464F/10^6$ hours. Due to the uncertainty in the method of derivation, the base failure rate (λ_b) was rounded to $0.5\ F/10^6$ hours.

10.5 References and Bibliography

References

1. Guth, George F., Development of Nonelectronic Part Cyclic Failure Rates, Martin Marietta Corporation, Final Technical Report, RADC-TR-77-417, December, 1977.

2. Arno, Robert G., Nonelectronic Parts Reliability Data, Reliability Analysis Center Publication NPRD-2, Summer, 1981.

3. IIT Research Institute, Electronic Reliability Design Handbook, Volume II, Contract Data Item, Contract F30602-78-C-0281, 1981.

4. Margolin, Bob, Time Delay Relays, DODOs, DOPIs and One-Shots, Electronic Products, May, 1979, pp 35-42.

5. Leach Relay Division, Technical Report, Failure Mode and Effects Analysis (FMEA) and MTBF Calculations, Leach Part No. TD-1161-1805, March, 1981.

6. Edwards, E., et.al., Avionic Environmental Factors For MIL-HDBK-217, IIT Research Institute, Final Technical Report, RADC-TR-81-374, January, 1982.

Bibliography

Arno, Robert G., Nonelectronic Parts Reliability Data, Reliability Analysis Center Publication NPRD-2, Summer, 1981.

Daniels, Leocadia, Time Delay Relays, Electronic Products, March, 1982, pp. 57-60.

Edwards, E., et.al., Avionic Environmental Factors For MIL-HDBK-217, IIT Research Institute, Final Technical Report, RADC-TR-81-374, January, 1982.

Fink, Donald G., and Christiansen, Donald, Editors, Electronics Engineers' Handbook, Second Edition, McGraw-Hill, 1982.

Guth, George F., Development of Nonelectronic Part Cyclic Failure Rates, Martin Marietta Corporation, Final Technical Report, RADC-TR-77-417, December, 1977.

IIT Research Institute, Electronic Reliability Design Handbook, Volume II, Contract Data Item, Contract F30602-78-C-0281, 1981.

Leach Relay Division, Thermal and Electrical Stress Analysis Data, Orbiter EEE Part Application, Leach Part No. EPH-391, Relay, Hybrid Driver, General Purpose, March, 1980.

IBID., Reliability Stress Analysis, Time Delay Relay, Model TD-1505-2001.

IBID., Model TD-1827-2001.

IBID., Model TD-1161-1805.

IBID., Worst-Case Analysis, Model TD-1505-2001 Time Delay Relay.

IBID., Technical Report, Failure Mode and Effects Analysis (FMEA) and MTBF Calculations, Leach Part No. TD-1161-1805, March, 1981.

Margolin, Bob, Time Delay Relays, DODOs, DOPIs and One-Shots, Electronic Products, May, 1979, pp 35-42.

Rauch, Ed, Prevention of ESD Damage During the Manufacture of Time Delay Relays, Coping with Static Electricity, Part XXXI, Evaluation Engineering, July/August, 1982.

Southwest Research Institute, Nuclear Plant Reliability Data System, 1979 Annual Reports of Cumulative System and Component Reliability, December, 1979.

Yudewitz, Norman, Back to Relay Basics, Magnecraft Electric Company Pamphlet, 1980.

IBID., Prediction Relay Life Mathematically, Magnecraft Electric Company Pamphlet, 1980.

11.0 CIRCUIT BREAKERS

11.1 Part Description

The NEMA (National Electrical Manufacturers' Association) definition of a circuit breaker is as follows: "A circuit breaker is a device for closing and interrupting a circuit between separable contacts under both normal and abnormal conditions. Normal indicates the interruption of currents not in excess of the rated continuous current of the circuit breakers. Abnormal indicates the interruption of currents in excess of rated continuous currents such as short circuits. Ordinarily, circuit breakers are required to operate relatively infrequently although some classes of breakers are suitable for frequent operation."

The attributes of circuit breakers in general are that they open automatically when required, are capable of carrying rated current and are capable of switching rated current. A circuit breaker must accomplish four fundamental duties:

(1) When closed it should be an ideal conductor.

(2) When open it should be an ideal insulator.

(3) When closed it must be able to interrupt its assigned current promptly without causing dangerous overvoltages.

(4) When open it has to be able to close promptly, possibly under short circuit conditions without contact welding.

Electromechanical circuit breakers considered in this study can be broken down into three major categories; thermal, magnetic and thermal-magnetic. Discussions of temperature compensated versions of thermal and thermal-magnetic circuit breakers are also included in this section. Each type of circuit breaker is available with one, two, three, four or more pole configuration.

A thermal circuit breaker is actuated when a bimetallic or trimetallic heat sensing element is exposed to temperature changes caused principally from load current heating. As heat is generated, the element binds or deforms and causes the contact mechanism to unlatch. In effect, the bimetal element pulls the trigger of a spring loaded switch which flies open. Thermal circuit breakers are best suited to protect wire since the thermal element within the circuit breaker is a reasonable analog of the performance of the protected wire. A typical thermal circuit breaker is given in Figure 11.1-1.

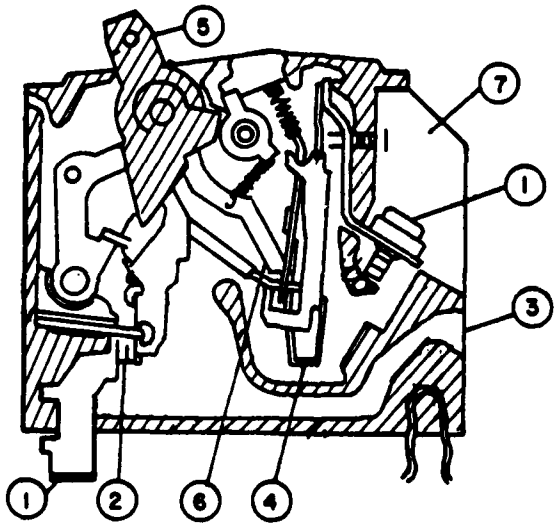

1 Terminals
2 Contacts
3 Blowout Vent
4 Bimetal Element
5 Handle
6 Latch
7 Case

FIGURE 11.1-1: OUTLINE OF TYPICAL THERMAL CIRCUIT BREAKER

Tripping action is caused by bimetals or trimetals. The deformation of the heat sensing element is caused by different thermal coefficients of expansion of the different metals in the bimetal or trimetal heat sensing

element. As relatively higher currents flow through the element, more heat is generated and faster bending of the element occurs. One metal used for the low expansion side of the element is invar. Copper is used in the center of a trimetallic element for low resistivity. For high resistivity, nickel is generally used. Various metals are used for the high expansion side.

Thermal circuit breakers have no instantaneous tripping point. A time delay is associated with all tripping actions. A typical graph of tripping time versus current overload is given in Figure 11.1-2. The actuation speed of a thermal circuit breaker varies directly with temperature and with the square of the current.

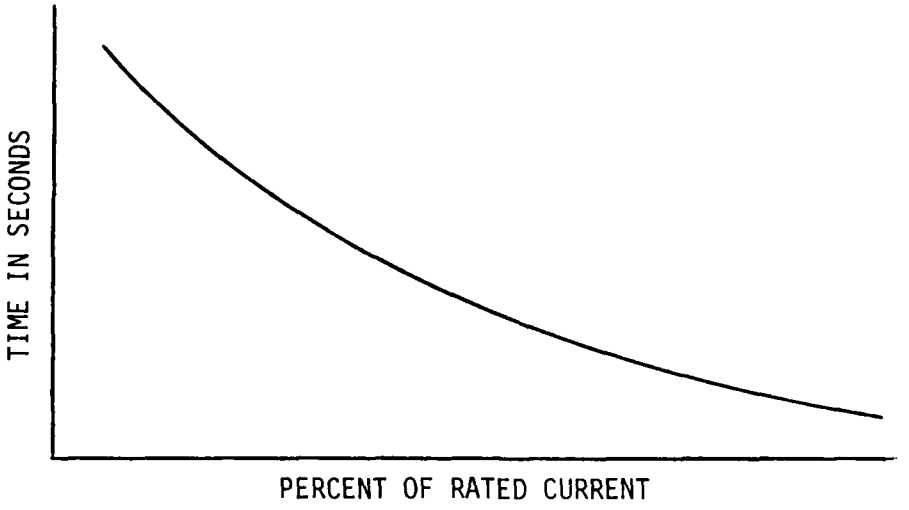

FIGURE 11.1-2: TRIP TIME CHARACTERISTICS OF A TYPICAL THERMAL CIRCUIT BREAKER

The deformation of the heat sensing element in thermal circuit breakers is dependent on temperature change. The circuit breaker will trip regardless of whether the temperature change is due to a current overload or a combination of current overload and increase in ambient temperature. The tripping time characteristics of thermal circuit breakers are highly dependent on ambient temperature. Because of this fact temperature compensated thermal circuit breakers are available. This type of circuit

breaker has an additional bimetal element which works in opposition to the overload element. The opposition bimetal element is isolated from heat generated by current overloads and therefore only deforms as a result of increased ambient temperature.

Magnetic circuit breakers depend on changes in magnetic flux which are caused by load current changes. The sensing and tripping functions are performed by separate elements; the solenoid coil and the armature. Magnetic circuit breakers contain a spring loaded movable iron core and a dampening fluid in a nonmagnetic tube with a solenoid coil wound around. As current increases, the iron core will move against the damping fluid because of increased magnetic flux. As the iron core moves towards the armature, the armature is attracted and the circuit breaker trips. If a critical magnetic flux value is reached (at approximately 1000% rated current) then the armature is attracted without movement of the iron core. This is the instantaneous tripping point for magnetic circuit breakers. Figure 11.1-3 shows the construction of a typical magnetic circuit breaker.

Time delay for magnetic circuit breakers is provided by the action of the fluid-damped movable iron core in the magnetic element. Overall delay characteristics are determined by several design variables. The most important design variable is the viscosity of the dampening fluid. Through adjustment of these variables, virtually any time-delay curve (trip time versus percent load) can be obtained. Ambient temperature has an effect on the viscosity of the dampening fluid and therefore effects trip time characteristics. Ambient temperature, however, has no effect on the instantaneous tripping current value.

Magnetic breakers are employed in circuits having high in-rush currents. A motor, for example, draws high current when power is first applied. As the motor comes up to running speed, the current requirements drop off quickly to normal. Because of the comparatively short duration of the high current demands, most circuitry and equipment can safely tolerate them. Therefore, it is not desirable to have circuit interruptions on these transient

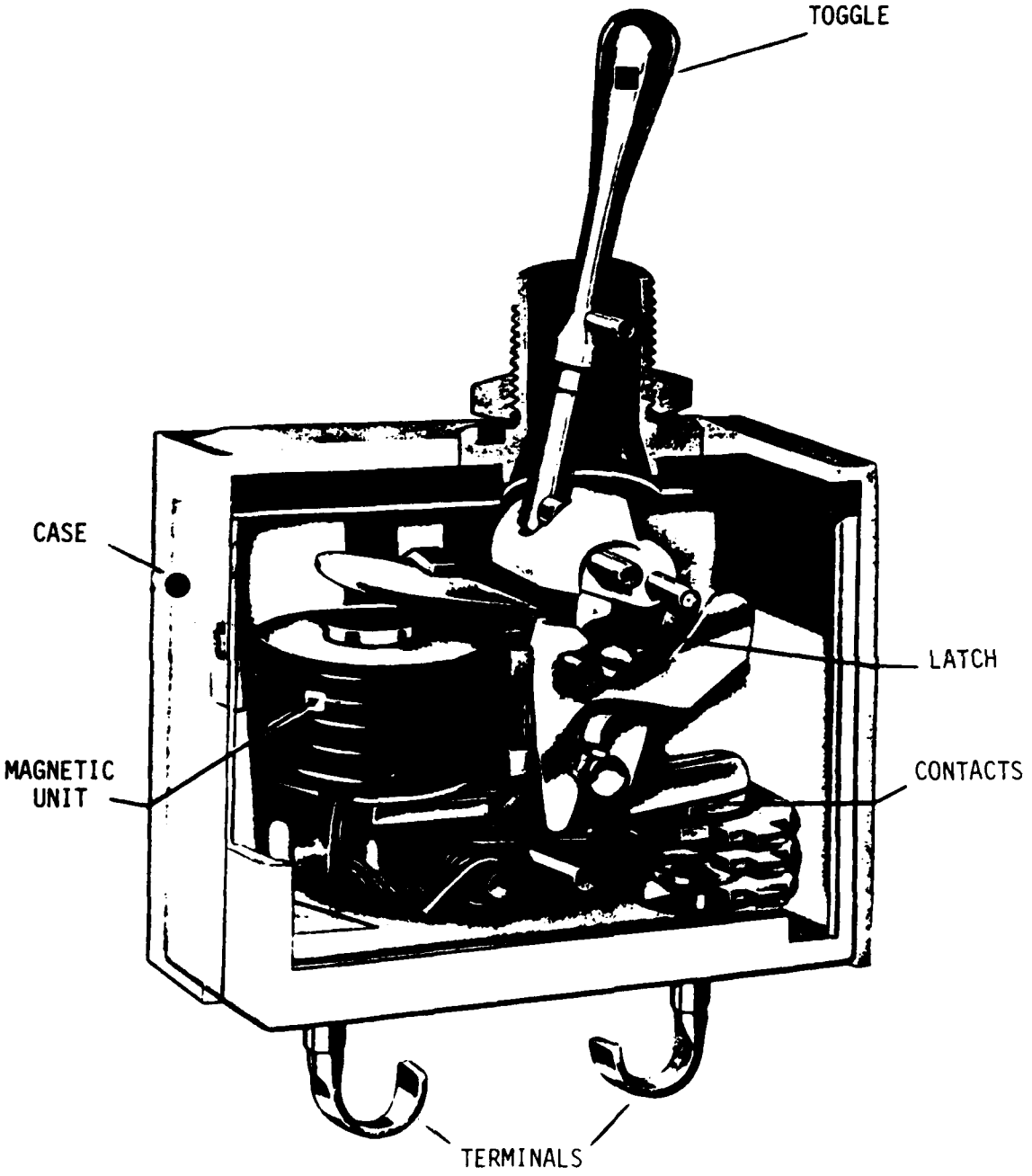

FIGURE 11.1-3: OUTLINE OF TYPICAL MAGNETIC CIRCUIT BREAKER

overloads, but it is necessary to interrupt prolonged or heavy overcurrents. The large number of possible time-delay curves is the reason that magnetic circuit breakers are ideal for these applications.

A thermal-magnetic circuit breaker is similar to a thermal circuit breaker until the point of contact opening. At this point the bimetallic element is assisted through the means of a magnet in tripping the contact mechanism. As the bimetallic element heats up, a magnetic field is also generated by the current. This magnetic field attracts the magnetic plate during high overloads and in turn causes the tripping of the device.

Thermal-magnetic circuit breakers are characterized by an instantaneous-trip point which is fixed at a specific percentage of the rated current. A coil can be used in series with the bimetallic element instead of a magnetic plate to activate the instantaneous trip. Figure 11.1-4 provides a graph of tripping time versus current overload for thermal-magnetic circuit breakers. As is the case with thermal circuit breakers, temperature compensated versions of thermal-magnetic circuit breakers are available.

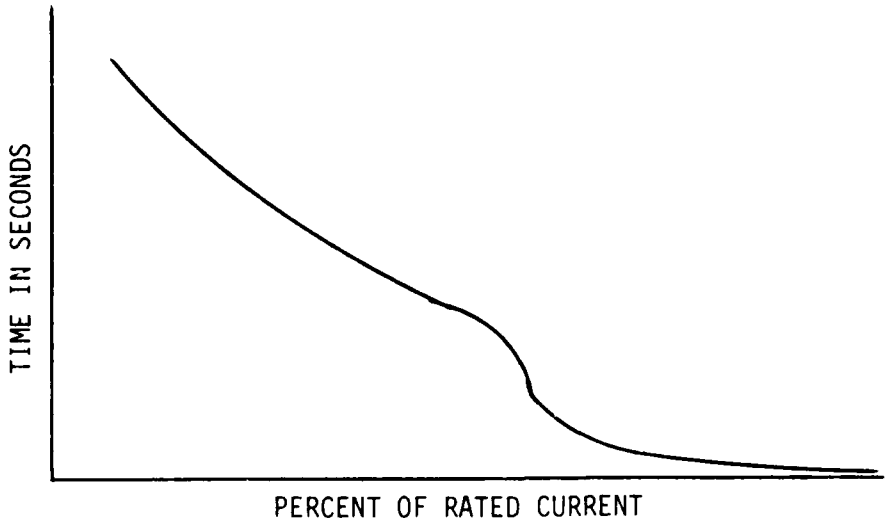

FIGURE 11.1-4: TRIP TIME CHARACTERISTICS OF A TYPICAL THERMAL-MAGNETIC CIRCUIT BREAKER

For each type of circuit breaker trip free construction is required in most applications. With this construction, the contact arm is independent of the manual operating handle while a fault exists. It is impossible to hold the contacts manually closed against an overload or short circuit. There are applications, primarily in aircraft operation, where a nontrip-free construction is desirable. These are cases where the function performed by the equipment is more important than the equipment itself; in these cases, non-trip-free construction permits the contacts to be held closed manually against the fault.

As can be deduced from this section, there are two basic means of circuit interruption for circuit breakers; thermal and magnetic. The use of a bimetal or trimetal heat sensing element is the distinguishing characteristic between the two basic types.

11.2 Failure Modes and Mechanisms

The failure modes and mechanisms for circuit breakers are similar to those of other electromechanical devices such as relays and switches. Reference 1 provides a failure mode distribution for circuit breakers in general, which is presented in Table 11.2-1.

TABLE 11.2-1: CIRCUIT BREAKER FAILURE MODE DISTRIBUTION

FAILURE MODE	FREQUENCY OF OCCURENCE
SHORT	38%
OPEN	38%
UNSTABLE	19%
ARCING	5%

All electromechanical devices such as circuit breakers would be expected to exhibit wearout type failures. Examples of possible wearout failure

mechanisms for circuit breakers are (1) fatigue induced failures of the bimetal element in thermal circuit breakers, (2) relaxation of the spring constant of springs used in circuit breakers, (3) contact surface degradation and (4) mechanical wear on moving parts. These wearout failure mechanisms would suggest that the failure rate of circuit breakers is an increasing function of time. However, empirical data to support this hypothesis is nonexistent. It cannot be determined whether the hazard rate of circuit breakers differs significantly from a constant value over the expected life of the equipment in which they are installed. Therefore until such data becomes available, the hazard rate of circuit breakers should be assumed constant.

All types of circuit breakers are susceptible to failures induced by environmental stress. Several different failure mechanisms which are accelerated by the environment are discussed in the following paragraphs.

At high altitudes contact arcing can occur at lower voltages and last longer as the contacts separate. This is mainly due to the fact that the dielectric strength of the air tends to decrease as barometric pressure decreases. Therefore when circuit breakers are used in high altitude applications, derated load and life specifications should be applied.

Insulating materials found in some circuit breakers may absorb moisture which decreases insulation resistance. Moisture may also condense on contact surfaces in a high humidity application and promote contact corrosion or galvanic action. Therefore, the selection of insulating material is important if the circuit breaker is to be applied in a high humidity environment.

In circuit breakers that use lubricants in bearing areas, high ambient temperatures may cause the flow of the lubricant onto the contacts or insulating surface. The reduction of lubrication on the moving parts may accelerate the wear of mechanical parts. Any film of lubricant deposited on

the insulating surfaces can capture dust and particles that reduce the dielectric strength and insulation resistance.

Very low ambient temperatures can decrease the viscosity of the lubricant and result in slower switching speed or even incomplete contact closure. Under certain atmospheric conditions ice may form causing higher and varying contact resistance. Increased contact forces tend to eliminate these problems.

Circuit breakers are more susceptible than switches to failure of the actuating mechanism. The actuating mechanisms in circuit breakers are not only more complex but are also susceptible to wear and fatigue from high impact loads. Incorrect operating and release forces are the main cause of failure. Premature switching or failure to switch may be due to mechanical misalignment of the actuation members, contamination, loose or defective parts, corrosion, or excessive wear on parts improperly installed.

A factor which obviously effects the reliability of circuit breakers is the configuration. A more complex circuit breaker (i.e. four pole) would be expected to have a higher failure rate than a less complex circuit breaker (i.e. one pole). This has been documented for other electromechanical devices (relays, switches) in MIL-HDBK-217D.

Poor manufacturing processes may also play an important role in the failure mechanisms of circuit breakers. Such anomalies as deformed contacts, loose or broken contacts, termination separation, and some external mechanisms may cause early failure of the circuit breaker. Loose or broken contacts are in many cases caused by inadequate welding of the leader, frame or support bracket. Shock or vibration can induce failures. Termination separation is the result of inadequate wire or terminal routing clearance. This can result in actuation mechanism interference, sharp bend radii resulting in the breakage of the wire, defective solder joints, overstressed solder joints, or defective welds. Failure mechanisms of this type can be eliminated by a thorough incoming inspection.

11.3 Circuit Breaker Failure Rate Prediction Model

This section presents the proposed failure rate prediction model for circuit breakers. The proposed model is:

$$\lambda_p = \lambda_b \pi_C \pi_Q \pi_E$$

where λ_p = predicted circuit breaker failure rate

λ_b = base failure rate

= 0.020 failures/10^6 hours, magnetic circuit breakers

= 0.038 failures/10^6 hours, thermal circuit breakers

= 0.038 failures/10^6 hours, thermal-magnetic circuit breakers

π_C = configuration factor (see Table 11.3-1)

π_Q = quality factor

= 1.0, MIL-SPEC quality

= 8.4, lower quality

π_E = environmental factor (see Table 11.3-2)

TABLE 11.3-1: CONFIGURATION FACTOR

Configuration	π_C
SPST	1.00
DPST	1.50
SPDT	1.75
3PST	2.00
4PST	2.50
DPDT	3.00
3PDT	4.25
4PDT	5.50
6PDT	8.00

TABLE 11.3-2: ENVIRONMENTAL FACTOR

Environment	π_E	Environment	π_E
G_B	1.0	A_{IA}	7.5
G_F	2.3	A_{IF}	10
G_M	8.2	A_{UC}	9.0
M_P	21	A_{UT}	8.0
N_{SB}	7.9	A_{UB}	15
N_S	7.9	A_{UA}	10
N_U	14	A_{UF}	15
N_H	32	S_F	1.0
N_{UU}	34	M_{FF}	21
A_{RW}	46	M_{FA}	29
A_{IC}	6.0	U_{SL}	62
A_{IT}	5.5	M_L	71
A_{IB}	10	C_L	N/A

11.4 Failure Rate Model Development

The approach utilized for model development was to identify significant parameters by analysis of circuit breaker field experience failure rate data. The model parameters were then quantified using the same data. At the conclusion of each step, the results were given a thorough analysis to determine whether they were consistent with theory. The circuit breaker failure rate data collected in support of this study is presented in Table 11.4-1. Data entries with zero failures and less than 500,000 part hours were merged with other data which were similar in regard to quality level, type, configuration and environment.

Application and construction variables were identified for circuit breakers and presented in Table 11.4-2. The application and construction variables represent factors which were determined whenever possible for all collected data. If sufficient detail could not be determined for a

TABLE 11.4-11. CIRCUIT BREAKER FAILURE RATE DATA

ENTRY NO.	QUALITY	TYPE	CONFIGURATION	ENVIRONMENT	TEMP (°C)	PART NO.	EQUIPMENT	FAILURES	PART HOURS
	MIL-SPEC	Magnetic	3PST	GF	25	M39019/5-70	AN/UYK-7	1	10,707,000
1	MIL-SPEC	Magnetic	DPST	GF	4	M39010/4-47	AN/FPS-108	0	28,512
2	MIL-SPEC	Magnetic	3PST	GF	25	M39019/1-218	AN/GYQ-18	0	355,902
3	MIL-SPEC	Magnetic	3PST	GF	25	M39010/1-248	AN/GYQ-18	0	355,902
	MIL-SPEC	Magnetic	3PST	NSB	45	M39019/5-70	AN/UYK-7	1	111,000
4	MIL-SPEC	Magnetic	SPST	AM	30	M39019/1-215	AN/TSQ-73	0	123,000
5	MIL-SPEC	Magnetic	SPST	AM	30	M39019/1-218	AN/TSQ-73	0	246,000
6	MIL-SPEC	Magnetic	SPST	AM	30	M39019/1-225	AN/TSQ-73	0	123,000
7	MIL-SPEC	Magnetic	SPST	GM	30	M39019/1-228	AN/TSQ-73	0	246,000
8	MIL-SPEC	Magnetic	SPST	GM	30	M39019/1-231	AN/TSQ-73	0	123,000
9	MIL-SPEC	Magnetic	SPST	GM	30	M39019/1-242	AN/TSQ-73	0	123,000
10	MIL-SPEC	Magnetic	SPST	GM	30	M39019/1-249	AN/TSQ-73	0	123,000
11	MIL-SPEC	Magnetic	SPST	AM	30	M39019/1-258	AN/TSQ-73	0	123,000
12	MIL-SPEC	Magnetic	DPST	AM	30	M39019/3-200	AN/TSQ-73	0	123,000
13	MIL-SPEC	Magnetic	3PST	GM	30	M39019/5-200	AN/TSQ-73	0	246,000
14	MIL-SPEC	Magnetic	3PST	GM	30	M39019/5-230	AN/TSQ-73	0	246,000
15	MIL-SPEC	Magnetic	3PST	GM	30	M39010/5-249	AN/TSQ-73	0	369,000
16	MIL-SPEC	Magnetic	DPST	GF	(4)	M55629/4-039	AN/FPS-108	0	28,512
17	MIL-SPEC	Magnetic	DPST	GF	(4)	M55629/4-046	AN/FPS-108	0	28,512
18	MIL-SPEC	Magnetic	DPST	GF	(4)	M55629/4-067	AN/FPS-108	0	28,512
19	MIL-SPEC	Magnetic	DPST	GF	(4)	M55629/4-095	AN/FPS-108	0	28,512
20	MIL-SPEC	Magnetic	DPST	GF	(4)	M55629/3-102	AN/FPS-108	0	142,560
21	MIL-SPEC	Magnetic	DPST	GF	(4)	M55629/3-130	AN/FPS-108	0	28,512
22	MIL-SPEC	Magnetic	SPST	GF	(4)	M55629/2-46	AN/FPS-108	0	28,512
23	MIL-SPEC	Magnetic	SPST	GF	(4)	M55629/2-107	AN/FPS-108	0	28,512
24	MIL-SPEC	Magnetic	3PST	GF	(4)	M55629/5-08	AN/FPS-108	0	28,512
25	MIL-SPEC	Magnetic	DPDT	GF	(4)	M55629/3-116	AN/FPS-108	0	114,048
26	MIL-SPEC	Magnetic	3PST	GM	(4)	M55629/5-132	AN/TSQ-73	0	123,000
27	Commercial	Magnetic	SPST	GF	25	(3)	AN/GYQ-18	0	1,067,706
28	Commercial	Magnetic	DPDT	GM	30	(3)	AN/TSQ-73	0	3,690,000
29	Commercial	Magnetic	SPST	GF	(4)	(3)	AN/FPS-108	0	28,512
30	Commercial	Magnetic	3PST	GF	(4)	(3)	AN/FPS-108	0	28,512
31	Commercial	Magnetic	3PST	GF	(4)	(3)	AN/FPS-108	0	28,512
32	Commercial	Magnetic	(4)	GF	(4)	(3)	AN/FPS-108	0	28,512
33	Commercial	Magnetic	(4)	GF	(4)	(3)	AN/FPS-108	0	28,512
34	Commercial	Magnetic	(4)	GF	(4)	(3)	AN/FPS-108	0	28,512
35	Commercial	Magnetic	(4)	GF	(4)	(3)	AN/FPS-108	0	28,512
36	Commercial	Magnetic	(4)	GF	(4)	(3)	AN/GYQ-18	0	355,902
37	Commercial	Magnetic	SPST	GF	25	(3)	AN/GYQ-18	0	355,902
38	Commercial	Magnetic	SPST	GF	25	(3)	AN/GYQ-18	0	355,902
39	Commercial	Magnetic	DPST	GM	30	(3)	AN/TSQ-73	0	123,000
40	Commercial	Magnetic	3PST	GM	30	(3)	AN/TSQ-73	0	123,000
41	Commercial	Magnetic	3PST	GM	30	(3)	AN/TSQ-73	0	246,000
42	Commercial	Thermal	SPST	GF	(4)	(3)	(4)	1	3,211,200
43	Commercial	Thermal	DPST	GF	(4)	(3)	(4)	2	3,211,200
44	Commercial	Thermal	3PST	GF	(4)	(3)	(4)	0	1,090,080
45	Commercial	Thermal	3PST	GF	(4)	(3)	(4)	2	1,090,080
46	Commercial	Thermal	3PST	GF	(4)	(3)	(4)	3	3,504,000
47	Commercial	Thermal	3PST	GF	(4)	(3)	(4)	0	1,477,520
48	Commercial	Thermal	3PST	GF	(4)	(3)	(4)	1	350,400
49	Commercial	Thermal	3PST	GF	(4)	(3)	(4)	1	425,088
50	Commercial	Thermal	3PST	GF	(4)	(3)	(4)	2	829,440
51	Commercial	Thermal	3PST	GF	(4)	(3)	(4)	3	929,440
52	Commercial	Thermal	3PST	GF	4)	(3)	4)	10	3,818,016
53	Commercial	Thermal	DPST	GF	4)	(3)	(4)	5	1,181,680
54	Commercial	Thermal	3PST	GF	4)	(3)	(4)	2	1,487,808
55	Commercial	Thermal	3PST	GF	(4)	(3)	(4)	2	1,912,896
56	Commercial	Thermal	3PST	GF	(4)	(3)	4)	3	1,062,720
57	Commercial	Thermal	DPST	GF	(4)	(3)	4)	0	363,360
58	Commercial	Thermal	3PST	GF	(4)	(3)	4)	0	425,088
59	Commercial	Thermal	DPST	GF	(4)	(3)	4)	0	17,200
60	Commercial	(4)	(4)	(4)	(4)	(3)	(4)	0	17,200
61	1	1	(4)	GF	(4)	(4)	(4)	236	113,398,000
62	1	1	(4)	GM	(4)	(4)	(4)	10	39,708,000
63	1	1	(4)	GF	(4)	(4)	(4)	2	10,340,970
64	1	1	(4)	GF	(4)	(4)	(4)	81	88,109,000
65	1	1	1	GF	(4)	(4)	(4)	1	9,872,000
66	1	1	1	NS	(4)	(4)	(4)	0	1,215,000
67	1	1	(4)	NS	(4)	(4)	(4)	1	1,622,488
68		Commercial	Under Volt.	(4)	GF	(4)	(3)	(4)	8	1,504,000
69		Commercial	Under Volt.	(4)	GF	(4)	(3)	(4)	0	744,000
TOTAL									379	324,197,690

NOTES

1. Data merged with other data entries of similar quality, type, configuration and environment.
2. Use of data questionable due to lack of detail
3. Commercial part numbers are proprietary.
4. Unknown.

TABLE 11.4-2: CIRCUIT BREAKER CONSTRUCTION AND APPLICATION VARIABLES

I. Type
   A. Thermal
   B. Magnetic
   C. Thermal-Magnetic
   D. Compensated Thermal
   E. Compensated Thermal-Magnetic

II. Pole Configuration
   A. Single Pole
   B. Double Pole
   C. Three Pole
   D. Four Pole

III. Construction Options
   A. Auxiliary Contacts
   B. Series Trip

IV. Seal
   A. Unsealed
   B. Panel Seal

V. Current Level
   A. Rated
   B. Actual

VI. Voltage Level
   A. Rated
   B. Actual

VII. Maximum Resistance or Impedence

VIII. Tripping Time Delay Characteristics (tripping time vs. % current overload)

IX. Actuator Operating Force

X. Operating Temperature
   A. Rated
   B. Actual

XI. Application Environment

XII. Manufacturing Quality Level

particular data entry, then it was not included in the model development process.

Theoretically the circuit breaker configuration is a significant variable effecting failure rate. To supplement the available data, the relation between configuration and failure rate was analyzed for other electromechanical devices with construction similarities to circuit breakers. The MIL-HDBK-217D failure rate prediction models for switches and relays include an identical factor based on device configuration. It was assumed that a configuration factor for circuit breakers would have a similar form. The factor for relays and switches is defined by the following equation.

$$\pi_C = 0.75PT - 0.25P + 0.50$$

where

π_C = device configuration factor
P = quantity of poles
T = quantity of throws

Assuming that the circuit breaker failure rate is best represented by a multiplicative model (i.e. $\lambda_p = \lambda_b \pi_1 \pi_2 \ldots$), inclusion of a factor in the form of the device configuration factor results in a nonlinear equation. As described in Section 3.1 regression analysis is difficult when the assumed model format is nonlinear. To solve this problem, the configuration factor which is applied to switches and relays was temporarily assumed to be correct for circuit breakers.

At the conclusion of the regression analysis, this assumption was examined to determine its feasibility.

Stepwise multiple linear regression analysis as described in Section 3.1 was applied to the circuit breaker failure rate data normalized by the assumed configuration factor. The data entries in Table 11.4-1 which included both sufficient detail and sufficient part hours to apply regression analysis are entry numbers 1, 29, 30, 44, 45, 46, 47, 48, 49, 50, 51, 52, 53, 54, 55, 56, 67 and 58. The regression analysis resulted in the following failure rate prediction model.

$$\lambda_p = \lambda_b \pi_C \pi_Q$$

where

λ_p = circuit breaker failure rate in failures/10^6 hours
λ_b = base failure rate
= 0.0450 failures/10^6 hours, magnetic circuit breakers
= 0.0884 failures/10^6 hours, thermal circuit breakers
π_C = configuration factor
π_Q = quality factor
= 1.0, MIL-SPEC
= 8.41, lower quality

It should be noted that the base failure rate values given above differ from the base failure rate values given in Section 11.3. This discrepancy is explained later in this section where environmental factors are introduced. The details of the regression analysis are given in Table 11.4-3. Base failure rate and quality factor were defined by the following equations. X_1 and X_2 are "dummy variables" used to quantify qualitative factors such as quality level and circuit breaker type.

$\lambda_b = \exp(\text{constant} + b_1 X_1)$
X_1 = 0, magnetic circuit breakers
X_1 = 1, thermal circuit breakers
$\pi_Q = \exp(b_2 X_2)$
X_2 = 0, MIL-SPEC
X_2 = 1, lower quality

TABLE 11.4-3: RESULTS OF CIRCUIT BREAKER REGRESSION ANALYSIS

Variable	Coefficient (b_i)	Standard Error	F-Ratio
X_1	-0.6747	0.5427	1.55
X_2	2.1300	0.8830	5.82
Constant	-2.4259	0.9023	

Degrees of Freedom = 15

Both variables (X_1, X_2) were significant at a 90% confidence level. The standard error statistic allows for the calculation of confidence intervals for base failure rate and quality level. Table 11.4-4 presents the point estimate, lower 20% confidence limit and upper 80% confidence limit for base failure rate and quality level.

TABLE 11.4-4: CONFIDENCE INTERVALS FOR CIRCUIT BREAKER PARAMETERS

Parameter	PT EST	Lower 20% CL	Upper 80% CL
Q	1.0	--	--
Q	8.41	3.90	18.14
b	0.0450	0.0281	0.0722
b	0.0884	0.0410	0.1910

Another regression analysis was performed without normalizing the data for configuration in order to re-examine the earlier assumption concerning the configuration factor. An exponential function of the number of poles was used to approximate the observed configuration factor. The results of this regression including point estimates, lower 20% and upper 80% confidence limits, and the configuration factor values currently in use for switches and relays are presented in Table 11.4-5. Analysis of these results reveal that there is no substantial difference between the assumed configuration factor and the observed approximate configuration factor. Therefore based on this regression analysis it was assumed that the configuration factor for switches and relays can also be applied to circuit breakers without

introducing error. The equation determined from the data to approximate the configuration factor is:

$$\pi_C = 0.857 \exp (0.154\ P)$$

where P = quantity of poles

TABLE 11.4-5: CONFIGURATION FACTOR ANALYSIS

Configuration	observed configuration factors $\pi_{c,\ 0.20}$	π_c	$\pi_{c,\ 0.80}$	assumed factors π_c
SPST	0.8	1.0	1.3	1.0
DPST	0.8	1.2	1.8	1.5
3PST	0.7	1.4	2.7	2.0

The assumed configuration factor was deemed preferable to the observed approximate configuration factor for several reasons. The assumed factor is an established documented factor and therefore should not be altered without substantial proof that it is inaccurate. The assumed factor was derived using data with higher pole configurations than was available for this study effort. If circuit breaker failure rate data could have been obtained with four or more poles, then the assumed and observed factors could have been aligned more precisely. Additionally, it was felt that the derivation of an additional factor based solely on the available data entries may have placed too high a burden on the available data and increased the probability of modeling "statistical noise".

Environment was not identified as a significant variable in the regression analysis. This does not imply, however, that environment is not a significant factor effecting reliability. The environment was omitted because the data used in the regression analysis was primarily from the ground fixed and ground mobile environment categories. The data collected in space flight, naval sheltered and air inhabited fighter environment categories was not used because sufficient detail regarding the circuit breakers was not obtainable. Theoretically, environmental stress has a

great effect on reliability and therefore an alternate approach was developed to derive a series of environmental factors.

The approach used to develop the environmental factors included comparison of circuit breaker failure modes and mechanisms with those of other electromechanical devices, primarily switches and relays. The anticipated effect of environmental stress on contact life, accelerated mechanical wear on moving components and other factors suggest similar environmental factors. The existing MIL-HDBK-217D environmental factors for relays, switches and connectors are given in Table 11.4-6. Relays and connectors each have two series of environmental factors depending on quality level.

TABLE 11.4-6: ENVIRONMENTAL FACTORS OF ELECTROMECHANICAL PARTS

Environment	Relays (MIL-SPEC)	Relays (Lower Quality)	Switches	Connectors (MIL-SPEC)	Connectors (Lower Quality)
G_B	1	2	1	1	1.5
S_F	1	(2.0)	1	1	1.5
G_F	2.3	4.6	2.9	1.2	4.7
N_{SB}	8	24	7.9	4.1	8.1
N_S	8	24	7.9	5.3	11
A_{IT}	4.0	8.0	5	5.0	15
M_P	21	63	21	8.5	17
M_{FF}	21	63	21	8.5	17
M_{FA}	29	82	29	12	24
G_M	8.2	25	14	8.3	25
N_H	32	96	32	13	26
N_{UU}	34	100	34	14	28
A_{UT}	12	30	50	5	15
N_U	14	38	20	13	27
A_{IF}	8.0	16	10	10	30
A_{RW}	46	140	46	19	37
U_{SL}	62	190	63	25	50
A_{UF}	24	60	100	10	30
M_L	71	210	71	29	58
C_L	N/A	N/A	1200	490	970

All data with recorded failures were merged according to environment to generate the environmental factors for circuit breakers. These data are

presented in Table 11.4-7. The failure rates given in Table 11.4-7 represent average values with respect to type, configuration and quality level. In order to use these data in conjunction with the existing environmental factors for electromechanical devices, a Chi-squared test was run to determine which of the five series of environmental factors given in Table 11.4-6 best represent the effect of environmental stress on circuit breakers. The Chi-squared test was set up with the average failure rates given in Table 11.4-7 equal to the observed values in the test and a series of predicted failure rates (as a function of the environmental factors given in Table 11.4-6) equal to the predicted values. The predicted failure rate value as a function of chosen environmental factor is given by,

$$\lambda_{pre} = (\Sigma\lambda_{obs}/\Sigma\pi_E)\pi_E$$

where

λ_{pre} = predicted average failure rate
λ_{obs} = observed average failure rate (Table 11.4-7)
π_E = environmental factor (Table 11.4-6)

This equation gives a best fit between observed and predicted values for each series of environmental factors given in Table 11.4-6. Then the Chi-squared test was applied to determine the optimal series of environmental factors. A brief discussion of the Chi-squared test is given in Section 3.1.

TABLE 11.4-7: CIRCUIT BREAKER FAILURE RATE DATA MERGED BY ENVIRONMENT

Environment	No. of Failures	Part hours($\times 10^6$)	Failure Rate ($f/10^6$hours)
SF	4	8.872	0.451
GF	107	146.519	0.730
GM	30	39.708	0.756
NS	1	1.215	0.823
AIF	236	119.998	1.967

The Chi-squared test results are given in Table 11.4-8. The relatively smaller Chi-squared values indicate a better fit between data and environmental factors. The results of the test indicate that the environmental factors currently applied to MIL-SPEC relays best represent the effects of the environment on circuit breakers. This result was intuitively satisfactory because of similarities between circuit breaker and relay failure modes and mechanisms.

The MIL-HDBK-217D environmental categories have been expanded to include additional avionic environments. Reference 5 presents the additional factors as well as the existing nonavionic environmental factors. The factors included in Reference 5 for MIL-SPEC relays are the proposed environmental factors for circuit breakers and they are the factors presented in Section 11.3.

TABLE 11.4-8: CHI-SQUARED TEST TO DETERMINE OPTIMAL ENVIRONMENTAL FACTORS

Environment	λ_{AVG}	MIL-SPEC Relays			Commercial Relays			Switches			MIL-SPEC Connect.			Commercial Connectors		
		π_{E1}	λ_1	x_1^2	π_{E2}	λ_2	x_1^2	π_{E3}	λ_3	x_1^2	π_{E4}	λ_4	x_1^2	π_{E5}	λ_5	x_1^2
[illegible]	0.451	1.0	0.172	0.453	2.0	0.132	0.780	1.0	0.132	0.771	1.0	0.183	0.392	1.5	0.098	1.270
[illegible]	0.730	2.3	0.395	0.284	4.6	0.304	0.598	2.9	0.383	0.315	1.2	0.220	1.183	4.7	0.308	0.579
[illegible]	0.756	8.2	1.410	0.303	25.0	1.650	0.485	14.0	1.849	0.646	8.3	1.521	0.385	25.0	1.634	0.475
[illegible]	0.823	8.0	1.375	0.222	24.0	1.584	0.366	7.9	1.043	0.046	5.3	0.971	0.023	11.0	0.720	0.015
[illegible]	1.967	9.0	1.375	0.255	16.0	1.056	0.785	10.0	1.320	0.316	10.0	1.832	0.010	30.0	1.964	0.000
Chi-Squared Values		$x^2 = 1.517$			$x^2 = 3.014$			$x^2 = 2.094$			$x^2 = 1.993$			$x^2 = 2.339$		

The regression analyses discussed previously consisted of data primarily in the ground fixed environment. In effect, the results of the regression were normalized to a ground fixed environmental factor equal to one. It was considered desirable that the series of environmental factors for circuit breakers be normalized to a ground benign environmental factor equal to one. Therefore, the previously derived base failure rates given in this section were divided by a factor of 2.3 (equal to the ground fixed environmental

factor). This could be done because of the multiplicative nature of the circuit breaker failure rate prediction model. The normalized base failure rates are as follows:

λ_b = base failure rate
= 0.0196 failures /10^6 hrs, magnetic circuit breakers
= 0.0384 failures /10^6 hrs, thermal circuit breakers

These values for base failure rate are identical to the base failure rate values given in Section 11.3 except for the number of significant digits. No failure rate data was available for thermal-magnetic circuit breakers. Based on theoretical considerations, the base failure rate developed for thermal circuit breakers was also applied to thermal-magnetic circuit breakers. The underlying factor was the use of a bimetal or trimetal heat sensing element to initiate tripping of the circuit breakers.

The determination of appropriate environmental factors and the normalization of the base failure rate values concludes the circuit breaker model development procedure. The development of modifying factors based on circuit breaker type, quality level, configuration and environment will greatly enhance failure rate prediction capabilities for these complex electromechanical devices.

11.5 References

1. Arno, R.G. (IIT Research Institute, Rome NY). Nonelectronic Parts Reliability Data, NPRD-2. Summer 1981.

2. Davis, W.B. (Airpax, Cambridge, MD). The Choice of Protection, 1979.

3. Machine Design, May 19, 1977, pp. 132-156.

4. Machine Design, May 13, 1982, pp. 139-146.

5. Edwards, E., Flint, S. and Steinkirchner, J. (IIT Research Institute, Rome, NY). Avionic Environmental Factors for MIL-HDBK-217, RADC-TR-81-374, January 1982.

12.0 I.C. SOCKETS

12.1 Device Description

I.C. (integrated circuit) sockets are constructed of an insulating housing containing female contact pins arranged geometrically to provide a mating capability with I.C. leads.

Socket housings are commonly made of thermoplastic materials such as glass filled nylon, polyesters, and polycarbonates. Thermosets such as DAP are also used. The latter provide excellent dimensional stability, but are generally more expensive. Many sockets, such as glass filled polyesters, come with a self-extinguishing 94 VO UL listing.

I.C. socket pins are available with three different types of terminations. The three types are solderless wrap, printed circuit and solder cup. The terminals are either plated with gold over nickel, or bright tin lead or bright acid tin over copper.

The I.C. socket contact is available in two basic design types. The contact design is either screw machined or stamped and formed. The screw machined contacts are close entry sleeves with machined, or stamped and rolled four leaf contact inserts. The stamped and formed contacts are available with several different design options. This type of contact can be designed with either a side wipe or a face wipe. The majority of all I.C. sockets make contact with the face of the I.C. lead. The stamped and formed contacts are also available with a single leaf or a double leaf configuration. For either type of contact design, the contact materials generally used are brass, beryllium copper, or phosphor bronze. The contacts are usually plated with either gold over nickel or tin over copper.

I.C. sockets are available which are compatible with a variety of I.C. pin quantities. The leading I.C. socket manufacturers offer sockets which are compatible with I.C.'s with up to 64 leads. Additionally, I.C. sockets

are available with either a standard profile or a low profile. Other I.C. socket construction options which are available to suit a particular application are right angle leads, zero insertion sockets, open body construction and anti-solder wicking barriers. Zero insertion force sockets have a sliding mechanism that provides effortless insertion and withdrawal of I.C.'s when the sockets are in the open position but locks them securely in place when the mechanism is closed.

12.2 Failure Modes and Mechanisms

Any use of I.C. sockets in field applications requires a reliability trade-off analysis. If the failure rate of the I.C. socket is high compared to the failure rate of the device inserted in the socket, then any other advantages offered by the sockets are negligible. Several failures modes and mechanisms applicable to I.C. sockets are discussed in this section.

One of the major I.C. socket failure modes is high contact resistance. If the socket is installed in a high contamination application, then there is the risk of oxides forming on the contacts or the accumulation of dust or dirt particles on the contacts. This condition creates a high contact resistance which may result in an intermittent or open connection. Additionally, increased contact resistance can be caused by repeated insertions of the I.C.. Repeated insertions can cause fatigue and deformation of the contact which results in the increased resistance. Contact and pin surfaces may also oxidize because of porous plating, scratched plating or overly thin plating.

Another failure mode experienced by I.C. sockets is the loss of insulation integrity. The I.C. socket housing should be an ideal insulator. In practice, changes in physical properties can occur because of high temperature operation or water absorption.

Another major reliability consideration for I.C. sockets is the compatibility of the I.C. socket plating and the I.C. lead plating. The

optimal combination is gold plated leads and gold plated contacts. The price of gold inhibits wide spread use of this combination. Other possible combinations are either tin plated leads and gold plated contacts or gold plated leads and tin plated contacts. In either case there is the possibility of galvanic corrosion caused by the contact of dissimilar metals. The fourth possible combination is tin plated leads and tin plated contacts. The possibility of galvanic corrosion is not present in this combination. However, tin plating is more porous than gold plating and therefore is more susceptible to the formation of oxides.

Side wipe contact construction has an inherent reliability problem. The method in which the I.C. lead is stamped results in a very rough edge. Insertion withdrawal cycles will very quickly cause the contact plating to be scraped off. Inadequate contact plating accelerates the oxidation process.

Caution should be applied in regard to I.C. socket usage in application environments with vibration stresses. When exposed to vibration the I.C. can "walk-out" of the socket. The probability of this failure mode is a function of the lead retention forces, the design of the socket and, of course, the magnitude and frequency of the vibration. To insure against occurrence of this failure mode, the use of sockets should be avoided in high vibration environments or the I.C.'s should be held securely in place by restraining straps.

More thorough discussions of I.C. socket failure modes and mechanisms are included in the documents listed in the bibliography of this section.

12.3 I.C. Socket Failure Rate Prediction Model

This section presents the proposed failure rate prediction model for I.C. sockets. The proposed model is:

$$\lambda_p = \lambda_b \times \pi_P \times \pi_E$$

where

λ_p = predicted I.C. socket failure rate

λ_b = base failure rate = 0.00042 failure/10^6 hours

λ_p = contact factor

$\lambda_p = \exp(\frac{N-1}{10})^{0.51064}$, N = number of active contacts

π_E = environmental factor (see Table 12.3-1)

TABLE 12.3-1: ENVIRONMENTAL FACTORS

Environment	π_E	Environment	π_E
G_B	1.0	A_{IA}	10*
G_F	3.1	A_{IF}	13*
G_M	17*	A_{UC}	10*
M_P	11*	A_{UT}	10*
N_{SB}	5.4	A_{UB}	13*
N_S	7.3*	A_{UA}	13*
N_U	18*	A_{UF}	20*
N_H	17*	S_F	1.0
N_{UU}	19*	M_{FF}	11*
A_{RW}	25*	M_{FA}	16*
A_{IC}	6.7*	U_{SL}	33*
A_{IT}	6.7*	M_L	39*
A_{IB}	10*	C_L	650*

* It is recommended that I.C. sockets should only be used in this environment if socketed device is restrained.

12.4 Failure Rate Model Development

The approach utilized for model development of I.C. sockets was to hypothesize a model form based on physics of failure information Quantification of all hypothesized parameters was not possible because of

limited data resources. However, a failure rate prediction model was derived based on several sound assumptions and analysis of the available data. A list of application and construction variables were determined for I.C. sockets and are presented in Table 12.4-1. The application and construction variables represent possible failure rate model parameters.

The preliminary model form which was hypothesized for I.C. sockets is given by:

$$\lambda_p = \lambda_b \, (N)^C \, \pi_Q \, \pi_E$$

where

λ_p = predicted I.C. socket failure rate
λ_b = base failure rate
λ_b = function of contact material, contact plating, contact design and I.C. lead plating
N = number of active contacts (active indicates electrical current flow through the contact)
c = constant
π_Q = quality factor
π_E = environmental factor

Insufficient field failure rate data were collected to quantify the hypothesized model. This was attributed to two major reasons. First, the use of sockets is very limited in military systems and therefore accurate data are scarce. Second, I.C. sockets are primarily used in ground, benign and ground, fixed environments. The failure rate of sockets operating in these environments is relatively low and therefore an extremely high number of part hours is required to observe a sufficient number of failures for modeling purposes. The field failure rate data which were collected are presented in Table 12.4-2.

TABLE 12.4-1: I.C. SOCKET CONSTRUCTION AND APPLICATION VARIABLES

I. Terminal Type
   A. Solderless Wrap
   B. Printed Circuit
   C. Solder Cup

II. Bond Material
   A. Diallyphthyalate (MIL-M-14, Type SDG-F)
   B. Nylon-Glass Filled (L-P-395, Type 1, Grade A, Class 1)
   C. Polyester-Glass Filled (MIL-M-24519)
   D. Polyphenylene Sulfide-Glass Filled (MIL-P-46174)
   E. Ether Polyurethane (MIL-P-47082)

III. Contact Material
   A. Brass (QQ-B-626)
   B. Beryllium-Copper (QQ-C-530 or QQ-C-533)
   C. Phosphor Bronze (QQ-B-750)
   D. Cupro-nickel alloy (CA725)
   E. Nickel-silver (CA770)

IV. Contact Plating
   A. Gold or Nickel
   B. Bright tin lead or bright acid tin over Copper

V. Terminal Plating
   A. Gold over Nickel
   B. Bright tin lead or bright acid tin over Copper

VI. Quantity of Pins

VII. Body Dimensions

VIII. Contact Design
   A. Screw Machined
   B. Stamped and Formed
      1. Dual Leaf vs. Single Leaf
      2. Face Wipe vs. Side Wipe

IX. Construction Options
   A. Right Angle Leads
   B. Zero Insertion Sockets
   C. Open Body Construction
   D. Anti-solder Wicking Barrier

X. Application Environment

XI. Manufacturing Quality Level

TABLE 12.4-2: I.C. SOCKET FAILURE RATE DATA

ENTRY NO.	QUALITY	CONTACT MATERIAL	CONTACT PLATING	TERMINAL TYPE	PINS/ SOCKET	ENVIRONMENT	EQUIPMENT	FAILURES	SOCKET HOURS
1	Commercial	Phosphor Bronze	Gold over Nickel	Solderless Wrap	24	GF	AN/GYQ-18	1	2,135,000
2	Commercial	Phosphor Bronze	Gold over Nickel	Solderless Wrap	16	GF	AN/GYQ-18	0	469,791,000
3	Commercial	Phosphor Bronze	Gold over Nickel	Solderless Wrap	16	GF	AN/GYQ-18	0	469,791,000
4	Commercial	Phosphor Bronze	Gold over Nickel	Solderless Wrap	14	GF	AN/GYQ-18	0	1,156,326,000
5	Commercial	Phosphor Bronze	Gold over Nickel	Solderless Wrap	14	GF	AN/GYQ-18	0	1,207,575,000
6	Commercial	Phosphor Bronze	Tin over Copper	Printed Circuit	16	GF	Computer	1	112,575,000
7	MIL-SPEC	Beryllium Copper	Gold over Nickel	Printed Circuit	16	NS	AN/SLQ-31	0	7,769,000
8	Commercial	(1)	(1)	(1)	16	GF	point of sales	0	20,736,000
9	Commercial	Beryllium Copper	Gold over Nickel	Solderless Wrap	16	GF	AN/GYQ-18	0	9,965,000
10	Commercial	Beryllium Copper	Gold over Nickel	Printed Circuit	14	GF	AN/GYQ-18	0	1,179,500
11	Commercial	Beryllium Copper	Gold over Nickel	Printed Circuit	16	GF	AN/GYQ-18	0	355,900
12	Commercial	Beryllium Copper	Gold over Nickel	Solderless Wrap	14	GF	AN/GYQ-18	0	18,507,000
13	Commercial	Beryllium Copper	Gold over Nickel	Solderless Wrap	24	GF	AN/GYQ-18	0	355,900
14	Commercial	Beryllium Copper	Gold over Nickel	Solderless Wrap	28	GF	AN/GYQ-18	0	355,900
15	Commercial	Beryllium Copper	Gold over Nickel	Printed Circuit	10	GF	AN/GYQ-18	0	711,800
								2	3,478,129,000

NOTES:

(1) Unknown

Field failure rate data were collected from only the ground, fixed and naval, sheltered environments. Therefore it was impossible to derive a complete series of environmental factors based solely on the data. Based on theoretical considerations, the environmental factors for lower quality connectors (Table 5.1.12.1-7 in MIL-HDBK-217D) were applied to I.C. sockets. This assumption was justified because the I.C. socket contact/I.C. lead interface is analogous to the interface between the male and female portions of a connector. The lower quality connector factors were applied because the I.C. lead is representative of a poor quality male connector due to the rough I.C. lead edges. The environmental factors for lower quality connectors range from a value of 1.5 for ground, benign and space, flight environments to a value of 970 for the cannon, launch environment. It was desirable to normalize the environmental factors to a value of one for the ground, benign environment. Table 12.4-3 presents both the existing lower quality connector environmental factors and the normalized factors to be applied to I.C. sockets. Additionally it is recommended that I.C. sockets should only be used in avionic and other high vibration environments if the socketed device is restrained to prevent "walkout".

The hypothesized I.C. socket failure rate prediction model assumed that failure rate was proportional to the number of active contacts raised by a constant. This hypothesized relation could neither be proved or disproved by the available data. Therefore the similarities between I.C. sockets and connectors were again analyzed. It was assumed that the relation between failure rate and number of contacts for connectors could also be applied to I.C. sockets. This relation is represented by a contact factor which is a multiplication factor and is given by the following equation:

$$\pi_p = \exp\left(\frac{N-1}{10}\right)^{0.51064}$$

where

π_p = contact factor

N = number of active contacts.

The great majority of the collected field experience data pertains to commercial quality level parts. One data record (entry number 3 in Table 12.4-2) was for military qualified I.C. sockets but it had zero observed failures. Therefore, development of a quality factor was not feasible. If it is assumed that commercial quality parts exhibit a higher observed failure rate, then a proposed model based on the collected data will predict a pessimistic failure rate for MIL-SPEC I.C. sockets.

TABLE 12.4-3: LOWER QUALITY CONNECTOR AND I.C. SOCKET ENVIRONMENTAL FACTORS

Env.	Lower Quality Connector π_E	Lower Quality Connector π_E, Normalized	Env.	Lower Quality Connector π_E	Lower Quality Connector π_E, Normalized
GB	1.5	1.0	AIA	15	10
GF	4.7	3.1	AIF	20	13
GM	25	17	AUC	15	10
MP	17	11	AUT	15	10
NSB	8.1	5.4	AUB	20	13
NS	11	7.3	AUA	20	13
NU	27	18	AUF	30	20
NH	26	17	SF	1.5	1.0
NUU	28	19	MFF	17	11
ARW	37	25	MFA	24	16
AIC	10	6.7	USL	50	33
AIT	10	6.7	ML	58	39
AIB	15	10	CL	970	650

The base failure rate for I.C. sockets was hypothesized to be a function of contact material, contact plating, contact design and I.C. lead plating. Due to the relative scarcity of failure rate data, an average base failure rate value was applied to all I.C. sockets. This assumption resulted in reduced accuracy for the proposed failure rate prediction model but was necessary because of the data deficiencies. The proposed model form is then given by:

$$\lambda_p = \lambda_b \times \pi_P \times \pi_E$$

where

λ_p = predicted I.C. socket failure rate
λ_b = base failure rate = constant
π_P = assumed contact factor
π_E = assumed environmental factor

To derive a numerical value for base failure rate, all data presented in Table 12.4-2 were normalized by environment and pin count. Normalized point estimate failure rates were calculated for each data entry by dividing observed failures by normalized part hours for data entries with observed failures and by calculating an upper 60% confidence limit for data entries without observed failures. These failure rate estimates are presented in Table 12.4-4. Dividing the summed failures by the summed normalized part hours resulted in a base failure rate estimate of 0.0000573 failures/10^6 hours. This potential base failure rate value was rejected for two reasons. First, the value was lower than any of the individual normalized failure rate estimates, which does not intuitively make sense. Second, the practice of merging failure rate data when the majority of data records have zero observed failures has questionable validity.

Therefore to derive a base failure rate estimate, the unweighted geometric mean of the normalized failure rate estimates for data entries 1 through 6 was computed. The data entries were not weighted because each data entry had either zero or one observed failure. Little failure rate estimation precision is offered in either case. If data entries had been available with greater than one observed failure, then those data entries would have been weighted accordingly. The geometric mean is preferable to the arithmetic mean for combining failure rate estimates. This technique is suggested in Reference 1. Data entries 7 through 15 were not included in the calculation because upper confidence limit failure rates for data records without observed failures are only meaningful if the failure rate estimate is

relatively low. This was not the case for data entries 7 through 15. The geometric mean of the normalized failure rates for data entries 1 through 6 is:

λ_b = 0.0000424 failures/10^6 hours

TABEL 12.4-4: I.C. SOCKET NORMALIZED FAILURE RATES

Entry No.	Normalized Failure Rate (f/10^6 hours)	Number of Observed Failures
1	0.0327	1
2	0.000184	0
3	0.000184	0
4	0.0000812	0
5	0.0000778	0
6	0.000838	1
7	0.00471	0
8	0.00416	0
9	0.00865	0
10	0.0796	0
11	0.242	0
12	0.00507	0
13	0.179	0
14	0.157	0
15	0.161	0

Inclusion of this numerical value into the proposed failure rate prediction model finalized the model development procedure for I.C. sockets. The proposed model offers the reliability analyst a method to assess the reliability of I.C. sockets. Currently, MIL-HDBK-217D does not consider I.C. sockets and the proposed model fills this void.

It should be noted that the proposed failure rate prediction model applies to I.C. socket failures observed at the socket housing and the socket/I.C. lead interface. The failure rate contribution of the I.C. socket terminal is accounted for by the interconnection assembly failure rate prediction model presented and developed in Reference 2.

12.5 References and Bibliography

References

1. Martz, H.F. and M.C. Bryson, A Statistical Model for Combining Biased Expert Opinions, Los Alamos Scientific Laboratory Rept. No. LA-UR-82-531.

2. Coit, David W., (IIT Research Institute), Printed Wiring Assembly and Interconnection Reliability, Final Technical Report, RADC-TR-81-318, November, 1981.

Bibliography

Augat Inc., Report of Test on 200 Series Low Profile DIP Socket with Beryllium Copper Contact, Test Report No. 178, December, 1979.

Augat Inc., Report of Test on 300 Series Low Profile DIP Sockets, Test Report No. 174, November, 1974.

Augat Inc., Report of Test on 500 Series Dual-In-Line Sockets, Test Report No. 173, February, 1973.

Bryant, N., D Hershberger and J. Coakley, Printed Circuit Board Assemblies from Countermeasures Set AN/ALQ-126; Failure Analysis of, Materials Test Report No. 67-77, August, 1977.

Burndy Electronic Products Laboratory, Test of DILB-P-108 Per MIL-S-83734A (USAF), Formal Report F7608-762, June, 1976.

Coit, David W., (IIT Research Institute), Printed Wiring Assembly and Interconnection Reliability, Final Technical Report, RADC-TR-81-318, November, 1981.

Erickson, J., W. Townes and J. Leary, R & M of Socketed I.C.'s, IEEE Transactions on Reliability, Vol. R-28, No. 5, December, 1979.

Erickson, J. and W. Townes, A Study of Integrated Circuit Mounting Techniques for Improved Reliability and Maintainability of FAA Airway Facility Systems, Report No. DELET-TR-79-7, March, 1979.

Gaynes Testing Laboratories, Qualification Testing of Socket, Plug-In, Part No. M83734/10, Order No. 9928-1215, January, 1978.

Howell, D., Socket or Solder, Electronic Products, Vol. 21, No. 1, June, 1978.

Robinson Nugent, Inc., Test Report on DIL I.C. Sockets for P.C.B. Applications, Report No. ICN-375, December, 1974.

13.0 THUMBWHEEL SWITCHES

13.1 Device Description

The switches which were considered in this study effort are thumbwheel, pushbutton and inline rotary switch types as specified by MIL-S-22710. The generic term "thumbwheel switch" was used as a notation to describe all three switch types. This term was selected for several reasons. First, thumbwheel switches are the most widely used of the three rotary switch types. Second, the pushbutton version of the MIL-S-22710 switch is physically similar to thumbwheel switches. Only the method of actuation is different. Third, the inline version of this switch type is rarely used. Although the term "thumbwheel switch" is used as a convenient notation in this discussion, the proposed failure rate prediction model applies to all three types of MIL-S-22710 rotary switches.

Thumbwheel switches typically consist of a thumbwheel with legend, a housing, a printed circuit board, contacts, a detent spring and eyelets. Generally there are two styles available. One version has a rotating printed circuit code disc and fixed contacts while the other version has rotating contacts and a fixed printed circuit board. In both versions the switch can operate in either direction. The switch position may be set in a variety of ways including use of a thumbwheel, lever, pushbutton or paddle lever. Detent action for the switch is provided by a plastic or metal spring, ball and spring combination, or an integral flexing member which is part of the spring housing.

Thumbwheel switches are typically designed with 2, 8, 10, 12, or 16 positions and are rated for operating temperatures ranging from -65°C to 125°C. Military versions of the switch are generally designed to meet military standards for thermal shock, vibration, explosion, salt spray, moisture, humidity and altitude.

Self extinguishing nylon and molded poylcarbonate are common materials used in the construction of the switch housing. Contacts are usually made of

beryllium copper with gold-over-nickel plating, which offers low contact resistance and long life. Epoxy glass printed circuit boards are standard.

A wide selection of thumbwheel switch models and options are available. Thumbwheel switch widths can range from 0.235" to 0.65". Overall switch height can range from 0.63" to 2.1" and depth behind the panel varies from 0.748" to 2.1". Standard indicator wheel markings include 0 to 7, 0 to 9 and 0 to 15. Character heights usually range from 0.09" to 0.25".

Thumbwheel switches are used wherever a man to digital device interface is required. By simply "dialing in" the required data on a multipole thumbwheel, an operator can program a wide variety of functions. The most common of these is to set operating limits. In some cases, operating the thumbwheel switch simply changes the configuration of an OR or AND gate matrix. In others applications, the thumbwheel switch is used to apply voltage to the appropriate pins of a microprocessor circuit. Depending on the device being controlled, the thumbwheel switch may be used to stop a process after a preset number of events has occurred, or at a predetermined voltage level.

Thumbwheel switches are also used to manually select channels in multichannel process controllers and data acquisition systems. With a thumbwheel switch, an operator can manually select a specific step in a lengthy program where an input terminal is not normally available.

Digital control of frequency synthesizers is another area for which the use of thumbwheel switches is well-suited. Such applications range from test equipment to radio transmitters. Thumbwheel switches are also used for the digital control of operations where a display of the preset instruction is required.

13.2 Failure Modes and Mechanisms

The failure modes and mechanisms of thumbwheel switches are similar to those of other rotary switch types. The expected failure modes include opens and shorts of the printed circuit board, jitter due to detent wear, and mechanical wearout problems. A more detailed discussion of rotary switch failure modes and mechanisms is given in Reference 1.

Contact life is a primary concern for all rotary switches. Several factors influence the integrity of the interface between the contacts and the printed circuit board code disc. All metal surfaces are susceptible to the formation of surface films. Airborne contaminants such as sulfides can condense on the contact surfaces and thus cause alterations of the physical and chemical properties of the contact plating material. When a surface film is softer than the contact material, the contact pressure will squeeze the film aside. However, when the film is harder than the contact material, there is a reduction of contact area and an increase in contact resistance. Brittle films will tend to be fractured away to expose the base metal during contact mating. Contact materials such as silver, platimum, palladium, tungsten, molybdenum and nickel are susceptible to the formation of oxide films. To make electrical contact through the tough and resistive oxide surface film requires relatively large contact forces. When high reliability is essential, gold plated contacts are recommended because they are virtually free from the formation of oxides.

13.3 Thumbwheel Switch Failure Rate Prediction Model

This section presents the proposed failure rate prediction model for thumbwheel switches. The proposed model is:

$$\lambda_p = (\lambda_1 + N\lambda_2)\ \pi_E \pi_{cyc} \pi_L$$

where

λ_p = predicted thumbwheel switch failure rate (failures/10^6 hours)

λ_1 = 0.0067 f/10^6 hours, MIL-SPEC quality

= 0.086 f/10^6 hours, lower quality

λ_2 = 0.062 f/10^6 hours, MIL-SPEC quality

= 0.089 f/10^6 hours, lower quality

N = number of active contacts

π_E = environmental factors (see Table 13.3-1)

π_{cyc} = cycling rate factor (see Table 13.3-2)

π_L = load type factor (see Table 13.3-3)

TABLE 13.3-1: ENVIRONMENTAL FACTORS

Environment	π_E	Environment	π_E
G_B	1	A_{IA}	15
G_F	2.9	A_{IF}	20
G_M	14	A_{UC}	10
M_P	21	A_{UT}	10
N_{SB}	7.9	A_{UB}	15
N_S	7.9	A_{UA}	15
N_U	20	A_{UF}	25
N_H	32	S_F	1
N_{UU}	34	M_{FF}	21
A_{RW}	46	M_{FA}	29
A_{IC}	8	U_{SL}	63
A_{IT}	8	M_L	71
A_{IB}	15	C_L	1200

TABLE 13.3-2: CYCLING RATE FACTOR

Switching Cycles	π_{cyc}
$\leq$ 1 cycle/hour	1.0
> 1 cycle/hour	number of cycles/hour

TABLE 13.3-3: LOAD TYPE FACTOR

Stress	Load Type		
S	Resistive	Inductive	Lamp
0.05	1.00	1.02	1.06
0.1	1.02	1.06	1.28
0.2	1.06	1.28	2.72
0.3	1.15	1.76	9.49
0.4	1.28	2.72	54.6
0.5	1.48	4.77	
0.6	1.76	9.49	
0.7	2.15	21.4	
0.8	2.72		
0.9	3.55		
1.0	4.77		

where

$$S = \frac{\text{operating load current}}{\text{rated resistive load}}$$

$$\pi_L = e^{(S/.8)^2} \text{ for resistive.}$$

$$= e^{(S/.4)^2} \text{ for inductive.}$$

$$= e^{(S/.2)^2} \text{ for lamp.}$$

CAUTION: This model applies to the switching function only. The model does not consider the contribution of any discrete components (e.g., resistors, diodes, lamp) which may be mounted on the switch. The failure rate of these devices must be calculated using the appropriate section in MIL-HDBK-217 and added to the failure rate of the switch.

This model applies to a single switch section. This type of switch is frequently ganged to provide the required function. The model must be applied to each section individually.

13.4 Failure Rate Model Development

The initial approach utilized for failure rate model development of thumbwheel switches was to identify and quantify significant failure rate model parameters by analysis of field experience data. The field experience failure rate data which were available are presented in Table 13.4-1. Application and construction variables were identified for thumbwheel switches and are presented in Table 13.4-2. The application and construction variables represent possible failure rate model parameters. The initial model development approach was unsuccessful due to field experience data limitations. Alternate model development approaches were explored because of the failure of the initial approach to yield an acceptable failure rate prediction model.

The alternate approach which was implemented for model development was based on analysis of the existing MIL-HDBK-217D failure rate prediction model for rotary switches (Section 5.1.11, MIL-HDBK-217D). The failure rate data presented in Table 13.4-1 were analyzed to determine whether the existing rotary switch model could be applied to thumbwheel switches without introducing error. Analysis of the the data did not invalidate the assumption that the existing rotary switch modifying factors based on cycling rate, load type and environment could be applied to thumbwheel switches. Therefore the assumption was made that a proposed failure rate prediction model for thumbwheel switches would be of the following form:

$$\lambda_p = (\lambda_1 + N\lambda_2)\,\pi_E\pi_{CYC}\pi_L$$

where

λ_p = predicted thumbwheel switch failure rate
λ_1, λ_2 = base failure rate constants (unique values for MIL-SPEC and commercial quality grades)
N = number of active contacts

TABLE 13.4-1: THUMBWHEEL SWITCH FAILURE RATE DATA

ENTRY NO.	NO. OF POSITIONS	NO. OF CONTACTS	LOGIC (1)	CYCLING RATE (CYCLES/HR.)	ENVIRONMENT	QUALITY	EQUIPMENT	FAILURES	PART HOURS
1.	10	11	Decimal	< 1.00	NSB	MIL-SPEC	AN/BRD-7	0	367,230
2.	8	4	BCO	< 1.00	NSB	MIL-SPEC	AN/BRD-7	0	367,230
3.	10	6	BCD	< 1.00	GM	MIL-SPEC	AN/TSQ-73	0	984,000
4.	16	6	BCH	< 1.00	GM	MIL-SPEC	AN/TSQ-73	0	246,000
5.	16	6	BCH	< 1.00	GM	MIL-SPEC	AN/TSQ-73	0	246,000
6.	8	5	BCO	< 1.00	GM	MIL-SPEC	AN/TSQ-73	0	1,476,000
7.	8	5	BCO	< 1.00	GM	MIL-SPEC	AN/TSQ-73	0	1,107,000
8.	10	6	BCD	< 1.00	GM	MIL-SPEC	AN/TSQ-73	0	369,000
9.(5)	8	5	BCO	< 1.00	GM	MIL-SPEC	AN/TSQ-73	0	246,000
10.	8	5	BCO	< 1.00	GM	MIL-SPEC	AN/TSQ-73	0	738,000
11.(5)	16	10	BCH(2)	0.01	AIC	MIL-SPEC	E-3A	0	78,310
12.	16	10	BCH(2)	0.25	AIC	MIL-SPEC	E-3A	2	130,520
13.	16	10	BCH(2)	0.11	AIC	MIL-SPEC	E-3A	1	208,820
14.	10	11	Decimal	< 1.00	GF	Commercial	Laboratory	12	4,426,000
15.	10	5	BCD	< 1.00	GF	Commercial	Traffic Control	1	3,200,000
16.	8	4	BCO	< 1.00	GF	Commercial	AN/GYQ-18	0	1,067,710
17.	10	6	BCD	< 1.00	GM	Commercial	AN/TSQ-73	0	3,936,000
18. (6)	10	5	(3)	< 1.00	GM	Commercial	AN/GRR-23	0 (6)	1,954,560
19. (6)	10	5	(3)	< 1.00	GM	Commercial	AN/GRR-23	0 (6)	1,954,560
20. (6)	10	5	(3)	< 1.00	GM	Commercial	AN/GRR-23	0 (6)	1,954,560
21. (6)	16	5	BCH	< 1.00	GM	Commercial	AN/GRR-23	0 (6)	1,954,560
22.	16	6	BCH	< 1.00	AIC	Commercial	(4)	3	189,200
Totals								19	5,485,000

NOTES: (1) BCO = binary coded octal, BCD = binary coded decimal, BCH = binary coded hexadecimal
(2) binary coded hexadecimal plus complement
(3) 9's complement of binary coded decimal
(4) unknown
(5) insufficient part hours to include in regression
(6) number of failures unverified

TABLE 13.4-2: THUMBWHEEL SWITCH CONSTRUCTION AND APPLICATION VARIABLES

I. Type
   A. Thumbwheel
   B. Inline
   C. Pushbutton

II. Number of Positions

III. Number of Contacts

IV. Logic
   A. Decimal
   B. Binary Coded
      1. Octal
      2. Decimal
      3. Hexadecimal
   C. Other

V. Housing and Thumbwheel Material
   A. Polycarbonate
   B. Self-extinguishing Nylon

VI. Contact Material
   A. Beryllium Copper
   B. Other

VII. Contact Plating
   A. Gold over Nickel
   B. Tin over Copper
   C. Other

VIII. Actuation Frequency (#Actuations per Unit Time)

IX. Application Environment

X. Manufacturing Quality Level

XI. Load Type
   A. Lamp
   B. Inductive
   C. Resistive

XII. Current Level
   A. Rated Resistive Current
   B. Actual Current

π_E = environmental factors
π_{cyc} = cycling rate factor
π_L = load type factor

To determine point estimate values for the two base failure rate constants, the data were separated by quality level and normalized for environment, cycling rate and load type using the assumed rotary switch failure rate model modifying factors. Each data entry was for thumbwheel switches which were switching a resistive load. The ratio of applied current to rated resistive current was unknown for the majority of data entries. The assumption was made that the ratio of applied current to rated resistive current was equal to 0.10 for all data entries. This is a realistic assumption because thumbwheel switches are used almost exclusively for switching decimal or binary logic circuits where a low current is required. Point estimate failure rates were calculated for each data entry by dividing the number of observed failures by the part hours for data entries with observed failures, and by calculating an upper 60% confidence limit value for data entries without observed failures. The normalization function and the resulting regression model are given by:

$$\lambda_N = \lambda_O/(\pi_E \pi_{cyc} \pi_L) = \lambda_1 + N\lambda_2$$

where

λ_N = normalized failure rate
λ_O = observed failures/part hours, data entries with observed failures
λ_O = upper 60% confidence limit, data entries w/o observed failures
π_E = assumed environmental factors
π_{cyc} = assumed cycling rate factor
π_L = assumed load type factor
= 1.02, resistive load stress = 0.10

Stepwise multiple linear regression analysis as described in Section 3.1 was applied to the data. The failure rate data had been separated by quality

level and therefore two regression analyses were required. The data records which were entered into the regression analyses are data entries 1-8, 10, 12-16 and 22 in Table 13.4-1. Data entries which were not included in the regression analyses either had insuffient part hours to estimate a failure rate without observed failures or lacked other requisites. The results of the two regression analyses are:

$$\lambda_{N,MIL\text{-}SPEC} = -0.5197 + 0.1317(N), \; R^2 = 0.60$$
$$\lambda_{N,commercial} = 0.0860 + 0.0888(N), \; R^2 = 0.30$$

The regression solution for commercial quality thumbwheel switches is satisfactory. However, the regression solution for military qualified thumbwheel switches is illogical, particularly because it predicts a normalized failure rate which is negative for thumbwheel switches with less than four contacts. Probable explanations for this result are (1) there was an inadequate number of data entries with observed failures to accurately apply regression analysis, and (2) no data entries were available for thumbwheel switches with less than four contacts. Therefore, the regression solution for military qualified thumbwheel switches was rejected and an alternate modeling approach was proposed.

The existing MIL-HDBK-217D equation for MIL-SPEC ceramic RF wafer rotary switches and MIL-SPEC medium power wafer rotary swtiches is given by:

$$\lambda_b = 0.0067 + 0.00003(N) \text{ failures}/10^6 \text{ hours}$$

where

N = number of active contacts

The dominant failure mechanisms associated with thumbwheel switches pertain to the switch contacts. Therefore the second base failure rate constant value in the above equation should not be applied to thumbwheel switches without verification with empirical data. However, it was assumed

that the first base failure rate constant could be applied to all types of rotary switches including thumbwheel switches. Therefore the failure rate equation for thumbwheel switches was assumed to be of the form:

$$\lambda_b = 0.0067 + \lambda_2(N) \text{ failures}/10^6 \text{ hours}$$

The failure rate data for MIL-SPEC thumbwheel switches was then analyzed to determine the remaining unknown base failure rate constant. The solution of a regression analysis which is forced through the origin and has only one independent variable, is given by:

$$Y = b_1 X_1$$
$$b_1 = \Sigma(X_{1,i} Y_i)/\Sigma(X_{1,i})^2$$

where

b_1 = regression coefficient
Y = dependent variable
X_1 = independent variable.

An additional variable was defined so the equation for MIL-SPEC base failure rate would be of this form. The additional dependent variable is defined as follows:

$$\lambda_R = \lambda_N - 0.0067$$

where

λ_R = additional regression dependent variable
λ_N = observed failure rate normalized for environment, cycling rate and load type.

The regression analysis model form was then modified to:

$$\lambda_R = \lambda_N - 0.0067 = \lambda_2(N)$$

and the second base failure rate constant (λ_2) for MIL-SPEC thumbwheel switches was derived by:

$$\lambda_2 = \Sigma(\lambda_R N)/\Sigma N$$
$$= 34.279/556 = 0.0617.$$

The complete base failure equation for MIL-SPEC thumbwheel switches was as follows:

$$\lambda_b = 0.0067 + 0.062(N).$$

Derivation of the second base failure rate constant for MIL-SPEC thumbwheel switches completed the model development process. The proposed model presented in its complete form including the assumed modifying factors for environment, cycling rate and load type was included in Section 13.3.

Thumbwheel switches are available with character illumination capabilities, or with diodes or resisters mounted on the external printed circuit board. The proposed failure rate prediction model for thumbwheel switches does not account for these additional components. The appropriate sections of MIL-HDBK-217D must be used in conjunction with the proposed thumbwheel switch failure rate prediction model for these hybrid types of thumbwheel switches.

13.5 References and Bibliography

References

1. Guth, G.F., Development of Nonelectronic Part Cyclic Failure Rates, Final Technical Report, RADC-TR-77-417, December, 1977.

Bibliography

Arno, R.G., Nonelectronic Parts Reliability Data, NPRD-2, Summer 1981.

Guth, G.F., Development of Nonelectronic Part Cyclic Failure Rates, Final Technical Report, RADC-TR-77-417, December, 1977.

Henriksen, D., Thumbwheel Switches, Electronic Products, July 1, 1979.

Pogmore, J., Selecting Switches for Harsh Environments, Electronic Products, June, 1982.

14.0 METERS

14.1 Part Description

The meters considered in this study are all ultimately either AC or DC electromagnetic current measuring devices.

DC meters utilize a core magnet and moving coil movement (D'Arsonval movement). DC meters are based on the principle that a current carrying conductor in a magnetic field will experience a force. If a conductor in the uniform magnetic field is constrained by a linear spring, the motion against the spring will be proportional to the current in the conductor. In this movement, a permanent magnet is enclosed by the moving coil and the return path of the flux is through the coil to an iron ring surrounding the coil. This type of movement is self shielding and is little affected by magnetic panels or stray magnetic fields. By using precision resistors, either internal or external to the meter, deflection can be made proportional to voltage.

AC meters including Radio Frequency meters normally use iron vane movements. This movement is designed around the fact that a piece of ferrous metal placed inside a coil is magnetized. When two pieces of metal (or vanes) are inside the same coil, they are identically magnetized and repel each other. By making one vane solid and pivoting the other, the movement responds to the rms value of current or voltage. By using rectifiers to produce positive average voltage, the core magnet movement is often used to give an rms reading of sinusoidal voltages.

Meters are categorized by function which includes:

- Primary Function
  - Ammeter
  - Voltmeter
  - Other

- o Application
  - AC
  - DC

The 'Other' application may be oil pressure, temperature, decibel, % load, VSWR gauge, etc. The most widely used AC meters are 60Hz for ground fixed, naval and ground mobile applications and 400Hz for airborne applications. Higher frequency meters up to 50KHz are available. A voltmeter, as the name indicates, is a voltage measuring instrument. This device is actually current sensitive, but by use of proper internal (or external) resistance is made to give a correct voltage indication. Meter movements are characterized by the amount of current required to deflect the pointer full scale (e.g. 50ua or 1 ma) and/or by the series resistance of the movement. Meters are characterized by their function, accuracy and input impedance. Input impedance is particularily important for voltage meters since it has a direct affect on the accuracy of the voltage reading. In most applications, ammeters use shunt resistors across the meter movement to accomodate higher current levels.

Meters are used as visual panel indicators on most military equipments.

14.2 Failure Modes and Mechanisms

The failure modes of meters are:

- o Degradated operation
  - spring relaxation
  - resistance drift in shunt or series resistances
  - shorted coil winding (partial)
  - leaky rectifier diode
  - balance weight shift
- o Catastrophic failure
  - bearing wear or dirty bearing
  - open coil winding

- shorted coil winding
- short/open shunt or series resistance
- short/open rectifier diodes
- bent or broken pointer

Drift in accuracy and/or catastrophic failure may result from exposure to high temperature, shock and vibration. Therefore application environment would be expected to be a significant variable effecting failure rate. The basic construction differences between AC and DC meter movements, the possible additional components (e.g. rectifier diodes) and the arrangement of internal resistors would indicate that function and current type would also be significant variables affecting reliability.

14.3 Meter Failure Rate Prediction Model

This section presents the proposed failure rate prediction model for meters. The proposed model is:

$$\lambda_p = \lambda_b \times \pi_A \times \pi_F \times \pi_Q \times \pi_E$$

where

λ_p = predicted meter failure rate
λ_b = base failure rate
= 0.090 F/10^6 hours
π_A = application factor
= 1.0, DC Current
= 1.7, AC Current
π_F = function factor
= 1.0, Ammeter
= 2.2, Voltmeter
= 2.8, Other (Note 1)
π_Q = quality factor
= 1.0, MIL-SPEC quality

= 3.4, lower quality

π_E = environmental factor (see Table 14.3-1)

Notes: (1) Includes meters whose basic meter movement construction is an ammeter but which contains internal conversion elements not normally found in an ammeter.

TABLE 14.3-1: ENVIRONMENTAL FACTOR

Environment	π_E	Environment	π_E
G_B	1.0	A_{IA}	42
G_F	3.8	A_{IF}	42
G_M	24	A_{UC}	50
M_P	26	A_{UT}	73
N_{SB}	11	A_{UB}	50
N_S	14	A_{UA}	73
N_U	36	A_{UF}	73
N_H	41	S_F	2.1
N_{UU}	29	M_{FF}	13
A_{RW}	60	M_{FA}	N/A
A_{IC}	21	U_{SL}	N/A
A_{IT}	42	M_L	94
A_{IB}	21	C_L	N/A

14.4 Failure Rate Model Development

The approach used for model development was to identify significant parameters by analysis of the meter field experience data. The model parameters were then quantified using the same data. The results were given a thorough analysis to determine if they were consistent with theory at the conclusion of each step. The meter failure experience data collected in support of this study are presented in Table 14.4-1.

TABLE 14.4-1: METER FAILURE EXPERIENCE DATA

Source	App (1)	Fun (2)	Qual	Env	No. Fail	OP Hrs	Equipment Type	Failure Rate ($F/10^6$ hrs) L 10%CL	PT EST	U 60%CL	U 90%CL
1	--	A	M	NSB	12	702,000	--	11.15	17.09		25.32
2	DC	A	C	GM	23	774,000	--	22.10	29.72		39.34
3	AC	A	M	GM	1	79,165	Mobile Generator	1.33	12.63		49.14
4	DC	V	M	GM	1	47,427	Mobile Generator	2.22	21.09		82.02
5	DC	A	M	GM	1	67,961	Mobile Generator		14.71		
6	AC	A	M	GM	3	67,961	Mobile Generator		44.14		
7	AC	V	M	GM	4	67,961	Mobile Generator		58.86		
8	AC	V	M	GM	0	47,427	--			19.27	54.48
9	AC	A	M	AIC	2	25,494	E3A	20.87	78.45		208.68
10	DC	A	M	AIC	0	25,494	E3A			35.85	90.41
11	DC	V	M	AIC	1	25,494	E3A	4.13	39.22		152.58
12	AC	V	M	AIC	0	25,494	E3A			35.85	90.41
13	--	A	M	GM	21	57,408,000	Hawk Support Equip	0.27	0.37		0.49
14	DC	A	M	NS	1	874,646	AN/SQS-26	0.12	1.14		4.45
15	--	A	M	ARW	16	81,000	--	137.49	197.53		277.15
16	--	A	M	ARW	12	14,000	--	559.28	857.14		1269.85
17	AC	A	M	NS	0	46,034	AN/SQS-26			19.85	
18	AC	N	M	NS	0	32,068	AN/SQS-26			28.50	
19	DC	F	M	GM	2	67,961	Mobile Generator	7.83	29.43		78.28
20	DC	KW	M	GM	5	67,961	Mobile Generator	35.83	73.57		136.48
21	DC	F	M	GM	1	47,427	Mobile Generator	2.22	21.09		82.02
22	DC	I	M	GM	0	67,961	Mobile Generator			13.49	
23	DC	I	M	GM	1	67,961	Mobile Generator	1.55	14.71		57.24
24	DC	I	M	GM	1	67,961	Mobile Generator	1.55	14.71		57.24
			Totals		108	60,798,858		1.56	1.78		2.02

Notes: (1) AC = Alternating Current, DC = Direct Current
(2) A = Ammeter
V = Voltmeter
N = Noise watt meter
F = Frequency meter
KW = kilowatt meter
I = Indicator: oil pressure, temperature or fuel level

Application and construction variables were identified for meters (Table 14.4-2). The application and construction variables represent factors which were determined whenever possible for all collected data.

TABLE 14.4-2: METER CONSTRUCTION AND APPLICATION VARIABLES

I. Type
   A. Ammeter
   B. Voltmeter
   C. Special Meter
   D. Other

II. Enclosure Type
   A. Nonwater Tight
   B. Water Tight

III. Application
   A. dc
   B. ac

IV. Environment

V. Manufacturing Quality Level

Stepwise multiple linear regression analysis as described in Section 3.1 was applied to the meter failure experience data. All functions other than ammeter and voltmeter were grouped under the heading 'other'. The first iteration of the regression program disclosed that the unknown applications (source 1, 13, 15, 16) had a significant impact on the results. The data sources with the unknown application factors were deleted since they had a significant impact on the regression, and a second regression was run. This second regression resulted in the following failure rate prediction model:

$$\lambda_p = \lambda_b \times \pi_F \times \pi_Q \times \pi_E$$

where

λ_p = meter failure rate in failures/10^6 hours
λ_b = base failure rate

$= 2.1687\ F/10^6$ hours

π_F = function factor

π_Q = quality factor

π_E = environment factor

The details of the regression are given in Table 14.4-3.

TABLE 14.4-3: RESULTS OF METER REGRESSION ANALYSIS

Variable	Coefficient (bi)	Standard Error	F-Ratio
Ammeter	1.0	--	--
Voltmeter	0.8089 (1)	0.7232	1.25
Other	1.0327 (1)	0.6662	2.40
MIL-SPEC Quality	1.0	--	--
Lower quality	1.2202 (1)	1.3220	0.85
G_M environment	1.0	--	--
N_{SB} environment	0.6702 (1)	1.3220	0.26
N_S environment	-0.3573 (1)	0.8064	0.20
A_{IC} environment	1.2233 (1)	0.7534	2.64
A_{RW} environment	3.8502 (1)	1.0057	14.66
λ_b	2.1687 (1)	--	--

Degrees of freedom = 16

Notes: (1) factor = exp(bi)

The variables voltmeter, other, A_{IC} and A_{RW} were significant at a 70% confidence level. The variable for quality level was significant at a 60% confidence level. The environment variables N_{SB} and N_S were forced-in by assigning a 0% confidence level. These variables were forced into the model by specifying a zero critical f ratio since they would be required to generate estimates for the entire range of environments. The standard error statistic allows for the calculation of confidence intervals for the variables. Table 14.4-4 lists the point estimate, lower 20% confidence bound and upper 80% confidence bound for the variables.

TABLE 14.4-4: CONFIDENCE INTERVALS FOR METER PARAMETERS

Parameter	PT EST	L 20% CL	U 80% CL
Ammeter	1.0	--	--
Voltmeter	2.2	1.2	4.2
Other Function	2.8	1.6	5.0
MIL-SPEC Quality	1.0	--	--
Lower quality	3.4	1.1	10.5
G_M environment	1.0	--	--
N_{SB} environment	2.0	0.6	6.1
N_S environment	0.7	0.4	1.4
A_{IC} environment	3.4	1.8	6.5
A_{RW} environment	47.0	19.8	111.4
λ_b	8.7	--	--

The construction differences between AC and DC meters indicate that one could expect to see a difference in the failure rate of AC and DC meters, and that there should be a factor in the prediction model to account for the difference. The data in Table 14.4-1 less the source 1, 13, 15 and 16 data were analyzed to see if a difference exists and, if so, to quantify the difference. The variables shown in Table 14.4-4 were used to normalize the operating hours to a G_M, MIL-SPEC, Ammeter condition. The data were then grouped by application (AC or DC). The normalized grouped data are given in Table 14.4-5.

TABLE 14.4-5: APPLICATION PARAMETERS ANALYSIS RESULTS

Application	Sample	Normalized OP HRS	No. Fail	Failure Rate (F/10^6 hrs) L10%CL	PT EST	U90%CL
AC	8	773,431	10	8.04	12.93	19.91
DC	8	4,845,272	37	6.08	7.64	9.51

The Chi-square goodness of fit test described in Section 3.1 was used to test the hypothesis that the failure rates for the AC and DC meters came from the same distribution. The test rejected the hypothesis at the 1% significance level. Therefore it is assumed that the failure rates are different and that application is a significant variable. The quantitative

difference was calculated by taking the ratio of the normalized observed failure rates. The results of this calculation are:

Application	π_A
DC	1.0
AC	1.7

The failure rate prediction model was then revised to include this factor. The revised model is:

$$\lambda_p = \lambda_b \times \pi_A \times \pi_F \times \pi_Q \times \pi_E$$

where

$\lambda_p = \lambda_b\ \pi_F\ \pi_Q\ \pi_E$ were defined previously
π_A = application factor

Only three of the environments (A_{IC}, G_M, A_{RW}) were identified as significant variables in the regression analysis. This does not imply, however, that environment is not a significant factor affecting reliability. Theoretically, environmental stress has a large effect on reliability and therefore an approach was developed to derive parameters for the remaining environments defined in reference 1. The approach used to develop the environmental factors was to apply regression techniques to the data and the environmental severity ratios presented in referen e 2, Figure 2.3-1. These severity ratios are presented in Table 14.4-7. Two regressions were run. The first assumed a model of the form:

$$\pi_{E,\ obs} = A\ S^n$$

where

$\pi_{E,\ obs}$ = observed environmental factors for A_{IC}, G_M and A_{RW}
S = environmental severity ratios
A & n = constants of regression

The second regression was run assuming a linear relationship of the form:

$$\pi_{E,\ obs} = A + nS$$

The results of these regressions are presented in Table 14.4-6.

TABLE 14.4-6: ENVIRONMENTAL FACTOR REGRESSION RESULTS

Regression	A	n	R*
1	0.0106	2.39	0.845
2	-17.35	2.25	0.968

*R = Correlation Coefficient

The second regression exhibits a better fit of the data. Two sets of environmental factors were calculated. These factors were normalized to a ground, benign environmental factor of 1.0 and are shown in Table 14.4-7. As the data indicates, the π_E's calculated from the models tend to cause the environmental factors to balloon at the environmental extremes. The linear model showed a better fit to the data, sparse as it was; therefore, the factors derived using this method were adopted for the prediction model. Since no severity ratios were available for the new avionic environmental factors (A_{IT}, A_{IA}, A_{IB}, A_{UT}, A_{UA}, A_{UB}), the severity ratio for fighters was applied to the trainer, fighter and attack environment and the severity ratio for transports was applied to the bomber and cargo environment. Since the ground, mobile environment was revised from 1.0 to 24 because of the normalization, and since the orginal regression was based on this factor, the base failure rate, λ_b, was revised from 2.1687 to 0.090 F/10^6 hours to accomodate the change. No environmental factor was given for the M_{FA}, U_{SL} and C_L environments because meters would not be used or at least would not be mission critical elements in these environments.

TABLE 14.4-7: CALCULATED ENVIRONMENTAL FACTORS

Environment	Linear Model	Non-linear Model	Severity Ratio
G_B	1.0	1.0	1.0
G_F	3.8	10.4	2.7
G_M	23.6	332.2	11.5
M_P	25.9	405.4	12.5
N_{SB}	11.3	70.2	6.0
N_S	14.2	112.1	7.3
N_U	35.5	821.9	16.8
N_H	40.9	1130.9	19.2
N_{UU}	29.0	1338.1	20.6
A_{RW}	59.9	2692.5	27.6
A_{IC}	20.7	249.4	10.2
A_{IT}	--	--	--
A_{IB}	--	--	--
A_{IA}	--	--	--
A_{IF}	41.6	1173.6	19.5
A_{UC}	49.7	1759.5	23.1
A_{UT}	--	--	--
A_{UB}	--	--	--
A_{UA}	--	--	--
A_{UF}	73.1	4278.3	33.5
S_F	2.5	5.7	2.1
M_{FF}	26.1	413.2	12.6
M_{FA}	37.3	918.5	17.6
U_{SL}	81.2	5460.4	37.1
M_L	93.8	7641.3	42.7
C_L	1619.1	6.5×10^6	720.6

14.5 References and Bibliography

References

1. Edwards, E., et.al., Avionic Environmental Factors For MIL-HDBK-217, Final Technical Report, RADC-TR-81-374, January, 1982.

2. Kremp, B.F. and Kimball, E.W., Revision of Environmental Factors For MIL-HDBK-217B, Final Technical Report, RADC-TR-80-299, September, 1980.

Bibliography

Arno, Robert G., Nonelectronic Parts Reliability Data, Reliability Analysis Center Document, NPRD-2, Summer, 1981.

Edwards, E., et.al., Avionic Environmental Factors For MIL-HDBK-217, Final Technical Report, RADC-TR-81-374, January, 1982.

IIT Research Institute, Electronic Reliability Design Handbook, Volume II, Contract Data Item, Contract F30602-78-C-0281, 1981.

Kremp, B.F., and Kimball, E.W., Revision of Environmental Factors For MIL-HDBK-217B, Final Technical Report, RADC-TR-80-299, September, 1980.

MIL-M-10304E, Military Specification, Meters, Electrical Indicating, Panel Type, Ruggedized, General Specification For, May, 1974.

MIL-STD-1279, Meters, Electrical Indicating, Selection and Use of, September, 1970.

QPL-10304-22, Qualified Products List, Products Qualified Under Military Specification MIL-M-10304, Meters, Electrical Indicating, Panel Type, Ruggedized, General Specification For, June, 1980.

15.0 FUSES

15.1 Device Description

A fuse is an intentionally weakened part of an electrical or electronic circuit. Its purpose is to protect the other elements of the circuit from a possibly damaging overload. Fuses are used to protect many different types of circuits. In some instances, fuses are used to protect only the wiring and prevent a fire. In other instances, they are used to protect a very sensitive meter or an electronic assembly.

Military type fuses are generally a glass-bodied cartridge with nickel-plated brass caps. High-amperage fuses are made of a punched zinc alloy element. Low-amperage fuses are constructed with a filament wire which can be of a variety of materials including copper, platinum and many alloys to accomplish the desired result.

Fuses are the safety valves of electrical circuits. Therefore, it is important that they operate or "blow" before damage occurs in either the equipment or the wiring being protected. Conversely, nuisance blowing is not desired. Thus, fuses must not blow too easily and cause open circuits when the equipment is operating normally.

It is obvious that time and current are the controlling factors in the function of a fuse. There is a time and current relationship at which the circuit will operate satisfactorily and cause no damage to equipment or wiring. There is also a time and current relationship at which the equipment will be damaged. In other words, the time-current characteristics of the fuse must conform to the time-damage characteristics of the equipment.

There are three basic types of fuses depending on the particular application. They are, (1) Fast-blowing fuses which are used for instrument protection where fast action is necessary in order to protect the equipment, (2) Medium-blowing fuses which are used for general applications and (3)

Slow-blowing fuses which are used for applications where a time lag is desirable.

Fast-acting fuses are designed to carry 100% of current rating and blow rapidly at very slight percentages of overload. For example, they typically require milliseconds to operate at high overload currents. The greater the overload, the more rapidly the circuit opens. There is very little mass in the filament used and therefore the reaction can take place very quickly under short-circuit conditions. This filament is generally made of silver, platinum, or other precious metal alloys. These fuses are manufactured with wire diameters as low as 0.000020 inches. Obviously this filament will open the circuit under adverse conditions before any damage can be done in other parts of the circuit.

Medium time delay fuses are by far the most widely used. These fuses are designed to protect a non-critical device, wiring, or equipment at minimum cost. In general, they are designed to carry 110% of rated current for a minimum of four hours. Circuits will be protected if an overload of 135% of rated current is applied to the fuse. In this case the fuse will open in less than one hour. If an overload of 200% of rating is placed on the circuit, the fuse will open the circuit in a maximum of 30 seconds. The action of these fuses is not as rapid as the fast-acting fuse. However, they are satisfactory in the majority of fuse applications.

The slow-blow fuse has a time-lag characteristic. Many circuits or pieces of equipment have a current in-rush which is normal for the operation of the equipment. The starting of a motor is an example. Until the motor is up to speed, the current is far higher than the normal operating current. This is normal operation for this circuit, so it is not desired that the fuse open the circuit during these conditions. Therefore, a fuse must be designed with sufficient mass or time lag to prevent nuisance blowing. In some highly inductive or capacitive electronic circuits, this same characteristic is required.

15.2 Failure Modes and Mechanisms

Fuses have two principal failure modes: open, and failure to open. Any premature interruption of the current flow such as a mechanical breaking of the fuse element would be classified as an open. A failure to open is when current flow levels exceed the fuse rating and the fuse element does not open the circuit. Failure to open is most commonly caused by electrically conductive material shorting the fuse terminals together. Even a very small increase in resistance due to corrosion, loose connections, poor mating of contact surfaces or loss of tension in the fuse holder clips can generate sufficient heat to cause fuse functioning without a change in circuit current.

Fuse and fuseholder parts are generally required to have a high copper content and therefore are subject to rapid corrosion in contaminated environments. This corrosion is usually in the form of nonconducting oxides. Plated fuse parts offer initial protection from corrosive environments, but will tarnish with time.

Fuses of the glass and ceramic types have been found to be resistive to high and low temperature, thermal shock, sand and dust, humidity, vibration and mechanical shock. The smaller the fuse in physical size, the more resistant it is to shock and vibration. Small dimension fuses resist shock tests well. There have been no reports of failure of any kind under the usual shock tests of 15G and 30G with an 11 millisecond duration. The reason that the relatively smaller fuses are resistant to shock and/or vibration stresses is that the fuse filament is short and does not easily resonate.

15.3 Fuse Failure Rate Prediction Model

This section presents the proposed failure rate prediction model for fuses. The proposed model is:

$$\lambda_p = \lambda_b \times \pi_E$$

where

λ_p = predicted fuse failure rate (failures/10^6 hours)
λ_b = base failure rate
λ_b = 0.010 failures/10^6 hours
π_E = environmental factor (see Table 15.3-1)

TABLE 15.3-1: ENVIRONMENTAL FACTORS

Environment	π_E	Environment	π_E
G_B	1.0	A_{IA}	12
G_F	2.3	A_{IF}	12
G_M	7.5	A_{UC}	13
M_P	8.1	A_{UT}	18
N_{SB}	4.4	A_{UB}	13
N_S	5.2	A_{UA}	18
N_U	10	A_{UF}	18
N_H	12	S_F	1.8
N_{UU}	12	M_{FF}	8.1
A_{RW}	16	M_{FA}	11
A_{IC}	6.8	U_{SL}	20
A_{IT}	12	M_L	22
A_{IB}	6.8	C_L	230

15.4 Failure Rate Model Development

The reliability modeling of fuses presents a unique problem. Unlike most other electrical and electromechanical parts, there is very little correlation between the number of fuse replacements and fuse failures. Generally when a fuse opens or "blows" something else in the circuit has created a current overload condition and the fuse is simply functioning as designed. Additionally, categorizing fuse field replacements as either fuse failures or fuse "functions" is very difficult. Isolated fuse replacements which would appear to be a failure may have been caused by a transient

current. Also the slow open failure mode is very difficult to identify. The desired modeling approach including utilization of regression analysis could not be applied because of the difficulties in collecting accurate fuse failure rate data. Therefore alternate approaches were explored.

Three different modeling approaches were attempted to derive a failure rate prediction model for fuses. The first approach was based on analysis of fuse life test data. The life test data was used to derive an equation for base failure rate. Environmental factors were derived by analysis of fuse replacement rate data. This approach proved to be unsuccessful, but is discussed in this section along with presentation of collected life test data. The second approach consisted of an analysis of the ratio of fuse replacement rate to fuse failure rate. This approach successfully yielded a failure rate prediction model but included some inherent difficulties. The third approach included derivation of environmental factors based on replacement rate data. The base failure rate in this approach was computed by assuming the observed average failure rate was equal to a documented numerical value. The proposed fuse failure rate prediction model was based on the agreement between the results obtained from approaches two and three.

Each potential approach to fuse failure rate modeling assumed that a series of applicable environmental factors could be derived by analyzing fuse replacement rate data. The method used to derive the environmental factors was based on the assumption that distributions of the ratios of replacement rate to failure rate are similar for each environmental category. Using this assumption as a rationale, the environmental factor derivation process described in Section 3.3 could be applied to replacement rates to derive a complete set of factors. Therefore, replacement rate data was collected for fuses and is presented in Table 15.4-1. The results of the environmental factor derivation process are given by the following equations:

$$\lambda = 0.227\ (S)^{0.8270}$$

$\pi_E = (S)^{0.8270}$, normalized to a GB factor = 1

where

r = average fuse replacement rate
π_E = environmental factor
S = environmental stress ratio

The complete series of environmental factors derived by this procedure is given in Table 15.3-1 in Section 15.3.

TABLE 15.4-1: FUSE REPLACEMENT RATE DATA

Entry No.	Env	Equipment	Replacements	Part Hours ($X10^6$)	Replacement Rate ($R/10^6$)
1	GF	radar	72	529.17	0.136
2	GF	AN/GYQ-18	2	0.36	5.619
3	GF	AN/GYQ-18	4	2.37	1.686
4	GF	AN/GYQ-18	0	0.71	1.284(1)
5	GF	AN/GYQ-18	3	2.37	1.264
6	GF	AN/GYQ-18	1	1.42	0.702
7	GF	W71-sensor	2	209.53	0.010
8	NSB	AN/BRD-7	0	1.65	0.553(1)
9	NS	AN/SQS-26C	6	48.58	0.124
10	SF	satellite	0	3.85	0.237(1)
11	AIF	AN/ALQ-126	1	0.10	9.980
Total			91	800.11	0.114

Note: (1) upper 60% confidence limit used to approximate replacement rate for data entries without observed replacements.

The fuse modeling approach which was initially thought to have the greatest merit was to analyze fuse life test data collected in the ground benign environment. Twelve fuse life test data records were obtained and are presented in Table 15.4-2. Fuse life testing is generally performed at 100% or 110% of rated current. Normal fuse operation is at approximately 80% of rated current. Stepwise multiple linear regression analysis as described in

TABLE 15.4-2: FUSE LIFE TEST DATA

Entry No.	Rated Current (amps)	Applied Current (amps)	Failures	Part Hours	Failure Rate ($f/10^6$)
1	0.38	0.34	11	22747	483.6
2	0.38	0.38	13	3366	3862.2
3	2.00	1.90	8	32405	246.9
4	2.00	2.60	16	3741	4276.9
5	7.00	7.00	0	40000	22.9(1)
6	7.00	8.75	13	4428	2935.9
7	15.00	15.00	4	38054	105.1
8	15.00	18.75	13	2896	4489.0
9	2.00	1.60	0	85000	10.8(1)
10	2.00	1.80	1	28200	35.5
11	2.00	2.00	6	16400	366.2
12	2.00	2.20	9	13715	656.2
Total			94	290952	323.1

Note 1: upper 60% confidence limit value used to approximate failure rate without observed failures.

Section 3.1 was applied to the fuse life test data. The regression analysis resulted in the following equation for fuse base failure rate,

$$\lambda_b = 271\ (I_a/I_r)^{11.29}\ \text{failures}/10^6\ \text{hours}$$

where

λ_b = base failure rate (Approach 1)
I_a = applied current (amps)
I_r = rated current (amps)

The base failure rate exponent was consistent with theory in that fuse derating significantly reduces the probability of "nuisance blows". However, the magnitude of the base failure rate constant was too high to be realistic. The base failure rate calculated for a fuse operating at 80% of rated current is 21.8 failures/10^6 hours. This value is significantly higher than both the existing MIL-HDBK-217D point estimate failure rate (0.1 failures/10^6 hours) and the replacement rates given in Table 15.4-1. Since

it is illogical for the fuse replacement rate to be lower than the failure rate, this approach was considered invalid. Three possible explanations for the failure of this approach to yield an acceptable model are:

(1) The life test conditions were not typical of field operating conditions. Additional operating stress caused by the particular test conditions could be responsible for the excessively high base failure rate constant.

(2) The relation between failure rate and fuse derating is a continuous function but too complex to be determined from the available data.

(3) The relation between failure rate and fuse derating should not be represented by a continuous function. Failure rate as a function of fuse derating hypothetically could be best represented by a step function. The failure rate may increase gradually with increased applied current until a point near unity ($I_a/I_r = 1$) where the failure rate increases dramatically.

The failure of the initial approach to produce a usable failure rate prediction model resulted in the development of several alternate approaches. The second approach was based on analysis of the ratio of replacement rate to failure rate. It is known that the replacement rate is greater than or equal to the failure rate for every conceivable fuse application. This must be true because a system normally cannot operate with a failed fuse in-place and therefore it must be replaced. It must also be true that the ratio of replacement rate to failure rate must be greater than or equal to one. In equation form, the relationships between replacement rate and failure rate are given by:

$$r_i \geq \lambda_i$$

$$\frac{r_i}{\lambda_i} \geq 1.0$$

where

r_i = replacement rate of the i^{th} data entry

λ_i = failure rate of the i^{th} data entry

The ratio (r_i/λ_i) is thought to be quite variable and depends upon many factors including equipment type, equipment complexity, type of maintenance, etc. As the number of available data entries becomes large, it is logical to believe that individual data entries would be found where the replacement rate was equal to the failure rate. In equation form this relation is given by:

$$\lim_{n\to\infty} \left(\min(r_i/\lambda_i)\right) = 1.0$$

where n equals the number of available data records, "min" denotes the minimum value function and "lim" denotes the limit function.

This relation cannot be disproved or verified by the fuse replacement rate data given in Table 15.4-1 for two reasons. First, the number of data records given in Table 15.4-1 is a relatively small number. Second, estimates of failure rate are not available for any of the data entries. However, the relation is intuitively correct.

The limiting function of the minimum ratio of replacement rate to failure rate was applied to the replacement rate data to obtain an estimate for base failure rate. To begin this procedure, all data were normalized for environment by using the environmental factors derived previously. Then it was assumed that the normalized replacement rates were greater than the unknown average base failure rate. This assumption was thought to be true because of the relatively few data records available for analysis. If all the normalized replacement rates are greater than or equal to the unknown average base failure rate, then the minimum normalized replacement rate can be used to provide an upper bound estimate of base failure rate. The following progression of equations show how the base failure rate estimate was obtained:

$$\lim_{n\to\infty} \left(\min(r_i/\lambda_i)\right) = 1.0$$

$$\lim_{n \to 12} \; (\min(r_i/\bar{\lambda}_b)) \geq 1.0$$

The average base failure rate can be factored out of the minimum value function because it was assumed to be a constant value.

$$(\min(r_i))/\bar{\lambda}_b \geq 1.0$$

$$\bar{\lambda}_b \leq \min (r_i)$$

The minimum normalized replacement rate was data entry number 7 in Table 15.4-1. Therefore, the estimate for base failure rate is:

$$\bar{\lambda}_b \leq .010 \div 2.3 = 0.00435 \text{ f/}10^6 \text{ hours}$$

where

r_i = normalized replacement rate of i^{th} data entry
λ_i = normalized failure rate of i^{th} data entry
$\bar{\lambda}_b$ = average base failure rate
2.3 = environmental factor for GF.

Multiplication of the average base failure rate value by the environmental factor completed the model development for this approach. The inherent difficulty with this approach is the use of several assumptions which can neither be proved or disproved. Also, the derived numerical base failure rate value ultimately is based on one data record. Therefore, extensive data quality control is required for proper application of this approach.

A third approach was deemed necessary because of the inadequacy of the first approach and the uncertainty of the second approach. This third approach assumed a fuse failure rate prediction model of the form:

$$\lambda_p = \lambda_b \times \pi_E$$

where

λ_p = predicted fuse failure rate
λ_b = base failure rate = constant value
π_E = environmental factor (Table 15.3-1)

The basis of the third approach was the assumption that the existing MIL-HDBK-217D average point estimate failure rate was an accurate measure of the average observed failure rate of data entries from a variety of application environments. This assumption was believed to be accurate because most of the criticism by reliability analysts was that the current model did not sufficiently discriminate against fuse reliability characteristics and not that the current model was an inaccurate measure of the average fuse failure rate. The data collected in support of this study (Table 15.4-1), $\bar{r}$ = 0.114 R/10^6 hours, also did not disprove this assumption. To derive the base failure rate value, the average fuse failure rate for the eleven environment categories included in MIL-HDBK-217C was assumed equal to the existing MIL-HDBK-217D average failure rate value of 0.1 failures/10^6 hours. The eleven environmental categories were used instead of the current 26 environments because the original use of the 0.1 value was not intended for such stressful environments as cannon, launch and underwater, sea launch. Therefore the base failure rate was obtained by:

$$0.1 \text{ failures}/10^6 \text{ hours} = \frac{1}{n} \sum_{i=1}^{n} (\lambda_b \pi_E)$$

$$0.1 = \frac{1}{11} (\lambda_b(1.0 + 2.3 + 7.5 + 5.2 + 10 + 6.8 + 12 + 13 + 18 + 1.8 + 22))$$

$$\lambda_b = 11(0.1)\ (1/99.6)$$
$$= 0.0110 \text{ failures}/10^6 \text{ hours}.$$

Neither approach two nor three had enough merit to be the sole basis of a failure rate prediction model. However, the relative proximity of the base failure rate values obtained from approaches two and three was sufficient justification for proposing a revised failure rate prediction model for

fuses. The base failure rate value obtained from approach three was included in the proposed model because it was the larger of the two values.

The proposed fuse failure rate modeling approaches described in this section present several attempts at deriving an equation for fuse failure rate. It was encouraging that two of the three modeling approaches yielded similar failure rate prediction models because of the severe field failure rate data collection problems associated with fuses.

15.5 Bibliography

Arno, R.G., Nonelectronic Parts Reliability Data, RAC publication NPRD-2, Summer, 1981.

Backe, R.J., Evaluation of Screening Methods to Obtain Long Life Subminiature Picofuses, Goddard Space Flight Center report no. PACER `4-004, November, 1980.

Ross, M., Corrosion Resistance of Silver Plated Copper and Brass Versus Unplated Copper and Brass, Federal Pacific Electric Co. Internal Report, August 1978.

Thomas E., The Mechanisms of Degradation and Failure in a Filamentary Fuse Wire, Goddard Space Flight Center report no. FMR 04-003, May, 1972.

16.0 QUARTZ CRYSTALS

16.1 Device Description

A crystal unit is an assembly which consists of a quartz resonator suitably mounted in a crystal holder. Quartz crystals are manufactured in a wide variety of mounting and holder configurations to suit many applications.

Quartz is useful in the electronics field because it is piezoelectric and has stable physical properties and manageable behavior over wide temperature ranges. The piezoelectric effect causes an electrical potential difference between two opposite faces of a quartz plate when the plate is mechanically stressed. Conversely, when a potential difference is applied to the two opposite sides of the quartz plate, mechanical stress and movement are generated.

Quartz plates which are cut to proper dimensions and appropriately mounted will vibrate in mechanical resonance at the desired frequency if an alternating voltage is applied to the opposite crystal faces. The unusually high stiffness and elasticity of this very hard crystalline material make it possible to produce electromechanical resonators that will operate over a wide range of frequencies extending from approximately 1000 Hertz to 150 Megahertz.

Figure 16.1-1 shows typical mounting variations used by various crystal manufacturers for a 1 MHz AT cut crystal in the standard MIL-HC-6/U holder. Figure 16.1-2 presents the construction and mounting of a larger low frequency crystal device. Figure 16.1-3 shows a typical edge-clamped mount which is widely used for mounting high frequency crystals. Electrodes are plated on the opposite crystal surfaces with the plating extended to opposite edges to provide attachment to the mounts. The crystal faces are only partially plated so that the effective electrode area is confined to a small circular region at the center of the blank. Thus, the capacitance is kept to

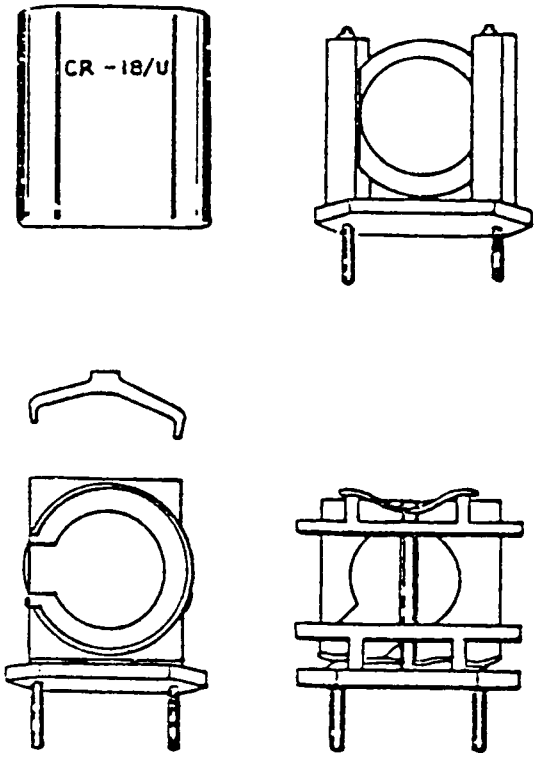

FIGURE 16.1-1: TYPICAL MOUNTING VARIATIONS FOR A 1MHz CRYSTAL

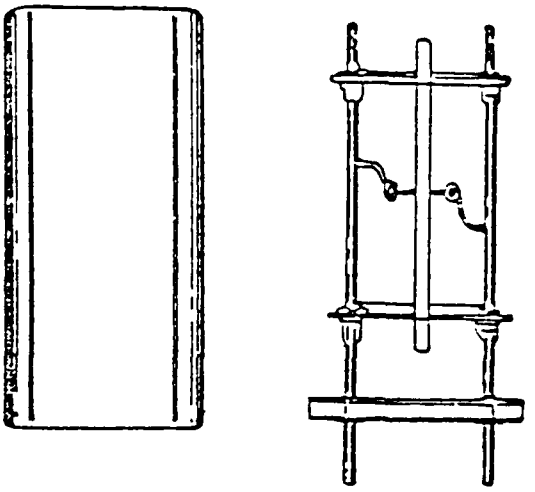

FIGURE 16.1-2: TYPICAL MOUNTING OF A LOW FREQUENCY CRYSTAL

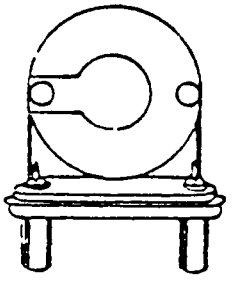

FIGURE 16.1-3: CEMENTED LEAD MOUNTING FOR HIGH FREQUENCY CRYSTALS

a minimum and the principal activity is confined to the center of the plate where it is most likely to be of uniform thickness. Both these factors contribute to frequency stability. The mounting wires are clamped or cemented at the edges, where activity of the crystal is low.

For high levels of shock and vibration, the wire mounts shown in Figure 16.1-3 are replaced by stiffer channel shaped mounts to keep the mount resonant frequency above 2 or 3 KHz. This ruggedized mounting requires some sacrifice in temperature stability and aging characteristics.

The most recent developments in crystal holders are in the use of cold welded cases and internal ribbon mounts. The cold-welded process eliminates exposure of the crystal to high temperatures and/or solder flux contaminants which can occur with the use of glass enclosures and conventional solder sealed cans. The use of a ribbon mount, as developed by Bell Telephone Laboratories, satisfies the requirement of high mount resonant frequency without inducing stress in the crystal blank.

One version of this type of internal ribbon mount employs three short ribbons which position the blank parallel to the base of a standard TO-5 can. In theory, three short ideal ribbons will remove the six degrees of freedom of the blank without any redundancies. In practice, this type of mount has resulted in a reduction of two orders of magnitude in vibration sensitivity as compared to the standard wire mount. At the same time, aging characteristics are not degraded and the lowest resonant frequency of the assembly is well above 2000 Hz. This type of mount appears to be particularly suited for high frequency applications where vibration modulation sensitivity is of concern.

16.2 Failure Modes and Mechanisms

Quartz crystals, if properly applied, are among the most reliable electronic components. Wearout failure mechanisms associated with the use of a quartz crystal are observed rarely when operated within

specifications. An example of a wearout failure mechanism which does occur is frequency drift. The majority of crystal failures can be categorized as catastrophic failures. There is a continuous aging process which decreases exponentially with time.

Operation above rated drive level will result in deterioration of stability, even though the dissipation is well below the level at which the crystal may shatter. High drive level will also accelerate the normal aging characteristics.

There are certain failure mechanisms associated with manufacturing which may or may not be detected prior to equipment installation. These failure mechanisms can result in either catastrophic failure or excessive drift after some period of operation. Some of the more common defects are listed below:

- Poor seal
- Excessive contamination
- Excessive internal mechanical stresses introduced by the blank mounting structure
- Poor electrical connections

A poor seal will result in a gradual frequency drift and an increase in crystal resistance due to entrance of moisture and other surface contaminants. The crystal may fail either by drifting out of tolerance or by an increase in resistance to the point that it may no longer oscillate.

The effect of excessive contamination is the same as that of a poor seal except that the contaminants are already present at the time of manufacture. This defect is relatively rare among quality manufacturers and the use of cold welded cases reduces the problem of contaminants, such as solder flux, being introduced during the sealing operation.

Occasionally the design of the internal mounting structure and/or the assembly techniques used will result in the blank being under mechanical stress in its mounted condition. Such stresses can also be introduced by high shock loads from improper handling. This condition increases the effective resistance of the crystal and can cause it to be temperature sensitive by either failing to operate or operating out of frequency tolerance at one of the temperature extremes. Units with this type of defect (when it is sufficient to cause the crystal to exceed the frequency tolerance limits) will usually be out of tolerance on the low side.

Poor electrical connections can cause failure for obvious reasons and may result in an intermittent connection or an open circuit depending on the nature of the solder joint defect.

16.3 Crystal Failure Rate Prediction Model

This section presents the proposed failure rate prediction model for crystals. The proposed model is:

$$\lambda_p = \lambda_b \times \pi_Q \times \pi_E$$

where

λ_p = predicted crystal failure rate

λ_b = base failure rate

$\lambda_b = 0.013\ (f)^{0.23}$ failures/10^6 hours, (f = frequency (MHz))

π_Q = quality factor

= 1.0, MIL-SPEC quality

= 2.1, lower quality

π_E = environmental factor (see Table 16.3-1)

TABLE 16.3-1: ENVIRONMENTAL FACTORS

Environment	π_E	Environment	π_E
G_B	1.0	A_{IA}	17
G_F	2.6	A_{IF}	17
G_M	10	A_{UC}	19
M_P	11	A_{UT}	28
N_{SB}	5.4	A_{UB}	19
N_S	6.5	A_{UA}	28
N_U	14	A_{UF}	28
N_H	16	S_F	1.0
N_{UU}	17	M_{FF}	11
A_{RW}	23	M_{FA}	15
A_{IC}	9.0	U_{SL}	30
A_{IT}	17	M_L	35
A_{IB}	9.0	C_L	500

16.4 Failure Rate Model Development

The approach used for development of a crystal failure rate prediction model was to identify and quantify model parameters by analysis of field experience data. The crystal failure rate data collected in support of this study effort are presented in Table 16.4-1.

Application and construction variables which were considered as possible crystal failure rate model modifying parameters are presented in Table 16.4-2. The application and construction variables were determined whenever possible for all collected data. The selection of variables to be included in the proposed crystal failure rate prediction model was based solely on the analysis of field experience data.

Stepwise multiple linear regression analysis as described in Section 3.1 was applied to the crystal failure rate data. Data records which were included in the regression analysis are data entries 1 through 13 in Table

TABLE 16.4-1: CRYSTAL FAILURE RATE DATA

ENTRY NO.	FREQUENCY (MHz)	DRIVE LEVEL (mW)	QUALITY	ENVIRONMENT	PART NO.	EQUIPMENT	FAILURES	PART HOURS
1	16.00	5.0	MIL-SPEC	GM	CR-60A/4	AN/TSQ-73	1	3,813,000
2	2.00	10.0	MIL-SPEC	AUT	CR-85/U	AN/ARN-118	0	2,481,000
3	2.00	10.0	MIL-SPEC	AUF	CR-85/U	AN/ARN-118	0	2,178,000
4	98.67	2.0	MIL-SPEC	AUT	CR-116/U	AN/ARN-118	4	2,481,000
5	98.67	2.0	MIL-SPEC	AUF	CR-116/U	AN/ARN-118	2	2,178,000
6	50.40	(3)	MIL-SPEC	AUT	(3)	AN/ARN-118	0	2,481,000
7	50.40	(3)	MIL-SPEC	AUF	(3)	AN/ARN-118	1	2,178,000
8	0.33	(3)	Commercial	AUT	(2)	AN/ARN-118	1	2,481,000
9	0.33	(3)	Commercial	AUF	(2)	AN/ARN-118	1	2,178,000
10	16.18	(3)	Commercial	AUT	(2)	AN/ARN-118	3	2,481,000
11	16.18	(3)	Commercial	AUF	(2)	AN/ARN-118	3	2,178,000
12	12.57	(3)	Commercial	GF	(2)	Communications	0	7,560,000
13	16.17	(3)	Commercial	GF	(2)	Communications	0	7,560,000
14 (1)	19.67	5.0	Commercial	GM	(2)	AN/TSQ-73	0	369,000
15 (1)	2.00	10.0	MIL-SPEC	ARW	CR-85/U	AN/ARN-118	0	63,000
16 (1)	98.67	2.0	MIL-SPEC	ARW	CR-116/U	AN/ARN-118	0	63,000
17 (1)	50.40	(3)	MIL-SPEC	ARW	(3)	AN/ARN-118	0	63,000
18 (1)	0.33	(3)	Commercial	ARW	(2)	AN/ARN-118	0	63,000
19 (1)	16.18	(3)	Commercial	ARW	(2)	AN/ARN-118	0	63,000
20 (1)	(3)	2.0	MIL-SPEC	NSB	CR-55A/U	AN/BRD-7	0	275,400
21 (1)	(3)	5.0	MIL-SPEC	NSB	CR-60A/U	AN/BRD-7	0	183,600
22 (1)	(3)	10.0	MIL-SPEC	NSB	CR-19A/U	AN/BRD-7	0	275,400
23 (1)	(3)	2.0	MIL-SPEC	NSB	CR-56A/U	AN/BRD-7	0	91,800
24 (1)	10.17	5.0	Commercial	NSB	(2)	AN/BRD-7	0	91,800
25 (1)	8.00	5.0	Commercial	NSB	(2)	AN/BRD-7	0	91,800
26 (1)	100.00	2.0	MIL-SPEC	AIT	CR-80/U	AN/ARC-164	0	273,600
27 (1)	106.00	2.0	MIL-SPEC	AIT	CR-80/U	AN/ARC-164	0	273,600
Totals							16	44,469,000

NOTES:

(1) Insufficient part hours.

(2) Commercial part numbers proprietary.

(3) Unknown.

TABLE 16.4-2: QUARTZ CRYSTAL CONSTRUCTION AND APPLICATION VARIABLES

I. Mode of Oscillation
   A. Fundamental
   B. Third Overtone
   C. Fifth Overtone

II. Frequency

III. Load Capacitance

IV. Quartz Plate Dimensions

V. Rated Drive Level

VI. Type of Cut
   A. AT
   B. BT
   C. CT
   D. DT
   E. NT

VII. Construction Options
   A. Cold-Welded Cases
   B. Internal Ribbon Mount

VIII. Mounting and Holder Configuration

IX. Operating Temperature
   A. Rated
   B. Actual

X. Application Environment

XI. Manufacturing Quality Level

16.4-1. Other data records included insufficient part hours to estimate a failure rate without observed failures. The regression analysis resulted in the following crystal failure rate prediction model.

$$\lambda_p = \lambda_b \times \pi_Q \times \pi_E$$

where

λ_p = predicted crystal failure rate in failures/10^6 hours
λ_b = base failure rate
λ_b = 0.0306 $(f)^{0.234}$ failures/10^6 hours, (f = frequency (MHz))
π_Q = quality factor
= 1.0, MIL-SPEC quality
= 2.1, lower quality
π_E = environmental factor
= 1.0, GF
= 4.4, GM
= 9.3, AUT
= 9.6, AUF

It should be noted that the base failure rate constant given above differs from the value given in section 16.3. This apparent discrepancy is due to normalization of the environmental factors. The regression analysis assumed a ground fixed environmental factor equal to one because no data were available from a ground benign environment. The proposed crystal failure rate prediction model environmental factors were normalized to a ground benign factor equal to one to be consistent with existing MIL-HDBK-217D models. The details of the regression analysis are given in Table 16.4-3. Base failure rate, quality factor and environment factor were defined by the following equations:

$$\lambda_b = (\exp(b_0))\ (f)^{b2}$$
$$\pi_Q = \exp(b_3 X_3)$$

X_3 = 0, MIL-SPEC

X_3 = 1, lower quality

π_E = $\exp(b_4X_4 + b_5X_5 + b_6X_6)$

X_4, X_5, X_6 = (0,0,0), GF

X_4, X_5, X_6 = (1,0,0), GM

X_4, X_5, X_6 = (0,1,0), AUT

X_4, X_5, X_6 = (0,0,1), AUF

The X_i variables are "dummy variables" used to quantify qualitative factors.

TABLE 16.4-3: RESULTS OF CRYSTAL REGRESSION ANALYSIS

Variable (X_i)	Coefficient (b_i)	Standard Error	F-Ratio
ln(f)	0.2336	0.0735	10.09
X_3	0.7471	0.3166	5.57
X_4	1.4902	0.6013	6.14
X_5	2.2346	0.4093	29.81
X_6	2.2606	0.4093	30.50
Constant	.4874	--	--

Degrees of Freedom = 7

Each of the variables given in Table 16.4-3 was significant at a 90% confidence level. The standard error statistic allows for the calculation of confidence intervals for quality factor, environmental factor and base failure rate exponent (b_2). Table 16.4-4 presents the point estimate, lower 20% confidence limit and upper 80% confidence limit for these factors.

TABLE 16.4-4: CONFIDENCE INTERVALS FOR CRYSTAL PARAMETERS

Parameter	PT EST	L 20% CL	U 80% CL
λ_b exponent	0.234	0.169	0.298
π_Q, MIL-SPEC	1.0	--	--
π_Q, lower	2.11	1.60	2.79
π_E, GF	1.0	--	--
π_E, GM	4.44	2.62	7.52
π_E, AUT	9.34	6.53	13.37
π_E, AUF	9.59	6.70	13.72

Analysis of the data allowed for determination of only four environmental factors. To improve the utility of the proposed model, a complete series of environmental factors was determined. There is no part type currently included in MIL-HDBK-217D whose environmental factors adequately represent the effects of environmental stress on crystals. Therefore, the methodology described in Section 3.3 was applied to the four observed environmental factors to derive an applicable series of factors. This method assumes that an environmental factor relation can be determined where environmental factor is a function of the "environmental stress ratios" given in Reference 1. The results of the environmental factor derivation are given by the following equations.

$$\pi_{E1} = 0.4105\ (S)^{0.9448}$$

$$\pi_{E2} = (S)^{0.9448}$$

where

π_{E1} = environmental factors normalized to a ground fixed $\pi_E = 1$
π_{E2} = environmental factors normalized to a ground benign $\pi_E = 1$
S = environmental stress ratio

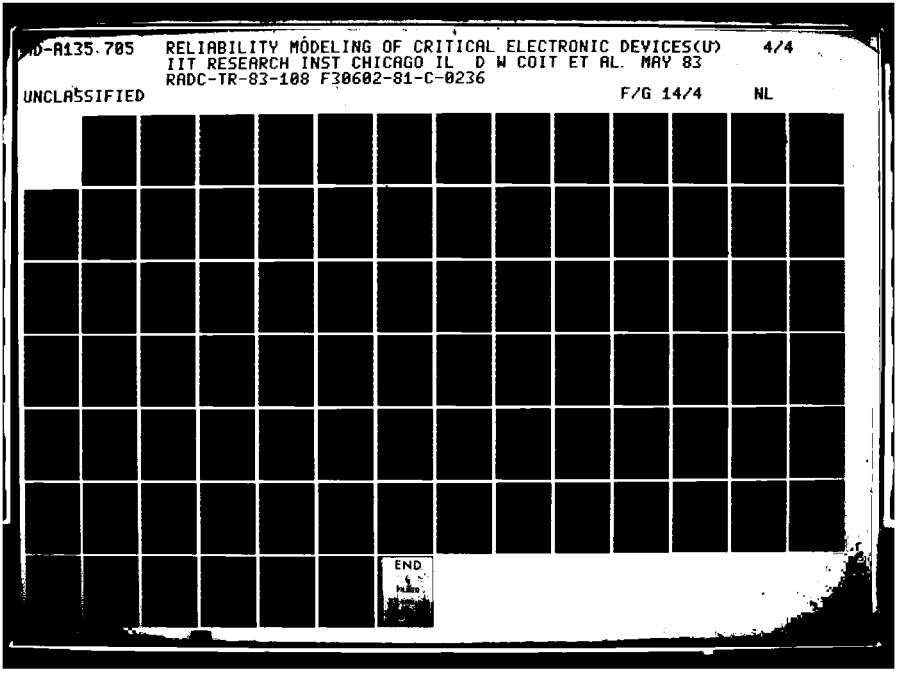

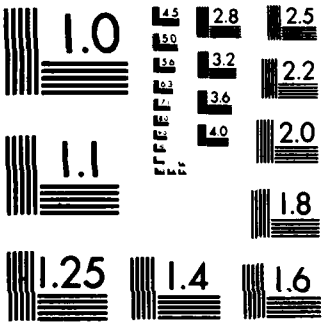

MICROCOPY RESOLUTION TEST CHART
NATIONAL BUREAU OF STANDARDS-1963-A

It was considered desirable for the environmental factors included in the proposed crystal failure rate prediction model to be normalized to a ground benign factor equal to one. The preliminary failure rate prediction model obtained by the regression analysis was normalized to a ground fixed environmental factor equal to one. Therefore, the base failure rate constant given previously in this section was multiplied by a factor of 0.4105 and the appropriate set of environmental factors (π_{E2}) was included in the proposed model. Thus, the equation for base failure rate becomes,

$$\lambda_b = 0.0126\ (f)^{0.234}\ \text{failures}/10^6\ \text{hours}$$

The complete set of environmental factors normalized to a ground benign factor equal to one is presented in Table 16.3-1.

Normalization of the base failure rate and the environmental factors concluded the failure rate prediction model development for crystals. The existing MIL-HDBK-217D failure rate prediction model for crystals consists of a single point estimate for all applications. The proposed model presents failure rate as a function of frequency, quality level and application environment and use of this proposed model will improve the reliability prediction capabilities for equipments designed with quartz crystals.

16.5 References and Bibliography

References

1. Kremp, B.F. and E.W. Kimball, Revision of Environmental Factors for MIL-HDBK-217B, RADC-TR-80-299, September 1980.

Bibliography

Fink, D.G. and D. Christianson, Electronics Engineers Handbook, Section 7, Second Edition, McGraw-Hill, 1982.

17.0 LAMPS

17.1 Incandescent Lamps

17.1.1 Device Description

Tungsten filament incandescent lamps are used extensively as miniature and subminiature indicator lamps. Construction options such as bulb size, filament type, light output, rated voltage and rated current are available in numerous combinations such that the optimal incandescent lamp type can be chosen for any particular application. Incandescent lamps are generally constructed of an envelope, a filament, a filament support, lead wires, a bead, an exhaust tip and a lamp base.

The envelope is commonly made of clear or colored glass. Envelopes for some high-powered lamps may be made of quartz or high-temperature glass. The envelope shape is coded by letter and by diameter in one eighth inch units. The letter codes used to specify envelope shape are T, G, S, B and RP corresponding to tubular, globular, straight-sided, blister, and pear-shaped reflector respectively. For example a T-2 bulb would be tubular with a diameter of two times one eighth inch (equal to one quarter inch).

Filaments can be classified into three categories. In general filaments are either coiled (coded C), straight (coded S) or coiled-coil (coded CC). The coiled type is more thermally efficient than the straight wire because heat can not escape as readily and therefore the filament becomes hotter for the same current. Filament supports are sometimes needed for the longer filaments which are required in high voltage, low current lamps. The supports cool the filament in their vicinity but are a liability in regard to vibration and filament notching.

Lead wires are low-resistance conductors usually having three purposes. They conduct electricity to the filament, they provide part of the filament support, and they carry the electricity through their mechanical seal with

the envelope glass. The connection to the filament is usually a crimp or a weld. Their ability to support the filament is improved by being short because the mechanical response to vibration is reduced. The thermal coefficient of expansion of the lead wire material must match the thermal coefficient of expansion of the glass through which they pass, or repeated heating and cooling of the lamp would soon fracture the seals. Having a hot filament at one end is most compatible with long internal lead wires, so the glass and the wire may change temperature gradually and simultaneously. Selection of the lamp internal lead length requires a compromise between shock/vibration response and seal-heating requirements.

The lamp bead provides a means of supporting the filament assembly both before it is mounted in the envelope and afterwards. Color of the bead offers a means of lamp identification.

The exhaust tube is used to evacuate the lamp. Most lamps have the filament in a vacuum. This reduces the loss of heat from the filament and produces more light output for the same filament current or applied voltage. Occasionally lamps are back-filled with argon, an argon-nitrogen mixture or another gaseous mixture to reduce tungsten evaporation from the filament. This will increase lamp life and reduce blackening within the envelope.

Lamp bases are commonly cemented to the envelope. The lead wires are usually soldered to the contacts. Use of soft solder is common though there is some advantage in the use of higher-temperature solders. In other cases a welded connection is made. The lamp base makes both electrical and mechanical contact to the equipment in which the lamp is installed. The base also provides a dimensional reference to the "light center".

Incandescent lamps are commonly used under high ambient light conditions as on-off indicator lights and for the internal illumination of panels in military equipment. They are used as the light source in projection alpha-numeric readouts, as well as the segment types of readout. Occasionally they

are used in pulsing or flashing circuits, and they may be used as a current-sensitive resistor in electronic circuits, such as automatic gain controls.

17.1.2 Failure Modes and Mechanisms

In AC operation, the predominant failure mechanism of an incandescent lamp is evaporation of the tungsten filament. Unlike most electronic devices, the lamp filament must be in a deterioration mode to operate (i.e. to illuminate). Ideally, the filament evaporates uniformly and the light intensity of the lamp gradually fades. In practice, however, the evaporation of the filament is not uniform and weak spots in the filament develop. Notching is the term generally used to describe this phenomenom of nonuniform evaporation of the filament. Failures are observed in the weak spot area when exposed to mechanical shock and/or vibration.

Several factors may increase the number of observed notching type filament failures. Higher voltage incandescent lamps require a longer, thinner filament. The thinner filament is more susceptible to failures induced by notching because the size of the notch and the rate of increase of the notch size are independent of filament diameter. Additionally filaments in high voltage lamps require filament supports becuase of their more fragile construction. The presence of the filament supports also tend to accelerate notching. The observed failure rate of incandescent lamps would be expected to be highly correlated to the rated voltage because of these factors.

Another factor influencing the evaporation rate of the filament is the ratio of applied voltage to rated voltage. As the ratio of applied to rated voltage is increased, internal lamp temperature is increased and the evaporation of the filament is accelerated. Lamp failure rate is related directly to filament evaporation rate.

In DC operation an additional failure mechanism is introduced which is dominant. DC operation results in electromigration of the tungsten filament in the direction of the applied electric field. Electromigration of the

tungsten in one direction reduces the minimum filament diameter. This increases the susceptibility of the lamp to failures from exposure to shock and/or vibration.

The life of an incandescent lamp relative to the life of the equipment in which it is installed is highly dependent on duty cycle. While the lamp is illuminating, the filament is in the process of evaporating and the average failure rate (in units of failures per equipment hr.) is relatively higher. Therefore the particular application of the incandescent lamp is of extreme importance in regard to the reliability. Applications for incandescent lamps range from a duty cycle of 1.0 (i.e., power on indication, constant illumination of dial/meter) to duty cycles approaching zero for certain warning indicator lamps. Generally the duty cycle of an incandescent lamp to be used as a warning indicator is unknown in the reliability prediction phase of equipment design.

Environmental stresses such as shock and vibration shorten lamp life by inducing failures in areas of the filament which have been weakened by either uniform evaporation, notching or electromigration of the filament. Therefore, application environment would be anticipated to have a significant effect on incandescent lamp failure rate. However, proper incandescent lamp selection can minimize the effects of the environment. Incandescent lamp manufacturers often offer lamps with similar specifications but different intended applications.

The instantaneous failure rate of an incandescent lamp is expected to be very time dependent. The dominant failure mechanisms for both AC and DC operation are degradation mechanisms such as uniform evaporation of the filament and filament notching. Collection of field experience data which allows analysis of failure rate time dependence is difficult and accurate estimates of Weibull or normal failure rate distribution parameters can not be determined.

17.1.3 Incandescent Lamp Failure Rate Prediction Model

This section presents the proposed failure rate prediction model for incandescent lamps. The proposed model is:

$$\lambda_p = \lambda_b \times \pi_u \times \pi_A \times \pi_E$$

where

λ_p = predicted incandescent lamp failure rate
λ_b = base failure rate in failures/10^6 hours
= $0.074\ (V_r)^{1.29}$ failures/10^6 hours, (V_r = rated voltage (volts))
π_u = utilization factor (see Table 17.1.3-1)
π_A = application factor
= 1.0, AC applications
= 3.3, DC applications
π_E = environmental factor (see Table 17.1.3-2)

TABLE 17.1.3-1: UTILIZATION FACTOR

Illuminate hours/equipment operate hours	π_u
< 0.10	0.10
0.10 to 0.90	0.72
> 0.90	1.0

TABLE 17.1.3-2: ENVIRONMENTAL FACTOR

Environment	π_E	Environment	π_E
G_B	1.0	A_{IA}	4.4
G_F	1.6	A_{IF}	4.4
G_M	3.4	A_{UC}	4.8
M_P	3.5	A_{UT}	5.8
N_{SB}	2.4	A_{UB}	4.8
N_S	2.7	A_{UA}	5.8
N_U	4.1	A_{UF}	5.8
N_H	4.4	S_F	1.4
N_{UU}	4.5	M_{FF}	3.5
A_{RW}	5.3	M_{FA}	4.2
A_{IC}	3.2	U_{SL}	6.1
A_{IT}	4.4	M_L	6.5
A_{IB}	3.2	C_L	27

17.1.4 Failure Rate Model Development

The methodology used to develop a failure rate prediction model for incandescent lamps included parameter identification and quantification by analysis of life test data, field experience data and theoretical reliability studies. The failure rate data collected in support of this study effort is given in Table 17.1.4-1.

As a prerequisite to collection of life test and field experience data, a list of construction and application variables were determined for incandescent lamps. The construction and application variables represent possible failure rate model parameters whose values were determined for all collected data whenever possible. The construction and application variables are given in Table 17.1.4-2.

TABLE 17.1.4-1: INCANDESCENT LAMP FAILURE RATE DATA

ENTRY NO.	BULB TYPE	RATED VOLTAGE (volts)	RATED CURRENT (amps)	AC/DC	FUNCTION	QUALITY	ENVIRONMENT	PART NO. (2)	EQUIPMENT (3)	FAILURES	PART HOURS
1	T-1 3/4	28	0.04	AC	constant illumination	MIL-SPEC	GB	327	life test	5	382,700
2	T-1 3/4	28	0.04	AC	" "	MIL-SPEC	GB	387	" "	3	587,900
3	T-1 3/4	28	0.04	DC	" "	MIL-SPEC	GB	327	" "	16	259,600
4	T-1 3/4	28	0.04	DC	" "	MIL-SPEC	GB	387	" "	16	273,200
5	T-1 3/4	28	0.04	DC	power indicator	MIL-SPEC	GF	387	AN/GYQ-18	4	1,423,600
6	T-1	28	0.02	DC	" "	MIL-SPEC	GF	6839	AN/GRC-171	63	523,000
7	T-1	5	0.06	DC	" "	MIL-SPEC	GF	685	AN/GRC-171	7	523,000
8	T-1	5	0.12	DC	warning indicator	MIL-SPEC	GM	718	AN/TSQ-73	0	492,000
9(1)	T-1 3/4	28	0.04	DC	" "	MIL-SPEC	GM	387	AN/TSQ-73	0	123,000
10	T-1	5	0.12	DC	" "	MIL-SPEC	AIT	715AS15	AN/ARC-164	1	3,283,200
11	T-1	5	0.06	DC	" "	MIL-SPEC	AIT	6832	AN/ALQ-117	1	2,090,400
12	T-1 3/4	28	0.04	DC	power indicator	MIL-SPEC	AIT	387	AN/ALQ-117	0	160,800
13	T-3 1/4	37.5	0.05	DC	power indicator	Commercial	GF	1828	AN/GRC-171	51	2,092,000
14	(5)	5	0.02	DC	warning indicator	Commercial	GM	7209	AN/TSQ-73	0	615,000
15	T-1 3/4	6	0.04	DC	" "	Commercial	NSB	345	AN/BRD-7	0	1,560,700
16	(5)	6	0.20	DC	power indicator	Commercial	GF	(4)	AN/GYQ-18	2	711,800
17	(5)	6	0.20	DC	test light	Commercial	GF	(4)	AN/GYQ-18	0	4,270,800
18	T-1	5	0.08	DC	power indicator	Commercial	GF	(4)	AN/GYQ-18	7	10,677,000
19	(5)	5	0.12	DC	status indicator	Commercial	GF	(4)	AN/GYQ-18	0	711,800
20	(5)	(5)	(5)	DC	warning indicator	MIL-SPEC	NS	(5)	AN/SQS-26	700	37,586,300
21	(5)	(5)	(5)	DC	warning indicator	MIL-SPEC	GF	(5)	radar	0	141,538,900
22	(5)	(5)	(5)	DC	warning indicator	MIL-SPEC	GM	(5)	(5)	2	196,600
23	(5)	(5)	(5)	DC	warning indicator	Commercial	GF	(5)	(5)	14	1,898,700
24	(5)	(5)	(5)	DC	warning indicator	Commercial	GF	(5)	(5)	1	1,451,400
Totals										893	213,433,400

NOTES:

(1) Insufficient part hours.
(2) American National Standards Institute (ANSI) part number.
(3) Test data is noted.
(4) Commercial part numbers are proprietary.
(5) Unknown.

TABLE 17.1.4-2: INCANDESCENT LAMP CONSTRUCTION AND APPLICATION VARIABLES

I. Type
   A. Large
   B. Miniature
   C. Subminiature
   D. Ultraminiature

II. Bulb Shape
   A. Globular
   B. Straight Side
   C. Tubular
   D. Other

III. Filament Type
   A. Coiled
   B. Straight
   C. Coiled-Coil

IV. Voltage Level
   A. Rated
   B. Actual

V. Current Level
   A. Rated
   B. Actual

VI. Function
   A. Light Source
   B. Power Indicator
   C. Warning Indicator
   D. Test Light
   E. Status Indicator
   F. Other

VII. Ratio of Illumination Time to Equipment Operating Time

VIII. Number of "On-Off" Cycles per Unit Time

IX. Application Environment

X. Operating Temperature
   A. Rated
   B. Actual

XI. Manufacturing Qaulity Level

The hazard rate of incandescent lamps would be anticipated to be increasing with time. However, incandescent lamp field experience data which allows for investigation of a time dependent failure rate model was not available. Therefore, average failure rate values were calculated for each data entry with observed failures by dividing the number of failures by the recorded part hours. An upper 60% confidence limit was used to approximate failure rate for the data entries without observed failures. These failure rates are equal to the catastrophic lamp failure rate plus an average wearout failure rate contribution.

Stepwise multiple linear regression analysis (described in Section 3.1) was applied to the incandescent lamp failure rate data. All data records except entry number 9 in Table 17.1-4-1 were entered into the regression analysis. Data entry number 9 had insufficient part hours to estimate a failure rate without observed failures. The rated voltage and rated current were unknown for data entries 20 through 24. An average rated voltage of twelve volts was assumed for these data entries. This assumption may slightly effect parameter estimation precision but was necessary to fully evaluate all factors influencing failure rate. The rated voltage and rated current were available for approximately 80% of all collected data and therefore any detrimental effects from this assumption are minimal.

The lamp utilization presented a unique problem in application of regression analysis. Generally a factor based on part utilization would be a function of a quantitative variable like duty cycle. However, the duty cycle of lamps used as warning indicators and test lights is unknown although thought to be relatively low (<0.10). The duty cycle of lamps functioning as status indicators is both unknown and variable over a range of values. The duty cycle of lamps functioning as power indicators is known to be approximately one. However, a factor could not possibly be based on this information. Therefore, the lamp utilization was treated as a qualitative variable similar to quality level or environment. "Dummy variables" of one and zero were used in the regression analysis to represent applications with periodic illumination and constant illumination respectively. Only one data

record was collected where a lamp functioned as a status indicator (data entry #19 in Table 17.1.4-1). Therefore, analysis of this type of lamp application could not be investigated by the regression analysis. The failure rate of status indicator lamps is considered later in this section. Treatment of lamp utilization as a qualitative variable not only aids the reliability modeling analyst but would also aid a reliability engineer performing an equipment reliability prediction. Reliability engineers using a proposed incandescent lamp failure rate prediction model would not have access to a precise measure of the anticipated duty cycle of a lamp functioning as a warning indicator. Therefore, a fixed numerical quantity for all warning indicator applications would provide maximum utility of the failure rate prediction model.

Both rated voltage and rated current were not included in the regression analysis because of a large negative correlation between the two variables. A properly applied regression analysis should include only variables which are independent. Rated voltage was chosen to be included in the analysis based on theoretical considerations.

The details of the regression analysis are given in Tables 17.1.4-3 and 17.1.4-4. Table 17.1.4-3 defines the variables introduced into the regression analysis and Table 17.1.4-4 presents the results of the analysis. Variables which are included in Table 17.1.4-3 but not Table 17.1.4-4 are those which could not be determined to have a significant effect on failure rate. An explanation of quantitative and qualitative regression is included in Section 3.1.

The results of the regression analysis indicate that bulb shape and quality level do not significantly effect the observed failure rate. This does not imply that quality level has no effect on failure rate. However, the relative difference in failure rate between MIL-SPEC and commercial quality incandescent lamps could not be distinguished from the data. Additionally only two out of five environmental factor variables were determined to be significant. These results are scrutinized in the following paragraphs.

TABLE 17.1.4-3: INCANDESCENT LAMP VARIABLE IDENTIFICATION

Parameter	Variables(s)	Factor
bulb/shape	X_1, X_2	$\exp(b_1X_1 + b_2X_2)$
miniature		$\exp(b_1)$
subminiature		$\exp(b_2)$
AC/DC	X_3	$\exp(b_3X_3)$
AC		1.0
DC		$\exp(b_3)$
quality	X_4	$\exp(b_4X_4)$
MIL-SPEC		1.0
lower		$\exp(b_4)$
rated voltage	$X_5 = \ln(V_r)$	$(V_r)^{b5}$
utilization	X_6	$\exp(b_6X_6)$
constant illum.		1.0
periodic illum.		$\exp(b_6)$
environment	X_7 - X_{11}	$\exp(b_7X_7 + \ldots + b_{11}X_{11})$
GB		1.0
GF		$\exp(b_7)$
NSB		$\exp(b_8)$
NS		$\exp(b_9)$
AIT		$\exp(b_{10})$
GM		$\exp(b_{11})$

TABLE 17.1.4-4: RESULTS OF THE REGRESSION ANALYSIS

Variable (X_i)	Coefficient (b_i)	Standard Error	F-Ratio
X_3	1.2057	1.2836	0 88
X_5	1.2890	0.5329	5.85
X_6	-2.2826	0.8376	7.43
X_9	3.0957	1.6674	3.45
X_{11}	1.9679	1.0571	3.47
Constant	-2.1926	--	--

Strict interpretation of the results given in Table 17.1.4-4 were that ground, benign; ground, fixed; naval, submarine and airborne inhabited, bomber environments have a similar effect on lamp reliability and that naval, sheltered ($X_{i\neq 9}=0$, $X_9=1$) and ground, mobile ($X_{i\neq 11}=0$, $X_{11}=1$) environments adversely effect lamp reliability. For the number of available data records and the anticipated "statistical noise", these results were not discouraging. Only the inclusion of airborne inhabited, bomber with ground, benign; ground, fixed and naval, submarine environment was considered questionable. The anticipated relatively smaller numerical differences between ground, benign; ground, fixed and naval, submarine environmental factors could not be distinguished by regression analysis unless more data records or more observed failures per data record were obtained. Nevertheless, derivation of a complete set of environmental factors is essential to properly discriminate against all incandescent lamp reliability characteristics. No part type currently included in MIL-HDBK-217D adequately represents the effects of environmental stress on lamps. Therefore, the methodology described in Section 3.3 was applied to the incandescent lamp data to derive an applicable series of environmental factors. This method assumes that an environmental factor relation can be determined where environmental factor is a function of the "environmental stress ratios" given in Reference 1. Before application of this method, all data was normalized by application, rated voltage and utilization. Referring again to Tables 17.1.4-3 and 17.1.4-4, the normalization function was obtained by the following progression of equations.

$$\lambda_p = \exp(b_0)\ \exp(b_3X_3)\ (V_r)^{b5}\ \exp(b_6X_6)\ \pi_E$$

$$\lambda_p/(\exp(b_3X_3)\ (V_r)^{b5}\ \exp(b_6X_6)) = \exp(b_0)\ \pi_E$$

$$\lambda_{p,\ norm} = \lambda_p/(\exp(b_3X_3)\ (V_r)^{b5}\ \exp(b_6X_6))$$

$$\lambda_{p,\,norm} = \exp(b_o)\ \pi_E$$

where

λ_p = incandescent lamp failure rate
π_E = environmental factor
$\lambda_{p,\,norm}$ = normalized failure rate

Various relations of normalized failure rate as a function of environmental stress ratio were attempted. The optimal relation and the corresponding environmental factor equation are given by,

$$\lambda_{p,\,norm} = 0.0735\ (S)^{0.495}$$

$$\pi_E = (S)^{0.495},\ (\text{normalized to } \pi_{E,GB} = 1)$$

where

S = environmental stress ratio

The series of environmental factors obtained by this method were given in Table 17.1.3-2 in the previous section. A result of normalizing the environmental factors to a value of one for a ground, benign environment was that refinement of the regression constant was necessary. The previously determined regression constant ($\exp(b_o) = \exp(-2.19) = 0.112$) represented an average value for the ground, benign; ground, fixed; naval, submarine and airborne inhabited, transport environments. The revised value ($\exp(b_o') = 0.075$) obtained from the environmental factor derivation process corresponds to the ground, benign environment.

The derived environmental factors based on the data are lower than those included in MIL-HDBK-217D for electronic parts. One explanation for this is that operating temperature and temperature cycling theoretically have very little effect on lamp life. The internal lamp illumination temperatures are

so high that elevated environmental temperatures and/or temperature cycling are essentially negligible in comparison. Therefore the derived incandescent lamp environmental factors are primarily a function of the other two primary failure activating stresses, shock and vibration.

The regression analysis identified the rated voltage as a significant variable effecting failure rate. The model indicates that failure rate is proportional to rated voltage raised by an exponent equal to 1.289. The rated voltage is a construction parameter which is the same for a particular lamp regardless of the application. Therefore, it was decided to include the rated voltage into a base failure rate relation. The base failure rate is therefore a function of the rated voltage and is given by,

$$\lambda_b = 0.074\ (V_r)^{1.29}$$

where

λ_b = base failure rate (failures/10^6 hours)
V_r = rated voltage (volts)

Applied voltage would also be anticipated to have a significant effect on lamp reliability. Consideration of this factor is discussed in the following paragraph.

All data collected in support of this study had an applied-to-rated voltage ratio either equal to one or unknown and assumed equal to one. This is not unusual because most design engineers do not "derate" lamp voltage. However, it has been documented that incandescent lamp failure rate in AC operation can be decreased by decreasing the applied voltage. References 2, 3, 5 and 6 include theoretical relations or examples of lamp life as a function of applied to rated voltage. An example of a theoretical relation between lamp life and applied to rated voltage is given below. This example is from Reference 6.

$$\text{Lamp life} \propto (V_r/V_a)^{13}$$

where

V_r = rated voltage
V_a = applied voltage

The theoretical relations only apply from 0.90 to 1.10 of rated voltage. The effect of reducing the applied voltage is more pronounced for low voltage lamps because of the sturdier tungsten filaments. Reducing the applied to rated voltage decreases internal lamp temperature and thus decreases the filament evaporation rate. Low voltage lamps most often fail due to the uniform evaporation of the filament. High voltage lamps have fragile filaments and more often experience catastrophic failures which are less dependent on evaporation rate. Therefore the relation is only directly applicable to low voltage lamps (rated voltage ≈ 5V). There are three major reasons why design engineers do not take advantage more often of the extended lamp life offered by derating lamp voltage. The first reason is that replacement of incandescent lamps in many applications is relatively easy and light output is of a greater concern than lamp reliability. The second reason is that higher voltage incandescent lamps (Vr ≈ 28v) are insensitive to the reliability differences caused by derating lamp voltage therefore the corresponding light output sacrifice is not warranted. The third reason is that lower voltage lamps already have inherently lower failure rates and therefore voltage derating is considered unnecessary. A factor based on the ratio of applied to rated voltage was not included in the proposed failure rate prediction model for two reasons. First, no data was available to either confirm or disprove the theoretical relations. Second, no documented theoretical relation was found which applies to higher voltage incandescent lamps.

The regression analysis for lamps included a factor based on whether the lamp is in AC or DC operation. A factor of one is assigned to lamps in AC operation and a factor of 3.3 is assigned to lamps in DC operation. This

factor was designated the application factor. These results are consistent with documented studies. Reference 2 states that "AC operation can increase lamp life from two to ten times the life obtainable with DC operation." Reference 3 states that "the life of an incandescent lamp energized by DC is 40 to 50% of life at the same voltage AC." Reference 4 found that "average life of filaments operating on DC at the designed voltage is less than one-third of that on AC." The observed failure rate ratio of 3.3 was based solely on the empirical data given in Table 17.1.4-1.

The utilization of an incandescent lamp was thought to be a significant factor in a failure rate prediction model. The results of the regression analysis indicate an order of magnitude difference between applications requiring constant illumination and those requiring periodic illumination. The effect which utilization has on failure rate was represented by a utilization factor (π_u). The numerical results are in complete agreement with theoretical reliablity considerations. However, sufficient data were available only for constant illumination, power indicator, warning indicator and test light applications. These applications represent the two extreme cases. Constant illumination and power indicator lamps are illuminating (and thus the filament is evaporating) for the entire time the equipment is in use. Warning indicator lamps and test lamps are usually not illuminating for the vast majority of the equipment operating time. Test lamps are generally activated briefly at the start and the end of a mission and accumulate very few illumination hours. Warning indicator lamps are intended to illuminate very rarely. The duty cycle of a warning indicator is very hard to predict but can be assumed to less than 10%. It should be noted that life limiting stresses occur while lamps are in both illumination and nonillumination modes. The problem with the regression solution is that status indicator lamps or other lamp applications with variable duty cycles were not included in the analysis. The one data record (entry #19, Table 17.1.4-1) where the lamp functioned as a status indicator has zero observed failures. The lack of precision in estimating a failure rate without observed failures is the reason that derivation of a numerical utilization factor value for status indicators was difficult. However, an important

attribute of all reliability modeling efforts is to produce a usable model which can be applied to all potential applications.

It was hypothesized that a continuous numerical relationship for utilization factor as a function of lamp duty cycle would not be linear. The hypothesized function was that the utilization factor would be relatively close to the duty cycle for low (<0.10) and high (>0.90) duty cycles, but would be higher than the duty cycle for intermediate duty cycle values. The hypothesized relationship for utilization factor as a function of duty cycle is presented in Figure 17.1.4-1. The reason for the hypothesized nonlinearity shown in Figure 17.1.4-1 is the anticipated effect of "on-off" power cycling. Applications with high and low duty cycles are subjected to relatively fewer on-off cycles and the observed failure rate is primarily a function of filament evaporation. Status indicator lamps with intermediate duty cycles are subjected to more on-off cycles and the failure rate is a function of both filament evaporation and on-off cycling. The amount of "on-off" cycling for low, intermediate and high duty cycles is illustrated in Figure 17.1.4-2. Based on the hypothesized relation, it was assumed that a proposed utilization factor for status indicators would fall between the value derived from constant illumination applications (1.0) and the arithmetic mean of the values derived from constant illumination and warning indicator applications (0.55). To determine a specific numerical quantity, upper confidence limit failure rates were calculated for data entry number 19. The upper 80% confidence limit satisfied the boundary limits assumed for a status indicator utilization factor. Therefore, the data was normalized and a utilization factor of 0.72 was calculated by the following equation. A discussion of Chi-squared confidence interval estimation is included in section 3.1.

$$\pi_{u,s} = \chi^2_{.80}/(2T\ \lambda_b\ \pi_E\ \pi_A)$$

where

$\pi_{u,s}$ = utilization factor for status indicators

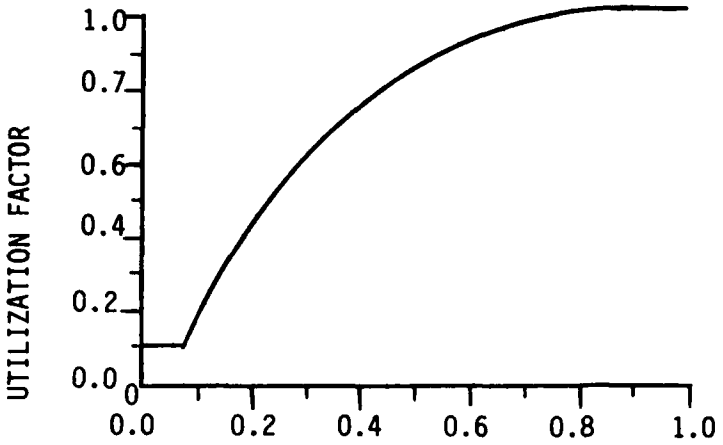

FIGURE 17.1.4-1: UTILIZATION FACTOR VS. DUTY CYCLE

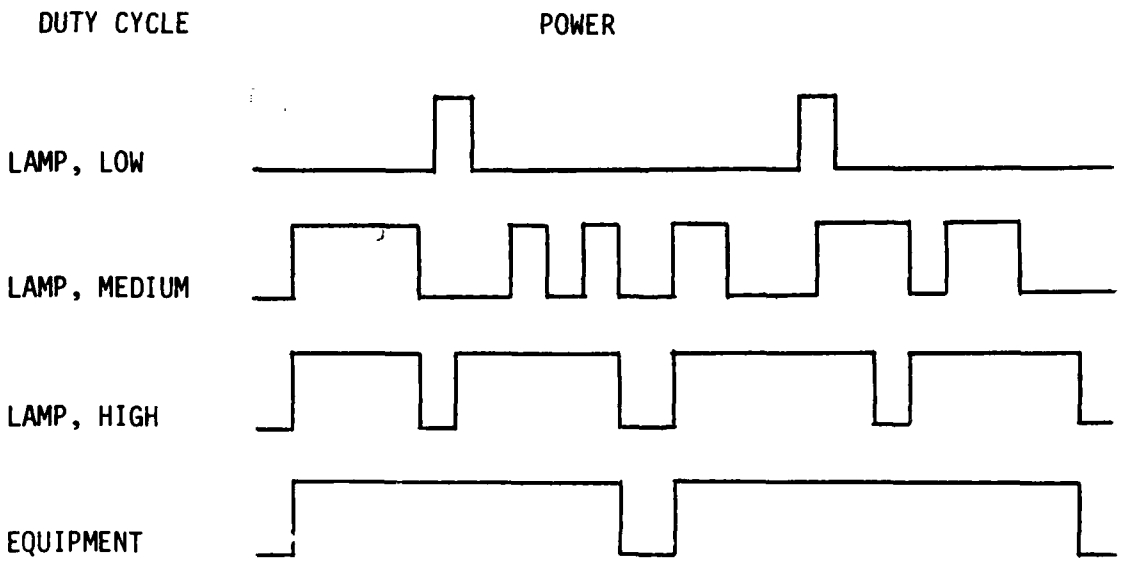

FIGURE 17.1.4-2: LAMP VS. EQUIPMENT POWER FOR VARIOUS DUTY CYCLES

$\chi^2_{.80}$ = Chi-squared statistic (α = 0.80, 2 degrees of freedom)

= 3.219

T = part hours X 10^6

= 0.7118

λ_b = base failure rate = 0.074 $(V_r)^{1.29}$ f/10^6 hrs.

= 0.074 $(5)^{1.29}$ = 0.590

π_E = environmental factor

= 1.6 for ground fixed

π_A = application factor

= 3.3 for DC

$\pi_{u,s}$ = 3.209/(2(0.7118)(0.590)(1.6)(3.3))

= 0.724

Although the method used to calculate this utilization factor value lacked precision, the numerical value is intuitively satisfactory. Status indicator lamps exhibit less filament evaporation but are subjected to more "on-off" cycling than constant illumination applications and a value close to the constant illumination value of one is logical. The interim utilization factors are presented in Table 17.1.4-5.

TABLE 17.1.4-5: INTERIM UTILIZATION FACTOR

Function	Duty cycle	π_u
power indicator	1.0	1.0
status indicator	?	0.72
warning indicator	0.10	0.10
test light	0.10	0.10

Another modification of the utilization factor was deemed necessary for two reasons. First, there are many applications for incandescent lamps and although Table 17.1.4-5 includes the majority of all lamp applications, many other applications exist such as illumination of a dial or meter. Second, particular applications of status indicators closely resemble power

indicator (constant illumination and little "on-off" cycling) or warning indicator (little or no illumination) and therefore should be assigned the more appropriate utilization factor value. Therefore a final utilization factor was determined and three general utilization types were defined and are presented in Table 17.1.4-6.

TABLE 17.1.4-6: UTILIZATION FACTOR

Utilization type	Illuminate hours/ equipment operate hrs.	π_u
A	> 0.90	1.0
B	0.10 to 0.90	0.72
C	< 0.10	0.10

The boundaries of the B category were chosen so that most applications would fall immediately into one category or another and that a specific numerical quantity of (illuminate hours/equipment hours) would not be required of the analyst preforming the reliability prediction. It should be noted that the three choices given in Table 17.1.4-5 represent three unique applications and that no attempt should be made to interpolate between the numerical values.

The effect of "on-off" cycling is not included directly in the proposed failure rate prediction model. However, the model accounts for "on-off" cycling two different ways. Missions within an environment category are similar in regard to mission duration. For example the typical helicopter mission would be expected to be much shorter than the typical mission in a ground fixed environment. Therefore the higher frequency of on-off cycles generally would occur in the helicoptor environment. Therefore the effect of on-off cycling is included in the environmental factor to the extent that the average frequency of on-off cycling is different between environment categories. The effect of on-off cycling is also included partially in the proposed utilization factor. For a particular environment category the relative frequency of on-off cycling is low for applications with both high

and low duty cycles (utilization types A and C in Table 17.1.4-6) and relatively higher for applications with an intermediate duty cycle.

The proposed failure rate prediction model offers greater sensitivity to incandescent lamp reliability characteristics. The existing MIL-HDBK-217D methodology for prediction of lamp failure rate was a point estimate failure rate for all lamp applications. The proposed model presents incandescent lamp failure rate as a function of rated voltage, environment, utilization and application. The proposed model offers the reliability analyst a more accurate and precise measure of lamp reliability and it is recommended that the proposed model be included in the latest revision of MIL-HDBK-217.

17.1.5 References and Bibliography

References

1. Kremp, B.F. and E.W. Kimball, Revision of Environmental Factors for MIL-HDBK-217B, RADC-TR-80-299, September 1980.

2. Sylvania Miniature Lightings Products, Properties of Miniature Lamps, Machine Design, Vol. 46, No. 30, Dec. 12, 1974.

3. Dombroski, C., Indicator Lamps - The Sooner the Brighter, Electronic Products, April 1978.

4. Koo, R.C. and J. Woodhouse, Observations on Electromigration and Improved Filament Life of Microminiature Lamps, Journal of the Society of Illuminating Engineers, Vol. 5, July 1976.

5. Chicago Miniature Lamp Works, Lamp Comparison and Evaluation of the Industry Standards No. 327 and No. 387 Subminiature Lamps.

6. Fink, D.G. and D. Christiansen, Electronics Engineer's Handbook, Second Edition, Section 11, McGraw-Hill Book Co., 1982.

Bibliography

Dawson, C.W., Nelson, J.L., et. al., Hot Spots and Their Effect on The Lives of Incandescent Filaments, Journal of the Society of Illuminating Engineers, July 1973.

Horacsek, O., Properties and Failure Modes of Incandescent Tungsten Filaments, IEE Proceedings, Vol. 127, Pt. A, No. 3, April 1980.

17.2 Lamps, Glow

17.2.1 Part Description

The following discussion was extracted primarily from reference 1. The glow lamp is basically a negative discharge device. It consists of two closely spaced electrodes housed in a glass envelope filled with rare gas (neon, argon, etc.). When a sufficient amount of voltage is applied across the terminals of a glow lamp, it exhibits what are called breakdown characteristics; that is, the gas ionizes and the voltage across the lamp drops very quickly to a reduced level which is called its maintaining voltage. When this condition occurs, there is the appearance of a glow surrounding the negative electrode.

Glow lamps have properties that permit them to be used as light sources or circuit components. As a light source, they permit a method of giving high voltage (115 volts) illumination in a small envelope. They are generally more rugged and more reliable than incandescent lamps. Illumination efficiency of standard brightness units is quite low, about 0.005 candlepower per milliamp, while for high brightness units it is about 0.013 candlepower per milliamp. This gives a brightness of about 0.0035 candlepower for a typical standard brightness unit and about 0.025 candlepower for high brightness units. Therefore, these units are not nearly as bright as typical incandescent lamps.

Glow lamps have many varied uses. In addition to being used as a lamp, they often serve as circuit components. Some of their uses include: indicator, voltage indicator, voltage regulator, low frequency generator, and leakage detector. Glow lamps are subject to "runaway" conditions; therefore, they must always be operated in series with a current limiting device, such as a resistor.

Glow lamps exhibit excellent environmental resistance and much higher vibration resistance than incandescent lamps. They should never be used

above 150°C and, in circuit applications, are not recommended above 75°C. When glow lamps are subjected to darkened environments, their breakdown voltage rises and ionization time increases. Lamps are available which include use of mild radioactive additives to reduce their susceptibility to darkened environments. Glow lamp operation is affected by electrostatic and electromagnetic fields. It is possible to ignite a glow lamp in a strong electromagnetic field with no applied voltage.

The definition of life differs with various glow types. Standard brightness indicator types are said to reach end of life when their light output decreases to 50% of initial. High brightness lamps remain essentially constant in light output through life, and fail when breakdown voltage reaches line voltage. Circuit component types reach end of life when their starting or maintaining voltage changes some definite value (usually 5 or 10 volts) from initial rating. References 2 and 3 state that the average useful life (time to 50% of initial output) for dc operation is 60% of the average useful life for ac operation.

17.2.2 Failure Modes and Mechanisms

The primary failure modes for glow lamps are as follows:

- o deterioration or destruction of the seal caused by defective materials and/or process, or handling problems. This will result in an open lamp because of the absence of a discharge between electrodes.
- o open lead wire in the base of the lamp or on wire leaded lamps external to the base caused by poor workmanship or defective materials. This will result in an open or intermittent lamp.
- o shorted lead wires in the base of the lamp caused by faulty workmanship. This will result in a shorted lamp with no light emission.
- o excessive current flow through the lamp or excessive voltage across the lamp causes an arc to form between the electrodes. This will result in rapid lamp deterioration.

17.2.3 Glow Lamp Failure Rate Prediction Model

This section presents the proposed failure rate prediction model for glow lamps. The proposed model is:

$$\lambda_p = 0.2F/10^6 \text{ hours}$$

The model is limited to neon glow lamps.

17.2.4 Model Development

The approach used was to hypothesize a model form based on physics of failure information. The model form would be verified and parameters would be quantified by analysis of data collected during the study. The model that was assumed is:

$$\lambda_p = \lambda_b \times \pi_E \times \pi_T \times \pi_Q \times \pi_A$$

where

λ_p = glow lamp failure rate ($F/10^6$ hours)
λ_b = base failure rate ($F/10^6$ hours) and where λ_b is a function of the lamp type
π_E = environmental factor
π_T = temperature factor
π_Q = quality factor
π_A = application factor

The rationale for including the factors given above is discussed in the following paragraphs.

Glow lamps may contain argon, neon or a mixture of gases. The circuit connection technique is either through a base or through lead wires. The deterioration characteristics of the gases differ. For instance, the

average of the specified lives from references 4, 5, 6 is approximately 14,900 hours for neon and 150 hours for argon glow lamps. Since the two connection techniques are so different it would be expected that their failure characteristics would be different. For example, from references 4, 5 and 6, the average of the specified lives is approximately 16,300 hours for wire lead devices and 21,100 hours for devices with a base. In addition, the failure modes of standard brightness indicators and high brightness lamps differ; therefore, the failure rate should differ. The construction of the glow lamp probably is correlated with the expected life of the device. The specified life of the devices varied from 7,500 to 100,000 hours for neon indicator lamps and from 500 to 25,000 hours for neon circuit component devices; however, the driving construction characteristic responsible for these differences was not obvious from the data (references 4, 5 and 6). It was assumed then that λ_b would vary as a function of gas type, construction basing mechanism and whether it is a standard or high brightness lamp.

Glow lamps behave differently in a darkened environment and in the presence of electrostatic and electromagnetic fields. Since they behave differently, it could be expected that their failure rate would differ depending on the environment. It was assumed that an environmental factor could be derived that would account for those differences in behavior.

Glow lamps have an upper temperature limit which should never be exceeded, and they exhibit a negative temperature coefficient. In addition, gas diffusion and bond strength are a function of temperature. These factors would indicate that device failure rate may be a function of temperature.

Glow lamps are manufactured devices and as such are subject to manufacturing deficiencies. In addition, glow lamps can be burned-in to reduce the number of infant mortality failures and to stabilize the breakdown and maintaining voltages. Failure rate then may be a function of manufacturing quality and whether or not a burn-in was performed.

Glow lamps are used for numerous applications including voltage detection, voltage regulation, low frequency generators and indicators. The definition of failure should vary for the various applications. The average of the specified lives from references 2, 3 and 4 is approximately 5,900 hours for circuit component neon lamps and 22,500 hours for neon indicator lamps. Failure rate then may be a function of how the lamp is used in the circuit.

Based on the above considerations, application and construction variables were identified (Table 17.2-1). These application and construction variables represent possible failure rate model parameters which were determined whenever possible for all collected data.

The glow lamp failure experience data collected in support of this study are presented in Table 17.2-2. As can be seen from the data, there is insufficient data to develop parameters for the model form assumed above. Also since all of the data are for the same basic lamp type used in the same application there was insufficient data to disprove the current MIL-HDBK-217D point failure rate estimate for neon lamps. It is proposed then that the current MIL-HDBK-217D model be retained. The low failure rate of the device and the fact that they are increasingly being replaced in circuit applications by solid state voltage regulators, and solid state and liquid crystal indicators may indicate that the current model is sufficient.

17.2.5 References and Bibliography

References

1. General Electric Company, Component Technology and Standardization Manual, Section 11.2.

2. Glowhite Product Catalog.

3. Xenell Corporation Product Catalog.

4. Herman H. Smith Product Catalog.

TABLE 17.2-1: GLOW LAMP CONSTRUCTION AND APPLICATION VARIABLES

I. Type
   A. Neon
   B. Argon
   C. Mixture

II. Bulb Shape
   A. Globular
   B. Straight Side
   C. Tubular
   D. Other

III. Mounting Method
   A. Base
   B. Lead

IV. Function
   A. Light Source
   B. Indicator
   C. Voltage Regulator
   D. Low Frequency Generator

V. Current Level
   A. Rated
   B. Actual

VI. Voltage Level
   A. Rated
   B. Actual

VII. Operating Temperature
   A. Rated
   B. Actual

VIII. Application Environment

IX. Manufacturing Quality Level

TABLE 17.2-2: GLOW LAMP FAILURE EXPERIENCE DATA

Source	Equip Type	Env	APP (3)	Tube Type	Voltage Rated	Voltage Actual	Current (A) Rated	Current (A) Actual	Temp (°C)	Qual (1)	No. Fail	OP Hrs ($\times 10^6$)	Failure Rate ($F/10^6$ hrs) (2)
1	TSQ-73	GM	I	NE-51	120	-	0.22	-	30	C	0	0.246	3.748
2	TSQ-73	GM	I	NE-2D	115	-	0.7	-	30	M	0	0.123	7.496
3	GRR-24	GM	I	NE-51H	120	-	0.22	-	--	C	1	1.701	0.588
4	GRR-23	GM	I	NE-51H	120	-	0.22	-	--	C	0	0.253	3.644
5	GYQ-18	GF	-	NE-51H	120	-	0.22	-	25	C	0	0.356	2.590
6	GYQ-18	GF	-	--	105/125	-	--	-	25	-	0	4.983	0.185
7	--	NS	-	--	-	-	--	-	--	-	26	53.215	0.489
Total											27	60.877	0.444

Notes: (1) C = Commercial quality, M = MIL-SPEC quality

(2) For zero failures entry is upper 60% confidence bound

(3) I = indicator

Bibliography

Arno, Robert G., Nonelectronic Parts Reliability Data, Reliability Analysis Center Document NPRD-2, Summer, 1981.

General Electric Company, Component Technology and Standardization Manual, Section 11.2.

Glowhite Product Catalog.

Herman H. Smith Product Catalog.

Xenell Corporation Product Catalog.

18.0 SURFACE ACOUSTIC WAVE DEVICES

18.1 Part Description

Surface Acoustic Wave (SAW) devices are any of a number of signal processing devices which operate by converting an electrical signal to an acoustic wave travelling along the surface of the medium. The surface acoustic wave has both longitudinal (compressive) and transverse (shear) components, and has the majority of its energy concentrated within one acoustic wavelength of the surface within the bulk. SAW devices are finding widespread use for a number of signal processing requirements at UHF and microwave frequencies.

In its simplest form, a SAW device consists of a pair of electrical conductors placed on each end of a piezoelectric crystal. When an electrical potential energizes one conductor pair, the piezoelectric crystal will mechanically distort, creating a surface wave which is transmitted through the crystal at a velocity dependant upon the material properties of the device. At the other end, the second pair of conductors detect the surface wave and outputs a corresponding electrical signal to the circuit. The velocity of a SAW is on the order of 10^{-5} that of electric field propagation in free space, making them useful as delay lines in electrical circuits.

By the addition of simple electrodes to otherwise standard piezoelectric delay lines, it is possible to use these delay lines to generate the convolution and correlation functions of an unknown signal with an arbitrary reference signal. By suitable choice of a reference signal, pulse compression and other signal processing operations may be performed.

Electrodes are usually fabricated in the form of an interdigitated structure as in Figure 18.1-1. The response of a SAW device may be controlled by altering the finger position width and amount of overlap.

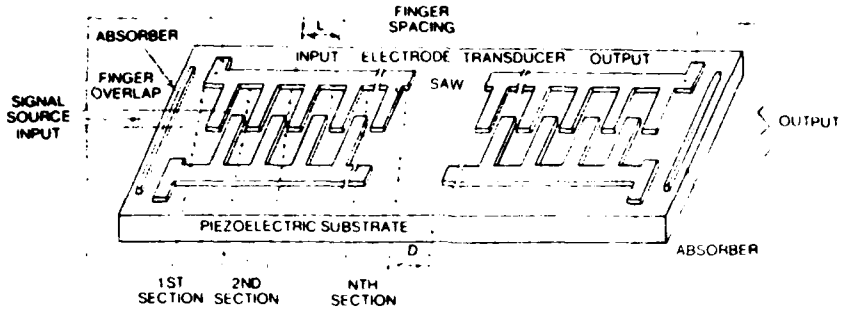

FIGURE 18.1-1: TYPICAL SAW CONSTRUCTION

The interdigitated structures are easily fabricated using conventional aluminum thin film deposition and lithographic techniques used by the microelectronic industry. For very high frequency devices, E-beam lithography must be used because the resolution of optical techniques is generally inadequate.

SAW devices offer the designer several attractive features, including the following:

- o Planar structures using conventional fabrication techniques
- o Relatively slow acoustic wave allows miniature devices to be made for operation at typical IF frequencies
- o Signal may be tapped during propagation, allowing complex signal processing
- o Sophistication of design is predominantly built into masks used to define electrode structures
- o Surface wave is stable and temperature insensitive. Devices are easily manufactured.

These devices have been fabricated from a wide variety of materials including quartz, lithium niobate, bismuth germanium oxide, barium sodium

niobate, cadmium sulfide, diamond, europium iron garnet, gallium arsenide, and many others.

The simplicity and versatility of surface acoustic wave devices makes them desirable for a number of high reliability state-of-the-art military systems including radar, communication, sonar, air traffic control, and display systems. Specific uses for SAW devices include delay lines, frequency filters, oscillators, matched filters, code generators, convolvers, and IF signal processing applications.

18.2 Failure Modes and Mechanisms

While the relative simplicity of these devices makes them reliable in a wide variety of applications, there are several failure modes and mechanisms to which these devices are susceptible. As their name might suggest, surface acoustic wave devices are susceptible to degradation as a result of surface contamination. It is important that the surface of high frequency devices be kept scrupulously clean. Small amounts of organic material can cause a large amount of surface wave attenuation.

Strain effects are very important in SAW devices. Unintentional strain results in devices with highly variable properties. This requires that particular care be exercised when bonding a SAW device to a substrate, so that no residual strain is present after the bonding operation. Also, if the operating temperature is to vary widely in use, it is important that thermal expansion rates for the SAW device and substrate be carefully matched.

Due to the extremely small finger dimensions on high frequency devices, the SAW component is very sensitive to electrostatic discharge (ESD) damage (at voltages as low as 150 volts on piezoelectric quartz and lithium niobate). ESD damage may manifest itself as a melting of interdigitated metal runs, a fracturing of the crystal surface, or both. As a consequence, it is imperative that SAW devices be manufactured, handled, and used in conditions where ESD protective measures have been implemented.

In addition to the above mentioned conditions, the surface wave device is vulnerable to the usual problems of crystal growth, thin film deposition, and lithographic defects, and packaging problems which are well documented in semiconductor and hybrid reliability studies. Table 18.2-1 lists the failure modes/mechanisms that have been either reported in the published literature or recorded with the data collected during the study.

TABLE 18.2-1: REPORTED FAILURE MODES/MECHANISMS

Source	Number of Occurrences*	Failure Mode/Mechanism
1	1	Wire bond failure.
2	1	Open ground wire connection.
3	-	Cracks in substrate during manufacture caused by rapid temperature change.
4	-	Polyimide used to bond SAW devices. If insufficient polyimide is used, it will tend to crack, effectively demounting the SAW.
5	-	Aluminum migration induced by high density acoustic fields.
6	-	Growth of aluminum oxide on the thin film aluminum metal induced by water vapor and a dc electric field within the transducer structure (Ref. 1).
7	-	Short fused (open) regions and melting of fingers and arc discharge regions across fingers induced by dc voltage transients as low as 150 volts (Ref. 2).

*'-' indicates, that the number of occurrences was not reported

18.3 SAW Failure Rate Prediction Model

This section presents the proposed failure rate prediction model for Surface Acoustic Wave Devices. The proposed model is:

$$\lambda_p = \lambda_b \times \pi_E$$

where

λ_p = predicted SAW failure rate ($F/10^6$ hours)
λ_b = base failure rate
= 2.1 $F/10^6$ hours
π_E = environmental factor (see Table 18.3-1)

TABLE 18.3-1: ENVIRONMENTAL FACTORS

Environment	π_E	Environment	π_E
G_B	1.0	A_{IA}	10.0
G_F	3.9	A_{IF}	15.0
G_M	11.0	A_{UC}	12.5
M_P	10.0	A_{UT}	10.0
N_{SB}	4.95	A_{UB}	20.0
N_S	8.5	A_{UA}	15.0
N_U	16.0	A_{UF}	20.0
N_H	15.5	S_F	1.6
N_{UU}	17.0	M_{FF}	10.5
A_{RW}	22.5	M_{FA}	14.5
A_{IC}	7.5	U_{SL}	30.5
A_{IT}	7.5	M_L	35.0
A_{IB}	12.5	C_L	600.0

18.4 Failure Rate Model Development

The model development approach used was to assume a model of the form: $\lambda_p = \lambda_b \pi_E$. A base failure rate ($\lambda_b$) estimate was then derived from the

observed data shown in Table 18.4-1. A failure rate prediction model of this form oversimplifies the reliability characteristics of SAW devices. However, the lack of available field failure rate data and the unavailability of data from SAW manufacturers necessitated this model format.

TABLE 18.4-1: SAW FAILURE EXPERIENCE DATA

Source (Note 1)	Env	No. Fail.	Sample Size	Operate Hours ($X10^6$)	Failure Rate ($F/10^6$ hours) L10%CL	PT EST (Note 2)	U90%CL
1	A_{IC}	1	--	0.062	1.70	16.10	62.64
2	G_B	1	32	0.691	0.15	1.45	5.63
8	S_F	0	--	0.788	--	1.17	2.92
9	G_F	0	46	0.036	--	25.68	64.21
Totals		2		1.577			

Notes:

1) Source 1: WIDE and Narrow Band Expanders and Compressors, equipment type unknown
   Source 2: 1393 MHZ Oscillator, life test data
   Source 8: Device Function unknown, equipment type unknown
   Source 9: Elastic Convolver, equipment type unknown

2) Upper 60% confidence limit for zero failure data

Because of the construction and reported failure mode/mechanism similarities between SAW and hybrid devices and because the acquired data were too sparse to develop environmental factors directly from the data, the environmental factors for hybrid device resistors, interconnections and packages presented in reference 1 were examined to determine their applicability for the SAW model. The ratio of the failure rates from the four data points were compared with the ratio of the environmental factors presented in reference 3 for hybrid device resistors, interconnections and packages. These data are shown in Table 18.4-2.

TABLE 18.4-2: ENVIRONMENTAL COMPARISONS

Env	MIL-HDBK-217 π_E Ratio	Upper 60% CL Failure Rate ($F/10^6$ hours)	Ratio of observed failure rates
G_B	1.0	2.9	1.0
S_F	1.6	1.2	0.4
G_F	3.9	25.7	8.9
A_{IC}	7.5	32.6	11.6

With the exception of the space flight environment factor, the progression of the observed factors track the progression of the current MIL-HDBK-217 factors for hybrids. One possible explanation for the space flight discrepancy is that the zero failures observed for the space flight data was an assumption made by the source of the data because the equipment was still operational. With the level of redundancy built into the equipment, this could be an optimistic assumption. Based on results shown above and the limited amount of data available (4 points and 2 failures), there is no reason to reject the assumption that the environmental factors presented in reference 3 for hybrids can be used to predict the failure rate of SAW devices.

The MIL-HDBK-217 π_E ratios given above were then used to normalize the data to the ground benign environment. The normalized data including point estimate failure rates, lower 10%, upper 60%, and upper 90% confidence limits are presented in Table 18.4-3.

TABLE 18.4-3: NORMALIZED FAILURE DATA

Source	No Fail	Env	Actual OPHRS ($X10^6$)	Normalized OPHRS ($X10^6$)	Normalized Failure Rate ($F/10^6$ hours) L10%CL	PT EST	U60%CL	U90%CL
1	1	A_{IC}	0.062	0.466	0.23	2.15	4.35	8.35
2	1	G_B	0.691	0.691	0.15	1.45	2.93	5.63
8	0	S_F	0.788	1.261	-	-	0.73	1.83
9	0	G_F	0.036	0.140	-	-	6.58	16.46
Total	2	-	-	2.558	0.21	0.78	1.21	2.08

It was then determined that the optimal base failure rate for SAWs was the 90% upper confidence level estimate of $2.08F/10^6$ hours. It was decided to apply this somewhat pessimistic value for base failure rate because of the relative scarcity of available data and the lack of discrimination in the proposed model against construction and usage variables. This estimate was rounded to two significant digits for inclusion in the handbook. The environmental factors presented in reference 3 for hybrid devices were then normalized to a ground benign value of 1.0 (see Table 18.3-1). A graph of the predicted to observed failure rates listed in Table 18.4-1 is shown in Figure 18.4-1. The upper 90% and lower 10% confidence limits are also shown on the graph.

18.5 References and Bibliography

References

1. Allen, Donald E., et. al., A Latent Failure Mechanism for Surface Acoustic Wave Components Utilizing Lithium Niobate, 18th Annual Reliability Physics Symposium, 1980.

2. Hickernell, F.S., DC Voltage Effects On SAW Device Interdigital Electrodes, 18th Annual Reliability Physics Symposium, 1980.

3. Edwards, E., et. al., Avionic Environmental Factors for MIL-HDBK-217, Final Technical Report, RADC-TR-81-374, January, 1982.

Bibliography

Allen, Donald E., et. al., A Latent Failure Mechanism for Surface Acoustic Wave Components Utilizing Lithium Niobate, 18th Annual Reliability Physics Symposium, 1980.

Annon., SAW Upsurge Likely in Avionics, Defense Electronics, February, 1981, p. 37.

Edwards, E., et. al., Avionic Environmental Factors For MIL-HDBK-217, Final Technical Report, RADC-TR-81-374, January, 1982.

Feinstein, Joseph, Passive Microwave Components, Electronics Engineers Handbook, Second Edition, McGraw-Hill, 1982.

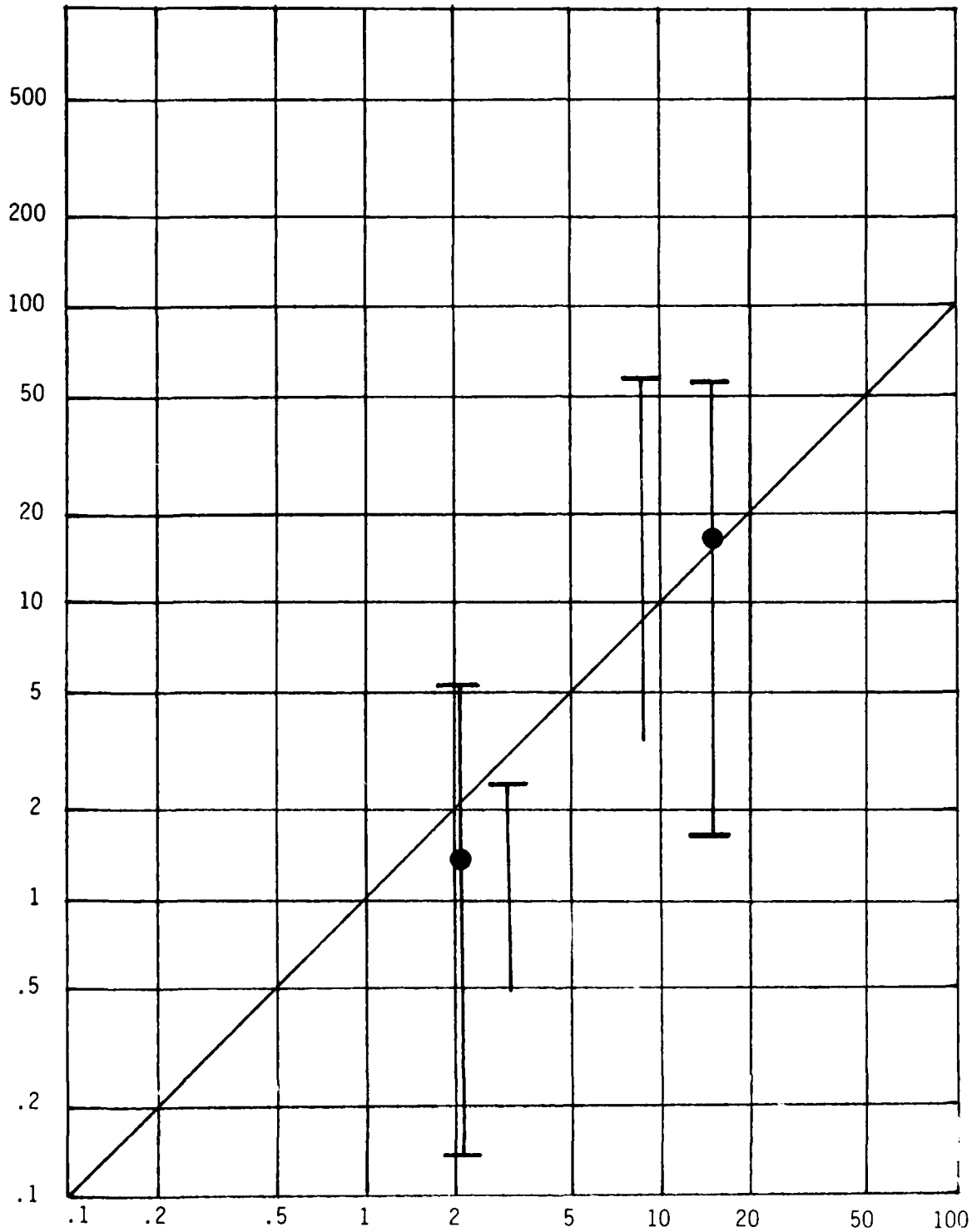

FIGURE 18.4-1: PREDICTED VS OBSERVED FAILURE RATES

Hickernell, F.S., DC Voltage Effects On SAW Device Interdigital Electrodes, 18th Annual Reliability Physics Symposium, 1980.

Hughes Aircraft Company, 2nd Quarterly Report, Contract No. N00014-81-C-2356, Broadband IOSA SAW Transducer Study, January, 1982.

Levine, B., SAW Technology Applications Probed, Source Annon.

Martin Marietta Corporation, Reliability Prediction Models for Microwave Solid State Devices, RADC-TR-79-50, April, 1979.

Murray, R.J., and White, P.D., SAW components answer today's signal-processing needs, Electronics, Vol. 54, September 8, 1981, pp. 120 - 124.

Reeder, T.M. et. al., Frequency Output Pressure Sensors Based on an Application of Surface Acoustic Wave Technology, Society of Automotive Engineers pamplet No. 760093.

Reible, Stanley A., Acoustoelectric Convolver Technology for Spread-Spectrum Communications, IEEE Transactions on Microwave Theory and Techniques, Vol. MTT-29, No. 5, May, 1981, pp. 463-473.

Shoquist, Tom, Sink Your Teeth Into a SAW, Electronic Products, May 1979, pp. 63-66.

Shreve, W.R., et. al., Power Dependence of Aging in SAW Resonators, preprint to be published in 1981 Ultrasonics Symposium Proceedings.

Yao, I. and Reible, S.A., Wide Bandwidth Acoustoelectric Convolvers, Ultrasonics Symposium Proceedings, September, 1979.

19.0 CONCLUSIONS AND RECOMMENDATIONS

19.1 Conclusions

Failure rate prediction procedures were developed for the following devices:

- o Vidicons
- o Semiconductor Lasers
- o Helium-Cadmium Lasers
- o Electronic Filters
- o Solid State Relays
- o I.C. Sockets
- o Thumbwheel Switches
- o Surface Acoustic Wave Devices

In addition, the prediction procedures for the following devices were revised:

- o Magnetrons
- o Electronic Time Delay Relays
- o Circuit Breakers
- o Meters
- o Fuses
- o Crystals
- o Incandescent Lamps
- o Cathode Ray Tubes

Both the new and the revised failure rate prediction procedures will greatly improve upon current failure rate prediction capabilities. The advantages offered by the proposed failure rate prediction procedures are discussed in the following paragraph.

Previously no single acceptable source of failure rates was available for the first group of devices given above. Their inclusion into MIL-HDBK-217 will allow for more consistent evaluations of reliability predictions, reliability trade-offs and life-cycle cost analyses. The revision of the failure rate prediction procedures for the second group of devices listed

above will provide greater sensitivity and increased accuracy in the predictions.

The failure rate prediction procedures for the following devices could not be revised:

- Helium-Neon Lasers
- Solid State Rod Lasers
- CO_2 Lasers
- Argon Ion Lasers
- Neon Glow Lamps

With the exception of Nd:YAG solid state lasers and neon glow lamps, these devices are not used to any great extent in military systems; consequently very little field failure experience data are available. The Nd:YAG laser is used in a number of military equipments; however, data were only available on three of these systems. This amount of data was insufficient to allow for the revision of the current model. Neon glow lamps are used sporadically throughout military equipments. Data were obtained from five military equipments; however, this amount of data was insufficient to allow for the revision of the current model. The low failure rate of this device and the fact that it is increasingly being replaced by solid state voltage regulators and both solid state and liquid crystal indicators would indicate that the current model is adequate.

None of the part failure rate models developed or revised during this study effort are as sophisticated as was originally intended. This was entirely due to lack of sufficient data or lack of detail in the data. The reasons for these data deficiencies are:

- Part types not normally used in military systems (e.g., Argon Ion, CO_2, Helium Neon and Helium Cadmium lasers).
- Part types are low population devices (e.g., neon lamps, SAWs).
- Data contributors are generally reluctant to incur any expenditure to further refine data and information they provide without charge.

- o Part failures are hard to define (e.g. fuses, circuit breakers).
- o Potential data contributors are hesitant to allow visitors access to their proprietary databases.

Consequently, many of the factors considered could not be included in the proposed models. Additionally, many of the factors that were included in the proposed models had to be developed from existing MIL-HDBK-217 models for similar devices, or had to be developed by other analytical methods and not directly from field experience data.

19.2 Recommendations

It is recommended that both the proposed new models developed during this study and the proposed revised versions of existing models be incorporated into MIL-HDBK-217.

Although the proposed failure rate prediction procedures greatly improve prediction capabilities, several recommendations are necessary in light of all available information. All of the devices studied could be classified as low population parts; consequently, most of the proposed models were based on limited data resources. Only a few of the devices do not exhibit sufficiently high failure rates and/or are not used in sufficient quantity to have a noticeable impact on predicted equipment reliability. These devices are:

- o Neon Glow Lamps
- o Incandescent Lamps
- o Fuses
- o Crystals
- o I.C. Sockets

The failure rate of any of the remaining devices may constitute a large portion of the total predicted equipment reliability; therefore, the respective failure rate prediction models should be investigated further to enhance their accuracy and sensitivity.

Several of the device types that were studied, including lasers and surface acoustic wave devices, could be considered emerging technologies. New lasing mediums are being introduced such as the blue-green Xenon-Chloride (XeCl) and Mercurous-Bromide (HgBr) lasers, and new techniques such as high pressure sealed CW CO_2 lasers. These types of lasers are currently not considered in MIL-HDBK-217. In addition, factors which are thought to impact laser reliability such as optical power density, tube power output, and incorporation of a simmer circuit in the solid state laser power supply are not currently considered in MIL-HDBK-217. Surface acoustic wave devices perform many functions (e.g., filter, delay, amplify, etc.) and can assume various levels of complexity. The proposed model does not address these factors which are thought to impact reliability. Every possible attempt should be made in the future to collect field failure rate data so that the failure rate prediction capability for these devices can be enhanced.

Analyses of the data and published information on many of the mature devices disclosed factors which were thought to impact the reliability of the device, but which either could not be investigated due to lack of data (e.g., focusing method on CRTs, environment on semiconductor lasers, etc.) or which could not be confirmed because of insufficient data (e.g., deflection method on CRTs, number of guns on CRTs, etc.). Every effort should be made to collect field failure rate data on these devices so that greater sensitivity and accuracy can be incorporated into their prediction procedures.

Air Force Regulation AFR 800-18 states: "to insure that every Air Force system is available for use when needed, will perform its assigned missions, and can be operated and supported economically, it is necessary to use and support GIDEP and the DoD Reliability Analysis Center." The following clause should be added to this statement: "and if data are to be available in sufficient quantities to provide support for reliability studies." The government provides funds for many maintenance support, life-cycle cost and reliability improvement warranty contracts which yield meaningful field failure experience data. A centralized point such as GIDEP or the Reliability Analysis Center should be on automatic distribution to receive

copies of the raw data collected during these contracts. These data would then be available for use in reliability studies such as the Reliability Modeling of Critical Electronic Devices effort.

It was noted during this study that many of the part and equipment manufacturers were reluctant to furnish uncontracted data free of charge. This reluctance may be due to material and manpower costs incurred in providing the data, or due to the proprietary nature of the data. The study contractor is normally not provided with sufficient funds to allow for the purchase of these data. The government should investigate methods of identifying when reliability data are generated, of analyzing the merits of the data, of providing a method of purchasing the data and of storing the data in a central repository which is available to all government contractors.

The proposed models for the non-mature devices (e.g., lasers, SAWs) should be updated and revised periodically, i.e., every three to five years. This would allow for changes in the state-of-the-art to be included on a timely basis.

Appendix A

Proposed Revision Pages

For

MIL-HDBK-217

5.1.2.9 Surface Acoustic Wave (SAW) Devices. The part operating failure rate model (λ_p) is:

$$\lambda_p = \lambda_b \pi_E \text{ failures}/10^6 \text{ hours}$$

where

λ_b = base failure rate

= 2.1 failures/10^6 hours

π_E = environmental factor (Table 5.1.2.9-1)

TABLE 5.1.2.9-1. ENVIRONMENTAL MODE FACTOR

Environment	π_E	Environment	π_E
G_B	1.0	A_{IA}	10.0
G_F	3.9	A_{IF}	15.0
G_M	11.0	A_{UC}	12.5
M_P	10.0	A_{UT}	10.0
N_{SB}	4.95	A_{UB}	20.0
N_S	8.5	A_{UA}	15.0
N_U	16.0	A_{UF}	20.0
N_H	15.5	S_F	1.6
N_{UU}	17.0	M_{FF}	10.5
A_{RW}	22.5	M_{FA}	14.5
A_{IC}	7.5	U_{SL}	30.5
A_{IT}	7.5	M_L	35.0
A_{IB}	12.5	C_L	600.0

5.1.3.11 Semiconductor Laser Devices

SPECIFICATION	DESCRIPTION
None	Aluminum gallium arsenide (AlGaAs), Double Heterojunction (DH), Stripe-geometry, Proton-isolated or Oxide-isolated structure, Optical Flux Density less than $3MW/CM^2$
None	Gallium Arsenide (GaAs), Single Heterojunction (SH), Stripe-geometry, Proton-isolated or Oxide-isolated structure, Optical Flux Density less than $3MW/CM^2$
None	Indium gallium arsenide/Indium gallium arsenide phosphorus (InGaAs/InGaAsP), DH, Stripe-geometry, Proton-isolated or Oxide-isolated structures, Optical Flux Density less than $3MW/CM^2$

The part failure rate model λ_p is:

$$\lambda_p = \lambda_b \pi_E$$

where

λ_p = total device failure rate ($F/10^6$ hours)

λ_b = average failure rate ($F/10^6$ hours)

π_E = environmental factor (Table 5.1.3.11-1)

The failure rate prediction procedure is as follows:

Step 1: Calculate the average failure rate (λ_b)

Step 1A: Calculate the average optical power output degradation rate using the following equation:

$$\tau_p = \tau_b \pi_T \pi_I \pi_C \pi_A \pi_F$$

where

τ_p = semiconductor laser optical power output degradation rate (%/1000 hours)

τ_b = base degradation rate (%/1000 hours) (Table 5.1.3.11-2)

π_T = temperature factor = $\exp\left[\frac{-E}{(T+273)}\right]$, T = Case Temperature (°C) (Table 5.1.3.11-3) and where E = apparent activation energy/Boltzman's Constant (Table 5.1.3.11-2). π_t is valid for +25°C $\leq$ T $\leq$ +100°C

π_C = construction factor (Table 5.1.3.11-4)

π_A = application factor (Table 5.1.3.11-5)

π_F = pulsed duty cycle factor (Table 5.1.3.11-6)

π_I = forward peak current factor (Table 5.1.3.11-7). (For Variable Current Sources use the initial current value). π_I is valid for 0 $\leq$ I $\leq$ 25 amps

Step 1B: Calculate the mean life of the device by the following procedure:

1) P_s = rated optical power output (mw)

2) define the required optical power output (Pr).

3) calculate the allowable degradation (D) as follows:

$$D(\%) = \frac{P_s - P_r}{P_s} \times 100$$

4) Mean life (U) = $D(\%)/\tau_p$

Note: Each laser must be replaced when it reaches P_r to make the calculated mean life (U) valid.

Step 1C: Calculate the average failure rate using:

$\lambda_p = 1/U$

Step 2: Calculate the average semiconductor laser failure rate using the equation:

$\lambda_p = \lambda_b \pi_E$

TABLE 5.1.3.11-1: ENVIRONMENTAL MODE FACTORS, π_E

Environment	π_E
G_B	1
G_F	2.4
G_M	7.8
M_P	7.7
N_{SB}	3.7
N_S	5.7
N_U	11
N_H	12
N_{UU}	13
A_{RW}	17
A_{IC}	2.5
A_{IT}	3.5
A_{IB}	3.5
A_{IA}	5.5
A_{IF}	8
A_{UC}	3
A_{UT}	5.5
A_{UB}	5.5
A_{UA}	8
A_{UF}	10
S_F	1
M_{FF}	7.8
M_{FA}	11
U_{SL}	23
M_L	26
C_L	450

TABLE 5.1.3.11-2: DEGRADATION EQUATION PARAMETERS

Device Type	E	τ_b ($\times 10^5$)
AlGaAs	4635	2.21
GaAs	4635	2.81
InGaAs/InGaAsP	5784	188

TABLE 5.1.3.11-3: TEMPERATURE FACTOR, π_T

T_C (°C)	AlGaAs or GaAs ($\times 10^{-6}$) π_T	InGaAs/InGaAsP ($\times 10^{-8}$) π_T
20	0.14	0.27
25	0.18	0.37
30	0.23	0.51
35	0.29	0.70
40	0.37	0.94
45	0.47	1.3
50	0.59	1.7
55	0.73	2.2
60	0.90	2.9
65	1.1	3.7
70	1.4	4.7
75	1.6	6
80	2	7.7
85	2.4	9.6
90	2.8	12
95	3.4	15
100	4	18

TABLE 5.1.3.11-4: CONSTRUCTION FACTOR, π_C

Construction	π_C
Facet Coat or Hermetic Package	1.0
No Facet Coat or Hermetic Package	3.3

TABLE 7.1.3.11-5: APPLICATION FACTOR, π_A

Application	π_A
Variable Current Source with optical feedback	1.0
Fixed Current Source	1.5

TABLE 7.1.3.11-6: PULSED DUTY CYCLE FACTOR, π_F

Duty Cycle	π_F*
1.0	1.00
0.9	0.95
0.8	0.90
0.7	0.85
0.6	0.75
0.5	0.70
0.4	0.65
0.3	0.55
0.2	0.45
0.1	0.30

*$\pi_F = \sqrt{\text{duty cycle}}$

TABLE 5.1.3.11-7: FORWARD CURRENT FACTOR, π_I

Forward Current, I (Ma)	π_I*
25,000	978
20,000	841
15,000	691
10,000	525
9,000	488
8,000	451
7,000	412
6,000	371
5,000	328
4,000	281
3,000	231
2,000	176
1,000	110
900	102
800	94
700	86
600	77
500	68
400	59
300	48
200	37
100	23
50	14

*$\pi_I = I^{0.68}$

Example 8.

Step (1) Given: A 10mw AlGaAs Double Heterostructure (DH) stripe geometry laser is used in a Ground, fixed environment, case temperature is 55°C, it has a facet coat, it has a fixed current source, the application is continuous wave (DC), the foward current is 100ma, and the minimum acceptable optical power output is 5mw.

Step (2) From Section 5.1.3.11 Step 1A

Calculate the average optical output degradation rate (τ_p)

$\tau_p = \tau_b \pi_T \pi_I \pi_C \pi_A \pi_F$

Step (3) Table 5.1.3.11-2 $\tau_b = 2.21 \times 10^5$ (%/1000 hours)

Step (4) Table 5.1.3.11-3 $\pi_T = 0.73$

Step (5) Table 5.1.3.11-7 $\pi_I = 23$

Step (6) Table 5.1.3.11-4 $\pi_C = 1.0$

Step (7) Table 5.1.3.11-5 $\pi_A = 1.5$

Step (8) Table 5.1.3.11-6 $\pi_F = 1.0$

Step (9) $\tau_p = 2.21 \times 10^5 (0.73) (23) (1.0) (1.5) (1.0)$

$= 5.56$ %/1000 hours

Step (10) From Section 5.1.3.11 Step 1B

Calculate the mean life of the device

Step (11) Allowable degradation (D)

$$D(\%) = \frac{P_s - P_s}{P_s} \times 100 = \frac{10mw - 5mw}{10mw} \times 100 = 50\%$$

Step (12) mean life (U)

$U = D(\%)/\tau_p = 50\%/5.56\%/1000$ hours $= 8993$ hours

Step (13) From Section 5.1.3.11 Step 1C

Calculate the average failure rate (λ_b)

$\lambda_b = 1/U = 111\ F/10^6$ hours

Step (14) From Section 5.1.3.11 Step 2

Calculate the average semiconductor laser failure rate (λ_p)

$\lambda_p = \lambda_b \pi_E = 111\ F/10^6$ hours (2.4) = $266.4\ F/10^6$ hours

5.1.4 Tubes, Electronic Vacuum

5.1.4.1 All Types Except Traveling Wave Tubes and Magnetrons. The operating failure rate model (λ_p) is:

$$\lambda_p = \lambda_b \times \pi_E \times \pi_L$$

where

λ_p = tube operating failure rate in failures/10^6 hr.
λ_b = base failure rate in failures/10^6 hr and is a function of tube type and operating parameters (see Table 5.1.4.1-1).
π_E = environmental factor (see Table 5.1.4.1-4).
π_L = learning factor (see Table 5.1.4.1-5).

TABLE 5.1.4.1-1: λ_b, BASE FAILURE RATE FOR TUBES
(Includes both random and wearout failures)

TUBE TYPE	λ_b (f./10^6 hrs.)
RECEIVER	
Triode, Tetrode, Pentode	5
Power Rectifier	10
CRT	9.6
THYRATRON	50
CROSSED FIELD AMPLIFIER	
QK681	260
SFD261	150
PULSED GRIDDED	
2041	140
6952	390
7835	140
TRANSMITTING	
Triode, Tetrode & Pentode — Peak Pwr≤200 kW, Freq≤200 MHz, Aver Pwr≤2kW	75
Triode, Tetrode & Pentode — If any of above limits are exceeded	100
	250
VIDICONS	
Antimony trisulfide (Sb_2S_3) photoconductive material	51
Silicon diode array photoconductive material	48

5.1.4.1-1

5.1.4.3 Magnetrons. The operating failure rate for magnetrons is:

$$\lambda_p = \lambda_b \times \pi_u \times \pi_E \times \pi_c$$

where

λ_p = total device failure rate (failure/10^6 filament hours)

π_u = utilization factor (see Table 5.1.4.3-1)

π_E = environmental factor (see Table 5.1.4.3-2)

π_c = construction factor

= 1, CW magnetrons (rated power < 5 Kw)
= 1, coaxial pulsed magnetrons
= 5.4, conventional pulsed magnetrons

λ_b = base failure rate (f/10^6 filament hrs)

= 18, CW magnetrons (rated power < 5 Kw)

= 19 $(f)^{0.73}$ $(P)^{0.20}$, pulsed magnetron (see Table 5.1.4.3-3)

where

f = frequency (GHz)
P = rated peak power (Mw)

TABLE 5.1.4.3-1: UTILIZATION FACTORS

Utilization (radiate hours/filament hours)	π_u
0.0	0.44
0.1	0.50
0.2	0.55
0.3	0.61
0.4	0.66
0.5	0.72
0.6	0.78
0.7	0.83
0.8	0.89
0.9	0.94
1.0	1.0

$\pi_u = 0.44 + 0.56(R)$, R = radiate hours/filament hours

TABLE 5.1.4.3-2: ENVIRONMENTAL FACTORS

Environment	π_E	Environment	π_E
G_B	1	A_{IA}	4
G_F	2	A_{IF}	20
G_M	4	A_{UC}	13
M_P	36	A_{UT}	16
N_{SB}	13	A_{UB}	19
N_S	13	A_{UA}	5
N_U	20	A_{UF}	30
N_H	56	S_F	1
N_{UU}	60	M_{FF}	36
A_{RW}	80	M_{FA}	50
A_{IC}	11	U_{SL}	106
A_{IT}	13	M_L	160
A_{IB}	13	C_L	2000

TABLE 5.1.4.3-3: BASE FAILURE RATE FOR PULSED MAGNETRONS

P (Power, Mw)	F(Frequency, GHz)													
	0.1	0.5	1	5	10	20	30	40	50	60	70	80	90	100
0.01	1.41	4.56	7.56	24.5	40.7	67.4	90.6	112	131	150	168	185	201	218
0.05	1.94	6.29	10.4	33.8	56.0	92.9	125	154	181	207	232	256	279	301
0.1	2.23	7.23	12.0	38.8	64.3	107	144	177	208	238	266	294	320	346
0.3	2.78	9.00	14.9	48.4	80.2	133	179	221	260	297	332	366	399	431
0.5	3.08	9.97	16.5	53.6	88.8	147	198	244	288	328	368	405	442	447
1	3.54	11.4	19.0	61.5	102	169	228	281	330	337	422	466	507	548
3	4.41	14.3	23.7	76.6	127	211	283	350	412	470	526	580	632	683
5	4.88	15.8	26.2	84.9	141	234	314	387	456	521	583	642	700	756

$$\lambda_U = 19(f)^{0.73}\ (P)^{0.20}$$

5.1.5 Lasers. This section presents failure rate models for laser peculiar items used in the following six major classes of laser equipment (see Bibliography Item 40):

Helium/Neon & Helium/Cadmium	Section 5.1.5.1
Argon Ion	Section 5.1.5.2
CO_2 Sealed	Section 5.1.5.3
CO_2 Flowing	Section 5.1.5.4
Solid State, Nd:YAG Rod	Section 5.1.5.5
Solid State, Ruby Rod	Section 5.1.5.6

The models and failure rates presented in this section apply to the laser peculiar items only, i.e., those items wherein the lasing action is generated and controlled. In addition to the laser peculiar items, there are other assemblies used with lasers that contain electronic parts and mechanical devices (pumps, valves, hoses, etc.). The failure rates for these parts should be determined with the same procedures as used for other electronic and mechanical devices in the equipment or system or which the laser is a part. The electronic device failure rates are in other parts of this Handbook and the mechanical device failure rates are in Bibliography Item 47.

The laser failure rate models have been developed at the "functional," rather than "piece part" level because the available data were not sufficient for "piece part" model development. Nevertheless, the laser functional models are included in this Handbook in the interests of completeness. These laser models will be revised to include piece part models and other laser types when the data become available.

Because each laser family can be designed using a variety of approaches, the failure rate models have been structured on three basic laser functions which are common to most laser families, but may differ in the hardware implementation of a given function. These functions are the lasing media, the laser pumping mechanism (or pump), and the coupling method.

The general laser failure rate model is:

$$\lambda_{LASER} = \lambda_{MEDIA} + \lambda_{PUMP} + \lambda_{COUPLING}$$

Examples of media-related hardware and influence factors are the solid state rod, gas, gas pressure, vacuum integrity, gas mix, outgassing, and tube diameter. The electrical discharge, the flashlamp, and energy level are examples of pump-related hardware and influence factors. The coupling function contributors are the "Q" switch, mirrors, windows, crystals, substrates, coatings, and level of dust protection provided.

The λ_{PUMP} term in the λ_{LASER} equation is zero for helium/neon, helium/cadmium, argon ion, CO_2 sealed and CO_2 flowing lasers because the pumping mechanisms for these lasers contain no laser peculiar items. Pumping is accomplished with electronic parts and circuitry. Failure rates for these parts are not included in this section but they should be included in the reliability analysis of the system or equipment containing the laser. Also, some of the terms in the above general λ_{LASER} equation have modifying factors depending upon the aser type. These factors are shown in the following subsections.

5.1.5.1 Helium/Neon and Helium/Cadmium Lasers

$$\lambda_p = \pi_E \lambda_{MEDIA} + \pi_E \lambda_{COUPLING}$$

where

λ_p = the laser failure rate in failures/10^6 operating hours.

π_E = the environmental application factor, and its value is determined from Table 5.1.5.7-1.

λ_{MEDIA} = the failure rate contribution of the lasing media, and its value is 84 failures/10^6 operating hours for helium/neon lasers, and 228 failures/10^6 operating hours for helium/cadmium lasers.

$\lambda_{COUPLING}$ = is the failure rate contribution of the laser coupling hardware, and its value is 0.1 failures/10^6 operating hours.

It should be noted that the laser failure rate prediction model can be simplified and rewritten as:

$$\lambda_{He/Ne} = 84.1\ \pi_E$$

$$\lambda_{He/Cd} = 228.1\ \pi_E$$

5.1.10.2 Solid State Relays (SSR)

Specification	Description
MIL-R-28750	Relay, Solid State

The part failure rate prediction procedure is as follows:

Step 1: If a Parts List and/or Schematic Diagram are available.

Step 1A: Calculate a failure rate for each particular component in the SSR assembly using the correct model from the following sections:

Integrated Circuits	Section 5.1.2
Discrete Semiconductors	Section 5.1.3
Resistors	Section 5.1.6
Capacitors	Section 5.1.7
Inductive Devices	Section 5.1.8
Relays	Section 5.1.10
Printed Wiring Assemblies	Section 5.1.13

Step 1B: Sum the failure rate contribution for each component. The SSR failure rate (λ_p) then is:

$$\lambda_p = \sum_{i=1}^{n} \lambda_i$$

where

λ_p = SSR failure rate (F/10^6 hours)

λ_i = failure rate of each individual component (F/10^6 hours)

Step 2: If a parts list but no schematic diagram is available, or if the part complement can be determined by other means (e.g., disection).

Step 2A: Calculate a failure rate for each component type and for the SSR as an assembly using the procedure discussed in Section 5.2.

Step 3: If no parts list or schematic diagram are available, calculate the SSR failure rate using the following model:

$$\lambda_p = \lambda_b \times \pi_Q \times \pi_E$$

where

λ_p = SSR failure rate (F/10^6 hours)

λ_b = base failure rate = 0.4 F/10^6 hours

π_E = environmental factor (Table 5.1.10.2-1)

π_Q = quality factor

= 1, MIL-SPEC quality
= 3, lower quality

TABLE 5.1.10.2-1: ENVIRONMENTAL FACTOR

Environment	π_E	Environment	π_E
G_B	1	A_{IA}	13
G_F	3.3	A_{IF}	22
G_M	13	A_{UC}	11
M_P	10	A_{UT}	16
N_{SB}	5.2	A_{UB}	40
N_S	7	A_{UA}	24
N_U	17	A_{UF}	38
N_H	16	S_F	0.85
N_{UU}	17	M_{FF}	10
A_{RW}	23	M_{FA}	14
A_{IC}	6.5	U_{SL}	31
A_{IT}	9.5	M_L	35
A_{IB}	24	C_L	590

5.1.10.3 Hybrid and Solid State Time Delay Relays (TDR)

Specification	Description
MIL-R-83726	Relay, Time Delay, Hybrid and Solid State

The part failure rate prediction procedure is as follows:

Step 1: If a Parts List and/or Schematic Diagram are available.

Step 1A: Calculate a failure rate for each particular component in the TDR assembly using the correct model from the following sections:

Integrated Circuits	Section 5.1.2
Discrete Semiconductors	Section 5.1.3
Resistors	Section 5.1.6
Capacitors	Section 5.1.7
Inductive Devices	Section 5.1.8
Relays	Section 5.1.10
Printed Wiring Assemblies	Section 5.1.13

Step 1B: Sum the failure rate contribution for each component. The TDR failure rate (λ_p) then is:

$$\lambda_p = \sum_{i=1}^{n} \lambda_i$$

where

λ_p = TDR failure rate (F/10^6 hours).

λ_i = failure rate of each individual component (F/10^6 hours)

Step 2: If a parts list but no schematic diagram is available, or if the part complement can be determined by other means (e.g. disection).

Step 2A: Calculate a failure rate for each component type and for the TDR as an assembly using the procedure discussed in Section 5.2.

Step 3: If no parts list or schematic diagram are available and the TDR is a hybrid electronic TDR, calculate the TDR failure rate using the current model for electronic time delay relays (Section 5.1.10).

Step 4: If no parts list or schematic diagram are available and the TDR is an all solid state TDR, calculate the TDR failure rate using the model:

$$\lambda_p = \lambda_D + \lambda_R$$

where

λ_p = TDR failure rate (F/10^6 hours)

λ_D = delay circuit failure rate (F/10^6 hours)

λ_R = relay circuit failure rate (F/10^6 hours)

Step 4A: Calculate the delay circuit failure rate (λ_D).

$$\lambda_D = \lambda_b \times \pi_E \times \pi_Q$$

where

λ_b = base failure rate = 0.5 F/10^6 hours

π_E = environmental factor (Table 5.1.10.3-1)

π_Q = quality factor
= 1, MIL-SPEC quality
= 4, lower quality

Step 4B: Calculate the relay circuit failure rate (λ_R) using the procedure given in Section 5.1.10.2.

Step 4C: Calculate the total TDR failure rate (λ_p).

$$\lambda_p = \lambda_D + \lambda_R$$

TABLE 5.1.10.3-1: ENVIRONMENTAL FACTORS

Environment	π_E	Environment	π_E
G_B	1	A_{IA}	18
G_F	4.5	A_{IF}	30
G_M	16	A_{UC}	15
M_P	12	A_{UT}	21
N_{SB}	8.4	A_{UB}	58
N_S	8.8	A_{UA}	33
N_U	20	A_{UF}	52
N_H	18	S_F	0.58
N_{UU}	20	M_{FF}	12
A_{RW}	26	M_{FA}	17
A_{IC}	8.8	U_{SL}	35
A_{IT}	12	M_L	40
A_{IB}	35	C_L	680

Thumbwheel:

TABLE 5.1.11-4: PREDICTION PROCEDURE FOR THUMBWHEEL SWITCHES

PART SPECIFICATION COVERED	DESCRIPTION
MIL-S-22710	Switches, Rotary (Printed Circuit), (Thumbwheel, In-line, And Pushbutton)

Part Operating failure rate model (λ_p)

$$\lambda_p = (\lambda_1 + N\lambda_2) \times \pi_E \times \pi_{cyc} \times \pi_L \ (f/10^6 \text{ hours})$$

where

λ_1 = 0.0067 $f/10^6$ hours, MIL-SPEC quality

= 0.086 $f/10^6$ hours, lower quality

λ_2 = 0.062 $f/10^6$ hours, MIL-SPEC quality

= 0.089 $f/10^6$ hours, lower quality

N = number of active contacts

π_E = environmental factors (see Table 5.1.11-5)

π_{cyc} = cycling rate factor (see Table 5.1.11-6)

π_L = load type factor (see Table 5.1.11-7)

CAUTION: This model applies to the switching function only. The model does not consider the contribution of any discrete components (e.g., resistors, diodes, lamp) which may be mounted on the switch. The failure rate of these devices must be calculated using the appropriate section of this handbook and added to the failure rate of the switch.

This model applies to a single switch section. This type of switch is frequently ganged to provide the required function. The model must be applied to each section individually.

TABLE 5.1.11-5: ENVIRONMENTAL FACTORS

Environment	π_E	Environment	π_E
G_B	1	A_{IA}	15
G_F	2.9	A_{IF}	20
G_M	14	A_{UC}	10
M_P	21	A_{UT}	10
N_{SB}	7.9	A_{UB}	15
N_S	7.9	A_{UA}	15
N_U	20	A_{UF}	25
N_H	32	S_F	1
N_{UU}	34	M_{FF}	21
A_{RW}	46	M_{FA}	29
A_{IC}	8	U_{SL}	63
A_{IT}	8	M_L	71
A_{IB}	15	C_L	1200

TABLE 5.1.11-6: CYCLING RATE FACTOR

Switching Cycles	π_{cyc}
$\leq$ 1 cycle/hour	1.0
> 1 cycle/hour	number of cycles/hour

TABLE 5.1.11-7: LOAD TYPE FACTOR

Stress	Load Type		
S	Resistive	Inductive	Lamp
0.05	1.00	1.02	1.06
0.1	1.02	1.06	1.28
0.2	1.06	1.28	2.72
0.3	1.15	1.76	9.49
0.4	1.28	2.72	54.6
0.5	1.48	4.77	
0.6	1.76	9.49	
0.7	2.15	21.4	
0.8	2.72		
0.9	3.55		
1.0	4.77		

where

$$S = \frac{\text{operating load current}}{\text{rated resistive load}}$$

$$\Pi_L = e^{(S/.8)^2} \text{ for resistive.}$$

$$= e^{(S/.4)^2} \text{ for inductive.}$$

$$= e^{(S/.2)^2} \text{ for lamp.}$$

Example 3

Given: A MIL-SPEC 2AMP resistive rated thumbwheel switch is installed in an airborne inhabited, cargo environment at a 40°C ambient temperature. The switch has five active contacts. It is cycled an average of 2 cycles per hour, and the load current is 5% of rated current and is resistive. The switch has four ¼watt, 10 ohm class M carbon composition (RCR) resistors mounted on the switch printed circuit card. The resistors are an integral part of the switch and cannot be removed and replaced if they fail.

Find: The failure rate of the switch as an assembly.

Step 1: Calculate Switch Failure Rate

$\lambda_1 = 0.0067$ f/10^6 hours

$\lambda_2 = 0.062$ f/10^6 hours

$N = 5$

$\pi_E = 8$

$\pi_{cyc} = 2$

$\pi_L = 1.02$

$\lambda_p = (\lambda_1 + N\lambda_2) \times \pi_E \times \pi_{cyc} \times \pi_L$

$\lambda_p = (0.0067 + (5 \times 0.062)) \times 8 \times 2 \times 1.00$

$\lambda_p = 5.067$ f/10^6 hours

Step 2: Calculate Resistors Failure Rate

From section 5.1.6.1.

$\lambda_p = \lambda_b \times \pi_E \times \pi_R \times \pi_Q$ (f/10^6 hours)

$\lambda_b = 0.00055$ f/10^6 hours (40°C, 0.4 stress)

$\pi_E = 3$

$\pi_R = 1$

$\pi_Q = 1$

λ_p = .00055 x 3 x 1 x 1

= 0.0016 f/10^6 hours

Step 3: Calculate total switch assembly failure rate

$\lambda = \lambda_{switch} + 4 \times \lambda_{resistors}$

λ = 5.067 f/10^6 hours + 0.006 f/10^6 hours

λ = 5.073 f/10^6 hours

5.1.11.2 Circuit Breakers

Specification	Description
MIL-C-55629	Circuit Breakers, Magnetic, Unsealed, Trip-Free
MIL-C-83383	Circuit Breakers, Remote Control, Thermal, Trip-Free
MIL-C-39019	Circuit Breakers, Magnetic, Low Power, Sealed, Trip-Free Service
W-C-375	Circuit Breakers, Molded Case; Branch Circuit and Service

5.1.11.2.1 Prediction Procedure For Circuit Breakers

The part operating failure rate model (λ_p) is:

$$\lambda_p = \lambda_b \times \pi_C \times \pi_Q \times \pi_E$$

where

λ_p = circuit breaker failure rate ($F/10^6$ hours)

λ_b = base failure rate

= 0.020 failures/10^6 hours, magnetic circuit breakers
= 0.038 failures/10^6 hours, thermal circuit breakers
= 0.038 failures/10^6 hours, thermal-magnetic circuit breakers

π_C = configuration factor (see Table 5.1.11.2-1)

π_Q = quality factor

= 1.0, MIL-SPEC quality
= 8.4, lower quality

π_E = environmental factor (see Table 5.1.11.2-2)

TABLE 5.1.11.2-1: CONFIGURATION FACTOR

Configuration	π_C
SPST	1.00
DPST	1.50
SPDT	1.75
3PST	2.00
4PST	2.50
DPDT	3.00
3PDT	4.25
4PDT	5.50
6PDT	8.00

TABLE 15.1.11.2-2: ENVIRONMENTAL FACTOR

Environment	π_E	Environment	π_E
G_B	1	A_{IA}	7.5
G_F	2.3	A_{IF}	10
G_M	8.2	A_{UC}	9
M_P	21	A_{UT}	8
N_{SB}	7.9	A_{UB}	15
N_S	7.9	A_{UA}	10
N_U	14	A_{UF}	15
N_H	32	S_F	1
N_{UU}	34	M_{FF}	21
A_{RW}	46	M_{FA}	29
A_{IC}	6	U_{SL}	62
A_{IT}	5.5	M_L	71
A_{IB}	10	C_L	N/A

5.1.12.3 Integrated Circuit (IC) Socket Prediction Procedure.

SPECIFICATION	DESCRIPTION
MIL-S-83734	Sockets, Plug-in Electronic Components

The part failure rate model is:

$$\lambda_p = \lambda_b \times \pi_E \times \pi_P$$

where

λ_p = total failure rate (f/10^6 hours)
λ_b = base failure rate = 0.00042 f/10^6 hours
π_E = environmental factor (Table 5.1.12.3-1)
π_P = contact factor (Table 5.1.12.3-2)

TABLE 5.1.12.3-1: ENVIRONMENTAL FACTORS

Environment	π_E	Environment	π_E
G_B	1.0	A_{IA}	10*
G_F	3.1	A_{IF}	13*
G_M	17*	A_{UC}	10*
M_P	11*	A_{UT}	10*
N_{SB}	5.4	A_{UB}	13*
N_S	[illegible]*	A_{UA}	13*
N_U	18*	A_{UF}	20*
N_H	17*	S_F	1.0
N_{UU}	19*	M_{FF}	11*
A_{RW}	25*	M_{FA}	16*
A_{IC}	6.7*	U_{SL}	33*
A_{IT}	6.7*	M_L	39*
A_{IB}	10*	C_L	650*

* It is recommended that I.C. sockets should only be used in this environment if socketed device is restrained.

TABLE 5.1.12.3-2: CONTACT FACTOR

Number of Active Contacts	π_P
6	2.02
8	2.30
10	2.58
14	3.14
16	3.42
18	3.71
20	4.00
22	4.31
24	4.62
28	5.26
36	6.66
40	7.42
48	9.06
50	9.50
64	12.93

$$\pi_P = \exp\left(\frac{N-1}{N_0}\right)^q$$

where

$N_0 = 10$

$q = 0.51064$

N = number of active contacts (active indicates electrical current current flow through the contact)

5.1.15 Meters

5.1.15.1 Prediction Procedure For Meters, Electrical Indicating

Specification	Description
MIL-M-10304	Meter, Electrical Indicating, Panel Type, Ruggedized.

The part operating failure rate model (λ_p) is:

$$\lambda_p = \lambda_b(\pi_A \times \pi_F \times \pi_Q \times \pi_E)$$

where

λ_p = meter failure rate in failures/10^6 hours

λ_b = base failure rate
= 0.090 F/10^6 hours

π_A = application factor
= 1.0, Direct Current
= 1.7, Alternating Current

π_F = function factor
= 1.0, Ammeter
= 2.2, Voltmeter
= 2.8, Other (meters whose basic meter movement construction is an ammeter with associated internal conversion elements)

π_Q = quality factor
= 1.0, MIL-SPEC quality
= 3.4, lower quality

π_E = environmental factor (see Table 5.1.15.1-1)

TABLE 5.1.15.1-1: ENVIRONMENTAL FACTOR

Environment	π_E	Environment	π_E
G_B	1.0	A_{IA}	42
G_F	3.8	A_{IF}	42
G_M	24	A_{UC}	50
M_P	26	A_{UT}	73
N_{SB}	11	A_{UB}	50
N_S	14	A_{UA}	73
N_U	36	A_{UF}	73
N_H	41	S_F	2.5
N_{UU}	29	M_{FF}	26
A_{RW}	60	M_{FA}	N/A
A_{IC}	21	U_{SL}	N/A
A_{IT}	42	M_L	94
A_{IB}	21	C_L	N/A

* N/A - Not normally applied

5.1.15.2 Example Failure Rate Calculations

Example 1.

Given: A MIL-M-10304 panel AC ammeter used in an airborne cargo inhabited environment.

Step 1.

The failure rate of the meter is found by substituting the values of λ_b, π_A, π_F, π_Q and π_E into the part failure rate model:

$$\lambda_p = \lambda_b(\pi_A \times \pi_F \times \pi_Q \times \pi_E) \text{ failures}/10^6 \text{ hours}$$

$$\lambda_p = 0.09(1.7 \times 1.0 \times 1.0 \times 21) \text{ failures}/10^6 \text{ hours}$$

$$\lambda_p = 3.2 \text{ F}/10^6 \text{ hours}$$

Example 2.

Given: A commercial panel type frequency meter with a construction similar to MIL-M-10304 panel meters. The meter operates the same as a DC ammeter. It is used in a ground, mobile application.

Step 1.

The failure rate of the meter is found by substituting the values of λ_b, π_A, π_F, π_Q and π_E into the part failure rate model:

$$\lambda_p = \lambda_b(\pi_A \times \pi_F \times \pi_Q \times \pi_E) \text{ failures}/10^6 \text{ hours}$$

$$\lambda_p = 0.09(1.0 \times 2.8 \times 3.4 \times 24) \text{ failures}/10^6 \text{ hours}$$

$$\lambda_p = 21 \text{ F}/10^6 \text{ hours}$$

5.1.16 Quartz Crystals

Specification	Description
MIL-C-3098	Crystal Units, Quartz

The part operating failure rate model (λ_p) is:

$$\lambda_p = \lambda_b * \pi_Q \times \pi_E$$

where

λ_p = quartz crystal failure rate ($F/10^6$ hours)

λ_b = base failure rate

$\lambda_b = 0.013\ (f)^{0.23}$ failures/10^6 hours (f = frequency (MHz))

π_Q = quality factor

= 1.0, MIL-SPEC quality
= 2.1, lower quality

π_E = environmental factor (see Table 5.1.16-1)

TABLE 5.1.16-1: ENVIRONMENTAL FACTOR

Environment	π_E	Environment	π_E
G_B	1	A_{IA}	17
G_F	2.6	A_{IF}	17
G_M	10	A_{UC}	19
M_P	11	A_{UT}	28
N_{SB}	5.4	A_{UB}	19
N_S	6.5	A_{UA}	28
N_U	14	A_{UF}	28
N_H	16	S_F	1
N_{UU}	17	M_{FF}	11
A_{RW}	23	M_{FA}	15
A_{IC}	9	U_{SL}	30
A_{IT}	17	M_L	35
A_{IB}	9	C_L	500

5.1.17.1 Lamps, Incandescent

SPECIFICATION	DESCRIPTION
MIL-L-6363	Lamps, Incandescent, Aviation Service
W-L-111	Lamp, Incandescent, (Electric, Miniature, Tungsten-Filament)

5.1.17.1.1 Prediction Procedure For Incandescent Lamps

The part operating failure rate model (λ_p) is:

$$\lambda_p = \lambda_b \times \pi_u \times \pi_A \times \pi_E$$

where

λ_p = incandescent lamp failure rate (F/10^6 hours)

λ_b = base failure rate

$\lambda_b = 0.074(V_r)^{1.29}$ f/10^6 hrs. (V_r = rated voltage (volts)) (see Table 5.1.17.1.1-1)

π_u = utilization factor (see Table 5.1.17.1.1-2)

π_A = application factor

= 1.0, AC applications
= 3.3, DC applications

π_E = environmental factor (see Table 5.1.17.1.1-3)

TABLE 5.1.17.1.1-1: BASE FAILURE RATE

V_r	λ_b
5	0.590
6	0.746
12	1.825
14	2.23
24	4.46
28	5.44
37.5	7.94

TABLE 5.1.17.1.1-2: UTILIZATION FACTORS

Utilization (Illuminate hours/ equipment operate hours)	π_u
< 0.10	0.10
0.10 to 0.90	0.72
> 0.90	1.0

TABLE 5.1.17.1.1-3: ENVIRONMENTAL FACTORS

Environment	π_E	Environment	π_E
G_B	1	A_{IA}	4.4
G_F	1.6	A_{IF}	4.4
G_M	3.4	A_{UC}	4.8
M_P	3.5	A_{UT}	5.8
N_{SB}	2.4	A_{UB}	4.8
N_S	2.7	A_{UA}	5.8
N_U	4.1	A_{UF}	5.8
N_H	4.4	S_F	1.4
N_{UU}	4.5	M_{FF}	3.5
A_{RW}	5.3	M_{FA}	4.2
A_{IC}	3.2	U_{SL}	6.1
A_{IT}	4.4	M_L	6.5
A_{IB}	3.2	C_L	27

5.1.17.3 Examples For Use of Lamp Models

Example 1:

Given: A 6.3 volt incandescent lamp, used as a tail warning radar indicator in the inhabited portion of a fighter aircraft. The voltage source is AC. The ratio of illuminate hours to equipment operate hours is less than 5%.

Step 1: Calculate the base failure rate (λ_b)

$\lambda_b = 0.074\ (6.3)^{1.29} = 0.795\ F/10^6$ hours

Step 2: From Table 5.1.17.1.1-1, $\pi_u = 0.10$

Step 3: From Table 5.1.17.1.1-2 A_{IF} service, $\pi_E = 4.4$

Step 4: Application factor AC service, $\pi_A = 1.0$

Step 5: Calculate the total lamp failure rate (λ_p)

$\lambda_p = \lambda_b \times \pi_u \times \pi_E \times \pi_A$

$\lambda_p = (0.795 \times 0.10 \times 4.4 \times 1.0)\ F/10^6$ hours

$\lambda_p = 0.350\ F/10^6$ hours

Example 2:

Given: A 12 volt incandescent lamp, used as a power indicator in a ground, fixed environment. The voltage source is DC. The ratio of illuminate hours to equipment operate hours is 1.0.

Step 1: Calculate the base failure rate (λ_b)

$\lambda_b = 0.074\ (12)^{1.29} = 1.83\ F/10^6$ hours

Step 2: From Table 5.1.17.1.1-1, $\pi_u = 1.0$

Step 3: From Table 5.1.17.1.1-2 G_F service, $\pi_E = 1.6$

Step 4: Application factor DC service, $\pi_A = 3.3$

Step 5: Calculate the total lamp failure rate (λ_p)

$\lambda_p = \lambda_b \times \pi_u \times \pi_E \times \pi_A$

$\lambda_p = (1.83 \times 1.0 \times 1.6 \times 3.3)\ F/10^6$ hours

$\lambda_p = 9.66\ F/10^6$ hours

5.1.18 Electronic Filters (Non-tunable) Prediction Procedure

Specification	Description
MIL-F-15733	Filters, Radio Frequency Interference
MIL-F-18327	Filters; High Pass, Low Pass, Band Pass, Band Suppression, and Dual Functioning (Non-tunable)

The part failure rate prediction procedure is as follows:

Step 1: If a Parts List and/or Schematic Diagram are available.

Step 1A: Calculate a failure rate for each particular component in the filter assembly using the correct model from the following sections:

Integrated Circuits	Section 5.1.2
Discrete Semiconductors	Section 5.1.3
Resistors	Section 5.1.6
Capacitors	Section 5.1.7
Inductive Devices	Section 5.1.8
Printed Wiring Assemblies	Section 5.1.13
Crystals	Section 5.1.16

Step 1B: Sum the failure rate contribution for each component. The filter failure rate (λ_p) then is:

$$\lambda_p = \sum_{i=1}^{n} \lambda_i$$

where

λ_p = filter failure rate ($F/10^6$ hours)

λ_i = failure rate of each individual component ($F/10^6$ hours)

Step 2: If a parts list but no schematic diagram is available, or if the part complement can be determined by other means (e.g. disection).

Step 2A: Calculate a failure rate for each component type and for the filter as an assembly using the procedure discussed in Section 5.2.

Step 3: If no parts list or schematic diagram are available, calculate the filter failure rate using the following model:

$$\lambda_p = \lambda_b \times \pi_Q \times \pi_E$$

where

λ_p = filter failure rate ($F/10^6$ hours)

λ_b = base failure rate

= 0.0219 $F/10^6$ hours for MIL-F-15733, ceramic-ferrite construction (styles FL 10-16, 22, 24, 30-32, 34, 35, 38, 41-43, 45, 47-50, 61-65, 70, 81-93, 95, 96)

= 0.120 $F/10^6$ hours for MIL-F-15733, discrete LC components (styles FL 37, 53, 74)

= 0.120 $F/10^6$ hours for MIL-F-18327, discrete LC components (composition 1)

= 0.265 $F/10^6$ hours for MIL-F-18327, discrete LC and crystal components (composition 2)

π_E = environmental factor (Table 5.1.18-1)

π_Q = quality factor

= 1, MIL-SPEC quality
= 2.9, lower quality

TABLE 5.1.18-1: ENVIRONMENTAL FACTOR

Environment	π_E	Environment	π_E
G_B	1	A_{IA}	8.8
G_F	2.1	A_{IF}	8.8
G_M	6	A_{UC}	10
M_P	6.4	A_{UT}	13
N_{SB}	3.7	A_{UB}	10
N_S	4.3	A_{UA}	13
N_U	7.9	A_{UF}	13
N_H	8.7	S_F	1.7
N_{UU}	9.2	M_{FF}	6.4
A_{RW}	11	M_{FA}	8.2
A_{IC}	5.5	U_{SL}	14
A_{IT}	8.8	M_L	16
A_{IB}	5.5	C_L	120

5.1.18.2 Examples

Example 1:

Step 1: Given: A MIL-F-18327, Composition 1 band pass filter that is used in a ground, fixed environment. A parts list is provided with the following part complement:

RF Coil, MIL-SPEC	- 4 each
Plastic Capacitor, MIL-SPEC	- 5 each
Paper/Plastic Capacitor, MIL-SPEC	- 2 each
Mica Capacitor, MIL-SPEC	- 1 each
Printed Wiring Board, 2-Sided	- 1 each
Solder Connections	- 24 each

Step 2: From Section 5.2 calculate a failure rate for each componenet type.

Plastic (CRH) .0085 f/10^6 hours
Paper/Plastic (CH) .049 f/10^6 hours
Mica (CM) .011 f/10^6 hours
RF Coil .011 f/10^6 hours
PW board .0029 f/10^6 hours
Connections .00017 f/10^6 hours

Step 3: From Section 5.2 calculate a failure rate for the filter assembly.

$$\lambda_p = (4 \times .011) + (5 \times .0085) + (2 \times .049) + (1 \times .011) + (1 \times .0029) + (24 \times .00017)$$

$$\lambda_p = 0.2025 \text{ f/}10^6 \text{ hours}$$

Example 2:

Step 1: Given: A MIL-F-18327, Composition 1 band pass filter that is used in a ground, fixed environment. No parts list or schematic diagrams are available and the part complement can not be determined.

Step 2: From Section 5.1.18 Step 3 Calculate a failure rate for the filter assembly.

$$\lambda_p = \lambda_b \times \pi_Q \times \pi_E$$

Step 2: $\lambda_b = 0.120$ f/10^6 hours

Step 2B: $\pi_Q = 1$

Step 2C: Table 5.1.18-1 $\pi_E = 2.1$, GF

Step 2D: $\lambda_p = 0.120$ f/10^6 hours x 1 x 2.1

$\lambda_p = 0.252$ F/10^6 hours

5.1.19 Fuse Prediction Procedure

SPECIFICATION	DESCRIPTION
W-F-1726	Fuse, Cartridge Class H
W-F-1814	Fuse, Cartridge, High Interrupting Capacity
MIL-F-5372	Fuse, Current Limiter Type, Aircraft
MIL-F-23419	Fuses, Instrument Type
MIL-F-15160	Fuses; Instrument, Power and Telephone (nonindicating), style FO1

The part operating failure rate model is:

$$\lambda_p = \lambda_b \times \pi_E$$

where

λ_p = total device operating failure rate (f/10^6 hours)

λ_b = base failure rate = 0.010 f/10^6 hours

π_E = environmental factor (see Table 5.1.19-1)

TABLE 5.1.19-1: ENVIRONMENTAL FACTORS

Environment	π_E	Environment	π_E
G_B	1.0	A_{IA}	12
G_F	2.3	A_{IF}	12
G_M	7.5	A_{UC}	13
M_P	8.1	A_{UT}	18
N_{SB}	4.4	A_{UB}	13
N_S	5.2	A_{UA}	18
N_U	10	A_{UF}	18
N_H	12	S_F	1.8
N_{UU}	12	M_{FF}	8.1
A_{RW}	16	M_{FA}	11
A_{IC}	6.8	U_{SL}	20
A_{IT}	12	M_L	22
A_{IB}	6.8	C_L	230

MISSION
of
Rome Air Development Center

RADC plans and executes research, development, test and selected acquisition programs in support of Command, Control Communications and Intelligence (C^3I) activities. Technical and engineering support within areas of technical competence is provided to ESD Program Offices (POs) and other ESD elements. The principal technical mission areas are communications, electromagnetic guidance and control, surveillance of ground and aerospace objects, intelligence data collection and handling, information system technology, ionospheric propagation, solid state sciences, microwave physics and electronic reliability, maintainability and compatibility.

END

FILMED

1-84

DTIC